

ÉCOLE DOCTORALE DES SCIENCES CHIMIQUES
UMR 7140

THÈSE présentée par :

Chaojie XU

soutenue le : **13 octobre 2015**

pour obtenir le grade de : **Docteur de l'université de Strasbourg**

Discipline/ Spécialité : Sciences Chimiques - Chimie

Tectonique Moléculaire :
**Réseaux de coordination hétérométalliques
basés sur des complexes d'Iridium(III) chiraux
et luminescents**

THÈSE dirigée par :

Pr. PLANEIX Jean-Marc
Pr. HOSSEINI Mir Wais

Professeur, Université de Strasbourg
Professeur, Université de Strasbourg

RAPPORTEURS :

Dr. BASSANI Dario
Pr. HOUSECROFT Catherine.

Directeur de recherche CNRS, Institut des Sciences Moléculaires
Professeur, Université de Bâle

AUTRES MEMBRES DU JURY :

Pr. SAUVAGE Jean-Pierre
Pr. FONTECAVE Marc

Professeur, Université de Strasbourg
Professeur, Collège de France

To my family

Acknowledgements

First of all, I would like to thank to all the members of my jury: Dr Dario Bassani, Pr. Catherine Houscroft, Pr. Jean-Pierre Sauvage, Pr. Marc Fontecave for their acceptance to evaluate my thesis work.

Three years' PhD life is a wonderful journey to see, to experience. I would like to thank to Pr. Mir Wais Hosseini, for giving me the opportunity to study in his lab. My dear prof, thank you for your encouragements, your patient guidance, and your opening door for discussion.

I would like to thank to Aurélie, thank you for her help in chemistry and in my life in Strasbourg. Without her patient guidance and help, I wouldn't learn so much not only in chemistry but also in French.

To my co-director of thesis, Pr. Jean-Marc Planeix, even you are not always in the lab, but your guidance from emails, your encouragements every time you come, helped a lot during my three years' PhD life.

Special thanks to our excellent crystallographer Nathalie Kyritsakas, without her great skills and patience in dealing with the crystals I obtained, my thesis project would not have been possible.

Thank you for all my present and past colleagues: Elena, Nicolas M., Nicolas Z., Dimby, Max, Cyril, Fan, Bowen, Patrick, Fabien, Mohammed, Sacha, Ivan, Antoine, and thank you for the learning atmosphere you have made. I am really appreciate all the great moments we spent in "Happy hours" and "O'Brien" and of course for the great times in labs, our discussions in chemistry and our stories in life. Aziz, Stephane, Audrey, Sylvie, Véro, Valérie, thank you for your helps in chemistry and in administration works.

A lot of thanks for the NMR and spectroscopy service. Thank you for Dr. Martine Heinrich's guidance for doing all my CD spectra. Thank you for the help of Dr. Elena Longhi and Dr. Chienwei HSU during luminescent measurements.

For all my Chinese friends in Strasbourg, Fan, Bowen, Huanhuan, Zhaohui, Yanan, thank you for your companion for cinemas and shopping.

At the end, thank you for Shaojun, thank you for the destiny to let us meet in Strasbourg and for you companion during the last two years.

Table of Contents

| | |
|---|-----------|
| RESUME EN FRANÇAIS..... | I |
| CHAPTER I: GENERAL INTRODUCTION..... | 2 |
| 1. Supramolecular Chemistry | 2 |
| 2. Molecular Tectonics | 3 |
| 3. Chiral or homochiral coordination polymers and their applications..... | 12 |
| 4. Luminescent Coordination Polymers and their applications..... | 22 |
| 5. Chirality in metal complexes..... | 26 |
| 6. Luminescent Ir(III) complexes | 30 |
| 7. Research Project | 34 |
| CHAPTER II: SYNTHESIS OF RACEMIC AND ENANTIOPURE CATIONIC IRIDIUM COMPLEXES FOR THE FORMATION OF COORDINATION NETWORKS | 42 |
| 1. Introduction..... | 42 |
| 2. Synthesis and characterization of the Ir(III) complexes based on terminal pyridyl coordinating sites as racemates..... | 48 |
| 3. Asymmetric synthesis and characterization of the enantiopure Ir(III) complexes based on terminal pyridyl coordinating sites | 57 |
| 4. Synthesis and characterization of racemic and enantiopure Ir(III) complexes based on terminal carboxylate coordinating sites..... | 66 |
| 5. Formation of a 1-D and 2-D coordination networks between racemic and enantiopure Ir(III) complex | 76 |
| 6. Conclusion of chapter | 85 |

| | |
|--|------------|
| CHAPTER III: SYNTHESIS OF NEUTRAL Ir(III) COMPLEXES FOR THE FORMATION OF COORDINATION NETWORKS..... | 90 |
| 1. Introduction..... | 90 |
| 2. Synthesis and characterization of the heteroleptic neutral Ir(III) complexes based on terminal pyridyl coordinating sites | 99 |
| 3. Synthesis and characterization of heteroleptic neutral Iridium(III) complexes based on terminal carboxylate coordinating sites..... | 108 |
| 4. Formation of coordination networks based on neutral Ir(III) complexes | 111 |
| 5. Conclusion of chapter | 119 |
| CHAPTER IV: CONCLUSIONS AND PERSPECTIVES | 122 |
| CHAPTER V: EXPERIMENTAL PART..... | 126 |
| 1. General..... | 126 |
| 2. Synthesis and characterization of compounds | 129 |
| 3. Crystallization and crystallographic data..... | 153 |
| 4. Powder X-ray diffraction data..... | 171 |
| LIST OF PRODUCTS | 176 |

RESUME EN FRANÇAIS

Tectonique moléculaire : Réseaux de coordination hétérométalliques basés sur des complexes d'Iridium(III) chiraux et luminescents

Les polymères de coordination (CPs) ou réseaux de coordination (CNs) également connus sous le nom de Metal-Organic Frameworks,¹ sont des architectures moléculaires cristallines infinies contenant des centres ou clusters métalliques reliés entre eux par des entités organiques (tectons organiques) *via* des liaisons de coordination. L'intérêt porté à ce type de matériaux, développé depuis une vingtaine d'années, découle de nombreuses possibilités synthétiques à explorer pour leur préparation ainsi qu'au grand nombre d'applications possibles dans les domaines du stockage de gaz,² de la catalyse,³ du transport de médicaments,⁴ ou de la détection.⁵ De plus, une attention particulière a été portée à l'obtention de polymères de coordination chiraux (homochiraux) en vue de leur utilisation notamment en catalyse asymétrique⁶ ou séparation énantiosélective⁷ basée sur leur aspect poreux. Cette porosité peut être exploitée pour effectuer au sein des pores offrant un environnement chiral, une catalyse asymétrique hétérogène permettant par la suite un recyclage facilité du catalyseur. D'autre part, la séparation chirale peut être envisagée en supposant qu'une reconnaissance chirale sélective entre un des deux énantiomères et les pores chiraux ait lieu. Différentes méthodes ont été développées pour obtenir des polymères de coordination chiraux.⁸ L'utilisation de tectons organiques énantiomériquement purs contrôlant la structure et la chiralité des architectures est actuellement l'approche la plus aboutie. En appliquant les concepts de la tectonique moléculaire,⁹ des polymères de coordination chiraux ont pu être obtenus en utilisant des tectons chiraux comportant des atomes de carbone asymétriques.¹⁰ Par ailleurs, des réseaux de coordination hétérométalliques (ou M'MOFs), une autre classe de réseaux de coordination, présentent également des propriétés intéressantes dans des domaines tels que la catalyse, la luminescence¹¹ ou le magnétisme.¹² Ce type d'architecture se compose de complexes métalliques, ou metallatectons, possédant des sites coordination périphériques capables de coordonner des ions métalliques. Ainsi, quelques polymères de coordination hétérométalliques et chiraux ont été décrits à partir de ligands BINAP,¹³ ou de métallo-salen chiraux¹⁴ en visant des applications en catalyse (Schéma 1a). Cependant, cette approche nécessite souvent une synthèse asymétrique multi-étapes afin d'obtenir les tectons énantiomériquement purs.

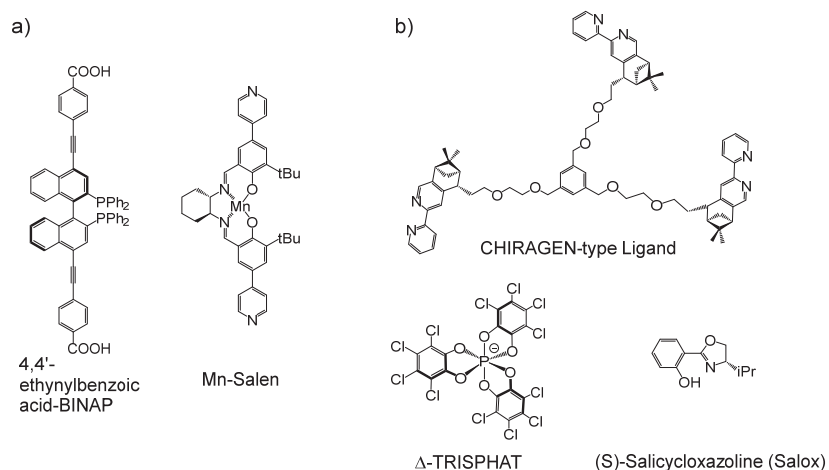


Schéma 1 : a) Exemples de ligands chiraux à base de BINAP et Mn-salen utilisés pour générer des réseaux de coordination homochiraux; b) Structures d'un exemple de ligands de type CHIRAGEN, de l'anion TRISPHAT et d'un ligand dérivé de l'oxazoline.

Les tectons chiraux précités sont soit des molécules possédant des centres stéréogènes (*e.g.* carbone de type sp^3 pour les ligands chiraux de type salen), soit sont basés sur des atropoisomères stables et non-interconvertibles du fait d'une grande barrière d'énergie conformationnelle (*e.g.* ligands de type BINAP ou BINOL). En 1911, Alfred Werner a démontré que, outre un carbone asymétrique tétraédrique, d'autres atomes, notamment les métaux de transition, adoptant d'autres géométries, pouvaient aussi jouer le rôle de centre stéréogène.¹⁵ Un cas particulier concerne les métaux adoptant une géométrie octaédrique et portant au moins deux ligands bidentates non contenus dans un même plan. Alors que les stéréodescripteurs *R* et *S* sont utilisés pour différencier deux énantiomères contenant un (ou des) atome(s) de carbone asymétrique, les descripteurs Δ et Λ sont alors employés pour distinguer l'hélice droite de l'hélice gauche dans les complexes métalliques octaédriques. Dans le cas de complexes d'Iridium (III) cyclométallés octaédriques, différentes méthodes ont été développées pour préparer des complexes énantiomériquement purs (Schéma 1b)¹⁶. Dans cette optique, A. von Zelewsky et ses collègues ont développé des ligands de type CHIRAGEN (CHIRALity GENerator) basés sur une unité pinène-pyridine pour former stéréosélectivement un des diastéréoisomères (Δ ou Λ).¹⁷ J. Lacour et ses collègues ont utilisé un anion enantiopure, le Trisphat, comme contre-ion afin de former et séparer des mélanges racémiques de complexes d'Iridium (III) binucléaires.^{16a} Ainsi, selon les différences de solubilité des stéréoisomères et la polarité des solvants employés, les paires d'ions diastéréomériques ainsi formés peuvent être séparées. Enfin, une autre approche basée sur l'emploi de ligands auxiliaires chiraux afin de former, par coordination du ligand sur un centre métallique, des diastéréoisomères séparables a également été développée. Après la résolution des diastéréoisomères, ces ligands auxiliaires chiraux labiles peuvent être remplacés par d'autres ligands choisis. P. Lusby et ses collègues ont ainsi exploité cette stratégie. En utilisant la L- et D-serine avec des dimères d'Iridium cyclométallés, les diastéréoisomères correspondant ont pu être

résolus. Les dimères d'Iridium énantio-pures ont ensuite été reformés par traitement acide et substitution des ligands chiraux labiles en conservant la configuration absolue des centres métalliques.¹⁸ Parallèlement, des ligands chiraux basés sur une unité de type oxazoline ont aussi été décrits par E. Meggers *et. al.* et ont montré leur efficacité pour former et isoler les diastéréoisomères résultants. La substitution de ces ligands labiles par d'autres ligands bidentates a permis la formation de complexes chiraux dont le seul élément de chiralité est le centre métallique.¹⁹ Cependant, il existe peu d'exemples de complexes d'Iridium (III) cyclométallés isolés sous forme énantio-pure. Dans l'optique de former des réseaux de coordination chiraux, seuls deux exemples de complexes possédant comme unique centre stéréogène un métal de géométrie octaédrique ont été décrits, à notre connaissance, pour la formation des réseaux de coordination homochiraux.²⁰ De plus, même si des complexes d'iridium ont déjà été employés comme métallatectons, seuls les mélanges racémiques ont été utilisés.²¹ Dans le cadre de ce travail, nous nous sommes intéressés à la possibilité de former des CPs énantio-purs en utilisant des complexes d'Iridium(III) énantio-purs. Il faut noter que les complexes d'Iridium (III) bis ou tris cyclométallés sont stables configurationnellement et ne racémisent pas en solution. Ils peuvent donc être utilisés comme briques élémentaires pour générer des MOFs homochiraux. En dehors de leur chiralité intrinsèque, de tels complexes sont également étudiés pour leurs propriétés photophysiques très intéressantes.^{20a-c} De ce fait, les réseaux de coordination homochiraux à base Iridium(III) devraient également présenter des propriétés de luminescence et de reconnaissance chirale permettant la détection optique de molécules encapsulées.

Ainsi, de nouveaux complexes d'Iridium(III) chiraux possédant trois ligands bidentates dont l'un est fonctionnalisé par des groupements périphériques coordinants ont été envisagés comme nouveaux métallatectons (Schéma 2). Deux des trois ligands bidentates sont des unités de type 2-phenylpyridine (ppy), groupements cyclométallants fréquemment utilisés pour obtenir des complexes luminescents. Afin de varier la longueur d'onde d'émission des complexes, le ligand fluoré 2-(2,4-difluorophenyl)pyridine (dFppy) a aussi été utilisé. Le troisième ligand bidentate est soit une unité de type 2,2'-bipyridine disubstituée (bpy, Y=N), soit une entité de type 2-phenylpyridine disubstituée (Y=C). L'utilisation d'un troisième ligand de type bpy entraîne la formation de métallatectons cationiques tandis que l'utilisation d'une unité ppy substituée génère des complexes neutres. De plus, ce troisième ligand est fonctionnalisé, en positions 5 et 5' de la bipyridine ou en positions 5 de la pyridine et 4 du groupement phényle du ligand 2-phenylpyridine, par des groupes périphériques coordinants tels que pyridine ou acide benzoïque. Les connecteurs choisis entre les sites périphériques de coordination et l'unité centrale de type bpy ou ppy sont des groupements éthyngyles afin d'assurer une coplanarité entre sites de coordinants centraux et terminaux induisant une conjugaison étendue au niveau du métallatecton. Comme mentionné ci-dessus, des propriétés luminescentes pour les réseaux de coordination obtenus par auto-assemblage des complexes d'Iridium avec des sels métalliques pourraient permettre la détection des molécules encapsulées.

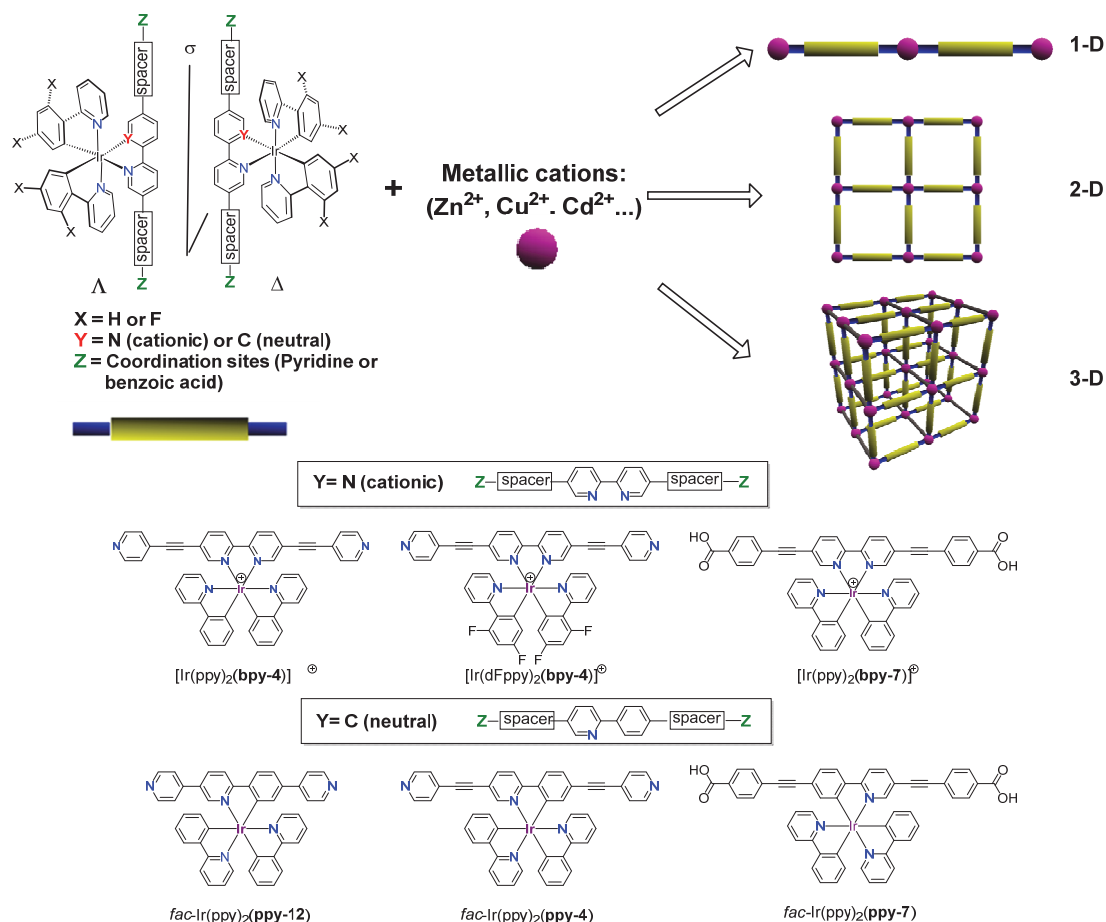


Schéma 2 : Structures des metallatectons cationiques et neutres basés sur des complexes d'Ir et représentations schématiques de la formation des réseaux de coordination 1-D, 2-D et 3-D.

Les objectifs de ce travail de thèse sont d'une part de la synthèse des complexes d'Iridium(III) racémiques (Δ et Λ) et énantiopurs (Δ ou Λ) et l'étude de leurs propriétés de luminescence, et, d'autre part, l'utilisation de ces complexes comme metallatectons pour générer des réseaux de coordination hétérométalliques homochiraux possédant des cavités chirales pour la reconnaissance de molécules chirales. Ce travail de thèse peut être divisé en deux grandes parties :

- 1) La synthèse des complexes d'Iridium cationiques sous leurs formes racémiques et énantiopures et la génération des réseaux de coordination à partir de ces metallatectons.
- 2) La synthèse de metallatectons à base de complexe d'Iridium neutres sous leur forme racémique uniquement et la génération des réseaux de coordination.

I. Synthèse des complexes cationiques d'Iridium sous forme racémique et enantiopure et formation de réseaux de coordination hétérométalliques

i. Synthèse de complexes discrets sous forme racémique

Deux ligands de type 2,2'-bipyridine, **bpy-4** et **bpy-7**, et possédant respectivement comme sites de coordinant périphériques une pyridine ou un acide benzoïque ont été synthétisés *via* des réactions de couplages de type Suzuki ou Sonogashira catalysées au palladium (Schéma 3).

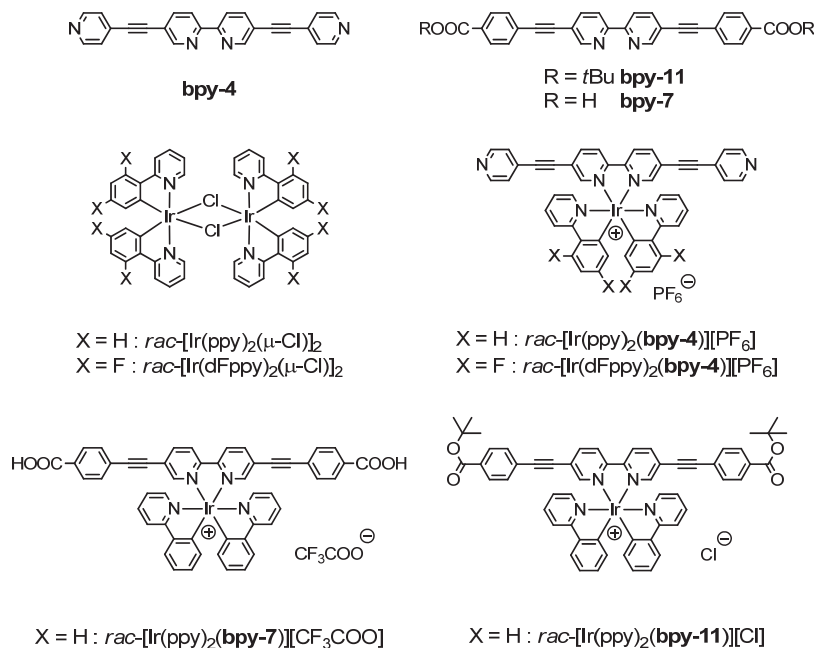


Schéma 3 : Structures des deux ligands **bpy-4** et **bpy-7**, des dimères d'Ir et des trois métallatectons cationiques ciblés, $\text{rac-}[\text{Ir}(\text{ppy})_2(\text{bpy-4})][\text{PF}_6]$, $\text{rac-}[\text{Ir}(\text{dFppy})_2(\text{bpy-4})][\text{PF}_6]$ et $\text{rac-}[\text{Ir}(\text{ppy})_2(\text{bpy-7})][\text{CF}_3\text{COO}]$ et de certains intermédiaires.

Le complexe d'Iridium(III) non-fluoré, $\text{rac-}[\text{Ir}(\text{ppy})_2(\text{bpy-4})][\text{PF}_6]$, a été synthétisé par réaction du dimère d'Iridium $\text{rac-}[\text{Ir}(\text{ppy})_2(\mu\text{-Cl})]_2$ avec le ligand **bpy-4** selon une procédure décrite précédemment.^{20d} La même procédure a été suivie pour obtenir le complexe d'Ir(III) possédant des fonctions acides carboxyliques protégées par des groupements *tert*-butyles, $\text{rac-}[\text{Ir}(\text{ppy})_2(\text{bpy-11})][\text{PF}_6]$. Puis, le composé final $\text{rac-}[\text{Ir}(\text{ppy})_2(\text{bpy-7})][\text{CF}_3\text{COO}]$ a été obtenu par hydrolyse acide des fonctions esters à l'aide de l'acide trifluoroacétique.

Pour la synthèse du complexe fluoré, $\text{rac-}[\text{Ir}(\text{dFppy})_2(\text{bpy-4})][\text{PF}_6]$, une autre approche a dû être développée, l'approche précédente aboutissant à un mélange non séparable de produits. Ainsi, la 5,5'-dibromo-2,2'-bipyridine (**bpy-1**) a été tout d'abord coordonnée au dimère $\text{rac-}[\text{Ir}(\text{dFppy})_2(\mu\text{-Cl})]_2$ pour obtenir le complexe $\text{rac-}[\text{Ir}(\text{dFppy})_2(\text{bpy-1})][\text{PF}_6]$. Ce complexe portant des bromes terminaux a ensuite été engagé dans une réaction de couplage de type Sonogashira avec la 4-éthynylpyridine conduisant à la formation du complexe final $\text{rac-}[\text{Ir}(\text{dFppy})_2(\text{bpy-4})][\text{PF}_6]$.

Tous les ligands et complexes ont été caractérisés par les méthodes classiques (*e.g.* ^1H -RMN, ^{13}C -RMN, microanalyses, spectrométrie de masse). De plus, leurs propriétés photophysiques ont été étudiées. Les trois complexes finaux présentent des longueurs d'onde d'émission entre 570 et 700 nm en solution avec un déplacement hypsochrome provoqué par la substitution des ligands ppy par les ligands dFppy. Ces complexes sont également émissifs à l'état solide. Leurs propriétés photophysiques sont comparables à celles déjà rapportées de complexes analogues. De plus, les trois complexes ont été caractérisés par diffraction des rayons X sur monocristal. Les paramètres géométriques observés sont similaires à ceux de complexes analogues décrits dans la littérature. Comme attendu, les deux énantiomères sont présents dans les structures cristallines.

ii. *Synthèse des complexes discrets énantiopurs*

Afin d'obtenir les complexes cationiques précédents de manière énantiopure, deux approches ont été suivies.

La première stratégie est basée sur la formation de paires d'ions en utilisant un anion énantiopure, soit le Trisphat (Schéma 1b), soit le binphat,²² pour générer des diastéréoisomères ioniques séparables par chromatographie ou recristallisation. Cependant, bien que cette méthode ait déjà été employée avec des complexes similaires d'Iridium, elle n'a pas permis ici d'isoler les diastéréoisomères pour les trois complexes employés dans le cadre de cette thèse.

La deuxième approche s'appuie sur l'utilisation de ligands bidentates auxiliaires chiraux induisant la formation de diastéréoisomères séparables. Une fois ces diastéréoisomères isolés, les ligands auxiliaires labiles peuvent être substitués par d'autres ligands achiraux, la configuration du centre métallique restant inchangée. Ainsi, en utilisant la méthode décrite récemment par Lusby *et al.*,¹⁸ les dimères d'Iridium énantiopures, $\Delta\Delta\text{-}[\text{Ir}(\text{ppy})_2(\mu\text{-Cl})_2]$ ou $\Lambda\Lambda\text{-}[\text{Ir}(\text{ppy})_2(\mu\text{-Cl})_2]$, ainsi que leur analogues fluorés ont pu être isolés par une synthèse en deux étapes utilisant comme auxiliaire chiral soit la L- soit la D-serine. Ces dimères possèdent comme seul centre stéréogène l'atome d'iridium, les ligands de ces complexes étant par ailleurs tous achiraux. De plus, aucune racémisation de tels complexes d'iridium n'est observée en solution, l'atome d'iridium conservant donc sa configuration absolue. Ainsi, les mêmes voies de synthèse développées pour les complexes racémiques peuvent être employées pour la synthèse des complexes cationiques énantiopurs en utilisant cette fois le dimère d'iridium énantiopure correspondant comme précurseur. Les deux énantiomères (Δ et Λ) des trois complexes cationiques ont donc pu être isolés. Tous les complexes chiraux ont été caractérisés par les techniques standards (^1H -RMN, ^{13}C -RMN, microanalyses, spectrométrie de masse) et par dichroïsme circulaire (CD) et polarimétrie. Des monocristaux de certains complexes énantiopures ont également été obtenus et étudiés par diffraction des rayons X sur monocristal confirmant ainsi la configuration absolue au sein de ces complexes (Schéma 4).

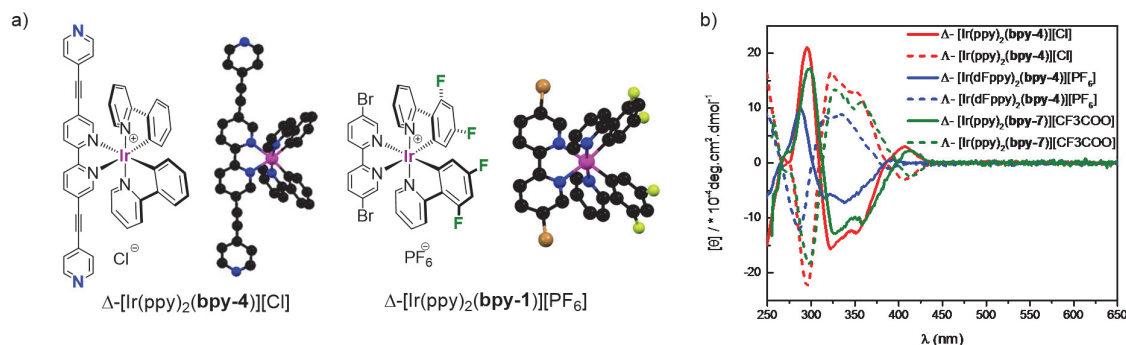


Schéma 4: a) Structures chimiques et cristallines de Δ -[Ir(ppy)₂(bpy-4)][Cl] et Δ -[Ir(dFppy)₂(bpy-1)][PF₆]. Les anions et molécules de solvant ont été omis par souci de clarté; b) Spectres CD à 293 K de Δ -[Ir(ppy)₂(bpy-4)][Cl] (trait plein rouge, CH₃CN), Δ -[Ir(ppy)₂(bpy-7)][CF₃COO] (trait plein vert, DMSO) et Δ -[Ir(dFppy)₂(bpy-4)][PF₆] (trait plein bleu, CH₃CN) (pour les énantiomères Λ , les mêmes couleurs que l'énantiomère Δ correspondant ont été utilisés mais les traits sont en pointillés).

iii. Synthèse des polymères de coordination hétérométalliques

L'auto-assemblage des métallatectons décrits précédemment avec différents sels métalliques (e.g. Cu²⁺, Co²⁺, Cd²⁺, Ag⁺) a été étudié en vue de la formation de polymères de coordination cristallins.

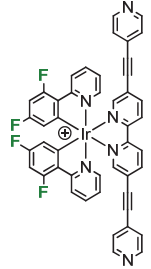
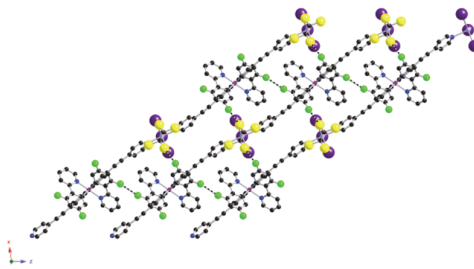
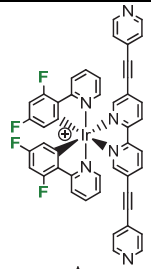
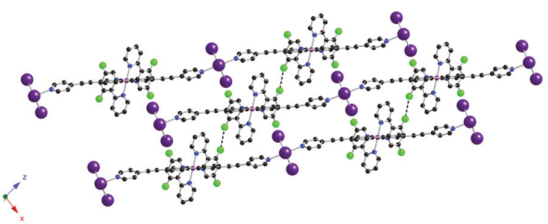
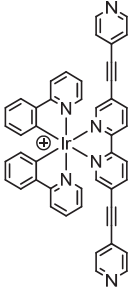
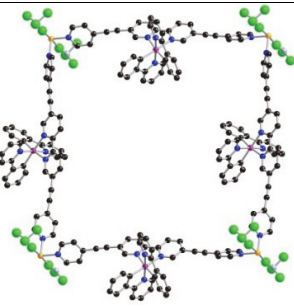
Malgré de nombreux essais, seuls trois réseaux de coordination ont pu être caractérisés par diffraction des rayons X sur monocristal. Les autres essais ont soit abouti à des poudres amorphes, soit à des cristaux maclés ou bien à des cristaux possédant un pouvoir diffractant trop faible. Ainsi, lorsque le métallatecton possédant des sites périphériques de type carboxylate a été employé, la structure des réseaux formés n'a pu être résolue, malgré des cristaux de bonne qualité, du fait d'un pouvoir de diffraction trop faible.

Par contre, la combinaison du métallatecton fluoré possédant des pyridines comme unités coordinantes terminales, [Ir(dFppy)₂(bpy-4)][PF₆], sous forme de racémate ou l'énantiomère Λ , avec des sels de Cd(II) a donné lieu à la formation de réseaux de coordination monodimensionnels (Tableau 1). L'obtention de ces chaînes infinies est due à l'échange des ions PF₆⁻ par des anions iodures au sein de la structure menant à un nœud métallique de formule [CdI₃]. Le cadmium adopte ainsi une géométrie trigonale plane au lieu de la géométrie octaédrique attendue. De plus, il est à noter que, dans le cas de *rac*-[Ir(dFppy)₂(bpy-4)][PF₆], bien que le cristal soit achiral, chaque chaîne est formée uniquement d'un seul des deux énantiomères. L'empilement des différentes chaînes homochirales consistent en une alternance de chaînes de chiralité opposée menant ainsi à une structure achirale. Dans le cas où seul l'énantiomère Λ est utilisé lors du processus d'auto-assemblage, le réseau monodimensionnel obtenu est similaire et comme attendu, l'empilement au sein du cristal mène à un matériau énantiopure. Dans le cas de ces deux réseaux, les propriétés de luminescence de

ont été étudiées et ont montré une faible influence du nœud métallique sur les propriétés d'émission centrées sur le complexe d'Iridium.

L'auto-assemblage du metallatecton analogue non fluoré *rac*-[Ir(dFppy)₂(bpy-4)][PF₆] avec un sel de Cu(I) oxydé en Cu(II) lors de la cristallisation a quant à lui permis l'obtention d'un réseau bidimensionnel (Tableau 1) de type grille comportant comme nœud métallique une unité Cu(BF₄)₂. A nouveau, chaque grille est homochirale comportant uniquement soit l'énantiomère Δ soit l'énantiomère Λ. L'empilement de ces grilles de manière légèrement décalée consiste en une alternance de plans de chiralité opposée et le cristal résultant est à nouveau achiral. Malheureusement, aucune émission de cette architecture de type de grille n'a pas pu être détectée, la présence de Cu(II) expliquant probablement l'extinction de luminescence.²³

Tableau 1 : Polymères de coordination hétérométalliques obtenus et caractérisés par diffraction des rayons X sur monocristal.

| Metallatecton | Nœud métallique | Structure cristalline des réseaux de coordination | Dimensionnalité |
|--|-----------------------------------|--|-----------------|
|  | [CdI ₃] ⁻ |  | 1D |
|  Δ | [CdI ₃] ⁻ |  | 1D |
|  | Cu(BF ₄) ₂ |  | 2D |

En conclusion, des polymères de coordination hétérométalliques basés sur des métallatectons centrés sur des complexes cationiques d'Iridium ont pu être générés et caractérisés à l'état solide. Cependant, cette stratégie présente deux inconvénients : i) les cavités au sein des réseaux ne sont pas seulement occupées par des molécules de solvant mais aussi par les contre ions des métallatectons (PF_6^-), réduisant ainsi l'espace disponible pour encapsuler des molécules; ii) dans le cas de l'emploi de CdI_2 , une métathèse d'anions du métallatecton et une coordination de l'iodure sur le Cd menant au nœud $[\text{CdI}_3]^-$ a été observée conduisant à une dimensionnalité inférieure du réseau.

II. Synthèse de complexes neutres d'Iridium sous forme racémique et formation de réseaux de coordination hétérométalliques

Ainsi, la présence d'anions peut être dommageable pour la formation de réseaux de coordination poreux et l'étude de leurs propriétés d'encapsulation. Des complexes neutres d'Iridium possédant trois unités de type phenylpyridine ont été envisagés comme approche complémentaire. Dans ce cas, le ligand de type bipyridine a été remplacé par une unité de type 2-phenylpyridine, les autres unités du ligand restant similaires. Ainsi, soit la 4-ethynylpyridine soit l'acide 4-ethynylbenzoïque ont été à nouveau utilisés comme sites périphériques de coordination (Schéma 5). Un troisième complexe ne possédant pas de connecteur a également été étudié (Schéma 5). De plus, de tels complexes d'Iridium cyclométallés ont été largement étudiés comme émetteurs triplets et présentent en général des rendements quantiques plus importants que leurs analogues cationiques.²⁴

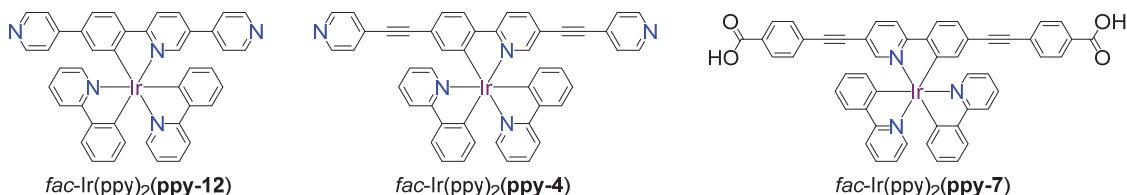


Schéma 5 : Structures chimiques de trois complexes d'Iridium tris-cyclométallés cibles, *fac-*

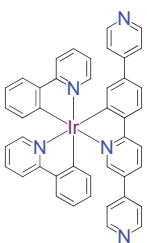
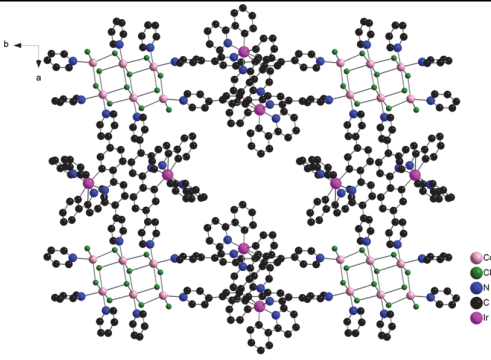
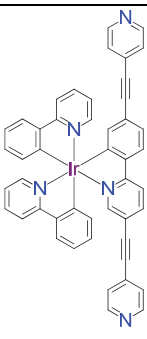
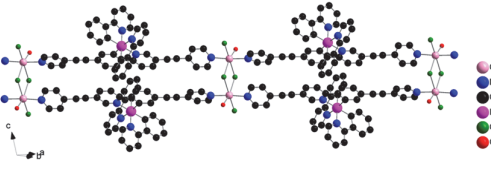
Ir(ppy)₂(ppy-12), *fac-Ir(ppy)₂(ppy-4)*, *fac-Ir(ppy)₂(ppy-7)*.

De manière générale, la synthèse de complexes d'Iridium(III) tris-cyclométallés nécessite des températures assez élevées et les isomères faciaux (*fac*), produits thermodynamiquement stables, sont généralement obtenus.²⁵ Cependant, un mélange de stéréoisomères peut également être obtenu et les rendements sont de ce fait généralement relativement faibles.^{24a} Dans un premier temps, nous nous sommes donc penchés sur l'optimisation des conditions de réactions pour former les trois complexes cibles (Schéma 5). Tous les complexes ont été caractérisés par les techniques habituelles (*e.g.* ^1H -RMN, ^{13}C -RMN, microanalyses, spectrométrie de masse). Pour les trois complexes, seul l'isomère *fac* a été isolé sous forme d'un mélange racémique (*fac,Δ* et *fac,Λ*) et il n'a pas été possible de résoudre ces deux énantiomères. La configuration faciale a été confirmée par RMN et par la structure cristalline obtenue par diffraction des rayons X sur monocristal (Schéma 5). Les propriétés luminescence des complexes neutres ont également été étudiées en solution et à l'état solide montrant

une émission dans le rouge entre 600 et 680 nm et des rendements quantiques et temps de vie similaires à des complexes analogues déjà décrits dans la littérature.

Afin de générer différents réseaux de coordination hétérométalliques par auto-assemblage en utilisant ces complexes neutres comme métallatectons, différents sels métalliques adoptant différentes géométries de coordination ont été utilisés. Ainsi, une architecture de type double-grille a été obtenue en combinant le complexe ne possédant pas de connecteur *fac*-Ir(ppy)₂(ppy-12) avec CdCl₂ (Table 2). Au sein d'une double-grille, les deux énantiomères du métallatecton sont présents et les nœuds métalliques consistent en un cluster de six atomes de Cd pontés par des atomes de chlore. La structure finale est de ce fait achirale. Par ailleurs, en utilisant le complexes possédant un connecteur de type ethynyl, *fac*-Ir(ppy)₂(ppy-4), un autre type de réseau a été obtenu en combinant ce métallatecton avec CdCl₂ (Tableau 2). En effet, cette fois, un réseau monodimensionnel composé de deux chaînes reliées entre elles par un cluster bimétallique de Cd est obtenu. Encore une fois, les deux énantiomères sont présents dans une double chaîne et le cristal est achiral. Dans les deux cas, les réseaux obtenus sont luminescents et les propriétés d'émission du complexe sont peu perturbées par la présence des atomes de Cd.

Tableau 2 : Polymères de coordination hétérométalliques obtenus et caractérisés par diffraction des rayons X sur monocristal

| Metallatecton | Nœud métallique | Structure cristalline des réseaux de coordination | Dimensionnalité |
|---|--|--|-----------------|
|  <p><i>fac</i>-Ir(ppy)₂(ppy-12)</p> | [Cd ₆ Cl ₁₂] ⁻ |  | 2D |
|  <p><i>fac</i>-Ir(ppy)₂(ppy-4)</p> | [Cd ₂ Cl ₄] ⁻ |  | 1D |

III. Conclusions et Perspectives

En conclusion, au cours de ce travail de thèse, la synthèse de nouveaux complexes d'Iridium bis-cyclométallés cationiques a été réalisée avec succès. Leur synthèse asymétrique a également pu être menée, menant à des complexes présentant comme unique centre stéréogène le centre métallique. Tous les complexes ont été caractérisés en solution et à l'état solide. En particulier, les propriétés photophysiques ont été étudiées et montrent une émission dans le rouge par excitation dans le visible. La formation de réseaux de coordination à l'aide de ces métallatectons a ensuite été étudiée en présence de divers sels métalliques. Il a notamment été possible de former par auto-assemblage un réseau monodimensionnel homochiral luminescent en combinant le métallatecton énantiopure avec un sel de Cd. D'autre part, la synthèse des complexes d'Iridium neutres tris-cyclométallés possédant comme troisième ligand un dérivé de 2-phenylpyridine fonctionnalisés par des sites de coordination périphériques de type pyridine ou acide benzoïque a été réalisée et optimisée. Les propriétés photophysiques de tels complexes ont également été étudiées. Enfin, la formation de réseaux de coordination hétérométalliques employant ces métallatectons neutres a été étudiée et des réseaux mono et bidimensionnels ont pu être obtenus.

Il est à noter que dans le cas des complexes neutres, il n'a pas été possible de résoudre les deux énantiomères de l'isomère *fac*. Une optimisation des conditions de réaction afin d'atteindre ce but reste encore à faire. De plus, plusieurs réseaux de coordination ont pu être formés en utilisant soit les métallatectons cationiques soit les métallatectons neutres mais n'ont pu être caractérisés par diffraction des rayons X, les monocristaux obtenus possédant un pouvoir de diffraction trop faible. Par ailleurs, d'autres sels métalliques doivent être testés pour générer de nouveaux réseaux de coordination stables et poreux afin d'exploiter leur propriétés de luminescence pour la détection de molécules encapsulées.

REFERENCES

- (1) (a) Furukawa, H.; Cordova, K. E.; O'Keeffe, M.; Yaghi, O. M. *Science* **2013**, *341*, 974; (b) Hosseini, M. W. *Acc. Chem. Res.* **2005**, *38*, 313.
- (2) Suh, M. P.; Park, H. J.; Prasad, T. K.; Lim, D. W. *Chem. Rev.* **2012**, *112*, 782.
- (3) Lee, J.; Farha, O. K.; Roberts, J.; Scheidt, K. A.; Nguyen, S. T.; Hupp, J. T. *Chem. Soc. Rev.* **2009**, *38*, 1450.
- (4) Horcajada, P.; Gref, R.; Baati, T.; Allan, P. K.; Maurin, G.; Couvreur, P.; Ferey, G.; Morris, R. E.; Serre, C. *Chem. Rev.* **2012**, *112*, 1232.
- (5) Cui, Y.; Yue, Y.; Qian, G.; Chen, B. *Chem. Rev.* **2012**, *112*, 1126.
- (6) (a) Song, F.; Wang, C.; Lin, W. *Chem. Commun.* **2011**, *47*, 8256; (b) Ma, L.; Abney, C.; Lin, W. *Chem. Soc. Rev.* **2009**, *38*, 1248; (c) Yoon, M.; Srirambalaji, R.; Kim, K. *Chem. Rev.* **2012**, *112*, 1196.
- (7) Peluso, P.; Mamane, V.; Cossu, S. *J. Chromatogr. A* **2014**, *1363*, 11.

- (8) Grosshans, P.; Jouaiti, A.; Bulach, V.; Planeix, J.-M.; Hosseini, Mir W.; Kyritsakas, N. *Eur. J. Inorg. Chem.* **2004**, 2004, 453.
- (9) (a) Simard, M.; Su, D.; Wuest, J. D. *J. Am. Chem. Soc.* **1991**, 113, 4696; (b) Mann, S. *Nature* **1993**, 365, 499; (c) Hosseini, M. W. *Coord. Chem. Rev.* **2003**, 240, 157.
- (10) (a) Larpent, P.; Jouaiti, A.; Kyritsakas, N.; Hosseini, M. W. *Chem. Commun.* **2013**, 49, 4468; (b) Marets, N.; Bulach, V.; Hosseini, M. W. *New J. Chem.* **2013**, 37, 3549; (c) Grosshans, P.; Jouaiti, A.; Bulach, V.; Planeix, J.-M.; Hosseini, M. W.; Nicoud, J.-F. *Chem. Commun.* **2003**, 1336; (d) Grosshans, P.; Jouaiti, A.; Bulach, V.; Planeix, J.-M.; Hosseini, M. W.; Nicoud, J.-F. *CrystEngComm* **2003**, 5, 414; (e) Jouaiti, A.; Hosseini, M. W.; Kyritsakas, N. *Chem. Commun.* **2002**, 1898.
- (11) Bo, Q. B.; Wang, H. Y.; Wang, D. Q.; Zhang, Z. W.; Miao, J. L.; Sun, G. X. *Inorg. Chem.* **2011**, 50, 10163.
- (12) (a) Liu, F.; Zeng, Y.; Jiao, J.; Li, J.; Bu, X.; Ribas, J.; Batten, S. R. *Inorg. Chem.* **2006**, 45, 6129; (b) Beziau, A.; Baudron, S. A.; Pogozev, D.; Fluck, A.; Hosseini, M. W. *Chem. Commun.* **2012**, 48, 10313; (c) Yan, C.; Li, K.; Wei, S.; Wang, H.; Fu, L.; Pan, M.; Su, C. *J. Mater. Chem.* **2012**, 22, 9846; (d) Sun, Y.; Yan, X.; Ding, F.; Gao, E.; Zhang, W.; Verpoort, F. *Inorg. Chem. Commun.* **2008**, 11, 1117.
- (13) (a) Falkowski, J. M.; Sawano, T.; Zhang, T.; Tsun, G.; Chen, Y.; Lockard, J. V.; Lin, W. *J. Am. Chem. Soc.* **2014**, 136, 5213; (b) Jouaiti, A.; Hosseini, M. W.; Kyritsakas, N.; Grosshans, P.; Planeix, J. M. *Chem. Commun.* **2006**, 3078.
- (14) Shultz, A. M.; Sarjeant, A. A.; Farha, O. K.; Hupp, J. T.; Nguyen, S. T. *J. Am. Chem. Soc.* **2011**, 133, 13252.
- (15) Werner, A. *Ber. Dtsch. Chem. Ges.* **1911**, 44, 1887.
- (16) (a) Auffrant, A.; Barbieri, A.; Barigelletti, F.; Lacour, J.; Mobian, P.; Collin, J. P.; Sauvage, J. P.; Ventura, B. *Inorg. Chem.* **2007**, 46, 6911; (b) Wenzel, M.; Meggers, E. *Eur. J. Inorg. Chem.* **2012**, 2012, 3168.
- (17) Hamann, C.; Von Zelewsky, A.; Neels, A.; Stoeckli-Evans, H. *Dalton Trans.* **2004**, 402.
- (18) Chepelin, O.; Ujma, J.; Wu, X.; Slawin, A. M.; Pitak, M. B.; Coles, S. J.; Michel, J.; Jones, A. C.; Barran, P. E.; Lusby, P. J. *J. Am. Chem. Soc.* **2012**, 134, 19334.
- (19) Huo, H.; Fu, C.; Harms, K.; Meggers, E. *J. Am. Chem. Soc.* **2014**, 136, 2990.
- (20) (a) Le Bozec, H.; Guerchais, V. *C.R. Chim.* **2013**, 16, 1172; (b) You, Y.; Nam, W. *Chem. Soc. Rev.* **2012**, 41, 7061; (c) Liang, A.; Ying, L.; Huang, F. *J. Inorg. Organomet. Polym. Mater.* **2014**, 24, 905; (d) Tinker, L. L.; McDaniel, N. D.; Cline, E. D.; Bernhard, S. *Inorg. Synth.* **2010**, 35, 168.
- (21) (a) Xie, Z.; Ma, L.; deKrafft, K. E.; Jin, A.; Lin, W. *J. Am. Chem. Soc.* **2010**, 132, 922; (b) Ho, M.-L.; Lin, M.-H.; Chen, Y.-T.; Sheu, H.-S. *Chem. Phys. Lett.* **2011**, 509, 162; (c) Li, L.; Zhang, S.; Xu, L.; Han, L.; Chen, Z.-N.; Luo, J. *Inorg. Chem.* **2013**, 52, 12323.
- (22) Damas, A.; Moussa, J.; Rager, M. N.; Amouri, H. *Chirality* **2010**, 22, 889.
- (23) (a) Ma, D. L.; He, H. Z.; Chan, D. S.; Wong, C. Y.; Leung, C. H. *PLoS One* **2014**, 9, e99930; (b) Lu, F.; Yamamura, M.; Nabeshima, T. *Tetrahedron Lett.* **2013**, 54, 779.
- (24) (a) Steunenberg, P.; Ruggi, A.; van den Berg, N. S.; Buckle, T.; Kuil, J.; van Leeuwen, F. W.; Velders, A. H. *Inorg. Chem.* **2012**, 51, 2105; (b) Kim, J.; Shin, I.; Kim, H.; Lee, J. *J. Am. Chem. Soc.* **2005**, 127, 1614.
- (25) (a) Tamayo, A. B.; Alleyne, B. D.; Djurovich, P. I.; Lamansky, S.; Tsyba, I.; Ho, N. N.; Bau, R.; Thompson, M. E. *J. Am. Chem. Soc.* **2003**, 125, 7377; (b) Schulz, G. L.; Chen, X.; Chen, S.; Holdcroft, S. *Macromolecules* **2006**, 39, 9157.

Chapter I: General Introduction

Nature is a great artist who makes masterpieces by bottom up strategy. Starting from atoms and molecules, Nature is able to fabricate a large variety of breathtaking functional architectures surrounding us, from inorganic entities such as snowflakes with different size and shape and a variety of quartz minerals for example, to organic materials such as DNA or seashells with different colors and embossed patterns (Figure I-1).

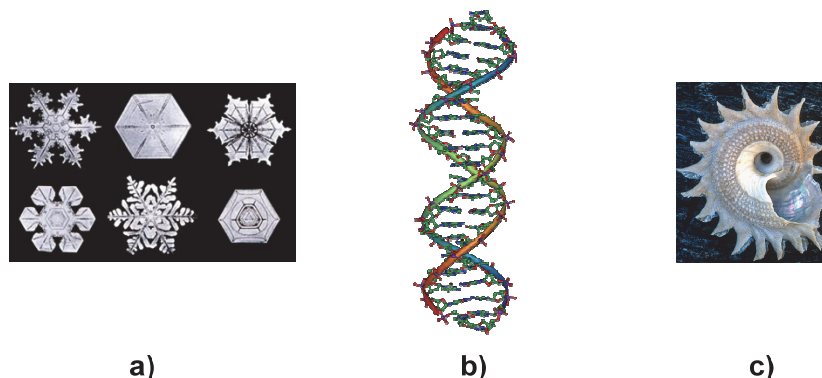


Figure I-1: Pictures of snowflakes (a)¹, the double helical DNA molecule (b)² and seashell (c)³.

Humans have been inspired by nature since the very first moments of evolution. As Leonardo da Vinci wrote: “When nature finishes to produce its own species, man begins using natural things in harmony with this very nature to create an infinity of species.” However, in order to mimic Nature, a one needs to learn about mechanisms and processes employed by Nature. Self-assembly of molecules is commonly encountered in nature based on combinations of different types of forces and interactions. As we shall see, besides covalent bonds, weak and non-covalent interactions play a significant role both in biological or inorganic structure formation. In the last decades, a new interdisciplinary science, covering chemistry, physics and biology, has emerged. This new branch of science is called “supramolecular chemistry”.

1. Supramolecular Chemistry

In 1978, Jean-Marie Lehn⁴ introduced a new concept in chemistry, which he defined as “chemistry beyond the molecule” in order to study organized entities of higher complexity that results from the association of two or more chemical species held together by intermolecular forces.^{4d} Thus, while only covalent bonds are considered in “classical” chemistry, supramolecular chemistry covers non-covalent interactions between molecules. These reversible interactions may be of different natures such as van der Waals forces, hydrogen bonds, coordination bonds, electrostatic or π - π interactions, *etc.* They are characterized by the direction of the interaction and its strength (*i.e.* its

energy). Taking into account the different recognition events between molecules governed by these weak intermolecular interactions, it is now possible to understand some of physical, biological and/or chemical properties of natural systems such as the supramolecular structure of DNA or abiotic systems. Supramolecular chemistry⁵ has now grown into a mature field and many synthetic supramolecular systems have been obtained by molecular self-assembly and recognition ranging from mechanically interlocked molecular architectures such as catenanes, rotaxanes or molecular knots, to systems that are designed to mimic biological systems.^{5b}

Mimicking biological systems remains however a challenge owing to their complexity and dynamic control of processes engaged in the functioning of biological systems. Dealing with self-assembly processes based on equilibrium between the different molecular components, the enthalpy-entropy compensation theory operates. The construction processes must lead to a lower Gibbs free energy, *i.e.* the assembled molecules must be thermodynamically more stable than the individual molecules.⁶ The programming of molecular recognition processes, in principle, should depend on the inherent properties of the molecules themselves. However, some of the weak interactions may also lead to the formation of unpredicted self-assembled architectures.

In order to impose the structure of final supramolecular architectures formed by molecular self-assembly processes, chemists design tectons or building blocks capable of generating molecular networks, periodic assemblies, in the crystalline phase with defined connectivity displaying specific functional features.

2. Molecular Tectonics

Molecular tectonics is a sub-branch of supramolecular chemistry. The term “molecular tectonics” was first introduced by Stephan Mann in 1993.⁷ The word “tecton” originates from Greek “TEKTON”, which means “builder”, and is the root for many words such as architect.^{7b} Chemists use tectons capable of interacting specifically with their neighbors. Indeed, molecular tectons, in order to lead to periodic architectures, must possess at least two complementary interaction sites organized in a divergent fashion. The localization and the number of the recognition sites determine not only the strength and directionality of interactions, but also the geometry of the selfassembled architectures.⁸ Recognition events,⁹ that is selective association between two complementary interactions sites of tectons, rely on different types of interactions such as H-bonding, electrostatic interactions, coordination bonding etc. detailed in the following sections. The repetition of recognition events leads to the formation of periodic architectures (networks). The number of iteration and translational orientation define the dimension (1D, 2D, 3D) of the networks in the crystalline phase. Thus, the energy and directionality of the supramolecular interactions as well as the geometry of molecular tectons are key parameters for the formation of molecular networks displaying 1D, 2D or 3D dimensionality.

2.1 Types of intermolecular interactions and their energy

Reversible interactions may be divided into six main categories: van der Waals interactions, hydrogen bonding, π - π interactions, electrostatic interactions, coordination bonds and halogen bonds (Figure I-2). All these reversible interactions may be used in molecular tectonics. Depending on the dominant interaction, the molecular networks will be named as, for example, H-bonded network or coordination network. The energy range for the above mentioned interactions is schematically represented in Figure I-2. We shall now give a short description of the characteristics of some of these intermolecular interactions.

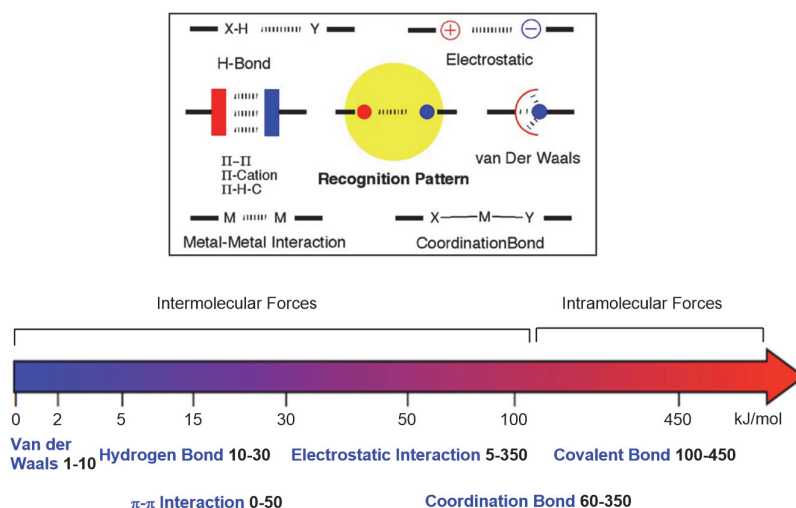


Figure I-2: Schematic representation of reversible intermolecular and intramolecular forces and their energy.^{9b}

The weakest interactions are van de Waals contacts with (energy in the 1 to 10 kJ/mol range). Although present in every molecular architecture, this type of interaction is the most difficult to be mastered.

The energy of π - π interactions¹⁰ ranges from 0 to 50 kJ/mol. It may play a significant role not only in molecular recognition¹¹ but also in the packing of solid state supramolecular architectures. For instance, a variety of molecular receptors based on rigid cyclic conjugated organic units have been designed for the formation of inclusion compounds. As illustrated in Figure I-3a, Kawase and coworkers reported the association of cyclic [n]paraphenyl acetylene moieties with C₆₀-fullerene derivatives in 1996.¹² Strong attractive interactions between the convex guest molecule and the concave receptors surfaces of the curved π - π conjugated systems were observed. π - π interactions may also be secondary interactions responsible for the crystal packing of molecular coordination networks.¹³ An example of 2-D coordination network based on 4-cyanobenzoic acid derivative and Ag⁺ cations was published by Guo's group (Figure I-3b).¹⁴ Coordination of the Ag⁺ cation either

through the CN coordinating site or by the carboxylate unit leads to a 2D-grid like network. The crystal packing is however mainly related to π - π stacking between phenyl rings of the organic linkers.

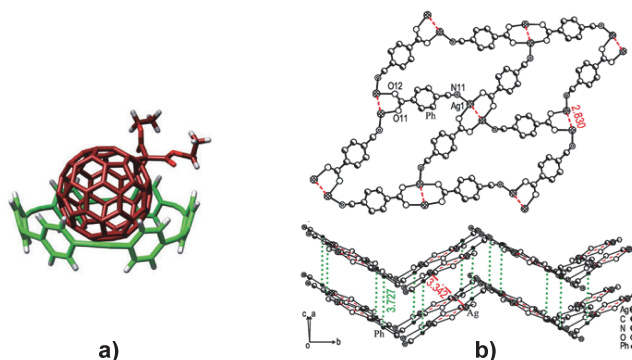


Figure I-3: a) X-Ray crystal structure of an inclusion complex resulting from the recognition of a C₆₀ derivative (red) by a rigid carbon nanoring (green)¹² and b) X-Ray crystal structure of a 2D-coordination network obtained upon combining p-cyanobenzoic acid with Ag⁺ ions (top) and crystal packing resulting from π - π interactions (bottom).¹⁴

The energy associated with hydrogen bonding ranges from 10 (weak) to 30 (strong) kJ/mol.¹⁵ A large variety of molecular architectures based on hydrogen bonding and/or charge-assisted hydrogen bonding has been reported.¹⁶ The hexagonal-type molecular network¹⁷ depicted in Figure I-4a is an example of a supramolecular architecture based on H-bonding between 1,3,5-cyclohexanetricarboxylic acid acting as hydrogen donor and 4,4'-bipyridine as hydrogen acceptor. In 2000,^{16b} our group reported the combination of 2,2'-bis-2-imidazolinium derivative **1** as hydrogen donor with ferrocenyldicarboxylate **2** acting as hydrogen acceptor. This combination leads to the formation of a 2D molecular network (Figure I-4b). The combination of H-bonding in dihapto mode with electrostatic charge-charge interactions imposes the connectivity mode and enhances the robustness of the network.

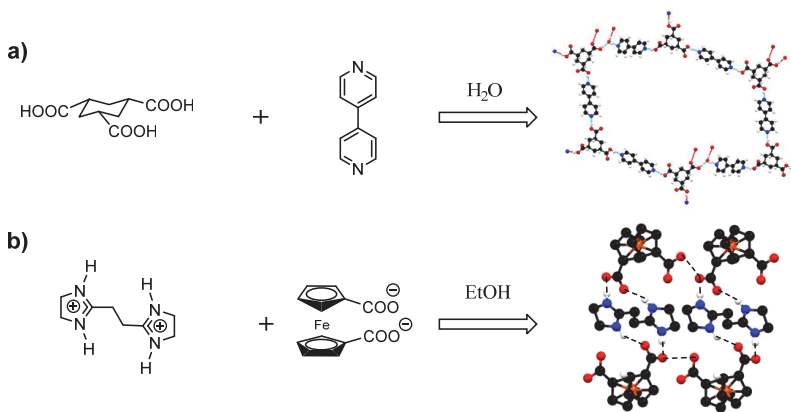


Figure I-4: Examples of molecular networks formed through a) hydrogen bonding¹⁷ or b) charge-assisted hydrogen bonding.^{16b}

Finally, coordination bonds with energy ranging from medium to strong (60-350 kJ/mol) have been extensively used recently¹⁸ to build supramolecular architectures of the metal organic type. The research project carried out in the context of this PhD is mainly centered on the design and formation of molecular networks employing coordination bonds as the dominant interaction. This type of networks is thus named coordination networks. Different examples of coordination molecular architectures resulting from interactions of organic coordinating tectons with metal centers is discussed below.

It should be noted that coordination networks (CNs) are also known as coordination polymer (CPs). Indeed, such infinite architectures are periodic molecular networks composed of metal centers or metal complexes bridged by organic linkers (tectons) through coordination bonds.¹⁹ For 2D and 3D porous crystals, the term Metal-Organic Frameworks (MOFs) or Porous Coordination Polymers (PCPs) is usually used in the literature.²⁰ The advantages of using coordination bond instead of weak hydrogen bond or van der Waals interactions for the generation of recognition patterns relies on two features. First, as mentioned above, the energy of a coordination bond is usually much higher than the one of a H bond, leading consequently to more stable and robust architectures. Secondly, metal centers may add other functionalities to the periodic architecture. Indeed, on one hand, the characteristics of the metal center governs the geometry and dimensionality of the network, and on the other hand, the metal center may offer interesting additional properties such as luminescence or magnetism etc.

In the following sections, the relationship between the topology (dimensionality) and geometry (size, shape...etc.) of networks and molecular features of tectons will be discussed. Some examples of 1D, 2D and 3D molecular networks, in particular, coordination networks reported in the literature are given below.

2.2 Geometry of the molecular tectons and molecular networks

Molecular receptors may be divided into two categories: *endo*-receptors and *exo*-receptors. *Endo*-receptors, based on convergent orientation of recognition sites, are designed to bind substrates and generate discrete complexes (Figure I-5). On the other hand, depending on the nature of substrates or connectors, *exo*-receptors, based on divergently oriented interactions sites may either form discrete complexes or infinite periodic molecular architectures (Figure I-6a). Thus, *endo*-receptors are commonly used in host-guest chemistry²¹ while *exo*-receptors are suitable for the generation of molecular networks (Figure I-6).

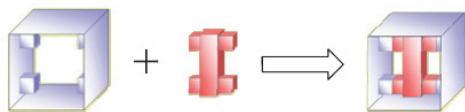


Figure I-5: Schematic representation of the formation of a discrete architecture with two endo-receptors.

The formation of either discrete or infinite molecular architectures using *exo*-receptors is determined by the localization, orientation and the number of interaction sites within the tecton backbone and the substrate or connecting moiety (Figure I-6).^{8a} If the number, localization and orientation of interaction sites on the substrate prevent iterative processes during the self-assembly discrete architectures are formed (Figure I-6a). On the contrary, infinite molecular architectures are obtained (see Figure I-6a, b and c for 1D, 2D or 3D architectures respectively).

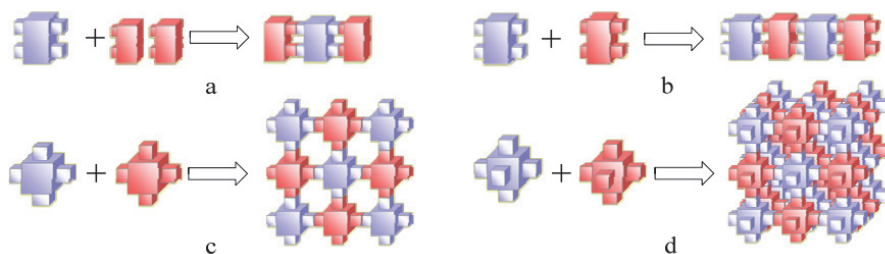


Figure I-6: Schematic representations of a discrete assemblies (a) or infinite molecular architectures (b,c,d) which may be formed upon combining *exo*-receptors with substrates or connectors.

Stang and coworkers described and classified possible discrete molecular architectures in a “molecular library” considering the number of interaction sites on the receptors and the angle between them.²² Thus, as illustrated in Figure I-7, ligands may be assembled into planar two dimensional systems such as triangles, squares or hexagons, as well as into non-planar three dimensional architectures such as polyhedrons and cubes.

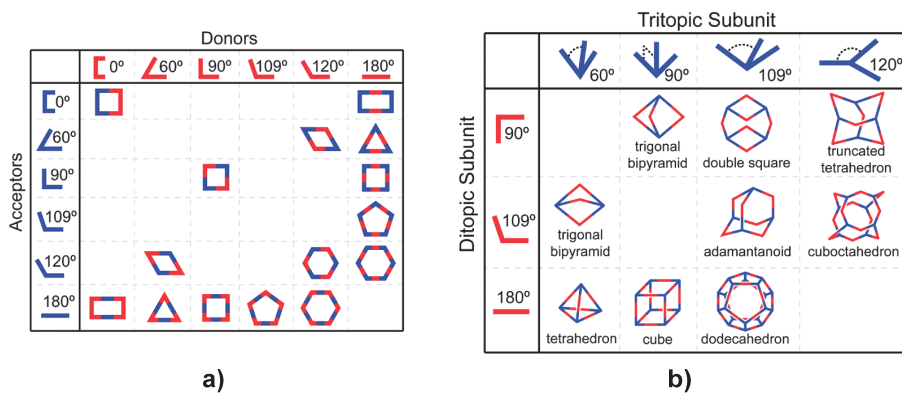


Figure I-7: “Molecular library” of discrete planar a) and non-planar b) molecular discrete architectures obtained using ditopic or tritopic subunits with predetermined angles.²²

For the formation of infinite molecular architectures, as mentioned above, according to the nature and geometry of molecular tectons, either 1D, 2D, or 3D molecular networks may be generated. Based on their dimensionality, different examples of coordination networks are discussed in the following sections.

2.2.1 One-dimensional molecular networks.

For the formation of 1D molecular networks, the repetition of recognition events, leading to assembling nodes, only take place along one direction (translational symmetry into one space direction).^{8a,b} As shown in Figure I-8, a one dimensional network may either be generated using a single component system based on a unique self-complementary tecton (a) or using a multicomponent system based on a combination of different complementary tectons (b). As illustrated in Figure I-8, only one type of assembling node is present when using a self-complementary tecton while one or two distinct assembling nodes may be present when using two different tectons possessing each two different interaction sites. Following this design principle, a wide variety of networks may be generated.

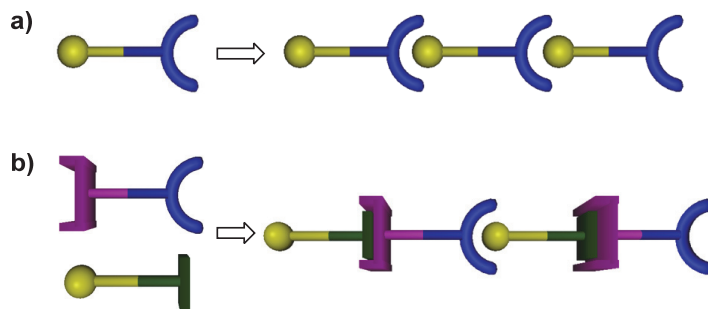


Figure I-8: Schematic representation of 1D molecular infinite architectures formed by self-complementary tecton (a) or by a combination of complementary tectons (b).

Different examples of 1D molecular networks of the cylinder, ladder, tube types have been reported.²³ They display different geometry ranging from linear,²⁴ zigzags,²⁵ to helical.²⁶

Here after is presented an example of 1D ladder type coordination network reported by our group. The flexible tecton **3** is based on an ethylene glycol fragment bearing at its extremities two benzonitrile groups as coordinating sites. The silver cation is coordinated to three nitrile groups belonging to three distinct tectons forming an infinite linear ladder chain.^{26b} (Figure I-9)

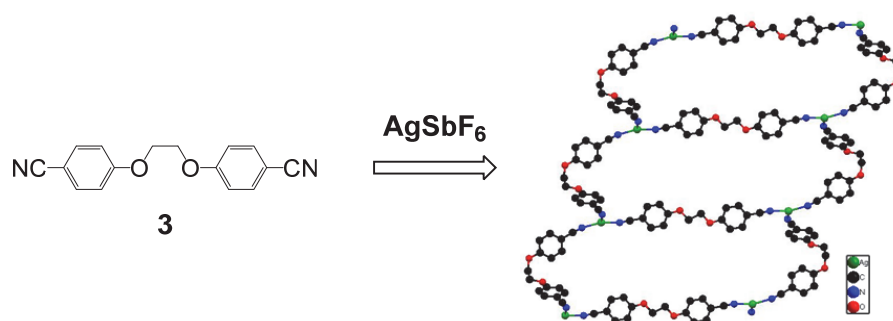


Figure I-9: Portion of the single crystal structure of a 1D ladder shaped coordination network formed upon combination of tecton 3 with AgSbF_6 .^{26b}

2.2.2 Two-dimensional molecular networks

Formation of 2D molecular networks requires the use of tectons bearing at least three divergently oriented recognition sites.^{8a,9b} Again, such architecture may either be generated by self-assembly of a unique self-complementary tecton or a combination of complementary tectons (Figure I-10a and b respectively). As illustrated in Figure I-10b, the use of a two-component system possessing two distinct complementary tectons may lead to the formation of two different assembling nodes (yellow-blue and green-violet nodes). Iteration of each of the nodes in two directions leads to formation of a 2D molecular network. The wide varieties of architectures that may be formed

换 d

□ 萑 撈 ㄣ 醴 怀 最 嶺

formation of non-desired architectures.

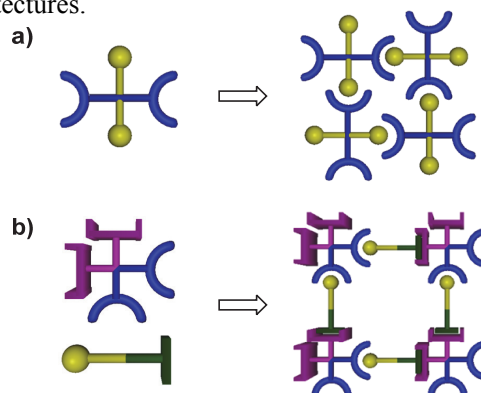


Figure I-10: Schematic representations of 2D molecular networks based on either one self-complementary tecton (a) or two distinct complementary tectons (b).

2D molecular networks may also exhibit planar, corrugated, slot or wavy geometries.²⁷ Dealing with grid-like arrangement, depending on the angle within the grid, this type of assembly may be divided into square, rhomboidal, rectangular or hexagonal types.

Two examples of 2D coordination networks are discussed below. A grid-type Cu(II)-Cd(II) heterometallic coordination network based on an imidazole-appended dipyrin ligand was synthesized

in our lab previously.²⁸ The molecular tecton **4** is a tetrahedral Cu(II) metal complex and is thus called a metallatecton. This metallatecton has two divergently oriented imidazole moieties that coordinate to Cd(II). The geometry around the Cd atom is octahedral with the square base of the octahedron occupied by four metallatectons and two chloride atoms in the apical positions. Thus, a grid-type 2D coordination network is generated. The distance between two consecutive Cd atoms is 26.35 Å (Figure I-11).

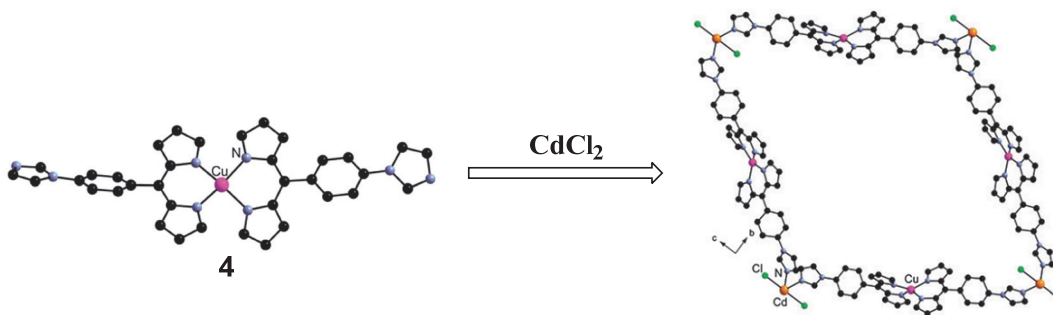


Figure I-11: Portion of the X-Ray structure of a 2D grid-type coordination networks combining a Cu(II) metallatecton with CdCl₂.²⁸

The other example is a rhomboidal distorted 2D coordination network based on tetrapyrrolyl substituted porphyrin **5** and Cu(hfacac)₂ (hfacac = 1,1,1,5,5,5-hexafluoroacetylacetonate).²⁹ In this case, the combination of the organic tecton **5** possessing four coordinating sites with Cu(hfacac)₂ (H₂O)₂ for which the two axial water molecules can be easily replaced by nitrogen donors belonging to the tecton **5** leads to the formation of 2D coordination network represented below (Figure I-12).

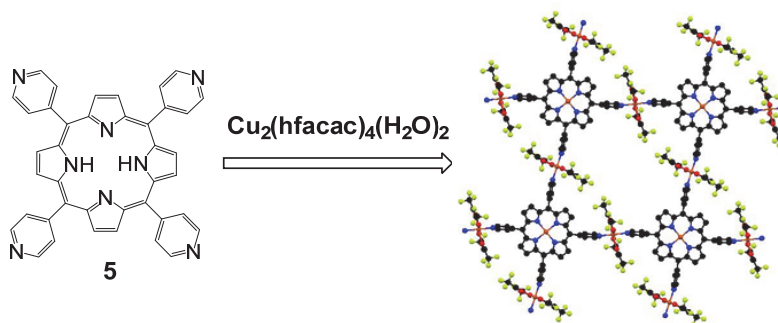


Figure I-12: 2D coordination networks formed combining the substituted porphyrin **5** with Cu(hfacac)₂(H₂O)₂.²⁹

2.2.3 Three dimensional molecular networks

For 3D molecular networks, the same or different assembling nodes must be translated in all three directions of space. The formation of 3D networks requires the specific design of tectons and the appropriate choice of the connecting metal.^{9b} Indeed, at least four non-planar divergently oriented

recognition sites are required to form a 3D molecular network. The recognition or interaction sites may be localized on the vertices of a tetrahedron, hexahedron, octahedron, *etc.* Here, only examples of tectons for which the recognition sites are occupying the vertices of an octahedron are discussed.

Again, as illustrated in Figure I-13, the 3D molecular networks may either be generated using a unique self-complementary tecton (a) or a multicomponent system with different complementary tectons (b).

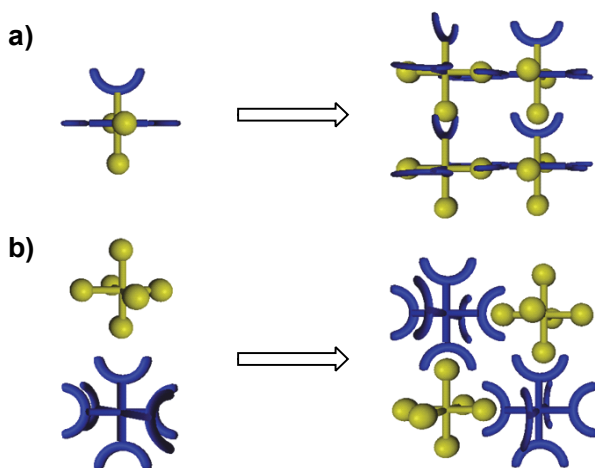


Figure I-13: Schematic representation of 3D molecular networks employing either one self-complementary tecton (a) or two distinct complementary tectons.

A library of 3D molecular networks has been developed in the past decades^{18a,30} displaying either tetrahedral, cuboid or octahedral shapes. Among them, **MOF-5**, obtained upon combining 1,4-benzenedicarboxylic acid with $\text{Zn}(\text{NO}_3)_2$ by Yaghi *et al.* is one of the most famous 3D MOFs which exhibits high porosity and stability (Figure I-14).³¹ In 2002, Yaghi and coworkers also expanded their work and demonstrated the synthesis of an isorecticular series of 3D MOFs based on octahedral Zn-O-C clusters and dicarboxylic acids as linkers. Increasing the length of the organic linker by using biphenyl, tetrahydropyrene, pyrene and terphenyl derivatives leads to the increase of pore sizes (Figure I-14).³²

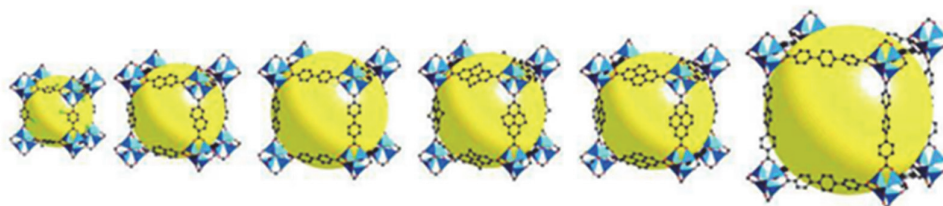


Figure I-14: 3D MOFs reported by Yaghi *et al.* using dicarboxylic acids and $\text{Zn}(\text{NO}_3)_2$ displaying different pore sizes.³²

Another approach has been developed recently to generate 3D coordination networks. In that case, dicarboxylic acid linkers are combined with pillars (e.g. 4,4'-bipyridine) to obtain robust and highly porous MOFs.³³ In our group, the formation of 3D cuboid coordination networks using this “pillar and linker” approach was achieved using a 4,4'-bipyridine moiety as linker with SiF_6^- anions acting as pillars able to form Zn-F coordination bonds.³⁴

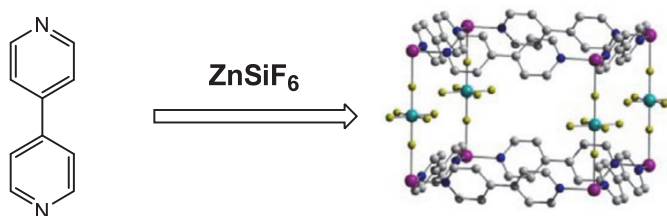


Figure I-15: A 3D cuboid coordination network resulting from the combination of 4,4'-bipyridine with ZnSiF_6 .³⁴

As presented and discussed above, a variety of coordination networks have been reported and their potential porosity for gas absorption and storage have been widely explored.^{32,35} Recently, multifunctionalized coordination networks, that is, combining their highly potential porosity with other properties such as chirality or luminescence has began to draw interests. Indeed, new perspectives in other attractive areas such as catalysis,³⁶ sensing³⁷ and enantioselective separation^{36d,38} may be expected.

We shall focus in the following sections on the formation of chiral and/or luminescent coordination networks and their applications in sensing, catalysis and separation.

3. Chiral or homochiral coordination polymers and their applications

In the past decade, interest in homochiral coordination networks has been growing because of their promising applications in heterogeneous asymmetric catalysis^{36b,39} or enantioselective separations.^{38,40} Indeed, crystals based on coordination networks offering potential large porosity have been reported. Some examples of heterogeneous catalysis within the pores of achiral coordination polymers have already been published.⁴¹ Owing to the possibility of recycling the catalyst due to its heterogeneous nature, asymmetric heterogeneous catalysis taking place within the chiral pores is of particular interest. Functionalized zeolites or other inorganic scaffolds have already been prepared and used as heterogeneous catalysts. However, homochiral coordination networks offer several unique advantages. One of them is their relative stability in different polar and non-polar solvents. Indeed, the majority of stable coordination networks are insoluble in usual solvents such as ethanol or halogenoalkanes enabling the catalytic reaction to take place in these solvents without degradation of the framework. Moreover, coordination polymers are highly organized architectures and their pore

size as well as their active sites distribution may be controlled through the design of tectons. Different methods for the preparation of chiral (or homochiral) coordination networks along with their potential catalytic properties are presented and discussed below.

Introduction of chirality into the pores or channels of a coordination networks may be achieved by two approaches. The first strategy is based on achiral organic tectons and metal centres or achiral metal complexes. In that case, the generation of chiral assemblies may be achieved by serendipity. For example, helical MOFs may be formed by combining achiral but flexible organic ligands with metal centers.⁴² The other strategy deals with the use of chiral tectons. The structure and topology of coordination networks generated using this strategy are more predictable and controllable.

3.1 Synthesis of homochiral coordination networks starting from achiral ligands

The best way to characterize those crystalline infinite architectures is to use X-Ray diffraction on single crystals which unravels the precise arrangements and positions of the atoms within the crystal. Moreover, the structural analysis also reveals whether the structure is chiral or not. Indeed, 230 different crystallographic space groups exist depending on the combination of all symmetry operations, such as reflection, rotation, improper rotation *etc.* Among these 230 types, 65 are orientation-preserving space groups and 11 out of 65 are intrinsically chiral.⁴³ Arrangement of the different atoms may result in a chiral space group and thus to a chiral material built without any chiral molecules, *i.e.* it is possible to obtain chiral coordination networks with achiral ligands.

Common literature examples include helical architectures formed with achiral and flexible ligands. A helix is defined as a smooth curve with clockwise (or anticlockwise) screw axis. A helix is intrinsically chiral since the left-handed helix (M) cannot be superimposed with the right-handed helix (P) with the two enantiomers being mirror images (Figure I-16).

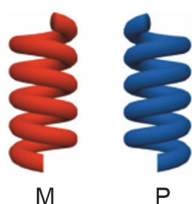


Figure I-16: Schematic representation of left-handed (M) and right-handed (P) helices.

Thus, a considerable amount of chiral helical coordination networks have been reported in literature.^{42,44} As an illustration, previous examples from our group are presented here (Figure I-17).^{42,44b,c} Formation of helical strands based on the combination of the *exo*-bischelate tecton **6** (Figure I-17) and silver cation was demonstrated.⁴² These macrocyclic tectons, because of the spacer groups connecting the two 2,2'-bipyridine units at positions 4 and 4', adopt a roof-type conformation. For that reason, when tectons **6** are interconnected by cations such as silver adopting the tetrahedral

coordination geometry, a single stranded helical network is formed (Figure I-17). Because of the achiral nature of the organic tecton, both *P* and *M* helices are present in the crystal affording thus a racemate.

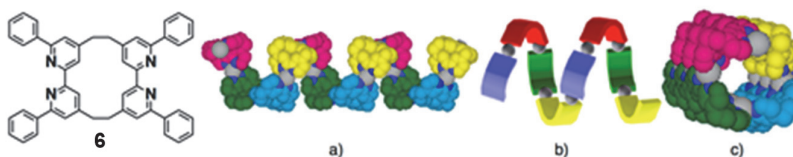


Figure I-17: Portions of the X-ray structure of the single-stranded helical coordination network formed upon combining silver cation with tecton **6** (a) and its schematic representation (b) and a lateral view (c). H atoms and phenyl groups are not represented for clarity.

Another example is based on the use of tecton **7** possessing two terminal coordinating pyridyl units connected by an oligoethyleneglycol spacer (Figure I-18). Combination of this bis-monodentate tecton **7** with Ag^+ salts led to the formation of crystalline double stranded interwoven infinite linear networks. The silver cation is coordinated to two pyridyl units belonging to two different tectons. The driving force for the formation of the helical architecture is related to the loop-type disposition (pseudo crown ether) of the oligoethyleneglycol unit leading to interactions between silver cations belonging to one strand and ether oxygen atoms of the other strand. Further studies showed that by increasing the length of the spacer or changing the orientation of the N atoms of the pyridyl rings, the pitch of the helical arrangement may be controlled. Again, the packing of *P* and *M* helices within the crystal (Figure I-18, b), the whole structure is achiral.

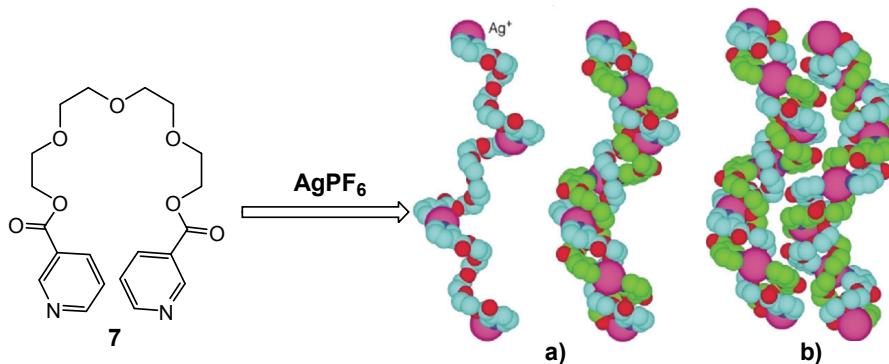


Figure I-18: Structure of tecton **7** and portions of the X-Ray structure of the double stranded helical coordination networks formed between silver cation and tecton **7** showing a) the *M* type single and double helices obtained upon coordination of Ag^+ cation and b) the packing of two double helices of opposite chirality.^{44b}

The formation of chiral coordination networks using achiral tectons may be achieved by adding a small amount of an enantiopure directing agent. The chiral auxiliaries may be a crystallization solvent, counter ions or chiral ligands. The enantiopure additives might either template the formation of the chiral structures or create an enantiomeric imbalance by promoting the crystallization of a given chiral form.⁴⁵ For instance, Bu *et al.* demonstrated that combining the achiral building block H₂thb (thiophene-2,5-dicarboxylic acid) with an In(III) salt in the presence of a small amount of either (-)-cinchonidine or (+)-cinchonidine, favors the formation of a chiral coordination network instead of the racemic ones.⁴⁶

3.2 Synthesis of homochiral coordination networks starting from chiral ligands

Compared to the former strategy, the use of chiral ligands for the formation of homochiral coordination networks proved to be more predictable and reproducible. At first, commercially available multitopic enantiopure ligands such as amino acids or hydroxyacids were used in order to introduce chirality within the framework. The porous homochiral materials obtained by this approach are designed for enantioselective separation or asymmetric catalysis. It appears that the use of amino acids and hydroxyacids as chiral building blocks suffer from two major drawbacks: 1) the high degree of flexibility of the tecton preventing the prediction of the final structure; 2) the rather restricted available space. Therefore it is important to design rigid homochiral tectons bearing appropriate coordinating sites to generate porous homochiral frameworks with the expected features.

In 2000, Kim *et al.* reported the first example of a homochiral coordination polymer showing enantioselective catalytic properties (Figure I-19). The chirality within this MOF named POST-1 originates from the chiral ligand **8** based on a tartaric acid scaffold. POST-1 was generated upon combining **8** with Zn(NO₃)₂. This chiral MOF exhibited asymmetric catalysis for transesterification reactions between 2,4-dinitrophenyl acetate with racemic 1-phenyl-2-propanol.^{36d}

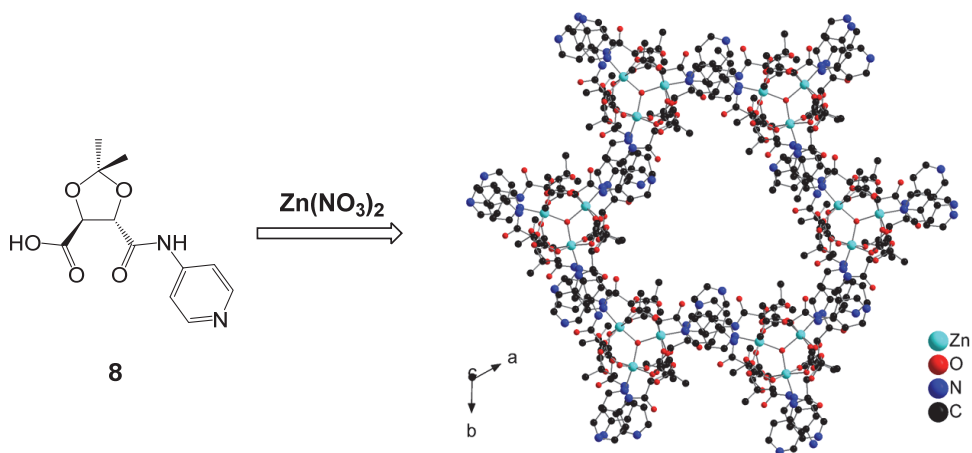


Figure I-19: Structure of tecton **8** and X-Ray structure of the homochiral MOF POST-1.^{36d}

Lin and co-workers have also reported the use of rigid chiral ligands based on BINOL derivatives. Such ligands possess two atropoisomers that cannot be interconverted because of the rather high conformational barrier between the two enantiomers. Moreover, BINOL is a well-known ligand in homogeneous catalysis and was thus foreseen as a potential useful linker in catalytically active MOFs. Combining ligand **9** with zinc cation afforded a 3D cubic homochiral coordination polymer.⁴⁷ (Figure I-20)

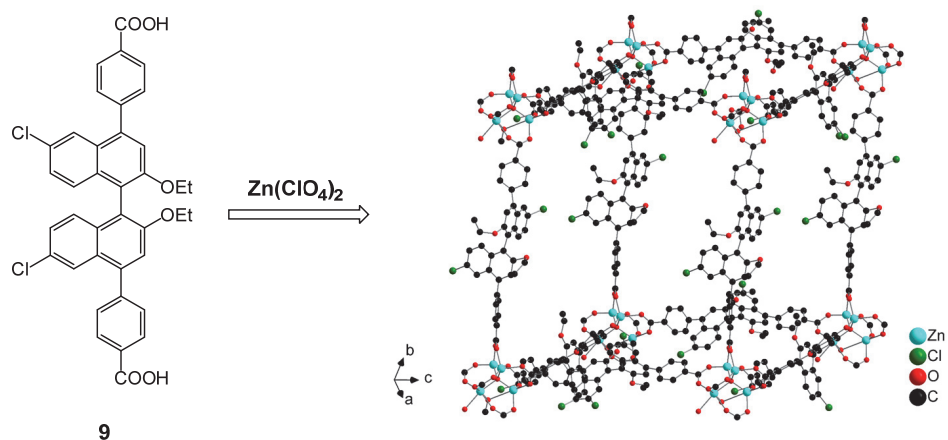


Figure I-20: Structure of tecton **9** and X-Ray structure of the 3D cubic homochiral MOF.

Several other chiral ligands based on stereogenic C atoms have been described since then.⁴⁸ And catalytically active homochiral MOFs have been reported as asymmetric heterogeneous catalyst for different reactions, such as cyanosilylation, asymmetric epoxidation and enantioselective ring-opening of epoxides.^{36b,49}

Furthermore, some heterometallic homochiral MOFs starting from chiral coordination complexes bearing peripheral coordinating sites have been described. Heterometallic MOFs (or Mixed Metal-Organic Frameworks, M'MOFs) consist in the self-assembly of a metallatecton or metalloligand, *i.e.* a coordination complex possessing peripheral coordination groups, acting as a linker and metal ions or clusters acting as metallic nodes.⁵⁰ For the chiral M'MOFs described, the chirality mainly originates from the organic parts such as BINOL,⁵¹ BINAP⁵² or chiral metallosalen^{36c,53} ligands and their applications in asymmetric catalysis were also reported (Figure I-21). These chiral ligands contain either a sp^3 carbon atom as stereogenic center (*e.g.* chiral salen ligands) or are based on two non-interconvertible atropoisomers (*e.g.* BINAP or BINOL ligands).

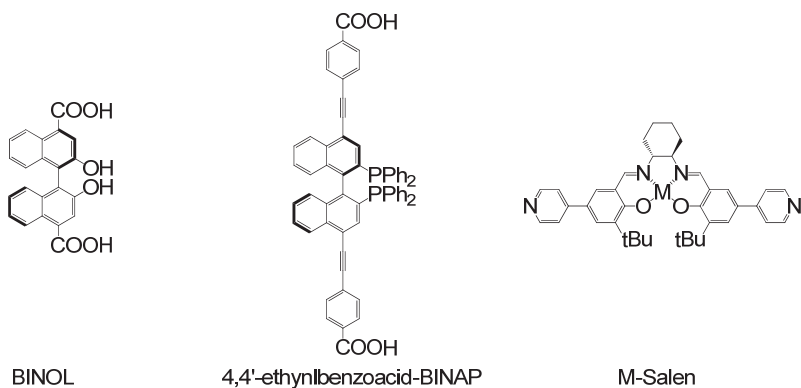


Figure I-21: Chemical structures of BINOL-, BINAP- and Mn-salen-based ligands used for the generation of homochiral heterometallic coordination networks.

Lin *et al.* also reported the preparation of a homochiral coordination network based on a chiral Mn-Salen ligand **10** functionalized with two carboxylate moieties as coordinating sites and zinc ions (CMOF-1) as metallic node. The presence of chiral cavities was proven by the X-Ray studies. CMOF-1 showed good asymmetric catalytic property in enantioselective epoxidation of alkenes (Figure I-22).^{36c}

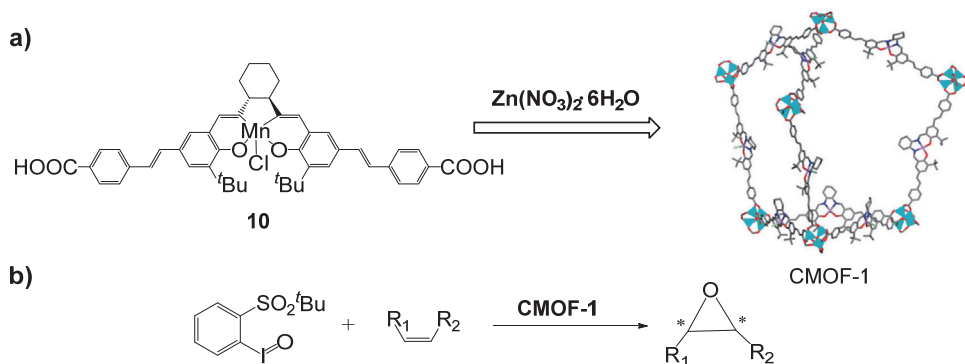


Figure I-22: a) Chemical structure of ligand **10** and the coordination polymer CMOF-1 obtained upon combining **10** with $\text{Zn}(\text{NO}_3)_2$ showing the presence of chiral cavities; b) an example of enantioselective epoxidation of alkene catalyzed by CMOF-1.^{36c}

As illustrated in Figure I-23,⁵³ Hupp and Nguyen *et al.* reported the synthesis of another Mn^{III} -salen-based MOF combining the Mn salen derivative **11** bearing two divergently oriented pyridyl coordinating units, a rigid pillar **12** based on four terminal carboxylic acid and zinc ion. A 3D cubic MOF was thus obtained (Figure I-23). Furthermore, by post-synthetic modification, they were able to exchange the Mn(III) ions with other metal ions such as Zn(II) or Ni(II). These porous MOFs were shown to be catalytically active.

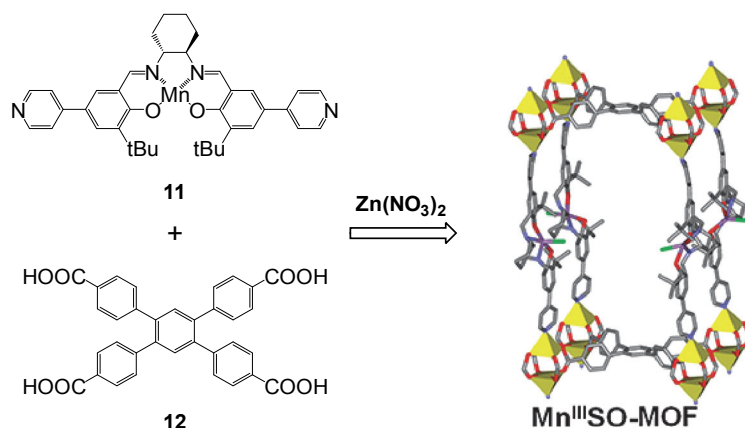


Figure I-23: Chemical structures of the two building blocks **11** and **12** combined with zinc nitrate to generate the 3D cubic MOF, $\text{Mn}^{\text{III}}\text{SO-MOF}$ represented in sticks.⁵³

In our laboratory, different chiral tectons containing asymmetric carbon atoms have been synthesized and homochiral H-bonded as well as coordination networks have been obtained subsequently.^{25a,54} The first type of tectons, based on the optically active *isomannide* backbone functionalized either with one or two pyridyl units using ester junctions, leads to the formation of helical networks (Figures I-24 and I-25). When only one pyridyl moiety (either 4- or 3-pyridyl for **13** and **14** respectively) is connected to the *isomannide* unit, the self-complementary tectons **13** and **14** are equipped with both H-bond donor (OH) and acceptor (pyridyl) sites (Figure I-24).^{54c}

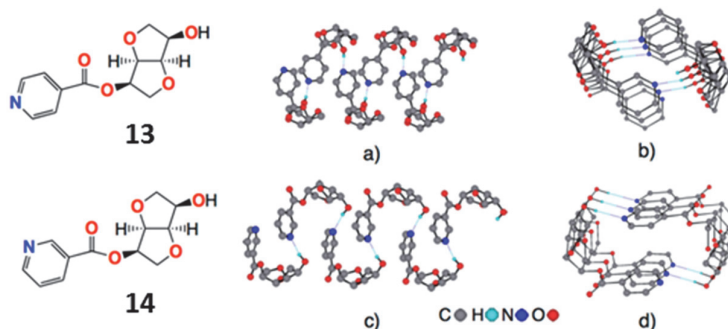


Figure I-24: Portions of the X-Ray structure of enantiomerically pure 1D helical H-bonded networks formed upon self-assembly of tectons **13** (a,b) or **14** (c,d).

Imposed by the stereochemistry of the *isomannide* unit, the pyridyl and the OH groups are divergently oriented towards the concave face of the bicyclic unit in both cases. Owing to their self-complementarity and enantiomerically pure nature, both tectons **13** or **14** lead to the formation of single-stranded H-bonded helical networks (Figure I-24 a,b and c,d for tectons **13** and **14** respectively). The mutual interconnection of consecutive tectons indeed takes place through H-bonding between the OH and pyridyl groups. For both helical networks, the *P* helicity is imposed by the predefined stereochemistry of *isomannide*.

The two enantiomerically pure tectons **15** and **16** are also based on the *isomannide* backbone but instead of only one pyridyl unit, two of them are connected to the *isomannide* moiety using ester junctions (Figure I-25a). The difference between tectons **15** and **16** is based on the orientation of the nitrogen atom of the pyridyl ring. The use of these two tectons leads to the generation of enantiopure helical coordination networks upon bridging of consecutive HgCl_2 by the N-based coordinating sites of the tecton.⁵⁵ Thus, combination of **15** with HgCl_2 leads to the formation of a single stranded helical coordination network with *P* helicity. The latter is imposed by the stereochemistry of *isomannide*. The infinite helical arrangement is obtained upon bridging of consecutive tectons **15** by mercury cations (Figure I-25b). It is interesting to note that the helical networks are packed in the *syn*-parallel fashion leading thus to a polar crystal (Figure I-25c). On the other hand, combining **16** with HgCl_2 leads again to the formation of an enantiomerically pure helical coordination network. Interestingly but unexpectedly, because of interactions between consecutive stands, a triple stranded helical network with *P* helicity is generated by bridging of consecutive tectons **16** by mercury cations (Figure I-25d). The triple stranded helices are again arranged in a parallel fashion.

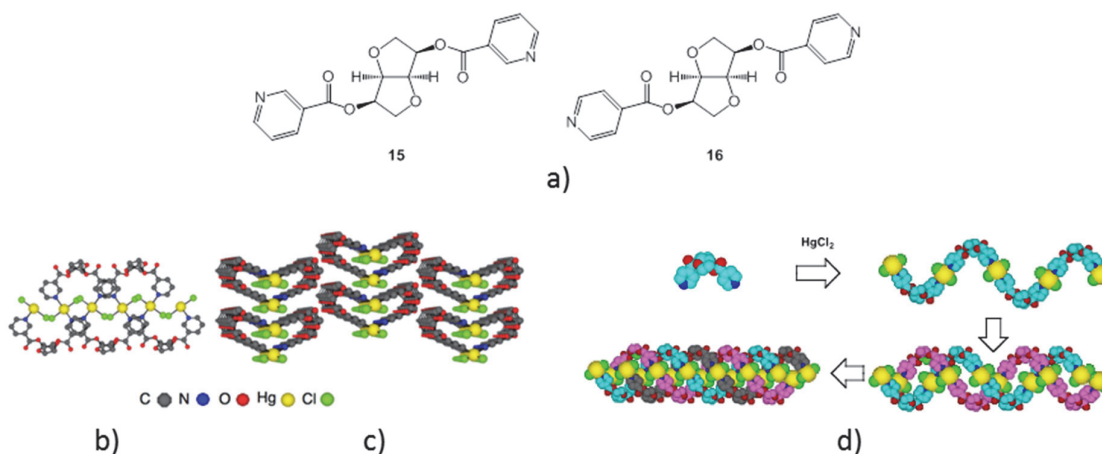


Figure I-25: a) Chemical structure of tectons **15** and **16**, b) portions of the crystal structure of the single-stranded helical coordination networks formed between HgCl_2 and tecton **15** and c) the *syn*-parallel packing of 1-D networks affording a polar crystal, d) generation of the triple-stranded helical coordination networks formed between HgCl_2 and tecton **16**.

In order to exploit directional physical properties, directional tectons based on dissymmetric organic tectons composed of a monodentate and a tridentate coordination poles such as **17** and **18** were designed (Figure I-26a). Combination of the latter with a transition metal complex such as CoCl_2 for which the metal adopts an octahedral coordination geometry and thus offers four coordination sites in square arrangement has been studied.⁵⁶ In both cases, bridging of the organic tectons and Co metallic nodes leads to neutral directional 1-D networks (Figure I-26d and e). The difference between the two networks is related to their packing. Indeed, for directional 1D networks, two packing

possibilities (*anti*-parallel (Figure I-26b) and *syn*-parallel (Figure I-26c)) may be envisaged. In the case of the achiral tecton **17**, as expected, the centric packing (Figure I-26d) with *anti*-parallel arrangement of the achiral 1D networks leading to an apolar crystal is observed. Because of the introduction of two optically active oxazoline moieties within the organic backbone of tecton **18**, a chiral and directional 1D coordination network is obtained (Figure I-26e). The directionality of the network is due to the acentric nature of the neutral c_2 -chiral organic tecton **18**. In marked contrast with the case mentioned above, here, a *syn*-parallel (Figure I-26c) arrangement of consecutive chiral 1D networks is observed. This packing mode leads to a polar solid.

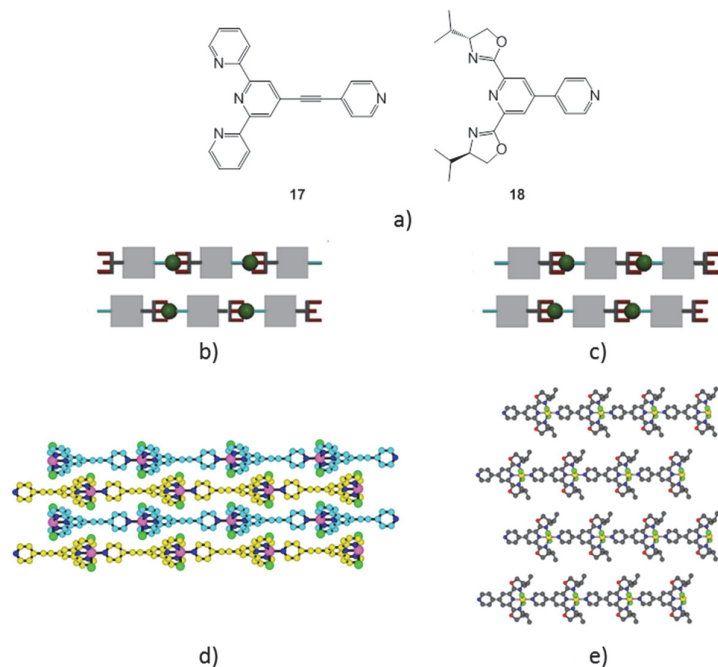


Figure I-26: Directional tectons **17** and **18** (a); schematic representation of *anti*-parallel (b) and *syn*-parallel (c) packing of two consecutive directional 1D networks. Portions of the X-ray structure of neutral network formed between CoCl_2 and tecton **17** (d) and **18** (e) showing the packing of consecutive directional 1D networks. In the case of tecton **17**, C atoms belonging to consecutive strands are differentiated by colour. H atoms are omitted for clarity

On the other hand, chiral porphyrins bearing pendant chiral alkyl chains and two divergently oriented pyridyl or ethynylpyridyl moieties were also used to generate chiral 1D and 2D zinc coordination networks.^{54b} Another recent example from our group was based on the use of the rigid enantiopure linear organic tecton **19** consisting in a diimide backbone derived from pyromellitic acid bearing two divergently oriented pyridyl coordinating units (Figure I-27). Combining ligand **19** with different metal salts such as HgCl_2 , $\text{Cu}(\text{hfac})_2$ or NiCl_2 afforded either 1D (zigzag or linear) or 2-D (grid type) homochiral coordination networks.

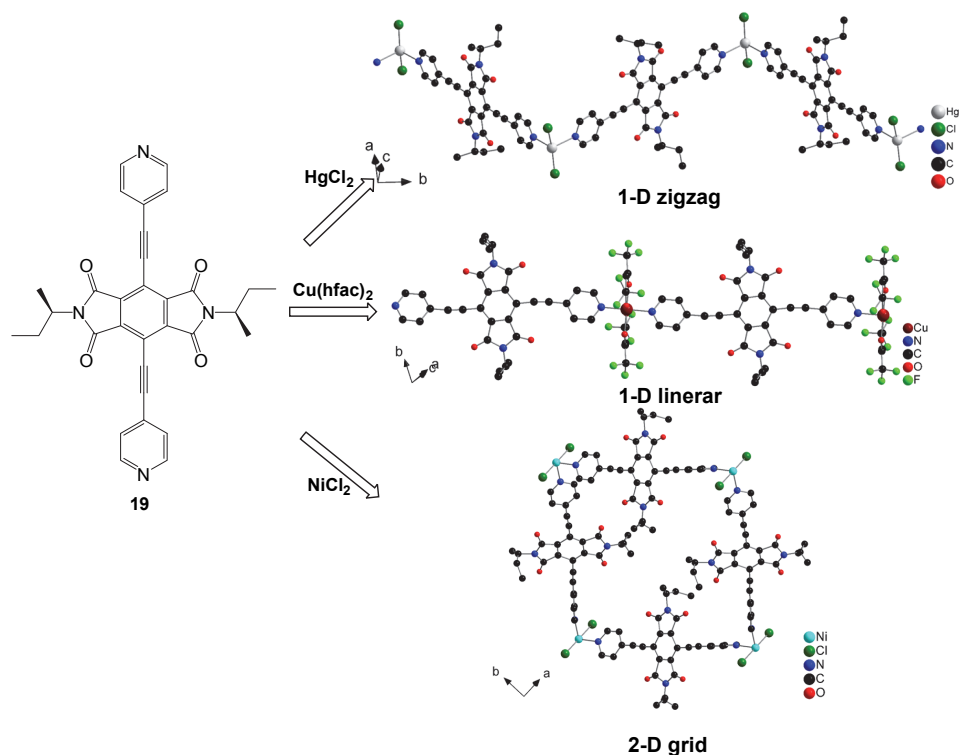


Figure I-27: Chemical structure of the enantiopure organic tecton **19** and portions of the X-ray crystal structures of 1D and 2D homochiral coordination networks formed by combining **19** with different metal salts.^{54d}

3.3 Synthesis of homochiral coordination networks by post-synthetic transformations

Another method to introduce chirality within a coordination network is based on post-synthetic modification. The term “postsynthetic modification” was first coined by Wand and Cohen in 2007 to describe the reaction of IRMOF-3 with acetic anhydride derivatives.^{50c,57} IRMOF-3 is a 3D cubic coordination network formed upon combining 2-amino-1,4-benzenedicarboxylate (**20**) with Zn(II) ions (Figure I-28a). The achiral coordination polymer thus obtained possesses free NH₂ sites that can react with different reagents through conventional covalent synthesis. In their first report, they used acetic anhydride generating an achiral MOF showing the efficiency of the approach.⁵⁷ Soon after, chiral reagents such as chiral acetic anhydride were utilized (Figure I-28b).^{50c} Apart from the free –NH₂ groups, other reactive groups such as aldehyde, azido as well as open coordinating sites for metal binding were introduced.⁵⁸

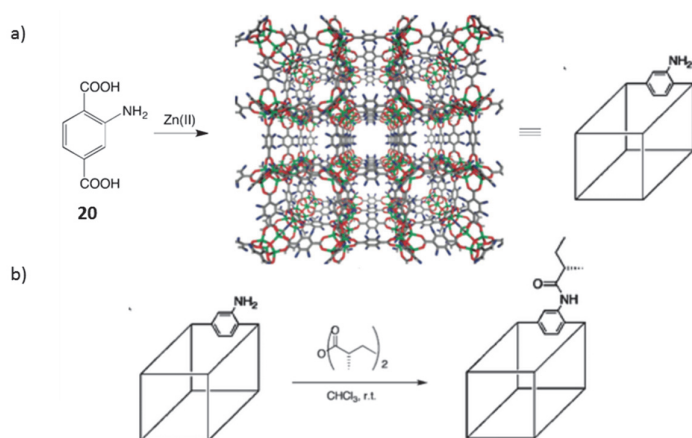


Figure I-28: a) Portions of the X-Ray structure of IRMOF-3 and schematic representation and b) an example to introduce chirality in IRMOF-3 by post-synthesis.^{50c}

It needs to be pointed out that this approach has some obvious drawbacks since narrow channels within the framework will prevent the postsynthetic reagent to enter. Thus, in some cases, only the surface of the crystals is modified.^{50c,59}

4. Luminescent Coordination Polymers and their applications

As mentioned above, coordination networks displaying luminescence are of interest. Because of the hybrid nature of MOFs, combining both an organic ligand and a metal ion (or clusters) within the framework, different modes of luminescence such as linker-based fluorescence or metal-based phosphorescence may be exploited.^{18a} Furthermore, luminescent MOFs are of particular interest for their applications in chemical sensing or explosive detection for example.^{37,60} Other appealing applications are mimicry of photosynthesis⁶¹ and photocatalysis.^{36a,62}

Thus, in the beginning of 2000, few examples of luminescent coordination polymers started to appear in the literature. In 2002, Wagner, Zaworotko *et al.* reported the synthesis of a 1D fluorescent coordination network mixing 4,4'-bipyridine and pyrene with Zn(NO₃)₂.⁶³ The Zn T-shaped nodes are coordinated to three bipyridine and two nitrate ions leading to a ladder-type coordination polymer (Figure I-29). The pyrene molecules are intercalated within the framework in a cofacial arrangement with the 4,4'-bipyridine allowing the formation of a 2:1 exciplex. The emission of both the monomer and the exciplex was observed and used to probe the local environment of the cavities within the framework.

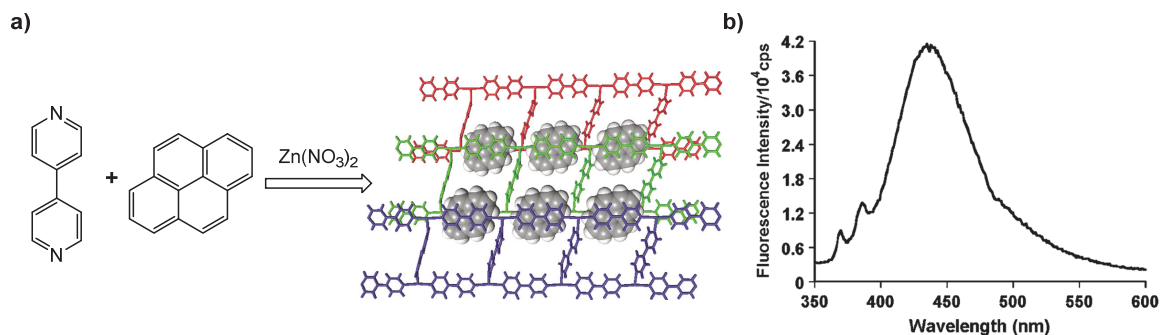


Figure I-29: a) Formation of the ladder coordination polymer upon reaction of 4,4'-bipyridine with Zn ion with pyrene molecules intercalated in the infinite architecture; b) emission spectra of the coordination polymer showing the monomer and exciplex emission⁶³

Since the first investigations of luminescent properties of MOFs at the beginning of 21st century, a large number of articles have been published including different reviews.^{18a,37,64} However, most of the luminescent coordination networks reported are homometallic based on either conjugated organic linkers and/or lanthanide ions which induce mainly ligand-centered or lanthanide-centered emission.⁶⁵

The example presented here is about a Cd(II) dipyrin-based MOFs that was reported by our group. Thus, a series of novel Cd(II) complexes based on α,β -unsubstituted dipyrin ligands (dpm) has been prepared and characterized (Figure I-30).⁶⁶

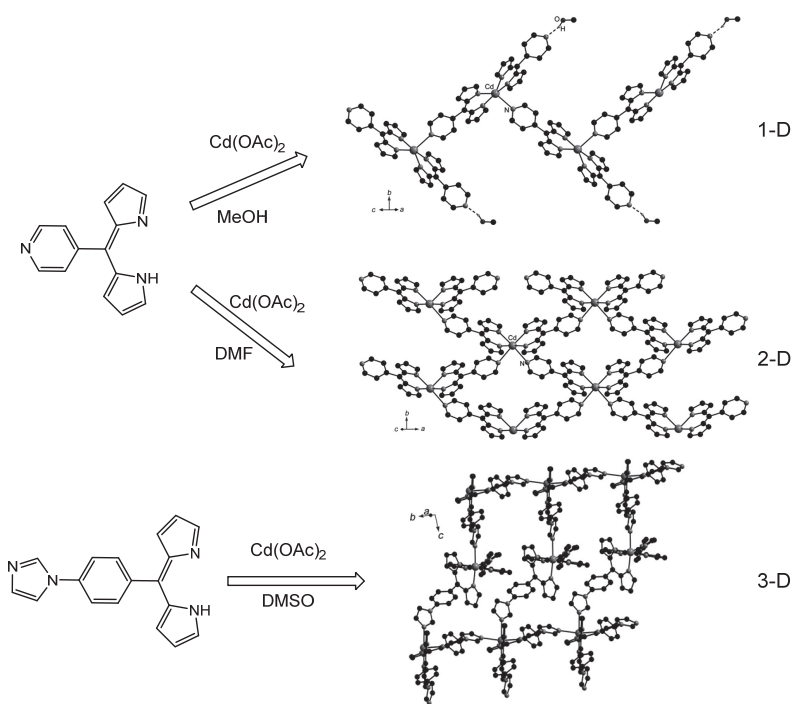


Figure I-30: Portions of the crystal structure of the luminescent 3D coordination polymer based on the self-assembled Cd(II) imidazole-based dipyrin complex.⁶⁶

These compounds are of the $[\text{Cd}(\text{dpm})_2]$ type, with the coordination sphere of the metal center occupied by two dpm chelates. Since the Cd(II) node is only four coordinated, it accepts two additional ligands. Furthermore, the dpm chelate possesses a secondary coordinating pole, *i.e.* pyridyl or imidazolyl units, that can coordinate to the Cd atom. Thus, by self-assembly, 1D, 2D and 3D coordination polymers were formed. These coordination polymers are orange to red emitting displaying emission bands around 550 nm to 650 nm attributed to ligand centered transitions.

The purpose of this PhD thesis was the formation of heterometallic luminescent coordination networks. For that reason, we shall mainly focus on some relevant examples of heterometallic networks. Heterometallic MOFs (HMOFs), generated through self-assembly of metal center with metallatectons, exhibiting good luminescence properties are currently attracting a great deal of interests.⁶⁷ In the same way as for homometallic MOFs, the luminescent heterometallic MOFs reported are mainly based on lanthanide nodes and lanthanide-based emission.⁶⁸ As an example, Jin *et al.*⁶⁹ reported a series of NIR-emitting (Ln,Ag) HMOFs. However, some examples based on Zn(II) porphyrins,⁷⁰ dipyrins⁶⁶ and polypyridine complexes⁷¹ as metallatectons exhibiting interesting luminescence properties have also been reported. Fewer examples based on metalloligands such as Ru(II), Ir(III), Os(III), Pt(II) have been reported.⁷² The use of transition metal complexes offers two unique features over purely organic linker as i) light absorption over the entire visible spectrum and ii) metal complexes (*e.g.* Ir, Ru, Os, Pt) may be phosphorescent exhibiting Metal-to-Ligand-Charge Transfer (MLCT) excited states and enabling thus harvesting of triplet excitons.

Since 2010, Lin *et al.* have reported a series of luminescent HMOFs based on Ru(II), Os(III) and Ir(III) complexes that exhibit in particular oxygen sensing properties. Some examples among them are discussed below. As illustrated in Figure I-31a, in 2011, Lin *et al.* reported on a luminescent MOF based on an heteroleptic Ru(II) complex Ru-1, H_2bpdc (H_2bpdc = [1,1'-biphenyl]-4,4'-dicarboxylic acid) and $\text{Zn}(\text{NO}_3)_2$.⁷³ A 3D two fold interpenetrated coordination polymers exhibiting large open channels filled with solvent molecules was obtained with a 1/4 Ru-1/bpdc ratio. The study of this photoactive MOF revealed an interesting diffusion-controlled quenching phenomenon. Indeed, diffusion in solution of amine quenchers into the MOF channels leads to a gradual quenching of the emission originating from the Ru-X bridging ligand *via* a redox quenching mechanism (Figure I-31b).

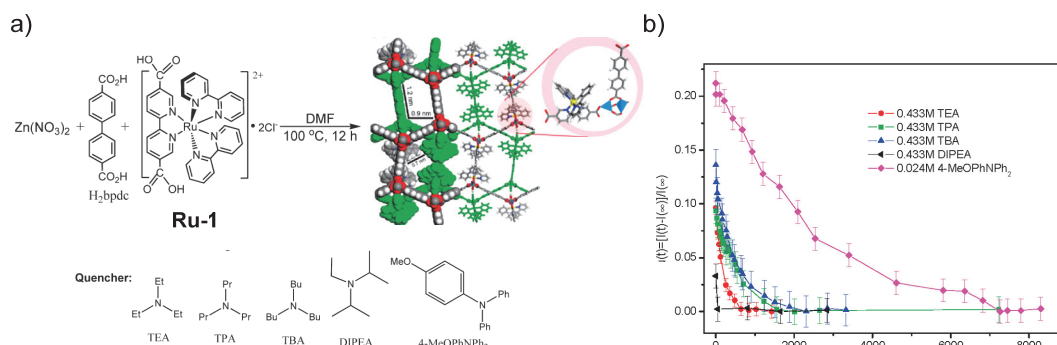


Figure I-31: a) Synthesis of the Ru-based Phosphorescent MOF and chemical structures of the amine quenchers investigated; b) Plots of the normalized time-dependent intensity $u(t) = [I(t) - I(\infty)] / I(\infty)$ vs t for different amine quenchers with $I(t)$ the time-dependent intensity and $I(\infty)$ the equilibrium intensity after a long time.⁷³

Another example selected from the publications of *Lin et al.* deals with the use of tris-cyclometalated Ir(III) complexes bearing 2-phenylpyridine units functionalized with carboxylic acids on the phenyl rings (Figure I-32). As will be discussed in Chapter III, highly porous and phosphorescent coordination polymers were obtained upon combining these Ir-based metallatectons with Zn ions displaying good oxygen sensitivity.⁷²

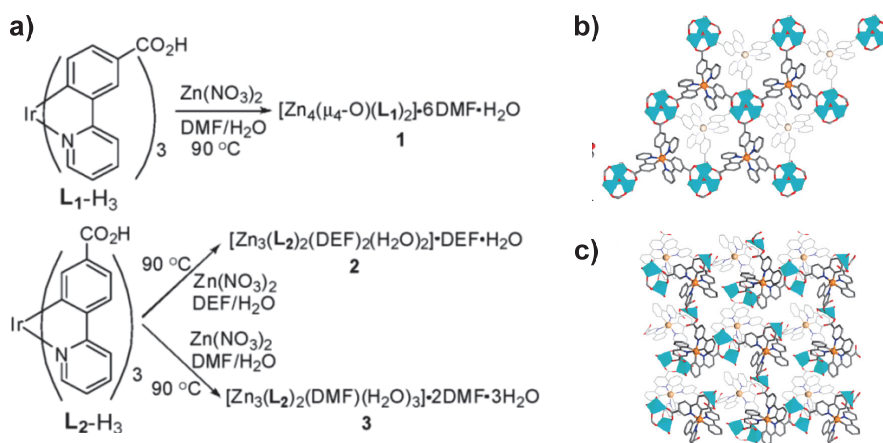


Figure I-32: Synthesis routes to obtain the Ir-based coordination polymers (a), and a top view of the 2D bilayer structures of 1(b) et 2(c).⁷²

From the different examples of either chiral or luminescent coordination polymers discussed above, it appears that luminescent and chiral properties within MOF architectures have lately become a flowering and rapidly expanding research area. The aim of this PhD project is to combine these two attractive features, luminescence and chirality, into a single heterometallic coordination network using an enantiopure luminescent metallatecton. In particular, chiral Iridium(III) complexes, displaying appealing luminescent properties, were synthesized in order to generate homochiral and luminescent coordination polymers.

Chirality in metal complexes adopting an octahedral geometry may originate from the use of chiral ligands possessing asymmetric carbon atoms or from the arrangement of ligands around the metal center itself (Λ or Δ configuration). In the section below, the origin of chirality in tris-chelate octahedral metal complexes, in particular Iridium(III) complexes, is discussed and methods for either resolution of complexes present as racemate or for their asymmetric synthesis are presented. A brief theoretical background on the photophysical properties of Iridium(III) complexes is also given.

5. Chirality in metal complexes

5.1 Origin of chirality in metal complexes

An object or a system is defined as chiral when it is distinguishable from its mirror image. Considering the symmetry elements, chiral objects cannot contain a center of inversion (i) or a plane mirror (σ). In nature, chiral objects as small as a single molecule, such as natural amino acids in proteins or as large as the horns of goats or the shells of sea snails can be easily found.

In chemistry, the concept of chirality is commonly associated with chiral organic molecules and the presence of asymmetric carbon atoms, that is a carbon atom connected to four different groups. The two resulting enantiomers are usually named S and R as stereochemical descriptors. However, arrangement of ligands around a metal center may also result in chiral inorganic or coordination compounds that are stereogenic at the metal.⁷⁴

In the 1910s, Alfred Werner was the first to evidence that chirality may not only be centered on C atoms but also on metal centers. In particular, he stated that octahedral tris-chelate metal complexes are inherently chiral. Notably, he succeeded in the resolution and isolation of a chiral tetranuclear Cobalt complex of general formula Δ -[Co₄(NH₃)₁₂(OH)₆]⁶⁺ known as Hexol (Figure I-33a) bearing no carbon atoms.⁷⁵ The latter is composed of achiral ligands with six bridging water molecules between the four Co atoms. It may also be described as one central cobalt atom coordinated to three chelating *cis*-(H₃N)Co(OH)₂ units through O atoms. The chiral information is here located directly on the metal and not on the ligand. Thus, bidentate achiral ligands coordinated to a metal center adopting an octahedral geometry will result in two enantiomers as illustrated in Figure I-33b. The Δ and Λ stereochemical descriptors are then used to describe the right-handed and left-handed enantiomers.

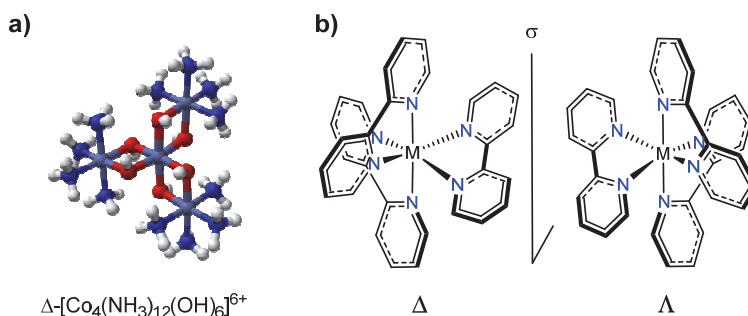


Figure I-33: a) Crystal structure of $\Delta\text{-[Co}_4\text{(NH}_3\text{)}_{12}\text{(OH)}_6\text{]}^{6+}$ and b) pair of enantiomers generated upon coordination of three bidentate chelating ligands on a metal center and stereochemical descriptors used. 2,2'-bipyridine is used as an example for the chelating ligand.

It should be noted that if the bidentate ligands are not symmetrical (e.g. 2-phenylpyridine), two diastereoisomers denoted as *fac* and *mer* isomers may exist. Both of them may then display two pairs of enantiomers (*fac*, Δ and *fac*, Λ) and (*mer*, Δ and *mer*, Λ).

Chiral metal complexes may display unique features with respect to chiral organic compounds based on asymmetric carbon.⁷⁶ First, easily accessible and commercially available achiral ligands may be used to synthesize active chiral coordination compounds such as catalysts. Secondly, because of the globular nature of octahedral complexes, their interaction with other molecules may be different compared to chiral organic molecules. They may thus be powerful structural scaffolds for selective recognition of nucleic acids for example. Multi-functionality may be achieved by coupling metal-centered chirality with the properties of the central metal ion, in particular transition metal ions. For instance, an enantiopure stereogenic-at-the-metal Ir(III) complex was used as photocatalyst in asymmetric reactions.⁷⁷ As for the preparation of enantiopure metal complexes, several techniques have been developed since the first isolation of a chiral coordination compound by Werner. We shall only describe in the following sections some of the methods that have proven successful also for Ir complexes, relevant to our work.

5.2 Methods developed to obtain enantiopure metal complexes

For the preparation of enantiopure metal complexes, three main strategies may be employed: i) resolution of a racemate; ii) stereoselective synthesis induced by a chiral ligand; iii) use of chiral auxiliary ligands, either to selectively form the desired enantiomers or to separate diastereoisomers. Conversion of complexes into diastereoisomers may be a simple way to separate them on the basis of their different physicochemical properties.

In order to isolate one enantiomer from its racemic mixture, specific recognition of this enantiomer is required. For example, differentiated interactions between the two enantiomers and a solid support based on hydrogen bonding, electrostatic interactions or van der Waals interactions may be explored. Furthermore, steric effects may also be exploited for enantioselective separation.

Several methods have been developed for the resolution of enantiomers bearing asymmetric carbon atoms: crystallization of diastereoisomers, liquid-liquid extraction (*e.g.* using a chiral solvent or a chiral ion) or chiral chromatography (HPLC, GC). These techniques may equally be applied to the resolution of chiral metal complexes.

Here, we focus only on the use of chiral counter ions and chiral auxiliary⁷⁸ or chiral ligands to obtain enantiopure metal complexes.

A-Resolution of metal complexes as racemate using chiral ions

When considering cationic metal complexes, chiral anions may be used to form diastereomeric ion pairs that may be separated by standard chromatography or solubility differences. In the 1990s, Lacour and coworkers developed a configurationally stable chiral anion based on a hexacoordinated phosphorus atom named TRISPHAT (Figure I-34).⁷⁹ In particular, its use as a chiral anion was shown to be successful to resolve octahedral Ru(II) complexes^{76b} as well as Ir complexes.⁸⁰ Thus, in 2007, Sauvage, Lacour and coworkers described the use of TRISPHAT to separate bimetallic Ir(III) complexes bearing 2-phenylpyridine unit and one bis-bipyridine ligand as bridging unit.⁸¹ This example will be further discussed in chapter II. Amouri *et al* described the resolution of planar cationic Ir complexes bearing Cp* (Cp* = pentamethylcyclopentadienyl) and *o*-quinone methide units by fractional crystallization of the TRISPHAT salts.^{80b}

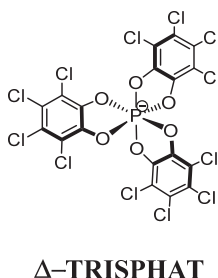


Figure I-34: Chemical structure of the resolving agent TRISPHAT.

B-Stereoselective synthesis induced by chiral ligands

When enantiomerically pure chiral ligands are coordinated to the metal center, either selective formation of one diastereoisomer is achieved or both diastereoisomers are formed in varying ratios.

In 1993, von Zelewsky and his coworkers first described the preparation of a series of CHIRAGEN (from CHIRality GENerator) ligands to form exclusively one enantiomerically pure octahedral Ru(II) complex with known absolute configuration at the metal center avoiding thus separation.⁸² These ligands, CHIRAGEN-1, are based on two bipyridine rings bearing a chiral pinene group on one of the pyridyl units and bridged by an aliphatic chain (Figure I-35a). They further extended this methodology to the synthesis of other Ru complexes using for example three bridged bipyridine units or aromatic linkers.⁸³ Furthermore, they applied this methodology to the

diastereoselective formation of chiral tris-cyclometalated Ir(III) complexes (Figure I-35b) using CHIRAGEN-2 as cyclometalating units.⁸⁴ However, despite its efficiency, this methodology requires first the synthesis of sophisticated chiral organic ligands.

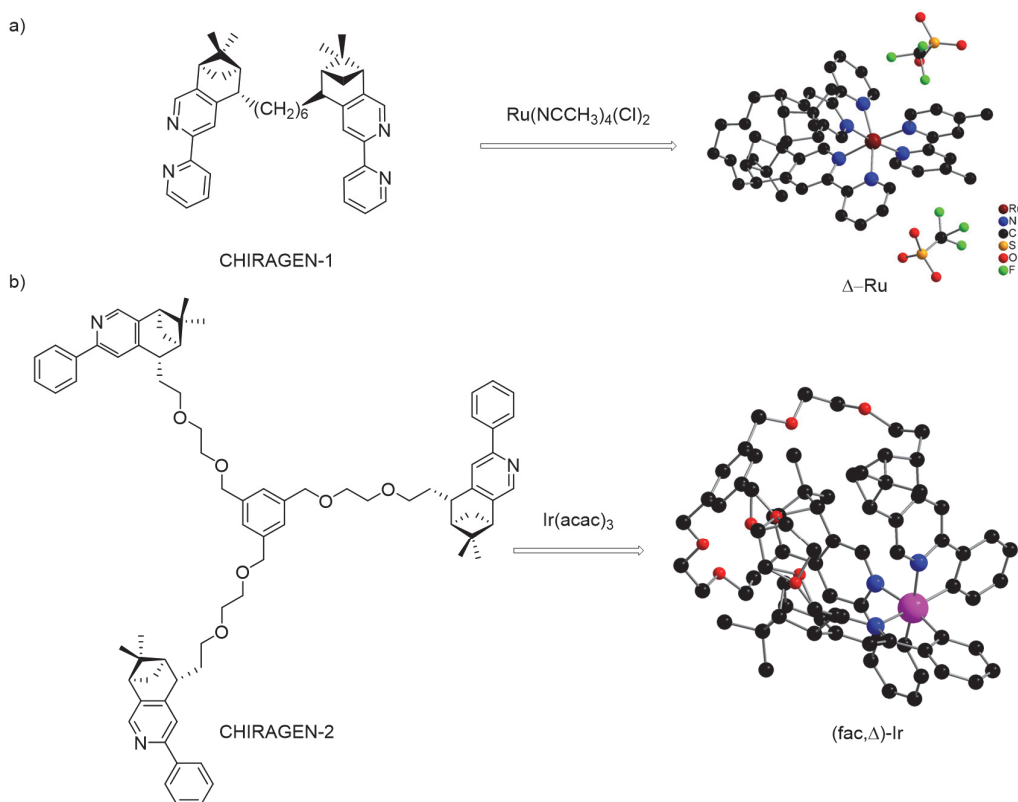


Figure I-35: a) chemical structure of CHIRAGEN-1 and crystal structure of the enantiomerically pure Ru complex⁸²; b) chemical structure of the chiral tris-phenylpyridyl ligand CHIRAGEN-2 and crystal structure of the enantiomerically pure Ir complex.⁸⁴

C-Preparation of Enantiopure metal complexes based on chiral auxiliary ligands

In order to avoid tedious synthesis of sophisticated chiral ligands, another approach, based on the use of simple commercially available chiral ligands, has emerged. The aim here is no more to drive the formation of only one diastereoisomer but to form two diastereoisomers that can be easily separated by classical methods such as chromatography or recrystallization. Furthermore, for labile auxiliary ligands, they can be replaced by the achiral ligand of choice.

Thus, this approach is based on a two-step procedure starting with the binding of the auxiliary enantiopure organic ligand to generate and subsequently separate the two diastereoisomers. The second step is based on the replacement of the labile chiral ligand by one achiral bidentate or two achiral monodentate ligands.

A series of oxazoline and chiral sulfoxide derivatives were prepared by Meggers *et al.* and they succeeded in the asymmetric synthesis of Ru as well as Ir octahedral metal complexes (Figure I-36a and b).^{76c,77b,85} Lusby *et al.* have also used this approach using serine-derivatives to resolve the diastereoisomers formed followed by asymmetric synthesis of the desired Ir complexes (Figure I-36c).⁸⁶ Some examples reported by those two groups are detailed in chapter II.

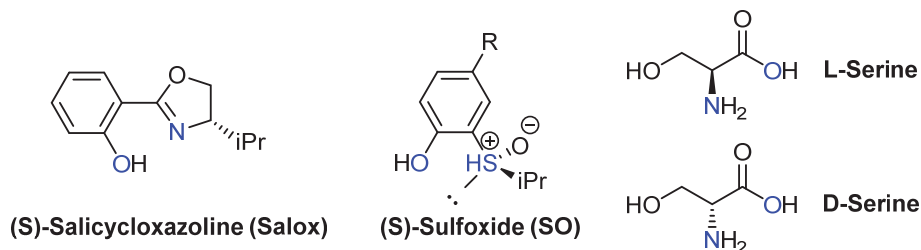


Figure I-36: Chemical structures of the chiral oxazoline, sulfoxide and serine derivatives used as chiral auxiliaries.

6. Luminescent Ir(III) complexes

As illustrated before, apart from chirality, during the last decade, the design and formation of luminescent coordination networks have attracted considerable interest. Luminescence may be defined as the emission of light from any substance in its electronically excited states. Depending on the nature of the excited state (singlet or triplet state), luminescence could be formally divided into two categories: fluorescence and phosphorescence. In the last decades, phosphorescent transition-metal complexes have attracted significant attention with respect to their potential applications in fabrication of chemical and biological sensors, photovoltaic devices and organic light emitting diodes (OLEDs).⁸⁷ In particular, the use of Ir(III) complexes as light emitters has been extensively studied because of their very high luminescence efficiencies and rather short phosphorescence lifetimes.

In the section below, the synthesis of bis- or tris-cyclometalated Ir(III) complexes is briefly commented and a brief theoretical background of their photophysical properties is given. More insights into the synthesis are given in the following chapters.

6.1 Synthesis of cyclometalated Iridium(III) complexes

It is worth noting that Iridium(III) forms a large variety of complexes, including mono-, bis- and tris-cyclometallated complexes,⁸⁸ bearing bidentate ligands such as polyimine⁸⁹ or diphosphine⁹⁰ ligands. The following paragraph is dedicated only to the synthesis of bis-cyclometallated Ir(III) complexes bearing a bipyridyl unit as third ligand ($[\text{Ir}(\text{C}^{\wedge}\text{N})_2(\text{N}^{\wedge}\text{N})]^+$) or tris-cyclometallated Ir(III) complexes ($\text{Ir}(\text{C}^{\wedge}\text{N})_2(\text{C}'^{\wedge}\text{N}')$) bearing two differentiated cyclometallating ligands.

In both cases, the first synthetic step consists in the formation of the Ir dimer $[\text{Ir}(\text{C}^{\wedge}\text{N})_2(\mu\text{-Cl})]_2$. The second step involves the substitution of the chloride ligands by a third ligand which could be

anionic ($C^{\wedge}N$) or neutral ($N^{\wedge}N$) (Figure I-37). The bis-cyclometallated Ir(III) complexes with general formula $[Ir(C^{\wedge}N)_2(N^{\wedge}N)]^{+}$ are cationic and rather mild reaction conditions may be employed as detailed in chapter II. In contrast, the synthesis of homo- and hetero-leptic tris-cyclometallated Ir(III) complexes $Ir(C^{\wedge}N)_2(C^{\wedge}N')$ requires harsh reaction conditions as discussed in chapter III.

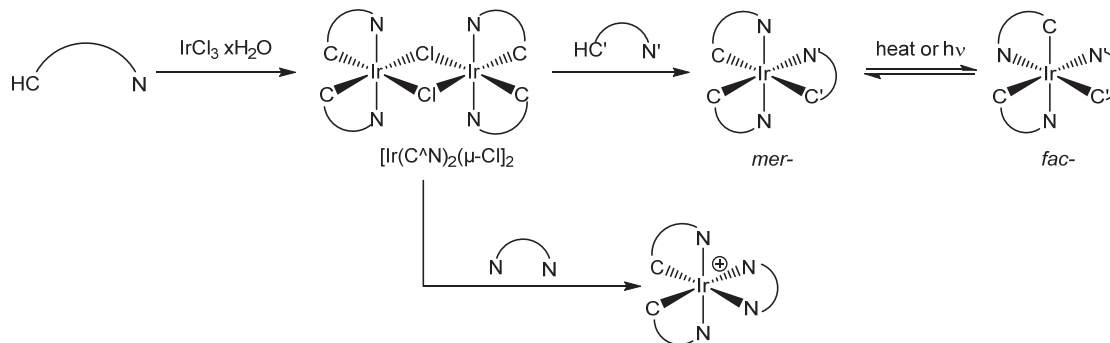


Figure I-37: Typical synthetic routes for the formation of tris-cyclometallated Ir complexes $Ir(C^{\wedge}N)_2(C^{\wedge}N')$ (top) and bis-cyclometallated Ir(III) complexes $[Ir(C^{\wedge}N)_2(N^{\wedge}N)]^{+}$.

6.2 Photophysical properties of Iridium(III) cyclometallated complexes

In the 1980s, Watts and coworkers initially discovered that the facial *fac*- $Ir(ppy)_3$ (ppy = 2-phenylpyridine) obtained as a side product in the synthesis of the chloro-bridged dimers $[Ir(ppy)_2(\mu-Cl)]_2$ exhibited interesting photophysical properties.⁹¹ Since then, tremendous efforts have been devoted to the development of related Ir complexes and impressive expansion of the literature on the luminescence of Iridium(III) complexes has been observed, as illustrated in Figure I-38.

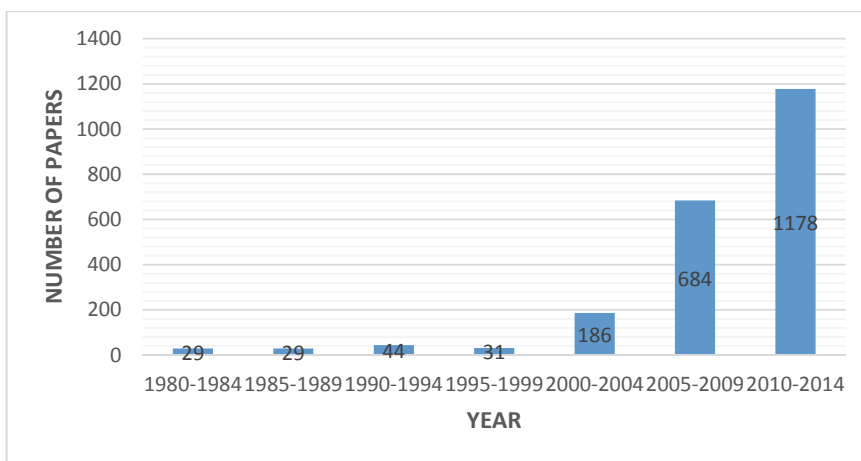


Figure I-38: Number of papers published from 1980 to 2014 containing the keywords “Iridium” and “Luminescence”, data obtained from “Scifinder”.

A-Theoretical Background

The Iridium(III) trication is a $5d^6$ center and according to the crystal field theory, the energy of the $5d$ orbitals could be modified and differentiated by a ligand-field splitting parameter (Δ). The value of Δ not only depends on the spatial extension of d orbitals, *i.e.* the effect is more pronounced for $5d$ orbitals with high principal quantum number than for $3d$ orbitals displaying a smaller principal quantum number, but also depends on the field strength exerted by the ligand. According to the spectrochemical series, ligands such as bipyridyl or phenylpyridyl are examples of ligands inducing the strongest effect.

It should be noted that photoexcitation in cyclometallated Ir(III) complexes may be associated with multiple electronic transitions states, such as ligand centered (LC) transitions or metal-centered (MC) transitions, or metal-to-ligand charge transfer (MLCT) transitions (Figure I-39). When dealing with heteroleptic tris-chelate Iridium(III) complexes, the electronic transitions are even more complicated as for example, ligand-to-ligand charge transfer (LL'CT) transitions can take place. In Figure I-39, some useful orbitals and electronic transitions in a typical cyclometallated Iridium(III) complexes are represented.

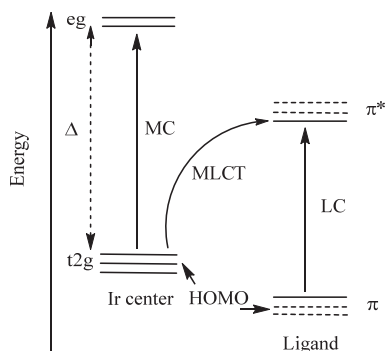


Figure I-39: Schematic representation of different orbitals and electronic transitions in cyclometallated Ir(III) complexes.

For Iridium(III) complexes, the ligand field splitting Δ is large and the MC levels are pushed so high in energy that usually they do not affect the emission properties. However, both emissive MLCT and LC transitions may be encountered. In addition, Iridium(III) center, as a heavy central metal atom, might strongly combine the emitting singlet and dark triplet states because of spin-orbit coupling (SOC), thus enabling triplet emission with high efficiency. Thus, the lowest excited states are either metal-ligand charge transfer (MLCT), in which the highest occupied molecular orbital (HOMO) is a combination of both metal d orbitals and ligand π orbitals, or solely ligand centered (LC), depending on the chemical structure of a ligand (Figure I-32).

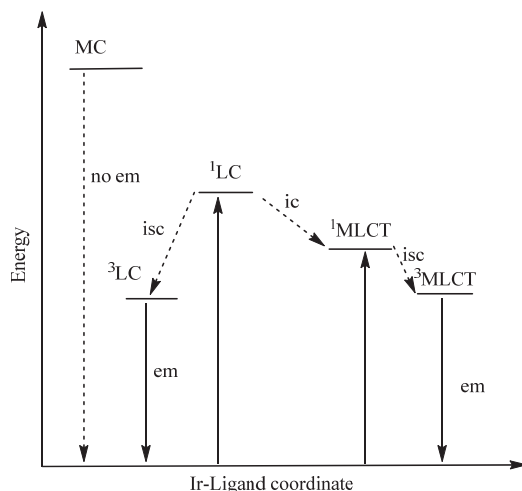


Figure I-40: Simplified schematic Jablonski diagram highlighting the mechanism of phosphorescence from Iridium(III) complex

The availability of these different close lying excited states explains why cyclometallated Iridium(III) complexes may show interesting emission properties in a wide emission wavelengths range. Based on the MO (molecular orbital) theory, color tuning, *i.e.* emission wavelengths shift, in cyclometallated Iridium(III) complexes, may be achieved by subtle change in the HOMO-LUMO energy bandgap (HOMO= highest occupied molecular orbital; LUMO= lowest occupied molecular orbital). Thus, a bathochromic shift of the emission, also called red shift, can be achieved by decreasing the HOMO-LUMO energy bandgap, while a hypsochromic shift of the emission, also known as a blue shift, can be achieved by increasing the HOMO-LUMO energy bandgap.

B-Color Tuning Strategies for Iridium(III) complexes

For the cationic bis-cyclometallated Iridium(III) complexes, owing to the relatively easy synthetic access, in order to gain more insights into their photophysical properties, various types of neutral ligands have been introduced. Mainly two approaches have been studied: i) introduction of electron-withdrawing or donating groups on chelating ligands; ii) use of different neutral ancillary ligands.

a) Introduction of electron-withdrawing or electron-donating groups on chelating ligands

From different investigations, the following conclusions were drawn. Electron-withdrawing groups such as -F, -CF₃ groups located on the cyclometallating unit tend to stabilize the HOMO by removing electron density from the metal centers, as demonstrated for instance by De Cola *et al.*⁹² and by Bernhard and coworkers,⁹³ whereas electron-donating groups such as -C(CH₃)₃ have the opposite effect. It is worth pointing out that the position of the substituents with respect to the coordinating carbon of the cyclometallating ligand strongly influences the HOMO-LUMO gap within the complex.⁹⁴

b) Introduction of different types of ancillary ligands.

The emission wavelength of heteroleptic cationic complexes could be varied using a third ancillary ligand. Again, varieties of ancillary ligand possessing different intrinsic features (steric hindrance, π -conjugated system) may be employed to influence the photophysical properties.⁹⁴⁻⁹⁵ For instance, Huang and coworkers prepared a series of cationic Iridium(III) complexes containing N^N ligands with different π -conjugated systems such as 2,2'-bipyridine to 2,2'-bisquinoline. As a result, the emission wavelengths were significantly influenced and ranged from 586 nm to 659 nm. Thompson and coworkers also demonstrated that, using ancillary ligands such as pzH (pzH = pyrazolyl) or dppe (dppe = bis (diphenylphosphino)-ethane) or CN-t-Bu (CN-t-Bu = *tert*-butylisocyanide), a blue shifting was obtained.^{95a}

It is worth noting that the influence of the third ancillary ligand or the chelating C^N ligands is largely determined by the nature of the C^N ligand. C^N chelating ligands possessing a relatively small π - π^* energy gap, as for ppy (phenylpyridine) or piq (phenylisoquinoline) ligands, exert less influence.^{95a} However, when C^N chelating ligands, such as difluorophenylpyrazole, offer larger π - π^* energy gap, the influence of the third ligand is strong and dominant.⁹⁶

Color tuning of the neutral tris-cyclometallated Iridium(III) complexes may also be achieved using the strategies mentioned above.⁹⁷ A notable feature for neutral tris-cyclometallated Iridium(III) complexes is its two diastereoisomer (facial isomer and meridional isomer) that may exhibit rather different photophysical properties.⁹⁸ Usually, the *fac*-isomers possess longer lifetimes and higher quantum efficiencies than their meridional counterparts.⁹⁹

Due to the variety features influencing the nature of the excited state in Iridium(III) complexes, their electrochemical and photophysical properties are not always easy to predict and explain. However, DFT calculations, by modeling orbital configurations and the energy of the lowest excited state, helps to better understand and thus explain experimental observations for new Iridium(III) complexes.

7. Research Project

To the best of our knowledge, coordination compounds only stereogenic at the metal have not been used to generate homochiral heterometallic coordination networks. We investigated the possibility of using chiral octahedral metal complexes, more specifically, chiral Iridium(III) complexes, as chiral metallatectons to form enantiopure MOFs. It is worth noting that cyclometallated Iridium(III) complexes are configurationally stable. This is a prerequisite if they were used as enantiopure building blocks for the generation of homochiral MOFs. As stated before, besides their intrinsic chirality, such complexes are well known for their highly efficient photophysical

properties.¹⁰⁰ Thus, chiral recognition as well as chemical sensing may be envisioned as potential applications for this type of organized solid-state materials.

Hence, we have designed new chiral Iridium(III) complexes bearing three chelating ligands equipped with peripheral coordinating sites as metallatectons (Figure I-41). Two of the bidentate ligands are 2-phenylpyridine cyclometallating units (ppy). This type of ligand is commonly used if luminescence is targeted. In order to tune the emission wavelength of the Ir(III) complexes, 2-(2,4-difluorophenyl)pyridine (dFppy) was also used as cyclometallating unit. The third ligand was either a disubstituted 2,2'-bipyridyl (Y = N) unit or a disubstituted 2-phenylpyridyl (Y = C) moiety. Thus, either cationic (Y = N) or neutral (Y = C) Ir(III) complexes have been considered. Furthermore, in order to form coordination networks based on combinations of the Iridium complex acting as metallatecton, and metal ions, the third ligand needs to be functionalized with coordinating groups such as pyridine or benzoic acid at 5,5' positions of the bipyridyl central unit (Y = N) or at positions 5 of the pyridyl unit and position 4 for the phenyl moiety of the central 2-phenylpyridyl unit. An ethynyl spacer between the terminal coordinating sites and the bipyridyl or phenylpyridyl units has been introduced in order to induce co-planarity of the ancillary ligand.

The aim of this PhD project (Figure I-41) was thus first to synthesize luminescent racemic and enantiopure cationic Iridium(III) complexes that are stereogenic only at the metal. The complexes obtained were further used as metallatectons to generate homochiral crystalline materials as detailed in chapter II. However, one of the drawbacks when using bis-cyclometallating cationic Ir(III) complexes is the presence of anions that may be deleterious for the formation of porous coordination networks. Chapter III describes the synthesis of neutral tris-cyclometallated Ir(III) complexes and their use as metallatectons for the generation of coordination polymers in the presence of different metallic nodes under self-assembly conditions

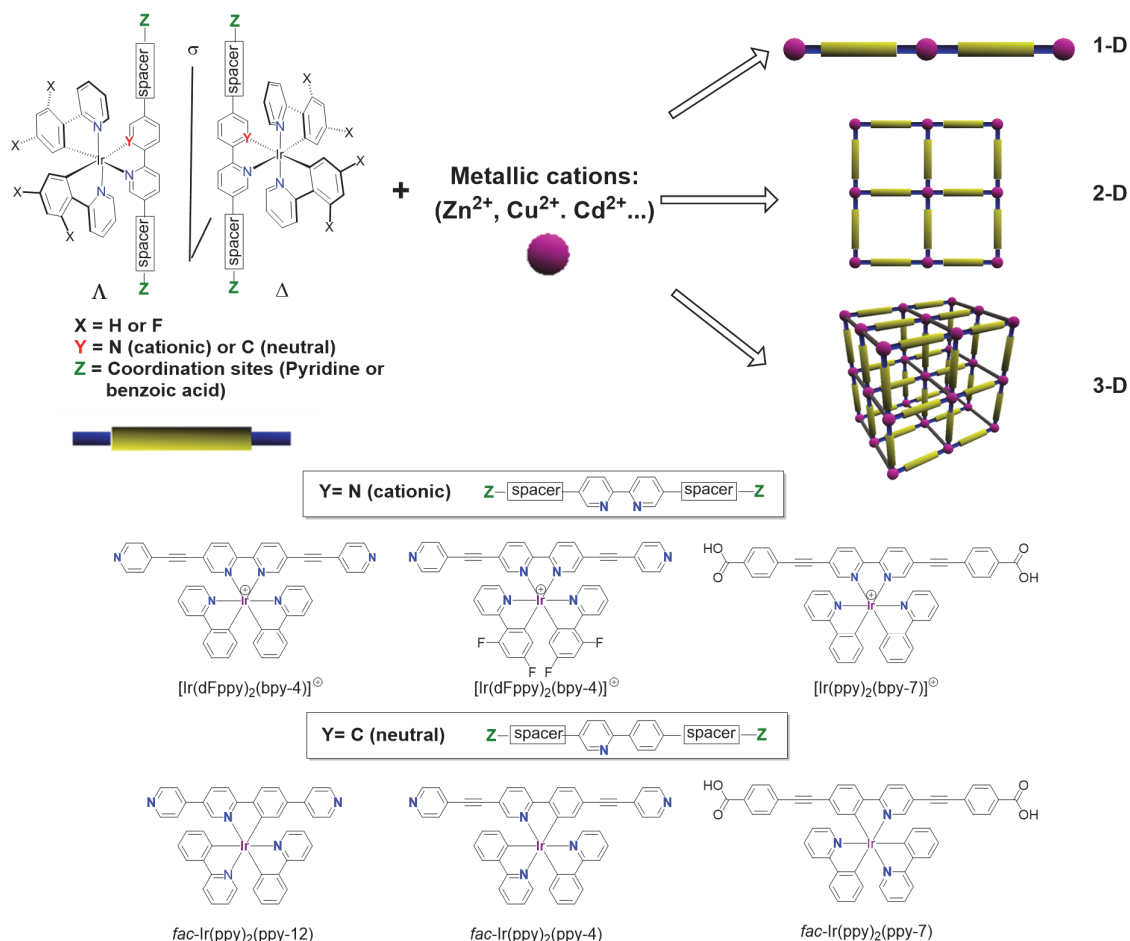


Figure I-41: Chemical structures of the different Ir-based chiral metallatectons and schematic representations of the possible 1D, 2D and 3D porous network formed upon combinations with metallic nodes.

REFERENCES

- (1) https://www.classzone.com/books/earth_science/terc/content/investigations/es0506/es0506page01.cfm.
- (2) http://en.wikipedia.org/wiki/Plant_genetics.
- (3) <https://www.pinterest.com/pin/8444318022350858/>.
- (4) (a) Lehn, J. M. *Pure Appl. Chem.* **1978**, *50*, 871; (b) Lehn, J. M. *Angew. Chem. Int. Ed. Engl.* **1988**, *27*, 89; (c) Lehn, J. M. *Angew. Chem. Int. Ed.* **1990**, *29*, 1304; (d) Lehn, J. M. *Supramolecular Chemistry: Concepts and Perspectives*; Wiley-VCH, 1995.
- (5) (a) Lehn, J. M. *Proceedings of the National Academy of Sciences* **2002**, *99*, 4763; (b) Steed, J. W.; Turner, D. R.; Wallace, K. *Core Concepts in Supramolecular Chemistry and Nanochemistry*, 2007.
- (6) (a) Liu, L.; Guo, Q.-X. *Chem. Rev.* **2001**, *101*, 673; (b) Boots, H. M. J.; De Bokx, P. K. *J. Phys. Chem.* **1989**, *93*, 8240; (c) Dunitz, J. D. *Chem. Biol.* **1995**, *2*, 709.
- (7) (a) Simard, M.; Su, D.; Wuest, J. D. *J. Am. Chem. Soc.* **1991**, *113*, 4696; (b) Mann, S. *Nature* **1993**, *365*, 499.

- (8) (a) Hosseini, M. W. *CrystEngComm* **2004**, *6*, 318; (b) Hosseini, M. W. *Coord. Chem. Rev.* **2003**, *240*, 157; (c) Hosseini, M. W. *Chem. Commun.* **2005**, 5825.
- (9) (a) Lehn, J. M. *La Chimie Supramoléculaire: Concepts et Perspectives*. **1997**; (b) Hosseini, M. W. *Acc. Chem. Res.* **2005**, *38*, 313.
- (10) (a) Tsuzuki, S.; Honda, K.; Uchimaru, T.; Mikami, M.; Tanabe, K. *J. Am. Chem. Soc.* **2002**, *124*, 104; (b) Hunter, C. A.; Sanders, J. K. M. *J. Am. Chem. Soc.* **1990**, *112*, 5525.
- (11) Perez, E. M.; Martin, N. *Chem. Soc. Rev.* **2008**, *37*, 1512.
- (12) (a) Kawase, T.; Darabi, H. R.; Oda, M. *Angew. Chem. Int. Ed. Engl.* **1996**, *35*, 2664; (b) Kawase, T.; Kurata, H. *Chem. Rev.* **2006**, *106*, 5250–5273.
- (13) Janiak, C. *J. Chem. Soc., Dalton Trans.* **2000**, 3885.
- (14) Wang, M.; Guo, S.; Li, Y.; Cai, L.; Zou, J.; Xu, G.; Zhou, W.; Zheng, F.; Guo, G. *J. Am. Chem. Soc.* **2009**, *131*, 13572.
- (15) Steiner, T. *Angew. Chem. Int. Ed.* **2002**, *41*, 48.
- (16) (a) Beatty, A. M. *Coord. Chem. Rev.* **2003**, *246*, 131; (b) Braga, D.; Maini, L.; Grepioni, F.; De Cian, A.; Felix, O.; Fischer, J.; Hosseini, M. W. *New J. Chem.* **2000**, *24*, 547; (c) Ward, M. D. *Chem. Commun.* **2005**, 5838.
- (17) Bhogala, B.; Vishweshwar, P.; Nangia, A. *Cryst. Growth Des.* **2002**, *2*, 325.
- (18) (a) Allendorf, M. D.; Bauer, C. A.; Bhakta, R. K.; Houk, R. J. *Chem. Soc. Rev.* **2009**, *38*, 1330; (b) Cohen, S. M. *Chem. Sci.* **2010**, *1*, 32; (c) James, S. L. *Chem. Soc. Rev.* **2003**, *32*, 276; (d) Batten, S. R.; Champness, N. R.; Chen, X.-M.; Garcia-Martinez, J.; Kitagawa, S.; Öhrström, L.; O'Keeffe, M.; Suh, M. P.; Reedijk, J. *CrystEngComm* **2012**, *14*, 3001.
- (19) Batten, S. R.; Champness, N. R.; Chen, X.-M.; Garcia-Martinez, J.; Kitagawa, S.; Öhrström, L.; O'Keeffe, M.; Paik Suh, M.; Reedijk, J. *Pure Appl. Chem.* **2013**, *85*, 1715.
- (20) Long, J. R.; Yaghi, O. M. *Chem. Soc. Rev.* **2009**, *38*, 1213.
- (21) Cram, J. D.; Cram, J. M. *Container Molecules and Their Guests* **1991**, *The Royal Society of Chemistry, Cambridge*.
- (22) Cook, T. R.; Zheng, Y. R.; Stang, P. J. *Chem. Rev.* **2013**, *113*, 734.
- (23) Leong, W.; Vittal, J. J. *Chem. Rev.* **2011**, *111*, 688.
- (24) (a) Hajeka, F.; Graf, E.; Cianb, A. D.; Fischerb, J.; Hosseini, M. W. *Dalton Trans.* **1996**, *37*, 1401; (b) Ferlay, S.; Jouaiti, A.; Loï, M.; Hosseini, M. W.; De Cian, A.; Turek, P. *New J. Chem.* **2003**, *27*, 1801; (c) Kozlova, M. N.; Ferlay, S.; Solovieva, S. E.; Antipin, I. S.; Konovalov, A. I.; Kyritsakas, N.; Hosseini, M. W. *Dalton Trans.* **2007**, 5126.
- (25) (a) Larpent, P.; Jouaiti, A.; Kyritsakas, N.; Hosseini, M. W. *Dalton Trans.* **2014**, *43*, 166; (b) Cheng, Y.-F.; Lu, X.-M.; Sun, X.-J. *Inorg. Chem. Commun.* **2014**, *49*, 127.
- (26) (a) Lin, M. J.; Jouaiti, A.; Kyritsakas, N.; Hosseini, M. W. *Chem. Commun.* **2010**, *46*, 115; (b) Bourlier, J.; Hosseini, M. W.; Planeix, J.-M.; Kyritsakas, N. *New J. Chem.* **2007**, *31*, 25.
- (27) (a) Ohmura, T.; Usuki, A.; Fukumori, K.; Ohta, T.; Ito, M.; Tatsumi, K. *Inorg. Chem.* **2006**, *45*, 7988; (b) Zhang, G.; Constable, E. C.; Housecroft, C. E.; Zampese, J. A. *Inorg. Chem. Commun.* **2014**, *43*, 51.
- (28) Beziau, A.; Baudron, S. A.; Pogozev, D.; Fluck, A.; Hosseini, M. W. *Chem. Commun.* **2012**, *48*, 10313.
- (29) Seidel, R. W.; Oppel, I. M. *CrystEngComm* **2010**, *12*, 1051.
- (30) (a) Agarwal, R. A.; Bharadwaj, P. K. *Cryst. Growth Des.* **2014**, *14*, 6115; (b) Suh, M. P.; Park, H. J.; Prasad, T. K.; Lim, D. W. *Chem. Rev.* **2012**, *112*, 782; (c) Furukawa, H.; Cordova, K. E.; O'Keeffe, M.; Yaghi, O. M. *Science* **2013**, *341*, 974.
- (31) Li, H.; Eddaoudi, M.; O'Keeffe, M.; Yaghi, O. M. *Nature* **1999**, *402*, 276.
- (32) Eddaoudi, M.; Kim, J.; Rosi, N.; Vodak, D.; Wachter, J.; O'Keeffe, M.; Yaghi, O. M. *Science* **2002**, *295*, 469.
- (33) (a) Pichon, A.; Fierro, C. M.; Nieuwenhuyzen, M.; James, S. L. *CrystEngComm* **2007**, *9*, 449; (b) Lee, C.-H.; Wu, J.-Y.; Lee, G.-H.; Peng, S.-M.; Jiang, J.-C.; Lu, K.-L. *Cryst. Growth Des.* **2014**, *14*, 5608; (c) Chang, Z.; Zhang, D. S.; Chen, Q.; Li, R. F.; Hu, T. L.; Bu, X. H. *Inorg. Chem.* **2011**, *50*, 7555.
- (34) Lin, M.-J.; Jouaiti, A.; Kyritsakas, N.; Hosseini, M. W. *CrystEngComm* **2011**, *13*, 776.
- (35) Li, J. R.; Kuppler, R. J.; Zhou, H. C. *Chem. Soc. Rev.* **2009**, *38*, 1477.

- (36) (a) Zhang, T.; Lin, W. *Chem. Soc. Rev.* **2014**, *43*, 5982; (b) Ma, L.; Abney, C.; Lin, W. *Chem. Soc. Rev.* **2009**, *38*, 1248; (c) Song, F.; Wang, C.; Lin, W. *Chem. Commun.* **2011**, *47*, 8256; (d) Seo, J. S.; Whang, D.; Lee, H.; Jun, S. I.; Oh, J.; Jeon, Y. J.; Kim, K. *Nature* **2000**, *404*, 982.
- (37) Kreno, L. E.; Leong, K.; Farha, O. K.; Allendorf, M.; Van Duyne, R. P.; Hupp, J. T. *Chem. Rev.* **2012**, *112*, 1105.
- (38) Peluso, P.; Mamane, V.; Cossu, S. *J. Chromatogr. A* **2014**, *1363*, 11.
- (39) Ma, L.; Lin, W. *Top. Curr. Chem.* **2009**, *293*, 175.
- (40) Duerinck, T.; Denayer, J. F. M. *Chem. Eng. Sci.* **2015**, *124*, 179.
- (41) Yoon, M.; Srirambalaji, R.; Kim, K. *Chem. Rev.* **2012**, *112*, 1196.
- (42) Kaes, C.; Hosseini, M. W.; Rickard, C. E. F.; Skelton, B. W.; White, A. H. *Angew. Chem. Int. Ed.* **1998**, *37*, 920.
- (43) Hahn, T.; Paufler, P. *International tables for crystallography, Vol. A. space-group symmetry D. REIDEL Publ. Co., Dordrecht, Holland/Boston, U. S. A., 1983, 854 Seiten, ISBN 90-277-1445-2; WILEY-VCH Verlag, 1984.*
- (44) (a) Jaunky, W.; Wais Hosseini, M.; Marc Planeix, J.; De Cian, A.; Kyrtsakas, N.; Fischer, J. *Chem. Commun.* **1999**, 2313; (b) Jouaiti, A.; Hosseini, M. W.; Kyrtsakas, N. *Chem. Commun.* **2003**, 472; (c) Schmaltz, B.; Jouaiti, A.; Hosseini, M. W.; De Cian, A. *Chem. Commun.* **2001**, 1242; (d) Withersby, M. A.; Blake, A. J.; Champness, N. R.; Hubberstey, P.; Li, W.-S.; Schröder, M. *Angew. Chem. Int. Ed.* **1997**, *36*, 2327; (e) Carlucci, L.; Ciani, G.; W. v. Gudenberg, D.; Proserpio, D. M. *Inorg. Chem.* **1997**, *36*, 3812.
- (45) Morris, R. E.; Bu, X. *Nat Chem* **2010**, *2*, 353.
- (46) Zhang, J.; Chen, S.; Wu, T.; Feng, P.; Bu, X. *J. Am. Chem. Soc.* **2008**, *130*, 12882.
- (47) Kesanli, B.; Cui, Y.; Smith, M. R.; Bittner, E. W.; Bockrath, B. C.; Lin, W. *Angew. Chem. Int. Ed.* **2005**, *44*, 72.
- (48) Bisht, K. K.; Parmar, B.; Rachuri, Y.; Kathalikattil, A. C.; Suresh, E. *CrystEngComm* **2015**.
- (49) Nickerl, G.; Henschel, A.; Grüner, R.; Gedrich, K.; Kaskel, S. *Chem. Ing. Tech.* **2011**, *83*, 90.
- (50) (a) Kitagawa, S.; Noro, S.-i.; Nakamura, T. *Chem. Commun.* **2006**, 701; (b) Andruh, M. *Chem. Commun.* **2007**, 2565; (c) Garibay, S. J.; Wang, Z.; Tanabe, K. K.; Cohen, S. M. *Inorg. Chem.* **2009**, *48*, 7341; (d) Burrows, A. D. *CrystEngComm* **2011**, *13*, 3623; (e) Das, M. C.; Xiang, S.; Zhang, Z.; Chen, B. *Angew. Chem. Int. Ed.* **2011**, *50*, 10510; (f) Kumar, G.; Gupta, R. *Chem. Soc. Rev.* **2013**, *42*, 9403; (g) Baudron, S. A. *CrystEngComm* **2010**, *12*, 2288.
- (51) (a) Cui, Y.; Ngo, H. L.; White, P. S.; Lin, W. *Chem. Commun.* **2003**, 994; (b) Jouaiti, A.; Hosseini, M. W.; Kyrtsakas, N.; Grosshans, P.; Planeix, J.-M. *Chem. Commun.* **2006**, 3078.
- (52) Falkowski, J. M.; Sawano, T.; Zhang, T.; Tsun, G.; Chen, Y.; Lockard, J. V.; Lin, W. *J. Am. Chem. Soc.* **2014**, *136*, 5213.
- (53) Shultz, A. M.; Sarjeant, A. A.; Farha, O. K.; Hupp, J. T.; Nguyen, S. T. *J. Am. Chem. Soc.* **2011**, *133*, 13252.
- (54) (a) Larpent, P.; Jouaiti, A.; Kyrtsakas, N.; Hosseini, M. W. *Chem. Commun.* **2013**, *49*, 4468; (b) Marets, N.; Bulach, V.; Hosseini, M. W. *New J. Chem.* **2013**, *37*, 3549; (c) Grosshans, P.; Jouaiti, A.; Bulach, V.; Planeix, J.-M.; Hosseini, M. W.; Nicoud, J.-F. *CrystEngComm* **2003**, *5*, 414; (d) Larpent, P.; Jouaiti, A.; Kyrtsakas, N.; Hosseini, M. W. *Dalton Trans.* **2014**, *43*, 2000; (e) Jouaiti, A.; Hosseini, M. W.; Kyrtsakas, N. *Chem. Commun.* **2002**, 1898.
- (55) (a) Grosshans, P.; Jouaiti, A.; Bulach, V.; Planeix, J.-M.; Hosseini, M. W.; Nicoud, J.-F. *Chem. Commun.* **2003**, 1336; (b) P. Grosshans; A. Jouaiti; V. Bulach; J.-M. Planeix; M. W. Hosseini; J.-F. Nicoud *C. R. Chimie.* **2004**, *7*, 189.
- (56) Jouaiti, A.; Hosseini, M. W.; De Cian, A. *Chem. Commun.* **2000**, 1863.
- (57) Wang, Z.; Cohen, S. M. *J. Am. Chem. Soc.* **2007**, *129*, 12368.
- (58) Tanabe, K. K.; Cohen, S. M. *Chem. Soc. Rev.* **2011**, *40*, 498.
- (59) Dau, P. V.; Kim, M.; Cohen, S. M. *Chem. Sci.* **2013**, *4*, 601.
- (60) (a) Hu, F.-L.; Wang, S.-L.; Li, H.-X.; Wu, B.; Lang, J.-P. *Inorg. Chem. Commun.* **2014**, *47*, 75; (b) Zhang, K. Y.; Liu, H.-W.; Tang, M.-C.; Choi, A. W.-T.; Zhu, N.; Wei, X.-G.; Lau, K.-C.; Lo, K. K.-W. *Inorg. Chem.* **2015**.
- (61) So, M. C.; Beyzavi, M. H.; Sawhney, R.; Shekhah, O.; Eddaoudi, M.; Al-Juaaid, S. S.; Hupp, J. T.; Farha, O. K. *Chem. Commun.* **2015**, *51*, 85.
- (62) Wang, C.; Wang, J. L.; Lin, W. *J. Am. Chem. Soc.* **2012**, *134*, 19895.

- (63) Wagner, B. D.; McManus, G. J.; Moulton, B.; Zaworotko, M. J. *Chem. Commun.* **2002**, 2176.
- (64) Maspoch, D.; Ruiz-Molina, D.; Veciana, J. *Chem. Soc. Rev.* **2007**, 36, 770.
- (65) Cui, Y.; Yue, Y.; Qian, G.; Chen, B. *Chem. Rev.* **2012**, 112, 1126.
- (66) Béziau, A.; Baudron, S. A.; Guenet, A.; Hosseini, M. W. *Chem. Eur. J.* **2013**, 19, 3215.
- (67) Heine, J.; Muller-Buschbaum, K. *Chem. Soc. Rev.* **2013**, 42, 9232.
- (68) Zhang, S.; Cheng, P. *CrystEngComm* **2015**, 17, 4250.
- (69) Jin, J.; Niu, S.; Han, Q.; Chi, Y. *New J. Chem.* **2010**, 34, 1176.
- (70) (a) Williams, D. E.; Rietman, J. A.; Maier, J. M.; Tan, R.; Greytak, A. B.; Smith, M. D.; Krause, J. A.; Shustova, N. B. *J. Am. Chem. Soc.* **2014**, 136, 11886; (b) Park, J.; Feng, D.; Yuan, S.; Zhou, H.-C. *Angew. Chem. Int. Ed.* **2015**, 54, 430; (c) Lee, C. Y.; Farha, O. K.; Hong, B. J.; Sarjeant, A. A.; Nguyen, S. T.; Hupp, J. T. *J. Am. Chem. Soc.* **2011**, 133, 15858; (d) Son, H.-J.; Jin, S.; Patwardhan, S.; Wezenberg, S. J.; Jeong, N. C.; So, M.; Wilmer, C. E.; Sarjeant, A. A.; Schatz, G. C.; Snurr, R. Q.; Farha, O. K.; Wiederrecht, G. P.; Hupp, J. T. *J. Am. Chem. Soc.* **2013**, 135, 862.
- (71) Du, D.-Y.; Qin, J.-S.; Sun, C.-X.; Wang, X.-L.; Zhang, S.-R.; Shen, P.; Li, S.-L.; Su, Z.-M.; Lan, Y.-Q. *J. Mater. Chem.* **2012**, 22, 19673.
- (72) Xie, Z.; Ma, L.; deKrafft, K. E.; Jin, A.; Lin, W. *J. Am. Chem. Soc.* **2010**, 132, 922.
- (73) Wang, C.; Lin, W. *J. Am. Chem. Soc.* **2011**, 133, 4232.
- (74) (a) von Zelewsky, A. *Stereochemistry of Coordination Compounds*; J. Wiley & Sons: Chichester, 1996; (b) Crassous, J. *Chem. Soc. Rev.* **2009**, 38, 830; (c) Meggers, E. *Eur. J. Inorg. Chem.* **2011**, 2011, 2911; (d) Crassous, J. *Chem. Commun.* **2012**, 48, 9687.
- (75) Werner, A. *Ber. Dtsch. Chem. Ges.* **1914**, 47, 3087.
- (76) (a) Sato, H.; Yamagishi, A. *J. Photochem. Photobiol., C* **2007**, 8, 67; (b) Hamelin, O.; Pécaut, J.; Fontecave, M. *Chem. Eur. J.* **2004**, 10, 2548; (c) Meggers, E. *Chem. Eur. J.* **2010**, 16, 752.
- (77) (a) Chen, L. A.; Tang, X.; Xi, J.; Xu, W.; Gong, L.; Meggers, E. *Angew. Chem. Int. Ed. Engl.* **2013**, 52, 14021; (b) Huo, H.; Fu, C.; Harms, K.; Meggers, E. *J. Am. Chem. Soc.* **2014**, 136, 2990; (c) Huo, H.; Shen, X.; Wang, C.; Zhang, L.; Rose, P.; Chen, L. A.; Harms, K.; Marsch, M.; Hilt, G.; Meggers, E. *Nature* **2014**, 515, 100.
- (78) Bauer, E. B. *Chem. Soc. Rev.* **2012**, 41, 3153.
- (79) Lacour, J.; Ginglinger, C.; Grivet, C.; Bernardinelli, G. *Angew. Chem. Int. Ed. Engl.* **1997**, 36, 608.
- (80) (a) Damas, A.; Moussa, J.; Rager, M. N.; Amouri, H. *Chirality* **2010**, 22, 889; (b) Moussa, J.; Chamoreau, L. M.; Amouri, H. *Chirality* **2013**, 25, 449.
- (81) Auffrant, A.; Barbieri, A.; Barigelletti, F.; Lacour, J.; Mobian, P.; Collin, J. P.; Sauvage, J. P.; Ventura, B. *Inorg. Chem.* **2007**, 46, 6911.
- (82) Hayoz, P.; Von Zelewsky, A.; Stoeckli-Evans, H. *J. Am. Chem. Soc.* **1993**, 115, 5111.
- (83) von Zelewsky, A. *Coord. Chem. Rev.* **1999** 190, 811.
- (84) Schaffner-Hamann, C.; von Zelewsky, A.; Barbieri, A.; Barigelletti, F.; Muller, G.; Riehl, J. P.; Neels, A. *J. Am. Chem. Soc.* **2004**, 126, 9339.
- (85) (a) Gong, L.; Mulcahy, S. P.; Devarajan, D.; Harms, K.; Frenking, G.; Meggers, E. *Inorg. Chem.* **2010**, 49, 7692; (b) Wenzel, M.; Meggers, E. *Eur. J. Inorg. Chem.* **2012**, 2012, 3168.
- (86) Chepelin, O.; Ujma, J.; Wu, X.; Slawin, A. M.; Pitak, M. B.; Coles, S. J.; Michel, J.; Jones, A. C.; Barran, P. E.; Lusby, P. J. *J. Am. Chem. Soc.* **2012**, 134, 19334.
- (87) (a) Ulbricht, C.; Beyer, B.; Friebe, C.; Winter, A.; Schubert, U. S. *Adv. Mater.* **2009**, 21, 4418; (b) Jayabharathi, J.; Thanikachalam, V.; Sathishkumar, R. *New J. Chem.* **2015**, 39, 235; (c) Tong, B.; Ku, H.-Y.; Chen, I. J.; Chi, Y.; Kao, H.-C.; Yeh, C.-C.; Chang, C.-H.; Liu, S.-H.; Lee, G.-H.; Chou, P.-T. *J. Mater. Chem. C* **2015**, 3, 3460.
- (88) Baranoff, E.; Cahill, J. F.; Flamigni, L.; Sauvage, J. P. *Chem. Soc. Rev.* **2004**, 33, 147.
- (89) (a) Dixon, I. M.; Collin, J.-P.; Sauvage, J.-P.; Flamigni, L.; Encinas, S.; Barigelletti, F. *Chem. Soc. Rev.* **2000**, 29, 385; (b) Basu, S.; Peng, S.-M.; Lee, G.-H.; Bhattacharya, S. *Polyhedron* **2005**, 24, 157.
- (90) Luo, S.-X.; Wei, L.; Zhang, X.-H.; Lim, M. H.; Lin, K. X. V.; Yeo, M. H. V.; Zhang, W.-H.; Liu, Z.-P.; Young, D. J.; Hor, T. S. A. *Organometallics* **2013**, 32, 2908.
- (91) (a) King, K. A.; Spellane, P. J.; Watts, R. J. *J. Am. Chem. Soc.* **1985**, 107, 1431; (b) Garces, F. O.; King, K. A.; Watts, R. J. *Inorg. Chem.* **1988**, 27, 3464.

- (92) Coppo, P.; Plummer, E. A.; De Cola, L. *Chem. Commun.* **2004**, 1774.
- (93) Lowry, M. S.; Goldsmith, J. I.; Slinker, J. D.; Rohl, R.; Pascal, R. A.; Malliaras, G. G.; Bernhard, S. *Chem. Mater.* **2005**, *17*, 5712.
- (94) Tsuzuki, T.; Shirasawa, N.; Suzuki, T.; Tokito, S. *Adv. Mater.* **2003**, *15*, 1455.
- (95) (a) Li, J.; Djurovich, P. I.; Alleyne, B. D.; Yousufuddin, M.; Ho, N. N.; Thomas, J. C.; Peters, J. C.; Bau, R.; Thompson, M. E. *Inorg. Chem.* **2005**, *44*, 1713; (b) Andreas F. Rausch; Mark E. Thompson; Yersin, H. *J. Phys. Chem. A* **2009**, *113*, 5927.
- (96) (a) Chang, C.-J.; Yang, C.-H.; Chen, K.; Chi, Y.; Shu, C.-F.; Ho, M.-L.; Yeh, Y.-S.; Chou, P.-T. *Dalton Trans.* **2007**, 1881; (b) Sajoto, T.; Djurovich, P. I.; Tamayo, A. B.; Oxgaard, J.; Goddard, W. A.; Thompson, M. E. *J. Am. Chem. Soc.* **2009**, *131*, 9813; (c) Howarth, A. J.; Davies, D. L.; Lelj, F.; Wolf, M. O.; Patrick, B. O. *Inorg. Chem.* **2014**, *53*, 11882.
- (97) Aoki, S.; Matsuo, Y.; Ogura, S.; Ohwada, H.; Hisamatsu, Y.; Moromizato, S.; Shiro, M.; Kitamura, M. *Inorg. Chem.* **2011**, *50*, 806.
- (98) Huo, S.; Deaton, J. C.; Rajeswaran, M.; Lenhart, W. C. *Inorg. Chem.* **2006**, *45*, 3155.
- (99) Tamayo, A. B.; Alleyne, B. D.; Djurovich, P. I.; Lamansky, S.; Tsyba, I.; Ho, N. N.; Bau, R.; Thompson, M. E. *J. Am. Chem. Soc.* **2003**, *125*, 7377.
- (100) (a) Le Bozec, H.; Guerchais, V. *C.R. Chim.* **2013**, *16*, 1172; (b) You, Y.; Nam, W. *Chem. Soc. Rev.* **2012**, *41*, 7061; (c) Liang, A.; Ying, L.; Huang, F. *J. Inorg. Organomet. Polym Mater.* **2014**, *24*, 905.

Chapter II: Synthesis of racemic and enantiopure cationic Iridium complexes for the formation of coordination networks

In this chapter, the synthesis of racemic and enantiopure cationic Iridium complexes based on two phenylpyridyl-derivatives (ppy) as cyclometallating ligands and one bipyridyl ligand bearing either pyridyl or carboxylate groups acting as peripheral coordinating sites will be described. Their use as metallatectons for the formation of coordination networks will be presented and different coordination networks formed upon their combinations with metal cations will be discussed.

1. Introduction

1.1 Preparation of cationic Ir(III) complexes as racemates

In the late 80s, a series of contributions from Watts and Güdel dealing with phosphorescent cyclometallated Iridium(III) complexes¹ demonstrated the relevance of Iridium(III) complexes to boost the performance of organic electroluminescence devices.² Since then, formation of octahedral Ir(III) complexes has known an ever growing interest and different ligands bearing oxygen and/or nitrogen donor atoms have been used.

As a third-row d⁶ transition metal, the synthesis of cyclometallated Iridium(III) proved to be difficult due to the great inertness of Iridium(III). As a consequence, harsh reaction conditions are sometimes required to substitute the classical chlorine ligands of the starting iridium dimeric salts. It is noteworthy that Iridium(III) is capable of forming a large range of complexes, including mono-, bis- and tris-cyclometallated complexes,³ and several cationic complexes have been reported with bidentate ligands, for instance, polyimine ligands⁴ and diphosphine⁵ ligands. Within the present chapter, the synthesis and characterization of cyclometallated Iridium(III) complexes bearing two cyclometallating C-N ligands and one N-N type chelate, *i.e.* 2,2'-bipyridine derivatives, will be discussed. The latter ligand being neutral, cationic complexes are obtained.

Cationic cyclometallated Ir(III) complexes are typically synthesized *via* a standard two-step procedure (Figure II-1). The first step, sometimes referred as the Nonoyama reaction,⁶ deals with the preparation of a bis-chloro-bridged dinuclear Iridium(III) complex by refluxing a mixture of aqueous and alcoholic solutions containing the HC-N ligand and hydrated Iridium (III) chloride. It should be noted that only the dimer depicted on Figure I-1, where all N atoms are in *trans* positions, is formed.⁷ The second step involves the substitution of the chloride atoms by a third bidentate neutral N-N ligand at RT to form heteroleptic mononuclear bis-cyclometallated cationic Iridium(III) complexes. Since,

starting from the chloro-bridged Ir(III) dimer, the synthesis of heteroleptic cationic Iridium(III) complexes with N-N type-ligands may be achieved under mild conditions, the formation of different isomers (*fac*, *mer*) may be avoided.

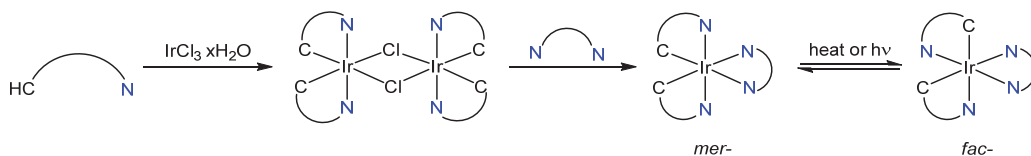


Figure II-1: Schematic representation of the two-step procedure for the formation of bis-cyclometallated cationic Ir(III) complexes bearing N-N ligand as the third ligand.

For the last decades, many reports have studied the reaction of the Ir dimer with different N-N ligands such as polypyridines⁸ or phenylpyrazoles⁹ leading to cationic Iridium(III) complexes. In most of the cases, solvents such as methanol, dichloromethane or acetonitrile are employed. Moreover, in order to facilitate the purification of the cationic complex, the chloride salt formed is converted into its PF₆ salt by metathesis with either NH₄PF₆ or KPF₆ aqueous solution. It should be noted that, although the synthetic strategy employed tends to control the formation of positional *fac*- or *mer*-isomers using Ir precursors with known stereochemistry, the optical isomerism, *i.e.* formation of Δ and Λ enantiomers, is not controlled leading thus to the cationic complex as a racemate.

1.2 Preparation of enantiopure Ir(III) cationic complexes

One of the challenges of this PhD project is the preparation of enantiopure Ir(III) cationic complexes. As briefly mentioned in the general introduction, in order to isolate enantiopure octahedral tris-chelate chiral complexes, different approaches have been followed. Thus, the use of chiral organic ligands may drive the formation of only one diastereoisomer (asymmetric synthesis) or allows the separation of pairs of diastereoisomers formed. In this approach, the chirality of the ligand is transferred to the metal centre. If the metal complex is charged, chiral resolution may be achieved employing chiral counter ions leading to the formation of pairs of diastereoisomers that can be separated by chromatography or by solubility differences. Another approach is based on a two-step procedure starting with the binding of an auxiliary enantiopure organic ligand such as oxazoline- or serine- derivatives to generate and subsequently separate the diastereoisomers. The second step is based on the replacement of the labile chiral ligand by one achiral bidentate or two achiral monodentate ligands.

In literature, examples regarding the preparation of enantiopure Ir(III) cationic complexes are scarce¹⁰ compared to other octahedral metal complexes such as Ru(II) complexes.¹¹ We shall give in the following section, an overview of the available methods already reported that can be of interest for our own study on cationic complexes.

In 2007, J.-P. Sauvage, J. Lacour and coworkers reported the separation of a binuclear bis-cyclometallated Ir(III) complex using Δ -TRISPHAT as chiral counter ions^{10a} (Figure II-2). Reaction of the enantiopure counter ion Δ -TRISPHAT with the binuclear Ir(III) complex afforded three different diastereoisomers (or diastereo ion-pairs) (a, b, c in Figure II-2). On preparative thin layer chromatography plates, three close and slightly overlapping bands were observed. The first two spots could be isolated with a decent diastereomeric excess and were assigned to the quasi-pure $\Lambda\Lambda$ - (b) and $\Delta\Delta$ - (a) diastereoisomers respectively.

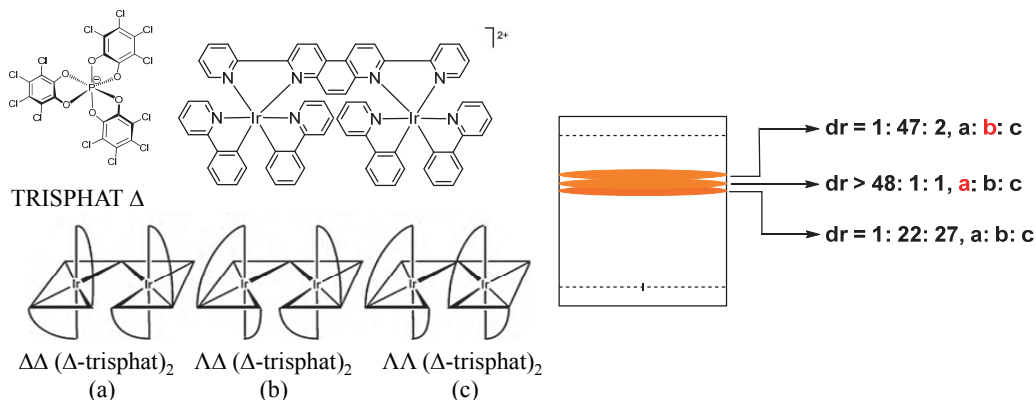


Figure II-2: Separation of a binuclear doubly charged Ir(III) complex using Δ -TRISPHAT as chiral counter ion.^{10a}

Another strategy dealing with the use of chiral labile auxiliary ligands was adopted recently by two groups in parallel.^{10b,12} This approach is based on a two-step procedure. First, the use of an enantiopure chiral auxiliary with the bis-cyclometallated chloro-bridged Ir dimer induces the formation of two diastereoisomers that can be separated by standard chromatography. The auxiliaries are either commercially available or easy-to-synthesize ligands. Again, it is worth noting that the Ir dimer employed in the first step consist only in the isomer where the Cl and C atoms are *trans* to each other.⁷ Three stereoisomers are thus possible for the Ir dimer ($\Delta\Delta$, $\Lambda\Lambda$ and the *meso* form, Figure II-3). Coordination of the chiral bidentate auxiliary leads thus to two diastereoisomers (Δ or Λ). The auxiliary is then removed without loss of the chirality centered on the metal and an achiral bidentate ligand (or two monodentate ligands) can be coordinated to the coordination sphere of the metal center.

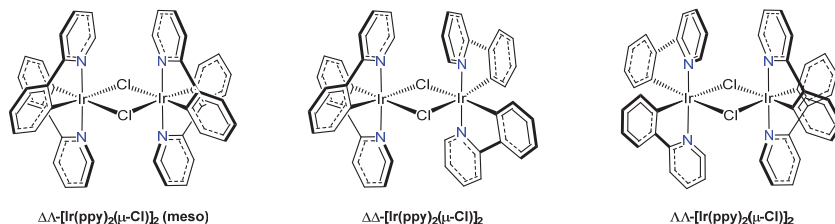


Figure II-3: Schematic representation of the stereoisomers of Iridium dimer bearing 2-phenylpyridine as cyclometallating ligand.

Following this approach, Lusby *et al.*¹² reported the use of L or D-serine as chiral ligands (Figure II-4) and achieved the resolution of the Ir(III) dimers. Thus, treatment of the dimer with L-serine afforded the two diastereoisomers Δ -[Ir(ppy)₂(L-serine)] and Λ -[Ir(ppy)₂(L-serine)] (abbreviated as $[\Delta, \text{L-serine}]$ and $[\Lambda, \text{L-serine}]$ respectively). The same holds when D-Serine is used. For each couple ($[\Delta, \text{L-serine}]$, $[\Lambda, \text{L-serine}]$ or $[\Delta, \text{D-serine}]$, $[\Lambda, \text{D-serine}]$), diastereoisomers were separated by column chromatography on silica gel. However, it is worth mentioning that the chromatographic separation of the intermediate serine-based diastereomeric complexes is quite tedious. Indeed, for the $[\Delta, \text{L-serine}]$, $[\Lambda, \text{L-serine}]$ couple, the first eluting diastereoisomer $[\Delta, \text{L-serine}]$ could be obtained analytically pure, whereas the slower eluting diastereoisomer corresponding to $[\Lambda, \text{L-serine}]$ was found to be always contaminated with $[\Delta, \text{L-serine}]$. Interestingly when using D-serine, the first eluting band which could be isolated as a pure compound was the $[\Lambda, \text{D-serine}]$ complex. Reformation of the chloro-bridged dimer was achieved by acid (HCl) treatment of $[\Delta, \text{L-serine}]$ or $[\Lambda, \text{D-serine}]$ to afford the enantiopure $\Delta\Delta$ - or $\Lambda\Lambda$ -[Ir(ppy)₂(μ -Cl)]₂ dimers. The enantiopure dimers were then combined with no loss of chirality at RT with 1,3,5-tricyanobenzene to form enantiopure coordination capsules.

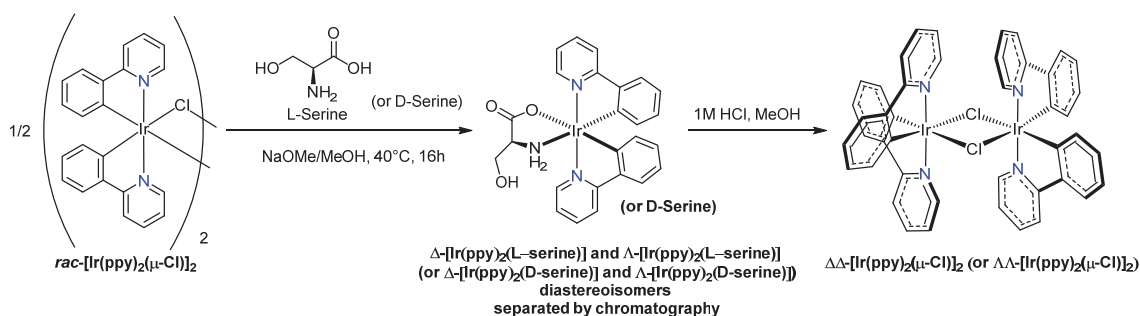


Figure II-4: Two-step procedure employed for the asymmetric synthesis of chiral octahedral tris-chelate Ir complexes using L- and D-Serine.¹²

On the other hand, Meggers *et al.*^{10b} used (S)-thiazoline-derived ligands (Figure II-5) to form two diastereoisomers (Δ , S and Λ ,S) that could be separated by chromatography. In a second step, stereospecific substitution of the chiral auxiliary by two acetonitrile molecules upon protonation with NH_4PF_6 afforded either the Δ -**3** or Λ -**3** pure enantiomers (ee > 99 %). These complexes have been used as asymmetric catalyst.^{10b,13}

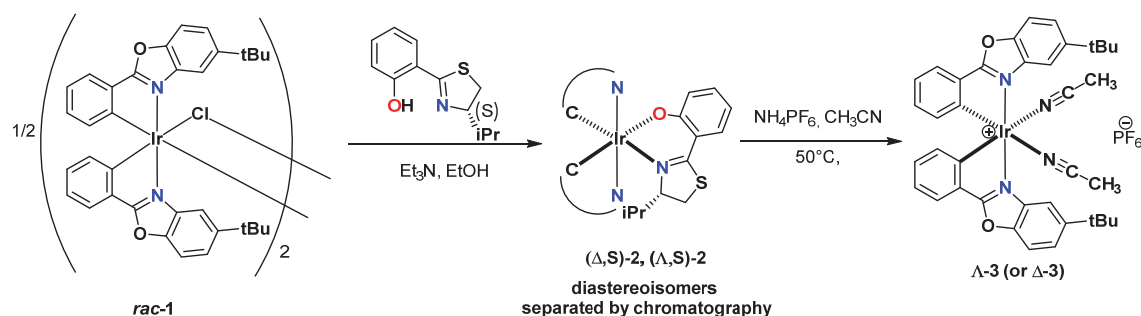


Figure II-5: Two-step procedure employed for the asymmetric synthesis of chiral octahedral tris-chelate Ir complexes using chiral thiazoline derivatives.^{10b}

In both cases, diastereoisomers were separated by standard silica gel chromatography and after replacement of the chiral auxiliary by achiral ligands, the enantiopure chiral-at-metal complex bearing only achiral ligands were obtained. Such “stereogenic at the metal” complexes are ideal precursors to generate more sophisticated enantiopure Ir(III) complexes. It should be noted that, under mild conditions, the two chiral complexes ($\Lambda\Lambda$ -[Ir(ppy)₂(μ -Cl)]₂ and Λ -3) are configurationally stable, *i.e.* no racemization of the complex occurs. Even for Λ -3 bearing two labile acetonitrile ligands, no configurational lability or decomposition was observed in solution.

1.3 Formation of coordination networks based on cationic Iridium complexes

Although several coordination networks based on bis-cyclometallated Ir(III) complexes as metalloligands¹⁴ or doping moieties have been reported, only few of them deal with cationic Iridium complexes. To the best of our knowledge, all the examples were reported by three groups: Lin *et al.*,¹⁵ Ho *et al.*,¹⁶ and Luo *et al.*¹⁷

For the reported examples, the Ir(III) complexes used as metallatectons were mainly functionalized with peripheral carboxylate groups as coordinating sites and were always used as racemates. As stated by Lin *et al.*¹⁸ in some cases, the disordered nature of the solvent molecules and counter ions in the MOF channels prevented their identification by single crystal X-Ray diffraction and only modeled structures based on Powder X-ray Diffraction (PXRD) and comparison with similar frameworks were reported.¹⁸ As previously reported for other coordination networks, the counter ions and the crystallization solvent used to form the periodic architectures influence the final architecture. Thus, in 2015, Ho *et al.*^{16b} described the formation of different heterometallic coordination polymers obtained upon combining Pb(II) salts with a bis-cyclometallated Ir(III) complex functionalized with a 2,2'-bipyridine chelate bearing two carboxylic groups. Varying the counter ions and/or the solvents afforded different networks.

Here, a selected example published by Luo *et al.*^{17a} in 2013 will be presented. A stable Zn(II)-Ir(III) heterometallic coordination network was obtained upon combining the Ir(III) complex

$[\text{Ir}(\text{ppy})_2(\text{dcbpy})]$ (ppy = 2-phenylpyridine, dcbpy = 2,2'-bipyridyl-4,4'-dicarboxylate) bearing peripheral carboxylic acid and $\text{Zn}(\text{NO}_3)_2$ acting as the metallic node (Figure II-6). Single crystals suitable for X-ray diffraction were generated. As depicted in Figure II-6a, the Zn atom adopts a tetrahedral coordination geometry and is coordinated to four carboxylate groups belonging to four different metallatectons. Each Ir complex bridges two Zn atoms forming a double stranded chain (Figure II-6a, dcbpy ligands belonging to either chain are colored in red or blue). The 3-D packing reveals the formation of pores within the architecture. The authors further investigated the luminescence properties of the MOFs and their application as sensor for nitroaromatic explosives. This highly luminescent (Zn,Ir)-MOF (solid state quantum yield of *ca.* 24 %) possesses good sensitivity for explosive molecules such as TNT in the ppm range. Indeed, quenching of the fluorescence originating from the MOF is observed even by naked eye.

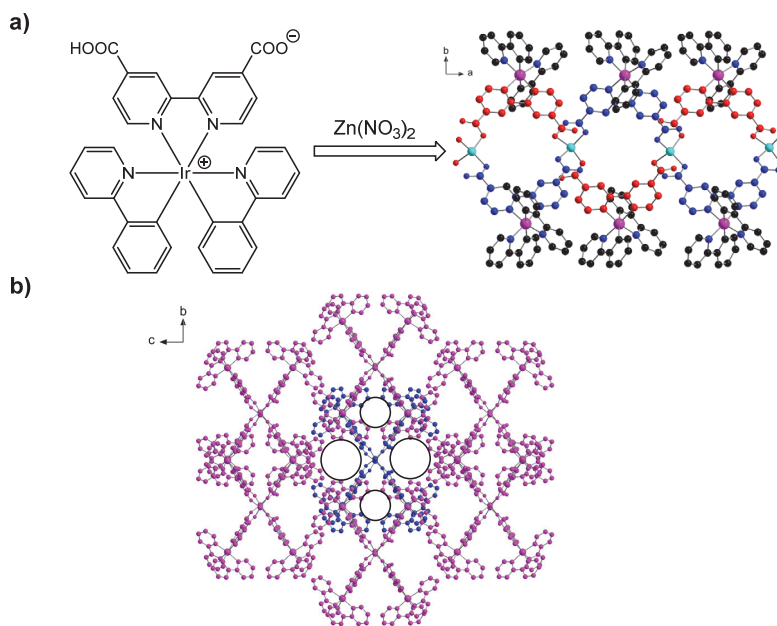


Figure II-6: Chemical structure of the Ir complex $[\text{Ir}(\text{ppy})_2(\text{dcbpy})]^+$ (a) and portions of the X-ray structure of $[\text{Ir}(\text{ppy})_2(\text{dcbpy})]$ -Zn MOF showing the torsional double-stranded chain structure (dcbpy units colored in red or blue for each chain)(a) and the 3D packing along the a axis and potential pores within the lattice (b).^{17a} Solvent molecules and H atoms have been omitted for clarity.

Thus, as exemplified above; Ir(III) complexes are ideal candidates as luminescent metallatectons to generate heterometallic coordination polymers. Furthermore, for sensing purposes, the presence of larger pores in the crystalline material should be of interest. In order to achieve this goal, one possibility could be to extend the bipyridyl ligand and add a spacer between the peripheral coordinating sites and the central bipyridine. Moreover, as mentioned earlier, octahedral tris-chelate Ir(III) complexes are intrinsically chiral. However, this interesting property has not been exploited so far. In the following sections, the synthesis and characterization of Ir(III) complexes as racemate and

enantiomerically pure species bearing terminal pyridyl moieties ($[\text{Ir}(\text{ppy})_2(\text{bpy-4})]^+$ and $[\text{Ir}(\text{dFppy})_2(\text{bpy-4})]^+$) or carboxylate groups ($[\text{Ir}(\text{ppy})_2(\text{bpy-7})]^+$) will be presented (Figure II-7). The heterometallic coordination networks obtained using these metallatectons will be discussed as well.

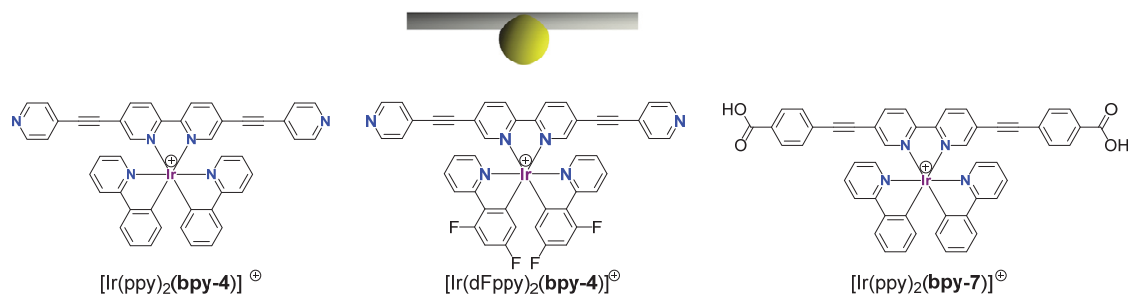


Figure II-7: Chemical structures of the three cationic Ir(III) complexes and the schematic representation of the linear metallatecton.

2. Synthesis and characterization of the Ir(III) complexes based on terminal pyridyl coordinating sites as racemates

2.1 Design and retrosynthesis

The design of the Ir(III) complex is based on an achiral extended 5,5'-substituted-2,2'-bipyridyl **bpy-4** (Figure II-8). The 2,2'-bipyridyl (bpy) unit is thus equipped in positions 5 and 5' with two 4-ethynylpyridyl moieties acting as peripheral coordinating sites. The presence of acetylene bridges enables the two peripheral pyridine groups to be coplanar to the bipyridyl central unit, inducing thus extension of conjugation. The other two bidentate ligands completing the coordination sphere of the Ir atom are either 2-phenylpyridyl (ppy) or 2-(2,4-difluorophenyl)pyridyl (dFppy) units.

Such complexes should be luminescent providing thus the possibility of sensing guest molecules within the voids of the porous architecture that may be formed upon self-assembly with metallic nodes. Moreover, insertion of fluorine atoms within the 2-phenylpyridyl (ppy) scaffold should induce a hypsochromic shift of the emission¹⁹ relative to its non-fluorinated analogue $[\text{Ir}(\text{ppy})_2(\text{bpy-4})]^+$ ensuring emission in the visible range. These metallatectons should behave as linear bridging units.

As mentioned before, the standard procedure to obtain cationic bis-cyclometallated Iridium(III) complexes with bipyridyl derivatives as the third ligand is based on the reaction of the dichloro-bridged Iridium dimers bearing the cyclometallating unit with the third bipyridyl ligand. For the formation of the desired complexes, $[\text{Ir}(\text{ppy})_2(\text{bpy-4})]^+$ and $[\text{Ir}(\text{dFppy})_2(\text{bpy-4})]^+$, two synthetic pathways have been followed depending on the cyclometallating unit employed (Figure II-8). The final organic ligand **bpy-4** may be directly coordinated to the Ir dimer (path A) or the 5,5'-dibromo-2,2'-bipyridyl ligand (**bpy-1**) may be first coordinated to the Ir dimer and the complex thus formed

subject to a Sonogashira coupling reaction to obtain the desired final complex (path B). Both pathways have been successful depending on the cyclometallating unit used.

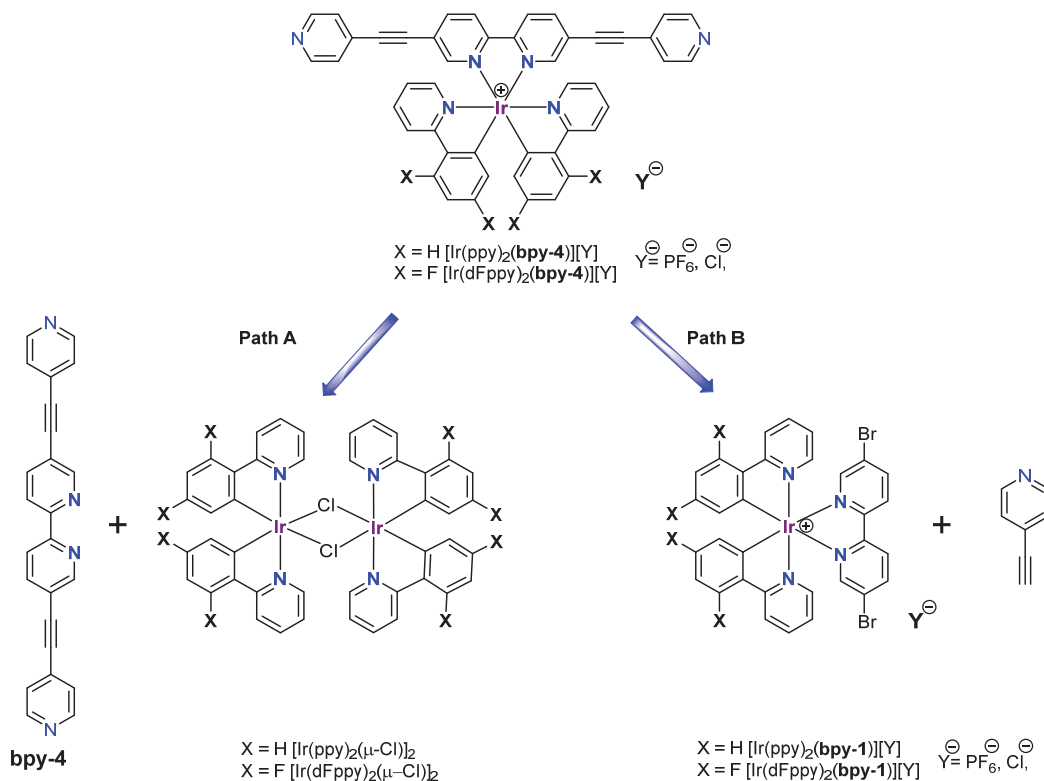


Figure II-8: Two possible retrosynthetic pathways to obtain the desired cationic Ir(III) complexes.

2.2 Synthesis of the racemic complexes *rac*-[Ir(ppy)₂(bpy-4)][PF₆] and *rac*-[Ir(dFppy)₂(bpy-4)][PF₆]

For the two strategies presented above, the synthesis of the Ir(III) dimers is a prerequisite. Thus, the dichloro-bridged Iridium dimer *rac*-[Ir(ppy)₂(μ-Cl)]₂⁷ and *rac*-[Ir(dFppy)₂(μ-Cl)]₂²⁰ were prepared following the procedure described in the literature starting from IrCl₃·xH₂O and the desired cyclometallating unit (Figure II-9). While 2-phenylpyridine is commercially available, ligand dFppyH was synthesized *via* a Suzuki coupling reaction as already reported.²¹ It is worth noting that for the formation of *rac*-[Ir(dFppy)₂(μ-Cl)]₂, the time of reaction (around 15 to 20 hours) is crucial as further refluxing increases the formation of other isomers or even partially defluorinated compounds (as evidenced by ¹⁹F NMR).²² As expected, the two Ir dimers were isolated as three stereoisomers (ΔΔ, ΛΛ and the *meso* form) with, in all three cases, the C atoms located in *trans* positions with respect to the Cl atoms.

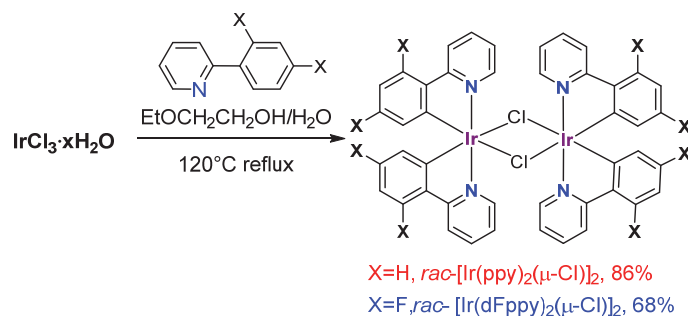


Figure II-9: Synthesis of $\text{rac-}[\text{Ir}(\text{ppy})_2(\mu\text{-Cl})]_2$ ⁷ and $\text{rac-}[\text{Ir}(\text{dFppy})_2(\mu\text{-Cl})]_2$ ²⁰

The two other precursors needed for the formation of the desired final Ir complex are the organic ligands **bpy-1** and **bpy-4** (Figure II-10).

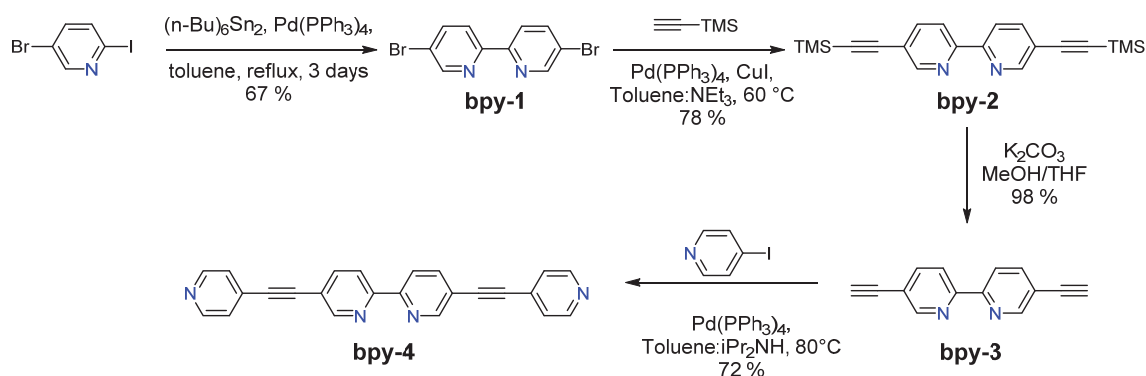
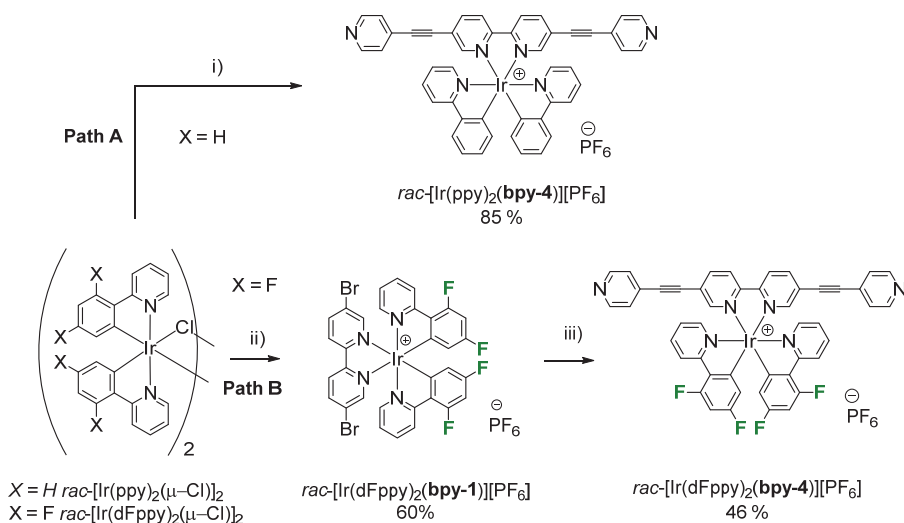


Figure II-10: Synthesis of ligands **bpy-i** (*i* = 1-4).

First, a homo-coupling reaction of 2-iodo-5-bromopyridine in the presence of the palladium catalyst $\text{Pd}(\text{PPh}_3)_4$, and 0.5 equivalent of the organotin reagent $\text{Sn}_2(\text{n-Bu})_6$, to generate *in-situ* the organostannane intermediate, in refluxing toluene afforded **bpy-1** in 67 % yield.²³ For the synthesis of **bpy-4**, starting from **bpy-1**, three other coupling and protection/deprotection steps are required. The ligand **bpy-3** was obtained in 76 % overall yield following the procedure described by Leigh *et al.*²³ by first a Sonogashira coupling reaction between **bpy-1** and ethynyltrimethylsilane in the presence of $\text{Pd}(\text{PPh}_3)_4$ and CuI followed by deprotection of the ethynyl groups with K_2CO_3 as a base. The last step leading to the final organic ligand **bpy-4** in 72% yield is again a Sonogashira reaction between **bpy-3** and 4-iodopyridine in the presence of $\text{Pd}(\text{PPh}_3)_4$ as catalyst. The overall yield starting from 5-bromo-2-iodopyridine is *ca* 37 %. It is interesting to note that no copper salt was necessary for the last coupling reaction. Furthermore, the last synthetic step had to be optimized to reach a decent yield and different coupling reaction conditions were tested (solvents and base: DMF, toluene, Et_3N ; catalyst: $\text{Pd}(\text{PPh}_3)_4$, $\text{Pd}(\text{PPh}_3)_2(\text{Cl})_2$; reaction temperatures : 60 °C to 120 °C). All **bpy-i** (*i* = 1-4) ligands were characterized by standard techniques ($^1\text{H-NMR}$, $^{13}\text{C-NMR}$, IR and elemental analysis).

Having the organic ligand **bpy-4** in hand, the first synthetic approach (path A, Figure II-11) was attempted to form the two desired Ir complexes.

The Iridium complex bearing the non-fluorinated cyclometallating units, $rac\text{-}[\text{Ir}(\text{ppy})_2(\text{bpy-4})][\text{PF}_6]$ was prepared in 85 % yield by reaction between the dichloro-bridged Iridium dimer $rac\text{-}[\text{Ir}(\text{ppy})_2(\mu\text{-Cl})_2]$ and ligand **bpy-4** (Figure II-11). The conditions used were adapted from those described by S. Bernhard *et al.*²⁴. Indeed, instead of using a mixture of dichloromethane and methanol as solvents, few drops of acetonitrile were added. As a result, the yield increased from 40 % to 85 % (overall yield obtained after metathesis of the chloride ions using an aqueous KPF_6 solution in both cases). This may be due to either a better solubility of the final product $rac\text{-}[\text{Ir}(\text{ppy})_2(\text{bpy-4})][\text{Cl}]$ in acetonitrile, or because acetonitrile, as a weakly coordinating solvent, may facilitate the cleavage of the chloro-bridged dimer. The final complex $rac\text{-}[\text{Ir}(\text{ppy})_2(\text{bpy-4})][\text{PF}_6]$ was characterized by standard techniques (^1H -NMR, ^{13}C -NMR, HRMS). Dark red single crystals suitable for X-ray diffraction were obtained in *ca.* four days by vapor diffusion of diethyl ether into a concentrated solution of the complex in acetonitrile (Figure II-12).



i) 1) **bpy-4**, $\text{CH}_2\text{Cl}_2/\text{CH}_3\text{OH}/\text{CH}_3\text{CN}$ 3/3/1, 60°C ; 2) KPF_6 , H_2O , 70°C ; ii) **bpy-1**, $\text{CH}_2\text{Cl}_2/\text{CH}_3\text{OH}$ 1/1, 60°C , 2) KPF_6 , H_2O , 70°C ; iii) 4-ethynylpyridine, $\text{Pd}(\text{PPh}_3)_4$, CuI , $\text{toluene}/\text{CH}_3\text{CN}/i\text{Pr}_2\text{NH}$ 40/3/16, 60°C .

Figure II-11: Synthesis of $rac\text{-}[\text{Ir}(\text{ppy})_2(\text{bpy-4})][\text{PF}_6]$ and $rac\text{-}[\text{Ir}(\text{dFppy})_2(\text{bpy-4})][\text{PF}_6]$.

Whereas path A was successful for the non-fluorinated complex $rac\text{-}[\text{Ir}(\text{ppy})_2(\text{bpy-4})][\text{PF}_6]$, and despite several attempts, this synthetic route turned out to be unsuccessful for the fluorinated complex $rac\text{-}[\text{Ir}(\text{dFppy})_2(\text{bpy-4})][\text{PF}_6]$. Indeed, as evidenced by ^{19}F -NMR which revealed the presence of more than the two signals expected for the F atoms located on the dFppy moieties, different fluorinated complexes were generated. Furthermore, mass spectrometry also revealed that different unknown products were formed. Purification by chromatography and recrystallization was attempted but was found to be unfeasible since the R_f values were too close.

Thus, the complex $rac\text{-}[\text{Ir}(\text{dFppy})_2(\text{bpy-4})][\text{PF}_6]$ was prepared *via* path B, consisting in coordination of the bromo derivative **bpy-1** followed by a coupling reaction performed on the

complex (Figure II-11). Complex *rac*-[Ir(dFppy)₂(bpy-1)][PF₆] could be obtained by reaction of *rac*-[Ir(dFppy)₂(μ-Cl)]₂ with ligand **bpy-1** in a mixture of dichloromethane and methanol at 60 °C overnight. In this case, the small proportion of unknown fluorinated complexes present as impurities could be removed by recrystallization. The pure complex *rac*-[Ir(dFppy)₂(bpy-1)][PF₆] was then reacted with 4-ethynylpyridine²⁵ to afford the final coupling product *rac*-[Ir(dFppy)₂(bpy-4)][PF₆] in *ca.* 46 % yield. The latter was characterized by standard techniques (¹H-NMR, ¹³C-NMR, HRMS). Orange single crystals suitable for X-ray diffraction were obtained by slow vapor diffusion of diethyl ether into a concentrated acetonitrile solution of *rac*-[Ir(dFppy)₂(bpy-4)][PF₆] in *ca.* one week (Figure II-14).

2.3 Characterization of *rac*-[Ir(ppy)₂(bpy-4)][PF₆] and *rac*-[Ir(dFppy)₂(bpy-4)][PF₆] as racemates

As mentioned earlier, all compounds were characterized by standard techniques including NMR. They all exhibit the expected features. Here, only the detailed X-ray structures for the two final complexes as well as their luminescent properties in solution and in the solid state are discussed. These features are of importance for the formation of heterometallic luminescent coordination networks.

A-Crystal structure of rac-[Ir(ppy)₂(bpy-4)][PF₆]

Dark red single crystals suitable for X-ray diffraction were obtained by vapor diffusion of Et₂O into a CH₃CN solution of the complex. Because of the severe disorder of solvent molecules of *rac*-[Ir(ppy)₂(bpy-4)][PF₆], the SQUEEZE command²⁶ was employed to remove the corresponding electron density. Complex *rac*-[Ir(ppy)₂(bpy-4)][PF₆] crystallizes in the triclinic system with *P*-1 as the space group (Figure II-12). The geometrical parameters (Table II-1) are similar to those described for other similar Iridium(III) complexes containing ppy and bpy ligands (bpy = 2,2'-bipyridyl).²⁷ The Ir center adopts a slightly distorted octahedral coordination geometry (see Table 1 for distances and angles) with the expected *trans* arrangement of the N donor atoms and *cis* arrangement of the C donor atoms of the cyclometallated ligand.^{1b,28} All three ligands are almost planar (average dihedral angle N-C-C-N of *ca.* -0.322° for the bpy ligand and N-C-C-C angle in the range -6.480 to 1.956 for the ppy ligands). The ethynyl spacers between the central and terminal pyridyl units of the bipyridyl ligand are almost linear (C-C-C angles in the 175.358-179.024° range) and the terminal pyridyl units are almost coplanar to the bpy unit. It should be noted that both enantiomers, Δ and Λ, are present in the structure as indicated by the achiral space group. The length of the metallatecton, *i.e.* the distance between the two N atoms of the terminal pyridyl units, is *ca.* 20.6 Å.

Table II-1: Selected average bond lengths (Å) and angles (°).

| | <i>rac</i> -[Ir(ppy) ₂ (bpy-4)][PF ₆] |
|---------------------------------------|--|
| Ir-C _{ppy} | 2.007 Å |
| Ir-N _{ppy} | 2.043 Å |
| Ir-C _{bpy} | 2.143 Å |
| N _{ppy} -Ir-N _{ppy} | 172.31° |
| N _{ppy} -Ir-C _{ppy} | 80.25° |
| N _{bpy} -Ir-N _{bpy} | 76.50° |

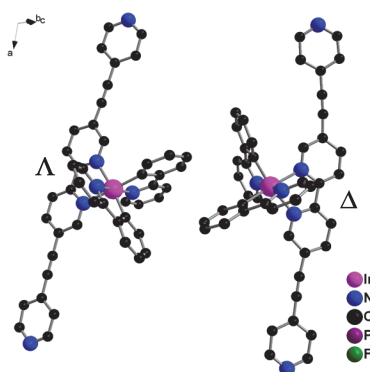


Figure II-12: Crystal structure of *rac*-[Ir(ppy)₂(bpy-4)][PF₆] showing the disposition of the two enantiomers in the lattice. Hydrogen atoms and PF₆⁻ ions as well as solvent molecules are omitted for clarity.

Furthermore, within the crystal, two crystallographically non-equivalent Ir complexes are present. Different π - π interactions between two neighboring **bpy-4** units belonging either to two Δ or two Λ enantiomers (shortest C-C distance of 3.496 Å for the two **bpy-4** ligands of two adjacent Δ enantiomers and 3.576 Å for the Λ enantiomers, for the Δ enantiomers, **bpy-4** ligands are colored in green and for the Λ enantiomers in orange) or between ppy ligands belonging to one Δ enantiomer and a neighboring Λ enantiomer (shortest C-C distance of 3.469 Å) are present in the lattice (Figure II-13a and b respectively).

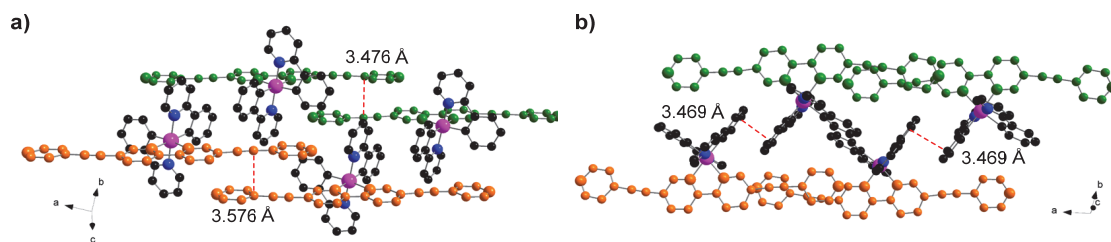


Figure II-13: Portions of the X-ray crystal structure of *rac*-[Ir(ppy)₂(bpy-4)][PF₆] showing the π - π interactions observed (red dashed lines) between bpy moieties (a) and ppy moieties (b). **bpy-4** ligands are colored in green for the Δ enantiomer and orange for the Λ enantiomer. Hydrogen atoms and PF₆⁻ ions as well as solvent molecules are omitted for clarity.

B-Crystal structure of *rac*-[Ir(dFppy)₂(bpy-4)][PF₆]

Orange single crystals suitable for X-ray diffraction were obtained by slow vapor diffusion of Et₂O into a CH₃CN solution of *rac*-[Ir(ppy)₂(bpy-4)][PF₆]. Complex *rac*-[Ir(dFppy)₂(bpy-4)][PF₆] also crystallizes in the triclinic system with *P*-1 as space group and exhibits similar geometrical parameters as for *rac*-[Ir(ppy)₂(bpy-4)][PF₆] (Figure II-14 and Table II-2). The substituted bipyridyl ligand is again almost planar and the ethynyl junctions are almost linear (C-C-C angles in the range 174.37 to 180.00°). As expected, both enantiomers are present in structure. As observed for the non-fluorinated analogue, the length of the metallatecton is *ca.* 20.6 Å.

Table II-2: Selected average bond lengths (Å) and angles (°).

| | <i>rac</i> -[Ir(ppy) ₂ (bpy-4)][PF ₆] |
|---------------------------------------|--|
| Ir-C _{ppy} | 2.011 |
| Ir-N _{ppy} | 2.041 |
| Ir-C _{bpy} | 2.136 |
| N _{ppy} -Ir-N _{ppy} | 171.71 |
| N _{ppy} -Ir-C _{ppy} | 80.65 |
| N _{bpy} -Ir-N _{bpy} | 76.81 |

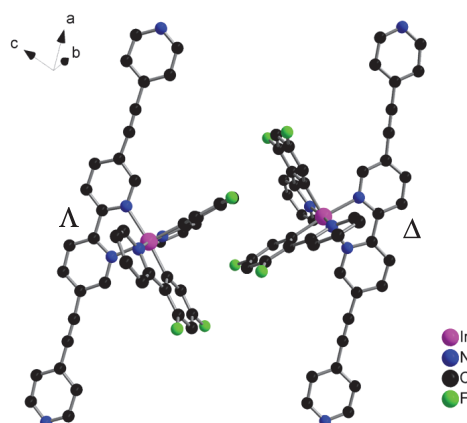


Figure II-14: X-ray crystal structure of *rac*-[Ir(dFppy)₂(bpy-4)][PF₆] showing the disposition of the two enantiomers in the lattice. Hydrogen atoms and PF₆⁻ ions as well as solvent molecules are omitted for clarity.

Similar to the non-fluorinated complex, within the crystal, two crystallographically non-equivalent Ir complexes are present. π - π interactions between the substituted bpy ligand belonging to two Δ enantiomers or two Λ enantiomers are also observed (shortest C-C distance 3.55 Å and 3.59 Å for the two non-equivalent Ir complexes) (Figure II-15).

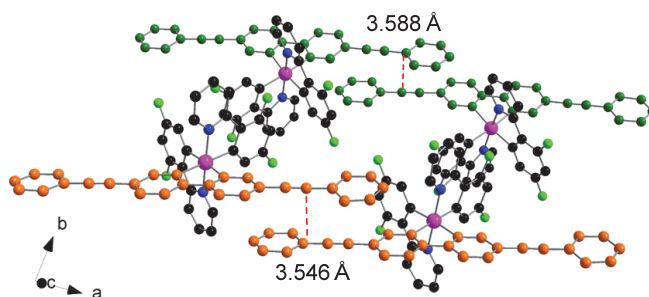


Figure II-15: Portions of the X-ray crystal structure of *rac*-[Ir(dFppy)₂(**bpy-4**)]PF₆ showing the π interactions (red dashed lines, **bpy-4** ligands are colored in green and orange for the Λ and Δ enantiomers respectively). Hydrogen atoms and PF₆⁻ ions as well as solvent molecules are omitted for clarity.

*C-Luminescent properties of *rac*-[Ir(ppy)₂(**bpy-4**)]PF₆ and *rac*-[Ir(dFppy)₂(**bpy-4**)]PF₆*

The photophysical properties of complexes *rac*-[Ir(ppy)₂(**bpy-4**)]PF₆ and *rac*-[Ir(dFppy)₂(**bpy-4**)]PF₆ were studied in solution as well as in the solid state (Figure II-16 and Table II-3).

rac-[Ir(ppy)₂(**bpy-4**)]PF₆ exhibits an intense absorption band between 240 and 450 nm in solution (Figure II-16a). This band can be attributed to spin-allowed ligand-centered (LC) transitions involving the ppy and the bpy moieties with a contribution of MLCT and LLCT (metal or ligand-to-ligand charge transfer) transitions as described previously.^{27a} In comparison, *rac*-[Ir(dFppy)₂(**bpy-4**)]PF₆ exhibits slightly blue shifted (*ca.* 5 nm) absorption bands (Figure II-16a). This can be rationalized by the strong electron-withdrawing nature of fluorine atoms in positions 2 and 5 on the dFppy units which could largely stabilize the HOMO by removing electron density from the Ir(III) metal centers.²⁹ Furthermore, the relatively intense absorption band around 300-360 nm is probably due to π - π^* transitions and conjugation over the bpy moieties as evidenced by the absence of this band in the absorption spectrum of *rac*-[Ir(dFppy)₂(**bpy-1**)]PF₆ (Figure II-16a) and as already observed on similar complexes bearing *p*-phenylene substituted bpy ligands.³⁰ In the solid state (Figure II-16c), a strong absorption band between 250 and 700 nm arising from LC, MLCT and LLCT transitions is observed.

The photoluminescence emission spectra recorded for *rac*-[Ir(ppy)₂(**bpy-4**)]PF₆ in degassed THF (Figure II-16b) and in the solid state (Figure II-16d) show an unstructured broad band with a maximum at *ca.* 695 nm (677 nm in the solid state), characteristic of charge transfer electronic transitions. As for the analogous compound [Ir(ppy)₂(bpy)]PF₆ (bpy = 2,2'-bipyridyl), the emission may be assigned to a mixture of ³MLCT (Ir→bpy) and ³LLCT (ppy→bpy) transitions.^{27a,31} The bathochromic shift observed compared to [Ir(ppy)₂(bpy)]PF₆ (λ_{em} = 590 nm, RT, THF)^{30a} can be attributed to the delocalization of the bipyridyl π system, stabilizing the LUMO as already described

in solution for ppy-cyclometallated Ir complexes bearing 2,2'-bipyridine ligand substituted in positions 5 and 5' with aryl rings^{27d} or oligo(arylene ethynylene) units.^{30a,c} Finally, in the solid state, a quantum yield (QY) of *ca.* 3 % was determined (Table II-3). This relatively weak QY value might be related to the presence of π - π interactions, as evidenced in the crystal structure, quenching thus partially the solid state emission. It should be noted that the PXRD pattern of the sample used for the luminescence measurements matches the simulated pattern based on the single crystal structure. Due to its rather photo-instability in solution, it was not possible to determine an accurate QY in solution.

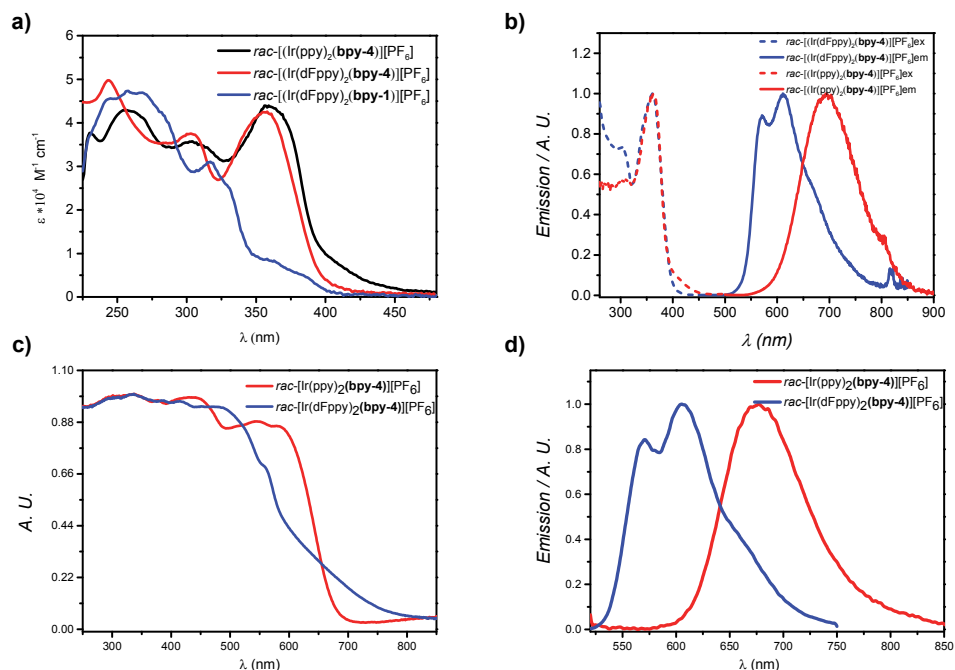


Figure II-16: Absorption spectra (a), excitation (dashed lines) and emission (solid lines) spectra in solution (b), reflectance spectra in the solid state (c) and emission spectra in the solid state (d) for *rac*-[Ir(ppy)₂(bpy-4)][PF₆] (red) and *rac*-[Ir(dFppy)₂(bpy-4)][PF₆] (blue).

Table II-3: Photophysical properties of *rac*-[Ir(ppy)₂(bpy-4)][PF₆] and *rac*-[Ir(dFppy)₂(bpy-4)][PF₆].

| Complexes | Absorption (CH ₃ CN, RT) | Absorption (THF, RT) | Emission (deaerated THF, RT) ^a | | | Emission (Solid, RT) ^c | |
|--|--|--|--|----------------|--------|--------------------------------------|-----|
| | λ (nm) (ε 10 ³ M ⁻¹ .cm ⁻¹) | λ (nm) (ε 10 ³ M ⁻¹ .cm ⁻¹) | λ (nm) | Φ ^b | τ (ns) | λ (nm) | Φ |
| <i>rac</i> -[Ir(ppy) ₂ (bpy-4)][PF ₆] | 256 (43.8), 303 (37.4), 359 (45.9). | 303 (40.4), 359 (48.8) | 694 | <i>n.d.</i> | 31 | 667 | 3 % |
| <i>rac</i> -[Ir(dFppy) ₂ (bpy-4)][PF ₆] | 243 (49.8), 303 (37.5), 356 (42.4). | 362 (45.2) | 571, 611 | 30 % | 1973 | 570, 605 | 2 % |

a: excited at 365 nm; b: using [Ru(bpy)₃][Cl]₂ as reference (Φ = 0.095 in deaerated CH₃CN)³²; c: excited at 390 nm; *n.d.* = not determined

In comparison with *rac*-[Ir(ppy)₂(**bpy-4**)]PF₆, *rac*-[Ir(dFppy)₂(**bpy-4**)]PF₆ exhibits emission peaks which are blue shifted by *ca.* 80 nm (Figure II-16b). Again, this hypsochromic shift is related to the presence of the strongly electron withdrawing F atoms on the dFppy ligand, stabilizing the HOMO as already reported for the analogue complex [Ir(dFppy)₂(bpy)]PF₆ (λ_{em} = 534 nm, RT, degassed CH₃CN) (bpyH₂ = unsubstituted 2,2'-bipyridyl).^{30b} However, unlike *rac*-[Ir(ppy)₂(**bpy-4**)]PF₆, it shows a structured band with two maxima at *ca.* 570 and 605 nm. In a first approximation, the emission could be attributed to a mixture of ³MLCT (Ir→bpy) and ³LLCT (ppy→bpy) transitions³¹ as described for [Ir(dFppy)₂(bpyH₂)]⁺. However, for *rac*-[Ir(dFppy)₂(**bpy-4**)]PF₆, owing to the structured emission, an increased ligand-centred character may be assumed for the lowest excited state. When compared to [Ir(dFppy)₂(bpyH₂)]⁺, a bathochromic shift is observed for *rac*-[Ir(dFppy)₂(**bpy-4**)]PF₆. Again, this may be attributed to the delocalization of the bipyridine π system, stabilizing its LUMO. It should also be noted that in solution, the emission lifetime is similar for *rac*-[Ir(dFppy)₂(**bpy-4**)]⁺ (τ = 1973 ns in degassed THF and τ = 1522 ns in degassed CH₃CN) and [Ir(dFppy)₂(bpyH₂)]⁺ (τ = 1,50 μ s, degassed CH₃CN)^{30b}. Finally, at room temperature, the complex *rac*-[Ir(dFppy)₂(**bpy-4**)]PF₆ exhibits in degassed THF solution and in the solid state quantum yields (QY) of 30 % and 2 % respectively. As described above for *rac*-[Ir(dFppy)₂(**bpy-4**)]PF₆, the presence of π - π interactions may account for the low QY in the solid state. It should be noted that the PXRD study of the sample used for the luminescence measurements in the solid state showed that the phase was pure.

3. Asymmetric synthesis and characterization of the enantiopure Ir(III) complexes based on terminal pyridyl coordinating sites

In this part, the different attempts to prepare enantiopure Ir(III) complexes using different methods will be discussed. Then, characterizations of those Ir(III) complexes, in particular by circular dichroism and single X-ray diffraction, will be reported.

3.1 Synthesis of the enantiomerically pure Ir precursors

A-Brief summary of the different strategies employed

In order to prepare the enantiopure Iridium complexes, Δ - and Λ -[Ir(ppy)₂(**bpy-4**)]PF₆ and Δ - and Λ -[Ir(dFppy)₂(**bpy-4**)]PF₆, chiral resolution of the racemic complexes or asymmetric synthesis should be performed. Besides standard techniques such as chiral HPLC, chiral resolution of metal complexes can be achieved employing two different methods based on either chiral counter ions (*e.g.* TRISPHAT and BINPHAT) or chiral ligands (*e.g.* oxazoline or amino-acids derivatives). These two methods were already successful in obtaining cyclometallated Iridium(III) complexes as presented in the introduction above.

Thus, as shown in Figure II-17, two approaches were tried to achieve either chiral resolution of the desired final cyclometallated Iridium(III) complexes (approach A) or their asymmetric synthesis using enantiopure metal complex precursors resolved using chiral auxiliary ligands (approach B).

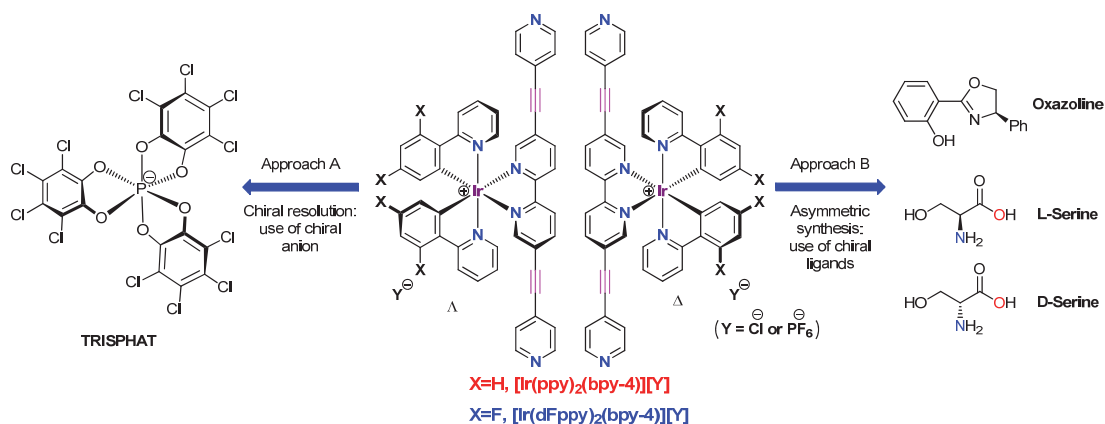


Figure II-17: Approaches attempted for the chiral resolution (A) or asymmetric synthesis (B) of the enantiopure Ir(III) complexes.

B-Approach A: use of chiral anions for the chiral resolution of the final Ir(III) complexes

As commented earlier, chiral resolution of cationic metal complexes may be achieved employing chiral counter ions such as TRISPHAT or BINPHAT leading to the formation of pairs of diastereoisomers that may be separated by chromatography or by solubility differences.

Thus, utilizing enantiopure TRISPHAT and BINPHAT as chiral anions with *rac*- $[\text{Ir}(\text{ppy})_2(\text{bpy-4})][\text{PF}_6]$ or *rac*- $[\text{Ir}(\text{dFppy})_2(\text{bpy-4})][\text{PF}_6]$ may enable separation of the different types of ion pairs formed by column chromatography or crystallization. It is worth noting that, because chiral BINPHAT is much more difficult to be prepared in large quantity than TRISPHAT,³³ BINPHAT is commonly used as chiral resolving agent in ^1H -NMR studies but not as reagent for the separation of enantiomers. It is indeed an efficient enantiodifferentiating agent in ^1H -NMR as long as the two enantiomers signals are differentiated upon formation of the two diastereo-ion pairs.³⁴

Thus, one equivalent of (Λ ,R)-BINPHAT was added to a CD_3CN solution of *rac*- $[\text{Ir}(\text{ppy})_2(\text{bpy-4})][\text{PF}_6]$ to study the influence of the chiral anion on the NMR spectrum of the complex. The two diastereo-ion pairs signals were differentiated. Indeed, some of the proton signals of *rac*- $[\text{Ir}(\text{ppy})_2(\text{bpy-4})][\text{PF}_6]$ were split proving thus the formation of the two diastereo-ion pairs (Figure II-18). However, no notable differences between the ^1H -NMR spectra of the PF_6 salt and TRISPHAT salt were observed when one equivalent or an excess of Λ -TRISPHAT were used.

For the chiral resolution of *rac*- $[\text{Ir}(\text{ppy})_2(\text{bpy-4})][\text{PF}_6]$, one equivalent of Λ -TRISPHAT was employed. In order to separate the two diastereoisomers, thin layer chromatography with different eluents (methanol/dichloromethane, acetonitrile/dichloromethane...) was performed. Unfortunately,

no substantial R_f differences were observed. Thus, separation by chromatography appeared to be not feasible. Crystallization of the two diastereo-ion pairs in different solvents and at different temperatures were also attempted, unfortunately without success. Adding more equivalent of Δ -TRISPHAT to force the formation of the TRISPHAT salt did not allow resolution of the mixture of two diastereoisomers either.

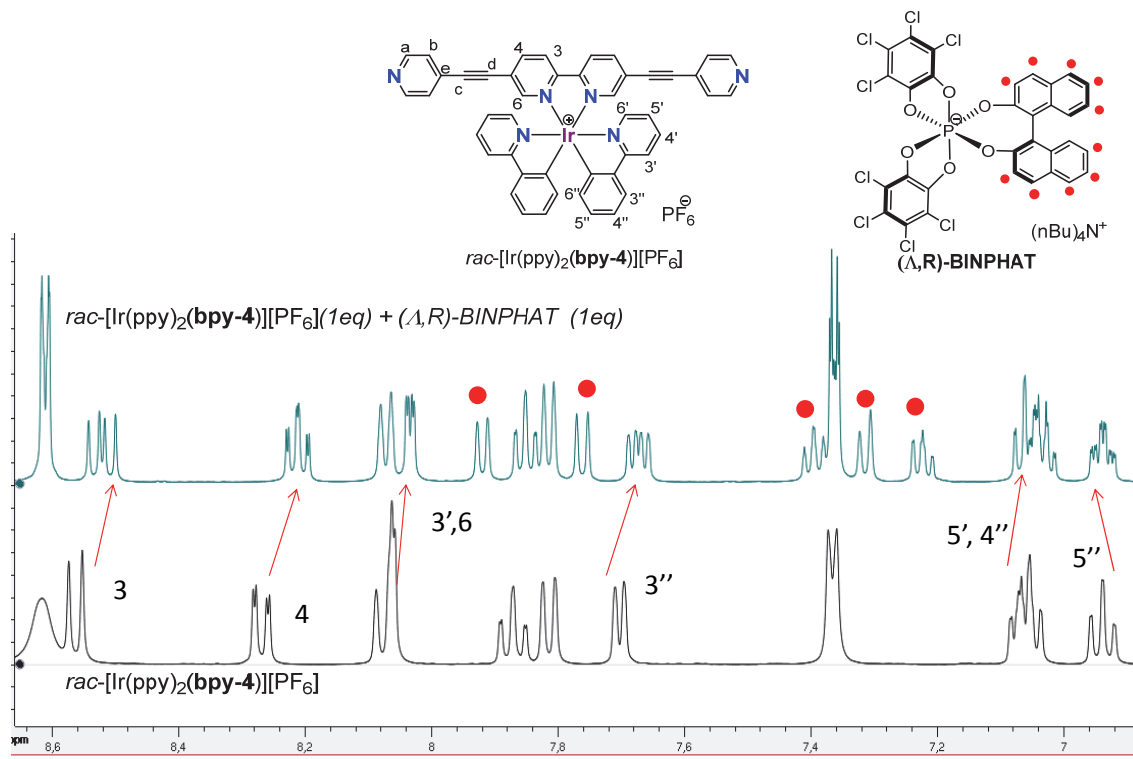


Figure II-18: Comparison of the ^1H -NMR spectra (CD_3CN , 400 MHz) of $\text{rac-}[\text{Ir}(\text{ppy})_2(\text{bpy-4})][\text{PF}_6]$ (bottom, black) and $\text{rac-}[\text{Ir}(\text{ppy})_2(\text{bpy-4})][\text{PF}_6]$ with 1 eq of (Δ, R) -BINPHAT (top, green).

C-Approach B: use of chiral auxiliary ligands for the chiral resolution of metal complexes precursors

The chiral resolution of metal complexes precursors using chiral auxiliary ligands (approach B) was conducted in parallel.

Based on the work done by E. Meggers *et al.*^{11,35} on chiral resolution of racemic Ru complexes precursors for the asymmetric synthesis of more sophisticated Ru complexes bearing only achiral bidentate ligands, oxazoline-derived ligands were employed. Thus, after isolation of the pure diastereoisomer bearing oxazoline derivative (either (Δ, S) and (Δ, S)), replacement of the chiral auxiliary with either labile ligands such as acetonitrile followed by coordination of **bpy-4** or direct replacement with the **bpy-4** ligand was envisaged. As illustrated in Figure II-19, the two diastereoisomers $(\Delta, S)\text{-Ir}(\text{ppy})_2(\text{Ox1})$ and $(\Delta, S)\text{-Ir}(\text{ppy})_2(\text{Ox1})$ were obtained by reaction of the

Iridium dimer with ligand (S)-**Ox1**. Unfortunately, it was not possible to differentiate the two isomers on thin layer chromatography (R_f too close) even using different solvents as eluents. As a consequence, the separation of the two diastereoisomers turned to be again unsuccessful in our hands.

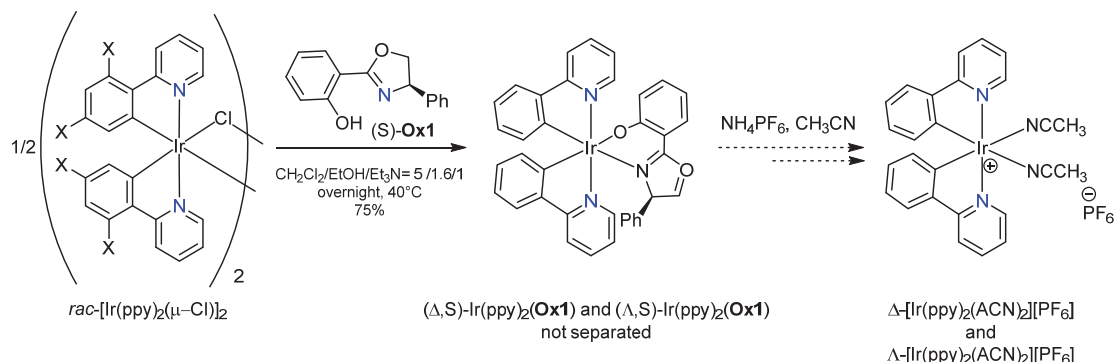


Figure II-19: Synthesis of the two diastereoisomers $(\Delta,S)\text{-Ir(ppy)}_2(\text{Ox1})$ and $(\Lambda,S)\text{-Ir(ppy)}_2(\text{Ox1})$ starting from the Iridium dimer and enantiopure oxazoline derivative (S)-**Ox1**.

During our search for other labile chiral auxiliary ligands, Lusby *et al.*¹² published a procedure for the chiral resolution of Iridium dimers using L- or D-serine as chiral auxiliaries (see paragraph 1.2 above for a detailed explanation). Thus, as illustrated in Figure II-20, following this method, the two enantiomers $\Delta\Delta\text{-}$ and $\Lambda\Lambda\text{-[Ir(ppy)}_2(\mu\text{-Cl})_2]$ were obtained *via* a two-step procedure in 43 % and 48 % yield respectively (overall yields for the two steps and based on $\text{rac-[Ir(ppy)}_2(\mu\text{-Cl})_2]$).

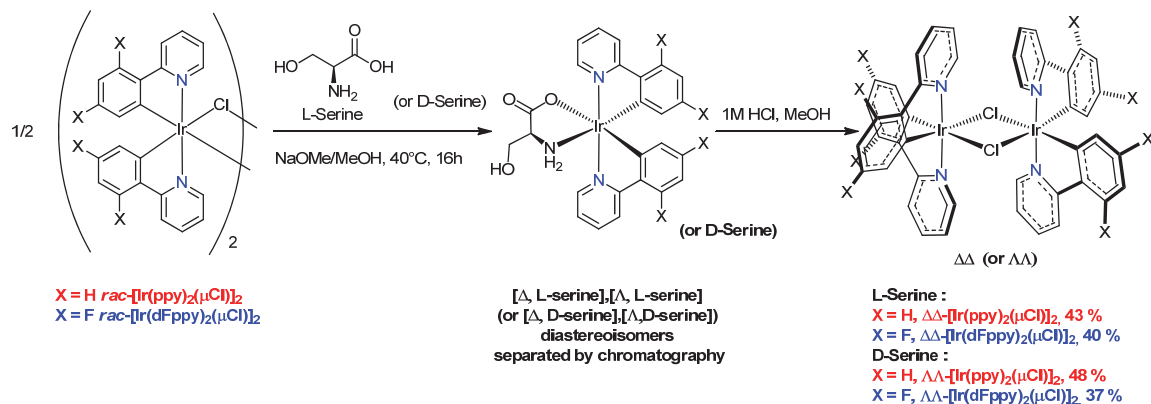


Figure II-20: Two-step procedure for the resolution of $\Delta\Delta\text{-}$ and $\Lambda\Lambda\text{-[Ir(ppy)}_2(\mu\text{-Cl})_2]$ and $\Delta\Delta\text{-}$ and $\Lambda\Lambda\text{-[Ir(dFppy)}_2(\mu\text{-Cl})_2]$.

The method was also successfully applied to the resolution of the fluorinated Iridium dimer $\text{rac-[Ir(dFppy)}_2(\mu\text{-Cl})_2]$. In that case, the difference of R_f values between the two serine intermediate diastereoisomers ($[\Delta, \text{L-serine}]$, $[\Lambda, \text{L-serine}]$ or $[\Delta, \text{D-serine}]$, $[\Lambda, \text{D-serine}]$) (0.18/0.19 using $\text{CH}_2\text{Cl}_2/\text{CH}_3\text{OH}$ 7 % as eluent) is even smaller than the non-fluorinated complexes (0.19/0.21 using $\text{CH}_2\text{Cl}_2/\text{CH}_3\text{OH}$ 6 %). These intermediates are also less stable on silica gel. As a consequence, the separation of the diastereoisomers is more tedious and the overall yields for the two enantiomers $\Delta\Delta\text{-}$ and $\Lambda\Lambda\text{-[Ir(dFppy)}_2(\mu\text{-Cl})_2]$ are lower (40 % and 37 % respectively) than the ones for the non-

fluorinated Iridium dimers. As stated by Lusby *et al.* when using ppy derivatives, and as verified for the fluorinated ones, while the first eluting diastereoisomer ([Δ ,L-serine] or [Λ ,D-serine]) can be obtained analytically pure, the slower eluting diastereoisomer ([Δ ,L-serine] or [Λ ,D-serine]) is always contaminated with the other isomer. This is also the reason why L- or D-serine intermediate complexes have to be used respectively to obtain the two dimers $\Delta\Delta$ - and $\Lambda\Lambda$ -[Ir(dFppy)₂(μ -Cl)]₂ analytically pure (Figure II-20).

All four enantiopure Iridium dimers were characterized by standard techniques including circular dichroism (CD) (Figure II-21) and polarimetric measurements ([α]_D, Table II-4). Pairs of enantiomers exhibit good opposite Cotton effects and opposite specific rotation [α]_D values could be observed.

Table II-4: [α]_D values of the enantiopure dimers (293K, 0.05 g/100 mL in CH₂Cl₂).

| [α] _D /complexes | [Ir(ppy) ₂ (μ -Cl)] ₂ | [Ir(dFppy) ₂ (μ -Cl)] ₂ |
|--------------------------------------|--|--|
| $\Delta\Delta$ - | +433° | +205° |
| $\Lambda\Lambda$ - | -468° | -183° |

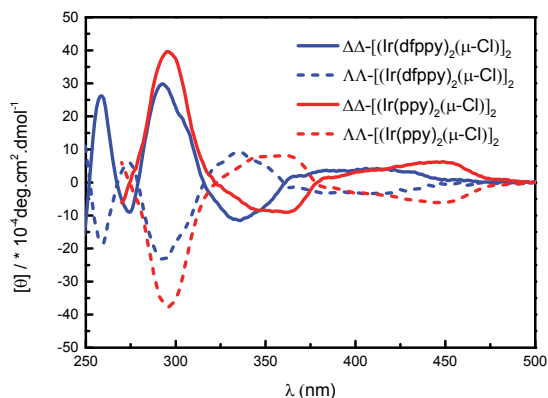
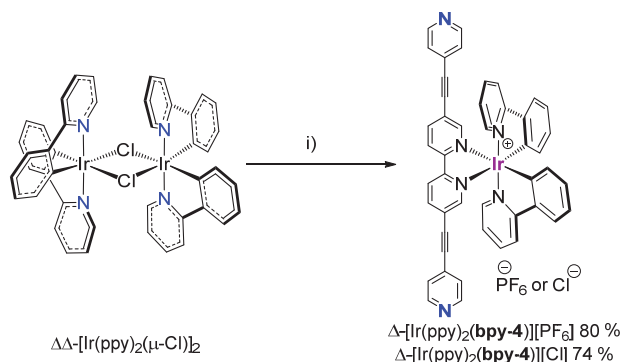


Figure II-21: CD spectra of the enantiopure dimers $\Delta\Delta$ - and $\Lambda\Lambda$ -[Ir(ppy)₂(μ -Cl)]₂ (red solid and dashed lines respectively) and $\Delta\Delta$ - or $\Lambda\Lambda$ -[Ir(dFppy)₂(μ -Cl)]₂ dimers (blue solid and dashed lines respectively) (293K, 20 μ M in CH₂Cl₂).

3.2 Asymmetric synthesis and characterization of *rac*-[Ir(ppy)₂(bpy-4)][PF₆]

Finally, following the synthetic route described above for the racemic complex, the two final Ir enantiomers, Δ - and Λ -[Ir(ppy)₂(bpy-4)][X] (X = Cl or PF₆), could be obtained starting either from the $\Delta\Delta$ - or $\Lambda\Lambda$ -[Ir(ppy)₂(μ -Cl)]₂ dimers. The two enantiomers were isolated either with chloride as counter ion (yield = 74 % and 76 % for the Δ and the Λ enantiomer respectively) or converted into

their PF₆ salt by metathesis with KPF₆ in water (yield = 80 % and 83 % for the Δ and Λ enantiomer respectively) (Figure II-22).



i) 1) **bpy-4**, CH₂Cl₂/CH₃OH/CH₃CN 3/3/1, 60 °C, 2) KPF₆, H₂O, 70 °C.

Figure II-22: Synthesis of Δ-[Ir(ppy)₂(bpy-4)][Y] (Y = Cl or PF₆). The same procedure was followed for the Λ isomer. The chloride salts can be isolated before performing the last metathesis step using KPF₆ (step (i)2)).

As expected, the PF₆ salts exhibit identical NMR and UV/Vis spectra as the ones obtained for the racemic mixture. Furthermore, the enantiomers exhibit mirror images CD spectra and opposite specific rotation values ([α]_D) (Figure II-23 and Table II-5). It should be noted that the same CD spectra are obtained for Δ-[Ir(ppy)₂(bpy-4)][PF₆] and Δ-[Ir(ppy)₂(bpy-4)][Cl]. The same holds for the Λ enantiomers.

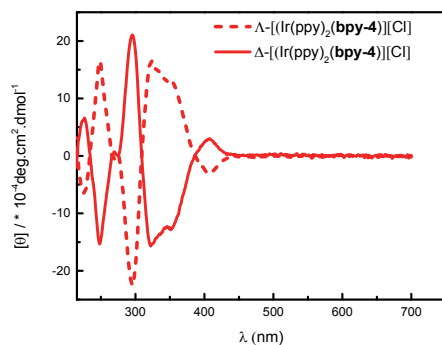


Figure II-23: CD spectra of the enantiopure complexes Δ- and Λ-[Ir(ppy)₂(bpy-4)][Cl] (293K, 10μM in CH₃CN)(solid and dashed lines respectively).

Table II-5: [α]_D values of the enantiopure complexes (293K, 0.06 g/100 mL in CH₃CN).

| [α] _D /complexes | [Ir(ppy) ₂ (bpy-4)][Cl] |
|-----------------------------|------------------------------------|
| Δ- | -317° |
| Λ- | +323° |

For the two enantiomers Δ- and Λ-[Ir(ppy)₂(bpy-4)][Cl], single crystals suitable for X-ray diffraction were obtained by slow diffusion of toluene into a 1/1 toluene/CH₃CN solution of the

desired complex (Figures II-24 a and b respectively). The X-ray structures confirmed the absolute configuration of the two enantiomers. Both complexes crystallize in the orthorhombic system with the chiral $P2_12_12$ space group. Their geometrical parameters are similar to those of *rac*-[Ir(ppy)₂(bpy-4)][PF₆] (selected average bond lengths and angles for Δ -[Ir(ppy)₂(bpy-4)][Cl]: Ir-C_{ppy} 2.017 Å, Ir-N_{ppy} 2.053 Å, Ir-N_{bpy} 2.146 Å, N_{ppy}-Ir-N_{ppy} 172.11°, N_{ppy}-Ir-C_{ppy} 80.39°, N_{bpy}-Ir-N_{bpy} 76.53°; selected average bond lengths and angles for Λ -[Ir(ppy)₂(bpy-4)][Cl]: Ir-C_{ppy} 2.016 Å, Ir-N_{ppy} 2.053 Å, Ir-N_{bpy} 2.140 Å, N_{ppy}-Ir-N_{ppy} 171.98°, N_{ppy}-Ir-C_{ppy} 80.31°, N_{bpy}-Ir-N_{bpy} 76.57°).

It should be noted that no suitable single crystals for X-Ray diffraction could be obtained for the PF₆ salt. This may be related to the non-innocent role played, in the crystalline phase, by one of the chloride ions that exhibits hydrogen bonds with the bipyridyl ligand (Cl1-C_a distance of 3.478 Å and Cl1-C_b 3.844 Å for the Δ enantiomer, Cl2-C_a 3.515 Å and Cl2-C_b 3.899 Å for the Λ enantiomers) bridging thus two Iridium complexes (Figure II-24). The other chloride ion which is not shown in the lattice for clarity is disordered over two positions. It is also hydrogen-bonded to H atoms of one ppy ligand (Cl-C distances ranging from 3.46 to 3.61 Å), one toluene molecule (Cl-C distances ranging from 3.72 to 3.74 Å) and one terminal pyridyl unit of the bpy ligand (Cl-C distances ranging from 3.64 to 3.83 Å).

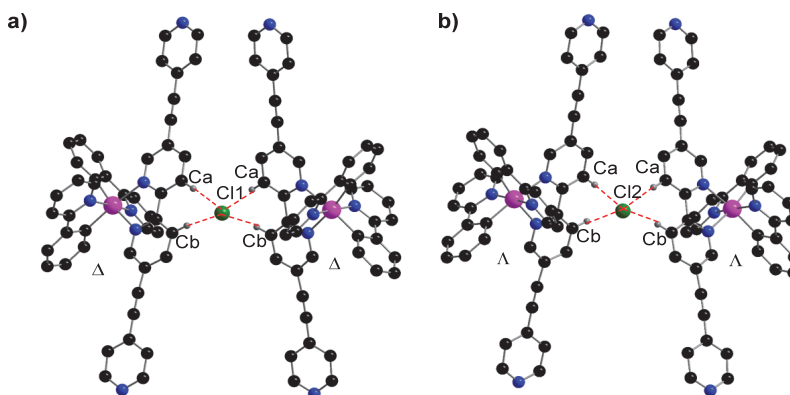


Figure II-24: X-ray structure of Δ -[Ir(ppy)₂(bpy-4)][Cl] (a) and Λ -[Ir(ppy)₂(bpy-4)][Cl] (b) showing the Hydrogen bonds between the protons linked to C_a and C_b atoms and one chloride ion (red dashed lines). Non-bonding hydrogen atoms, chloride ions and solvents molecules are omitted for clarity.

In solution, a comparison of the ¹H-NMR spectra in CD₃CN of Δ -[Ir(ppy)₂(bpy-4)][PF₆] and Δ -[Ir(ppy)₂(bpy-4)][Cl] also reveals the formation of hydrogen bonds between proton H₃ and an adjacent chloride ion. As shown in Figure II-25, a downfield shift of *ca.* 0.09 ppm of the signal of proton H₃ when going from the PF₆ salt to the Cl salt is observed. This is probably due to the electron withdrawing influence of chloride ion on this proton. It should be noted that such an observation has

already been reported by E. Constable *et al.*³⁶ for similar Ir(III) complexes in the solid state and in solution.

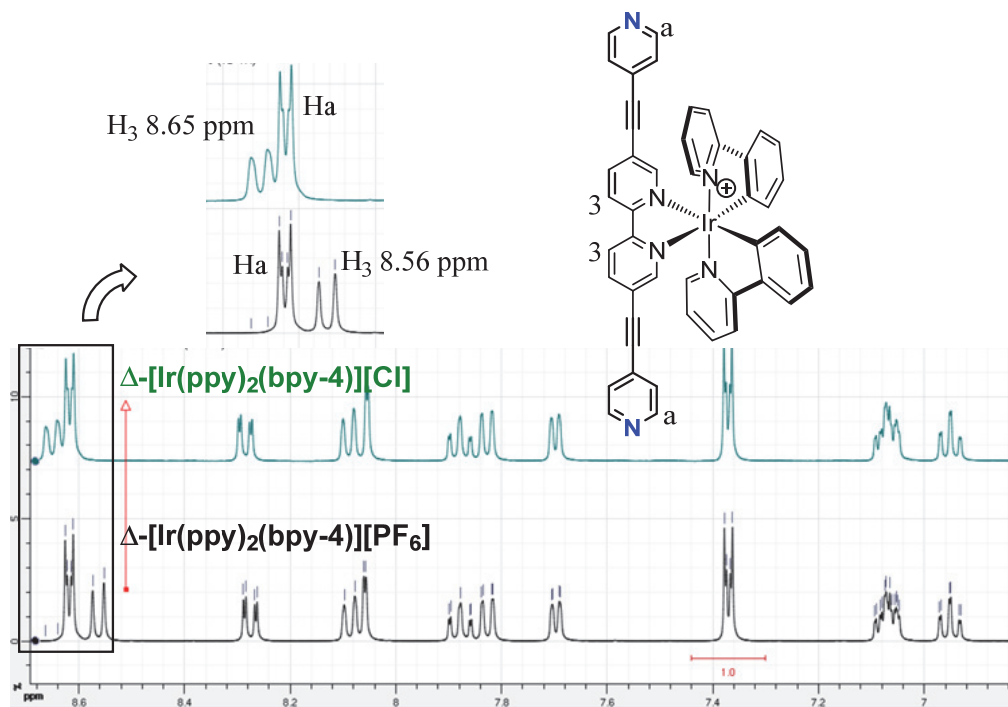
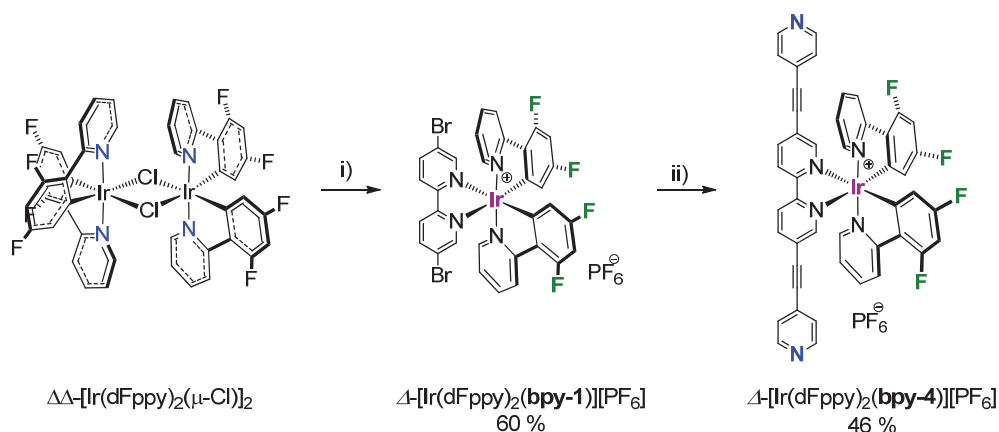


Figure II-25: Portions of the ^1H -NMR spectra (CD_3CN , 400 MHz) of Δ -[Ir(ppy) $_2$ (bpy-4)][PF $_6$] (bottom, black) and Δ -[Ir(ppy) $_2$ (bpy-4)][Cl] (top, green).

3.3 Asymmetric synthesis and characterization of *rac*-[Ir(dFppy) $_2$ (bpy-4)][PF $_6$]

The fluorinated Iridium enantiomers, Δ - and Λ -[Ir(dFppy) $_2$ (bpy-4)][PF $_6$], were also obtained following the same route described above for the fluorinated complex as a racemate (Figure II-26). Thus, the enantiopure Δ - and Λ -[Ir(dFppy) $_2$ (bpy-1)][PF $_6$] complexes were obtained by reaction of the corresponding enantiopure dimers, $\Delta\Delta$ - or $\Lambda\Lambda$ -[Ir(ppy) $_2$ (μ -Cl)] $_2$, in 60 % and 55 % yield respectively. A Sonogashira coupling reaction between Δ - and Λ -[Ir(dFppy) $_2$ (bpy-1)][PF $_6$] with 4-ethynylpyridine afforded the two enantiopure Δ - and Λ -[Ir(dFppy) $_2$ (bpy-4)][PF $_6$] complexes in 46 % and 45 % yield respectively. It should be noted that the dibromo intermediate as well as the final cationic Ir complexes could only be isolated as their PF $_6$ salts as purification of their chloride salts was not possible. All chiral complexes exhibit identical NMR and UV/Vis spectra as those observed for the racemic mixture. As expected, the enantiomers exhibit mirror images CD spectra (Figure II-27) and pairs of enantiomers also show opposite specific rotation ($[\alpha_D]$, Table II-6). It is important to note that the configuration of the metal center (Δ or Λ) is retained during the coupling reaction.



i) **bpy-1**, $\text{CH}_2\text{Cl}_2/\text{CH}_3\text{OH}$ 1/1, 60 °C, 2) KPF_6 , H_2O , 70 °C; ii) 4-ethynylpyridine, $\text{Pd}(\text{PPh}_3)_4$, CuI , toluene/ $\text{CH}_3\text{CN}/i\text{Pr}_2\text{NH}$ 3/0.2/1, 60 °C.

Figure II-26: Synthesis of $\Delta\text{-}[\text{Ir}(\text{dFppy})_2(\text{bpy-4})][\text{PF}_6]$. The same route was followed to obtain the Λ isomer.

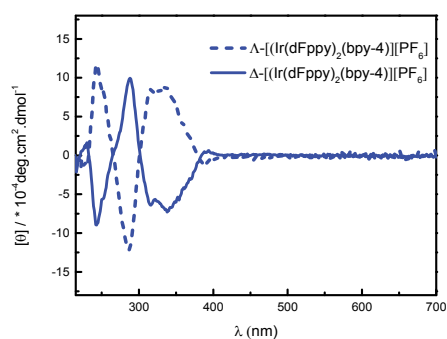


Figure II-27: CD spectra of the enantiopure complexes $\Delta\text{-}$ and $\Lambda\text{-}[\text{Ir}(\text{dFppy})_2(\text{bpy-4})][\text{PF}_6]$ (solid and dashed lines respectively) (293K, 10 μM in CH_3CN).

Table II-6: $[\alpha]_D$ values of the enantiopure complexes (293K, 0.06 g/100 mL in CH_3CN).

| $[\alpha]_D/\text{complexes}$ | $[\text{Ir}(\text{dFppy})_2(\text{bpy-4})][\text{PF}_6]$ |
|-------------------------------|--|
| $\Delta\text{-}$ | -209° |
| $\Lambda\text{-}$ | +213° |

No single crystals suitable for X-ray diffraction could be obtained for the two final complexes, $\Delta\text{-}[\text{Ir}(\text{dFppy})_2(\text{bpy-4})][\text{PF}_6]$ and $\Lambda\text{-}[\text{Ir}(\text{ppy})_2(\text{bpy-4})][\text{PF}_6]$. However, the structure of the intermediate complex $\Delta\text{-}[\text{Ir}(\text{dFppy})_2(\text{bpy-1})][\text{PF}_6]$ could be determined (Figure II-28) and confirmed the configuration of the metal center. Indeed, single crystals of the latter complex were grown by slow diffusion of ether into an acetonitrile solution containing the desired complex. As expected, $\Delta\text{-}[\text{Ir}(\text{ppy})_2(\text{bpy-1})][\text{PF}_6]$ crystallizes in a chiral space group (orthorhombic, $C222_1$). The Ir atom adopts a distorted octahedral geometry with one bipyridyl (**bpy-1**) and two dFppy moieties displaying the

expected *cis*-arrangement of the C atoms and *trans*-arrangement of the N atoms. The average bond lengths and angles around the Ir center (Ir-C_{ppy} 1.996 Å; Ir-N_{ppy} 2.041 Å; Ir-N_{bpy} 2.136 Å; N_{ppy}-Ir-N_{ppy} 173.98°; N_{ppy}-Ir-C_{ppy} 77.38°; N_{bpy}-Ir-N_{bpy} 80.67°) are similar to those observed for the racemic Iridium complexes reported above.

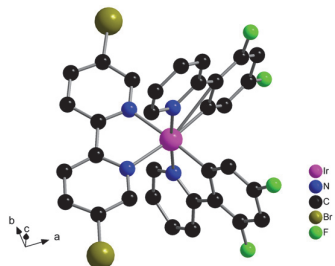


Figure II-28: Crystal structure of Δ -[Ir(dFppy)₂(bpy-1)][PF₆]. H atoms, PF₆[−] ion and solvent molecules are omitted for clarity.

4. Synthesis and characterization of racemic and enantiopure Ir(III) complexes based on terminal carboxylate coordinating sites

In order to expand the scope of the linear Ir metallatectons described above, terminal carboxylate coordinating sites (instead of pyridyl) appeared as candidate of choice to obtain other types of heterometallic coordination polymers. In this part, the different attempts to synthesize the racemic Ir(III) complexes bearing carboxylate terminal coordinating sites, *rac*-[Ir(ppy)₂(bpy-7)][Y] (Y = Cl or PF₆) will be discussed (Figure II-29). After optimization of the reaction conditions, the asymmetric synthesis of the metallatecton will be presented. Finally, the characterizations of the Ir(III) complexes, in particular the single crystal X-ray structure and luminescent properties, will be detailed for some of the complexes.

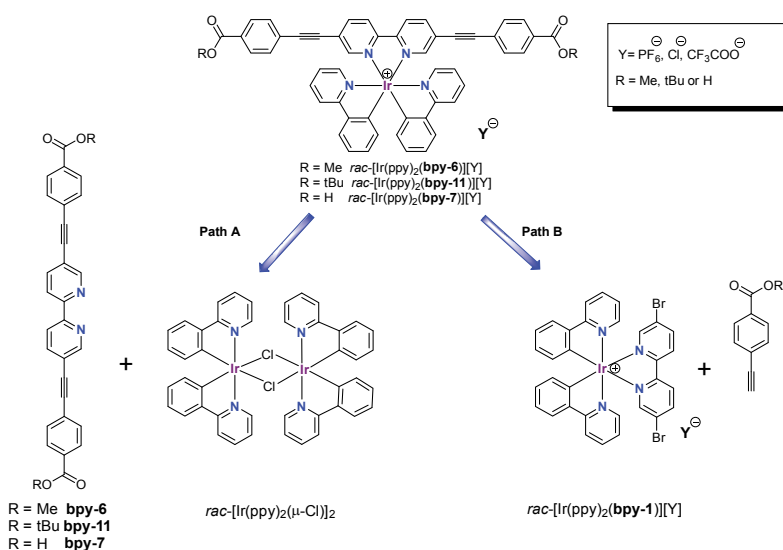


Figure II-29: Two possible retrosynthetic pathways to obtain the desired cationic Ir(III) complexes.

4.1 Synthesis and characterization of the racemic Ir(III) complexes *rac*-[Ir(ppy)₂(bpy-7)][Y] (Y = Cl or CF₃COO)

As for the pyridyl derivatives presented above, two synthetic pathways may be followed to prepare the desired Ir(III) complexes *rac*-[Ir(ppy)₂(bpy-7)]⁺. Due to the expected low solubility of ligand **bpy-7** in organic solvents such as dichloromethane or acetonitrile owing to the presence of carboxylic acids, the latter must be protected with alkyl groups such as methyl-, ethyl- or *tert*-butyl-groups to facilitate purification of the corresponding complexes. The final Ir(III) complexes containing the carboxylic acid as terminal coordinating sites will then be obtained by saponification of the ester groups. The targeted Ir complexes are thus *rac*-[Ir(ppy)₂(bpy-6)]⁺ and *rac*-[Ir(ppy)₂(bpy-11)]⁺ depending on the terminal ester groups (R = Me or *t*Bu respectively).

*A-Synthesis and characterization of the ester derivatives *rac*-[Ir(ppy)₂(bpy-6)]⁺ and *rac*-[Ir(ppy)₂(bpy-11)]⁺ and the carboxylic acid derivative *rac*-[Ir(ppy)₂(bpy-7)]⁺*

Again, following path A, the synthesis of the ester protected **bpy-6** is required to subsequently coordinate it to the Ir dimer. As a first attempt, methyl was used as protecting group for the carboxylic acid as its use was already reported for similar Ir-based metallatectons.¹⁸ The synthesis is illustrated in Figure II-30 starting from **bpy-3** previously synthesized. A Sonogashira coupling reaction between **bpy-3** and methyl 4-iodobenzoate in the presence of Pd(PPh₃)₄ and CuI was conducted in the presence of Pd(PPh₃)₄ and CuI in a mixture of toluene and *i*Pr₂NH as solvent and base affording **bpy-6** in *ca.* 22 % yield. Even varying the reaction conditions (toluene and dmf used as solvents, temperature of 60 °C and 100 °C) did not afford a better yield.

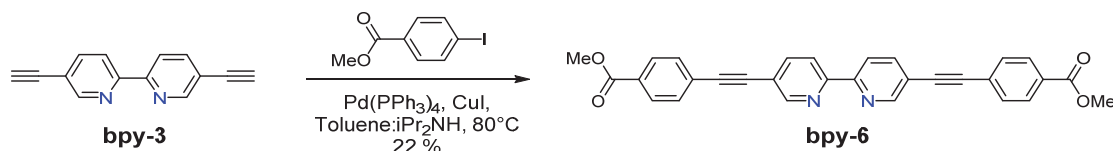
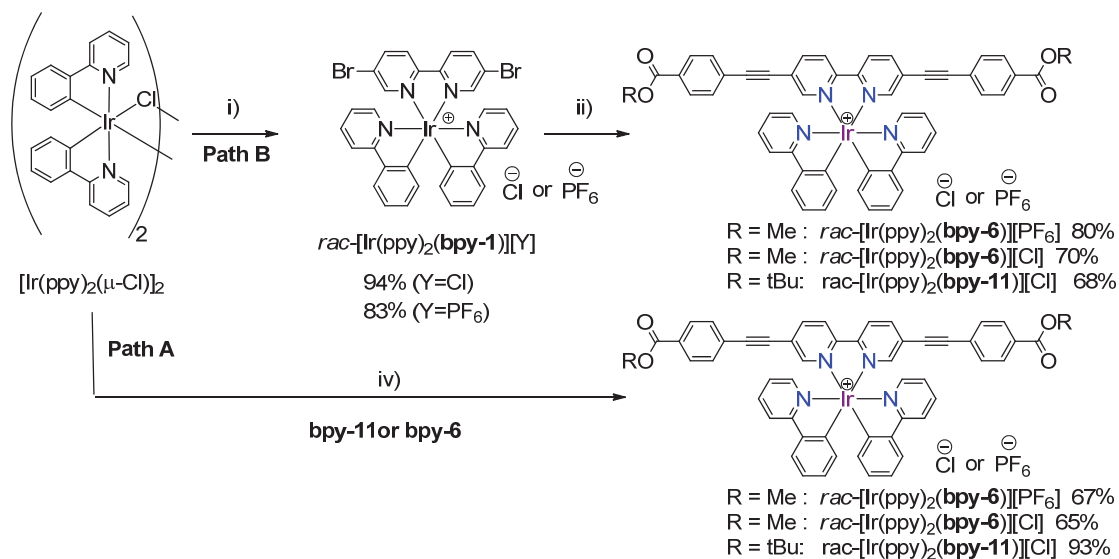


Figure II-30: Synthesis of ligand *bpy-6*.

Coordination of ligand **bpy-6** on the Ir dimer was then performed using reaction conditions described for the previously described Ir complexes (Figure II-31 bottom). Thus, *rac*-[Ir(ppy)₂(bpy-6)][Y] (Y = Cl or PF₆) was obtained as a chloride salt in 65 % yield or as a PF₆ salt in 67 % yield after metathesis of the chloride salt with a KPF₆ aqueous solution. When considering the PF₆ salt, the chloride salt intermediate was not isolated and the yield is an overall yield over the two steps.



i), 1) $\text{CH}_2\text{Cl}_2/\text{CH}_3\text{OH}$ 1/1, 60 °C, 2) (only for $\text{rac-[Ir(ppy)}_2(\text{bpy-1})][\text{PF}_6]$) KPF_6 , H_2O , 70 °C;; ii) **5** or **10**, $\text{Pd(PPh}_3)_4$, CuI, toluene/ $\text{CH}_3\text{CN}/\text{Et}_3\text{N}$ 3/0.2/1, 60 °C to 70 °C; iii) $\text{CF}_3\text{COOH}/\text{CH}_2\text{Cl}_2$ 1/1, rt or HCl 37 %/1,4-dioxane 1/4, rt ; iv) **bpy-6** or **bpy-11**, $\text{CH}_2\text{Cl}_2/\text{CH}_3\text{OH}/\text{CH}_3\text{CN}$ 1/1/0.5, 60 °C.

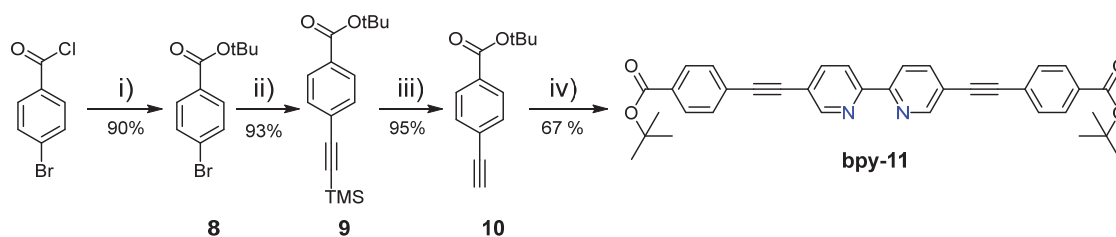
Figure II-31: Synthesis of the ester derivatives Ir complexes $\text{rac-[Ir(ppy)}_2(\text{bpy-6})][\text{Y}]$ (Y = Cl or PF_6) and $\text{rac-[Ir(ppy)}_2(\text{bpy-11})][\text{Cl}]$

In parallel and considering the low yield obtained for the synthesis of ligand **bpy-6**, the preparation of $\text{rac-[Ir(ppy)}_2(\text{bpy-6})][\text{Y}]$ (Y = Cl or PF_6) following path B was conducted (Figure II-31 top). Thus, the bromo derivative $\text{rac-[Ir(ppy)}_2(\text{bpy-1})][\text{Y}]$ (Y = Cl or PF_6) could be obtained using the same reaction conditions described for the pyridyl-substituted complex $\text{rac-[Ir(dFppy)}_2(\text{bpy-1})][\text{PF}_6]$ (see section 2.1). Reaction of the Ir dimer $\text{rac-[Ir(ppy)}_2(\mu\text{-Cl})_2$ afforded the chloride salt $\text{rac-[Ir(ppy)}_2(\text{bpy-1})][\text{Cl}]$ in 94 % yield. $\text{rac-[Ir(ppy)}_2(\text{bpy-1})][\text{PF}_6]$ was obtained in the same way in 85 % overall yield performing a metathesis step with a KPF_6 aqueous solution at the end of the reaction. Then, *via* a Sonogashira coupling reaction between $\text{rac-[Ir(ppy)}_2(\text{bpy-1})][\text{Y}]$ (Y = Cl or PF_6) and methyl 4-ethynylbenzoate (compound **5**)³⁷, the ester-substituted complex $\text{rac-[Ir(ppy)}_2(\text{bpy-6})][\text{Y}]$ (Y = Cl or PF_6) was obtained as a chloride salt in 70 % yield or as a PF_6 salt in 80 % yield.

According to the procedure reported in literature for a similar bis-cyclometalated Ir complex,¹⁸ the last deprotection step should be easily performed in good yields by KOH treatment in a mixture of THF/EtOH as solvent at 60 °C for *ca.* one hour (TLC showed the absence of the initial product). The pure carboxylic acid-substituted Ir complex could then be obtained by acidification of the reaction mixture (aqueous HCl) followed by precipitation. However, in our case, the $^1\text{H-NMR}$ spectrum of the crude product shows several unknown signals in addition to the expected signals for the desired $\text{rac-[Ir(ppy)}_2(\text{bpy-7})][\text{Cl}]$ complex. The impurity could not be removed by recrystallization or by exchanging the Cl^- counter ion by PF_6^- ion in order to modify the solubility of the complexes in solution.

As a matter of fact, similar outcomes were observed for saponification of rac -[Ir(ppy)₂(bpy-6)][PF₆] obtained through the path B, *i.e.* the presence of non-removable unknown impurities contaminating the desired product.

After several unsuccessful attempts, *tert*-butyl group, a well-known leaving group, was used. Thus, as illustrated in Figure II-31, the ester derivative rac -[Ir(ppy)₂(bpy-11)][Cl] was synthesized following both path A and path B with good overall yields. Again, the synthesis of **bpy-11** was required for path A (Figure II-32). A two-step synthesis starting from 4-bromobenzoyl chloride afforded *tert*-butyl 4-ethynylbenzoate (ligand **10**) in 79 % overall yield following reported procedures.³⁸ Ligand **10** was then reacted with **bpy-1** in the presence of Pd(PPh₃)₄ and CuI in a mixture of toluene/dmf /iPr₂NH solvents to afford **bpy-11** in 67 % yield. Coordination of **bpy-11** to the Ir dimer was then achieved to afford rac -[Ir(ppy)₂(bpy-1)][Cl] in 93 % yield (Figure II-31).



i) pyridine/CH₂Cl₂, *tert*-butanol, RT; ii) ethynyltrimethylsilane, Pd(PPh₃)₄, CuI, toluene/Et₃N 1/1, 60 °C; iii) K₂CO₃, MeOH, RT; iv) **bpy-1**, Pd(PPh₃)₄, CuI, Toluene/DMF/*i*Pr₂NH, 80 °C

Figure II-32: Synthesis of **bpy-11**

For path B, the intermediate rac -[Ir(ppy)₂(bpy-1)][Cl] complex was obtained in 94 % yield using the procedure described earlier. A Sonogashira coupling reaction with *tert*-butyl 4-ethynylbenzoate **10** afforded the final complex rac -[Ir(ppy)₂(bpy-11)][Cl] in 68 % yield (Figure II-31). The similar overall yields for the two paths A and B (49 % for path A and 54 % for path B) shows that both synthetic pathways are suitable for the preparation of rac -[Ir(ppy)₂(bpy-11)][Cl].

Removal of the *tert*-butyl groups was performed using two different reaction conditions (Figure II-33). At first,³⁹ an excess of trifluoroacetic acid was added to the ester derivative rac -[Ir(ppy)₂(bpy-11)][Cl] in CH₂Cl₂ at room temperature for one hour. After evaporation of the solvents, the pure deprotected complex rac -[Ir(ppy)₂(bpy-7)][CF₃COO] was obtained quantitatively with CF₃COO⁻ ion as counter ion as evidenced by ¹⁹F NMR. The complex rac -[Ir(ppy)₂(bpy-7)][CF₃COO] shows rather low solubility in most polar and non-polar solvents such as alcohols and chlorinated solvents. Even in DMF or DMSO, the complex is only slightly soluble which limits the reaction conditions for the future formation of coordination networks *via* crystallization. It was thus decided to use another counter ion in order to enhance the solubility of the complex. Deprotection of rac -[Ir(ppy)₂(bpy-11)][Cl] was achieved in *ca.* 80 % yield using an HCl aqueous solution and 1,4-dioxane as solvent at RT within 6 h to afford the pure product rac -[Ir(ppy)₂(bpy-7)][Cl].

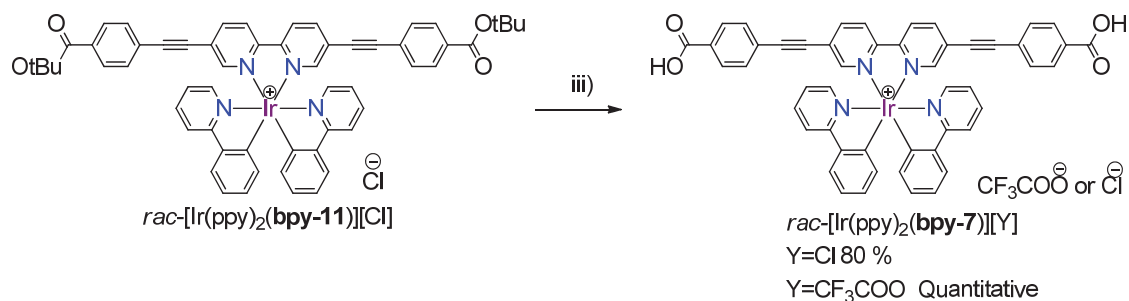


Figure II-33: Saponification of the ester-derivative to obtain $rac-[Ir(ppy)_2(\text{bpy-7})]^+$.

The different organic ligands and Ir complexes obtained were characterized by standard techniques (1H -NMR, ^{13}C -NMR, elemental analysis and HRMS). Crystallographic data were also obtained on single crystals for $rac-[Ir(ppy)_2(\text{bpy-6})][PF_6]$ and $rac-[Ir(ppy)_2(\text{bpy-7})][CF_3COO]$ and the luminescent properties of the final Ir complexes were studied and will be discussed in the next sections.

B-Crystal structures of $rac-[Ir(ppy)_2(\text{bpy-6})][PF_6]$ and $rac-[Ir(ppy)_2(\text{bpy-7})][CF_3COO]$

Red single crystals of $rac-[Ir(ppy)_2(\text{bpy-6})][PF_6]$ were obtained upon slow vapor diffusion of diethyl ether into a concentrated acetonitrile solution containing the desired complex in *ca.* one week. The crystal structure obtained by X-ray diffraction is shown in Figure II-34. Similar to the pyridyl-terminated complexes $rac-[Ir(ppy)_2(\text{bpy-4})][PF_6]$ and $rac-[Ir(dFppy)_2(\text{bpy-4})][PF_6]$, the ester complex also crystallizes in the triclinic *P*-1 space group and exhibits similar geometrical parameters (Figure II-34a and Table II-7). The Ir center is in a distorted octahedral environment and the C atoms of the ppy moieties are in *cis* positions while the N atoms are in *trans* positions. The three chelating ligands are almost planar (dihedral angle N-C-C-N of 1.25 for the bpy unit and -0.22 and 3.87 for the two ppy moieties). The terminal ester moieties are not coplanar with the central bpy unit (dihedral angle in the range 16.05 ° to -23.05 °) and the ethynyl junctions are slightly bent (C-C-C angles in the range 174.48 ° to 177.98 °). Both enantiomers are present in the solid state (Figure II-34a). Again, π - π interactions between two neighboring **bpy-6** ligands are present (Figure II-34b). The shortest C-C distance between two interacting bpy units is of 3.581 Å for the two **bpy-6** ligands of two adjacent Λ (or Δ) enantiomers (Figure II-34b).

Table II-7: Selected bond lengths (Å) and angles (°).

| | $rac-[Ir(ppy)_2(\text{bpy-6})][PF_6]$ | $rac-[Ir(ppy)_2(\text{bpy-11})][CF_3COO]$ |
|---|---------------------------------------|---|
| Ir-C_{ppy} | 2.013(3), 2.012(3) | 1.999(11), 2.004(11) |
| Ir-N_{ppy} | 2.043(2), 2.054(2) | 1.999(11), 2.057(9) |
| Ir-C_{bpy} | 2.142(2), 2.147(2) | 2.138(9), 2.146(9) |
| N_{ppy}-Ir-N_{ppy} | 172.63(9) | 173.7(4) |
| N_{ppy}-Ir-C_{ppy} | 80.44(10), 80.44(11) | 79.7(5), 81.1(5) |
| N_{bpy}-Ir-N_{bpy} | 76.73(9) | 76.0(3) |

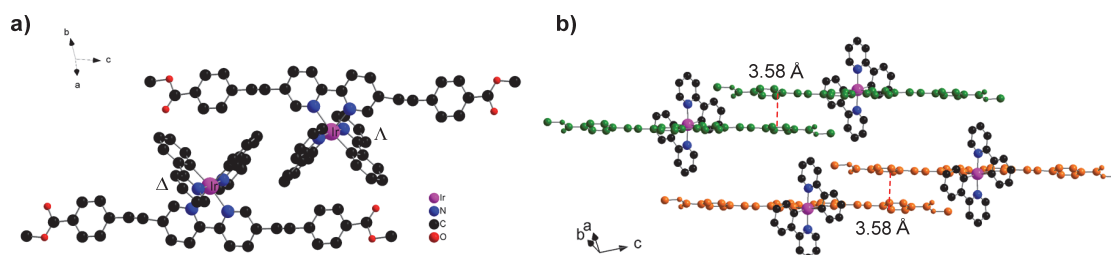


Figure II-34: Crystal structure of *rac*-[Ir(ppy)₂(bpy-6)][PF₆] showing the presence of the two enantiomers within the lattice (a) and π - π interactions between neighboring **bpy-6** ligands (**bpy-6** ligands are colored in green and orange for the Λ and Δ enantiomers respectively) (b). H atoms, PF₆ anions and solvent molecules are omitted for clarity.

Red single crystals of *rac*-[Ir(ppy)₂(bpy-7)][CF₃COO] were obtained upon slow vapor diffusion of diethyl ether into a concentrated DMF solution containing the complex in *ca.* one week. Some structural information are presented in Figure II-35. As for the previous racemic complexes, *rac*-[Ir(ppy)₂(bpy-7)][CF₃COO] crystallizes in the triclinic system with *P*-1 as space group. The geometrical parameters (Figure II-35 and Table II-7) are similar to those of the previous complexes. The Ir center is again in a distorted octahedral geometry. The three chelating ligands are almost planar (dihedral angle N-C-C-N of -0.69 for the bpy unit and -0.77 and 1.47 for the two ppy moieties). The ethynyl junctions are slightly bent (C-C-C angles in the range 173.96° to 178.46°) and the terminal benzoic acids are again not coplanar with the bpy unit (distortion angle ranging from 9.37° to 24.57°). Both enantiomers Λ and Δ are present in the crystal (Figure II-35a). Again, π - π interactions between two adjacent **bpy-7** ligands are observed (Figure II-35b). The shortest C-C distance is *ca* 3.575 Å for the two **bpy-7** ligands of two adjacent Λ enantiomers or Δ enantiomers (Figure II-35b red dashed lines). Furthermore, two types of Hydrogen bonds are observed between the carboxylic acid groups of the Ir complex and dmf molecules (see Figure II-35a for H-O distances ranging from 1.82 Å to 2.56 Å).

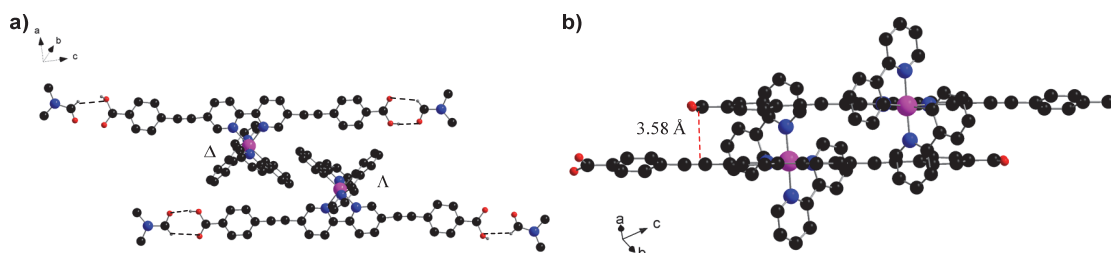


Figure II-35: Portions of the X-ray crystal structure showing the two enantiomers and the H-bonds between the COOH moieties of the complexes and dmf molecules (a) and π - π interactions between neighboring **bpy-7** ligands (b). Hydrogen atoms, CF₃COO⁻ anions and the solvent molecules not interacting through H-bonding are omitted for clarity.

C-Luminescent properties of rac -[Ir(ppy)₂(bpy-11)][Cl] and rac -[Ir(ppy)₂(bpy-7)][CF₃COO]

The photophysical properties of complexes rac -[Ir(ppy)₂(bpy-11)][Cl] and rac -[Ir(dFppy)₂(bpy-7)][CF₃COO] were investigated both in solution and in the solid state (Figure II-36 and Table II-8).

Both complexes, rac -[Ir(ppy)₂(bpy-11)][Cl] and rac -[Ir(ppy)₂(bpy-7)][CF₃COO] exhibit similar absorption spectra highlighting a negligible influence of the *tert*-butyl group. The absorption maxima are also similar to the one observed for the terminal pyridyl-substituted metallatecton rac -[Ir(ppy)₂(bpy-4)][PF₆] even though the absorption coefficients (ϵ) are lower for the pyridyl-substituted Ir complex. As for the above discussed complex rac -[Ir(ppy)₂(bpy-4)][PF₆], the intense absorption band between 240 and 450 nm for the two complexes in THF (Figure II-36a) can be attributed to spin-allowed ligand-centered (LC) transitions involving the ppy and the bpy moieties with a contribution of MLCT and LLCT (metal or ligand-to-ligand charge transfer) transitions as described previously.^{27a} Again, the intense absorption around 320-380 nm is probably due to conjugation over the **bpy-11** or **bpy-7** moieties (π - π^* transitions) as already observed for similar complexes.³⁰ In the solid state (Figure II-36c), a strong absorption band between 250 and 650 nm arising from LC, MLCT and LLCT transitions is observed.

Figure II-36b shows that the photoluminescence spectra of the two complexes measured at room temperature are broad without defined structure. Again, as for rac -[Ir(ppy)₂(bpy-4)][PF₆] discussed earlier, the emission may be attributed to a mixture of ³MLCT and ³LLCT transitions. Moreover, the large red shift of the emission wavelength of both complexes (686 nm for rac -[Ir(ppy)₂(bpy-11)][Cl] and 673 nm for rac -[Ir(dFppy)₂(bpy-7)][CF₃COO]) when compared to [Ir(ppy)₂(bpy)][PF₆] (λ_{em} = 590 nm, RT, THF)^{30a} could be again explained by the presence of extra aromatic systems contributing to the conjugated π system and thus to a decrease of the energy level of the LUMO. Lifetime and quantum yield measurements in solution for the two complexes (54 ns and 0.007 for rac -[Ir(ppy)₂(bpy-11)][Cl] and 113 ns and 0.04 for rac -[Ir(dFppy)₂(bpy-7)][CF₃COO]) are comparable with those reported for red light emitting cationic complexes.⁴⁰ The relatively shorter lifetime and quantum yield for complex rac -[Ir(ppy)₂(bpy-11)][Cl] may be due to the presence of *tert*-butyl groups as a source of nonradiative deactivation pathways of the emissive excited state. Finally, in the solid state, the two complexes exhibit a broad emission band at *ca.* 682 nm. The presence of bulky *tert*-butyl groups might prevent π - π stacking in the solid state and explain the negligible difference of the emission wavelength maxima in solution and in the solid state for rac -[Ir(ppy)₂(bpy-11)][Cl].

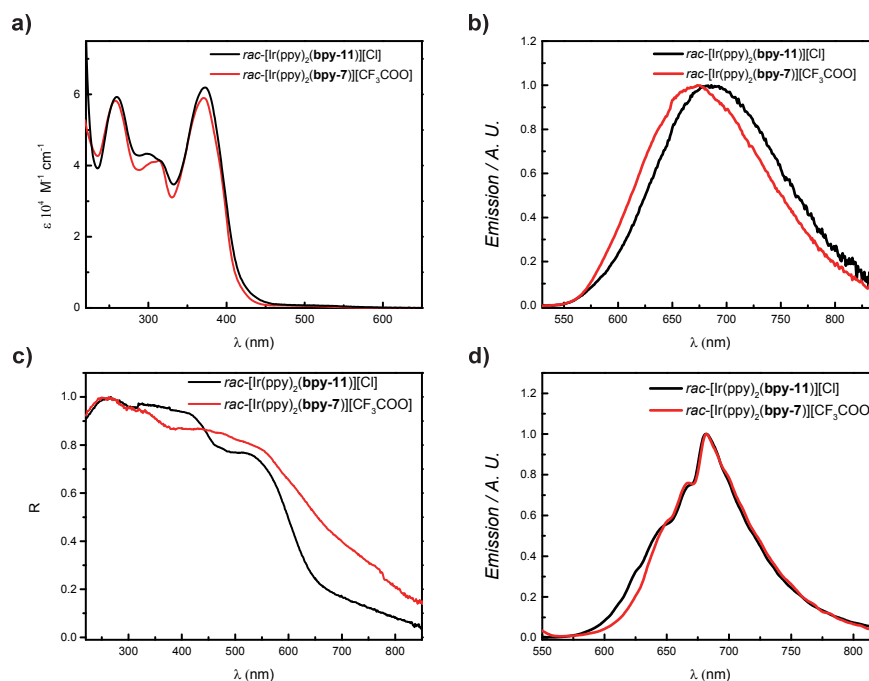


Figure II-36: Absorption spectra (a), reflectance spectra (c) and emission spectra in solution (b) and in the solid state (d) for *rac*-[Ir(ppy)₂(bpy-11)][Cl] (black) and *rac*-[Ir(ppy)₂(bpy-7)][CF₃COO] (red).

Table II-8: Photophysical properties of *rac*-[Ir(ppy)₂(bpy-11)][Cl] and *rac*-[Ir(ppy)₂(bpy-7)][CF₃COO]

| Complexes | Absorption (THF, r.t.) | Emission (deaerated THF, RT) ^a | | | Emission (Solid, RT) |
|---|--|--|----------------|---------------------|-------------------------|
| | λ (nm) (ε 10 ³ M ⁻¹ .cm ⁻¹) | λ (nm) ^a | Φ ^b | τ (ns) ^c | λ (nm) |
| <i>rac</i> -[Ir(ppy) ₂ (bpy-11)][Cl] | 260 (59.3), 297 (43.3), 373 (62.0). | 686 | 0.007 | 53 | 682 |
| <i>rac</i> -[Ir(ppy) ₂ (bpy-7)][CF ₃ COO] | 258 (58.2), 304 (40.9), 371 (59.0) | 673 | 0.032 | 113 | 682 |

a : excited at 390 nm; b: measured using [Ru(bpy)₃][Cl]₂ in degassed acetonitrile as reference (Φ = 0.095);³² c: The emission decay fits better with two components, weighted-average single lifetime are listed.

4.2 Synthesis and characterization of the enantiopure Δ- and Λ-[Ir(ppy)₂(bpy-7)][CF₃COO]

Following the route described for the racemic complexes, the two final Ir enantiomers Δ- and Λ-[Ir(ppy)₂(bpy-7)][CF₃COO] could be obtained starting from the ΔΔ- or ΛΛ-[Ir(ppy)₂(μ-Cl)]₂ dimers obtained previously (see section 3.1). Thus, the two enantiomers Δ- and Λ-[Ir(ppy)₂(bpy-11)][Cl] were isolated in good yields (80 % and 75 % for the Δ and the Λ enantiomers respectively) following path B. Then the Δ- and Λ-[Ir(ppy)₂(bpy-7)][CF₃COO] enantiomers were synthesized

quantitatively by stirring the enantiopure ester complexes in DCM in the presence of TFA. All complexes were fully characterized by standard techniques (^1H -NMR, ^{13}C -NMR and HRMS) as well by circular dichroism (CD) and polarimetric measurements ($[\alpha]_D$).

The isolation of the enantiopure Δ - and Λ - $[\text{Ir}(\text{ppy})_2(\text{bpy-7})][\text{CF}_3\text{COO}]$ complexes could be corroborated by good and opposite Cotton effects observed on the CD spectra as well as by the quasi-opposite $[\alpha]_D$ values (Table II-9). The CD spectra and $[\alpha]_D$ values of Δ - and Λ - $[\text{Ir}(\text{ppy})_2(\text{bpy-7})][\text{CF}_3\text{COO}]$ complexes as well as those of the intermediate products Δ - and Λ - $[\text{Ir}(\text{ppy})_2(\text{bpy-11})][\text{Cl}]$ are illustrated in Figure II-37 and Table II-9 respectively.

Table II-9: $[\alpha]_D$ values of the enantiopure complexes (293K).

| $[\alpha]_D$ /complexes | $[\text{Ir}(\text{ppy})_2(\text{bpy-11})][\text{Cl}]$ | $[\text{Ir}(\text{ppy})_2(\text{bpy-7})][\text{CF}_3\text{COO}]$ |
|-------------------------|---|--|
| Δ - | -277 ° a | -257 ° c |
| Λ - | +280 ° b | +254 ° c |

a: 0.064 g/100 mL in CH_3CN ; b: 0.066 g/100 mL in CH_3CN ; c: 0.068 g/100 mL in DMSO.

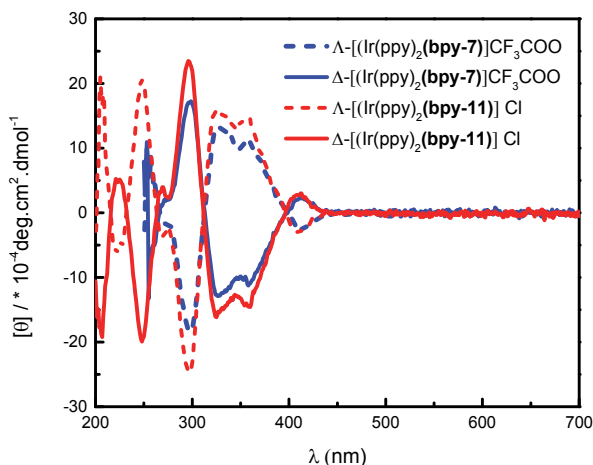


Figure II-37: CD spectra of the enantiopure complexes, Δ - $[\text{Ir}(\text{ppy})_2(\text{bpy-7})][\text{CF}_3\text{COO}]$ (blue solid line) and Λ - $[\text{Ir}(\text{ppy})_2(\text{bpy-7})][\text{CF}_3\text{COO}]$ (blue dotted line) (293K, 10 μM in DMSO) and of Δ - $[\text{Ir}(\text{ppy})_2(\text{bpy-11})][\text{Cl}]$ (red solid line) and Λ - $[\text{Ir}(\text{ppy})_2(\text{bpy-11})][\text{Cl}]$ (red dotted line) (293K, 10 μM in CH_3CN).

Furthermore, red single crystals of Δ - $[\text{Ir}(\text{ppy})_2(\text{bpy-11})][\text{Cl}]$ suitable for X-Ray diffraction could be obtained upon slow evaporation of a mixed solution of toluene and acetonitrile containing Δ - $[\text{Ir}(\text{ppy})_2(\text{bpy-11})][\text{Cl}]$. The structural investigation confirmed the absolute configuration of the enantiopure complex. The complex Δ - $[\text{Ir}(\text{ppy})_2(\text{bpy-11})][\text{Cl}]$ crystallizes in the trigonal system with $P321$ as space group. The geometrical parameters are similar to those described for Δ - $[\text{Ir}(\text{ppy})_2(\text{bpy-4})][\text{Cl}]$. The central **bpy-11** ligand and the two cyclometallating ligands are quasi planar (distortion

angle ranging from -1.61 to 4.29°) and the ethynyl junctions are almost linear with C-C-C angles ranging from 171.78° to 178.89° . The terminal benzoic acid moieties are slightly deviated from coplanarity with the central bpy units (dihedral angles ranging from -23.43° to -17.40°). Selected distances and angles are listed in Table II-10.

Table II-10: Selected bond lengths (Å) and angles ($^\circ$) of Δ -[Ir(ppy)₂(bpy-11)][Cl].

| | Δ -[Ir(ppy) ₂ (bpy-11)][Cl] |
|---|---|
| Ir-N_{bpy} | 2.129(11), 2.133(10) |
| Ir-N_{ppy} | 2.002(7), 2.041(12) |
| Ir-C_{ppy} | 2.004(12), 2.009(14) |
| N_{ppy}-Ir-N_{ppy} | 173.2(4) |
| N_{ppy}-Ir-C_{ppy} | 81.2(5), 81.4(6) |
| N_{bpy-11}-Ir-N_{bpy-11} | 76.7(4) |

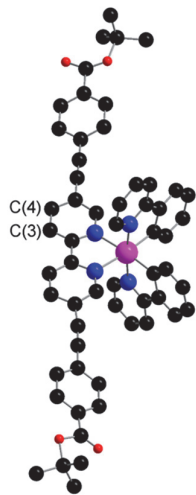


Figure II-38: X-ray structure of Δ -[Ir(ppy)₂(bpy-11)][Cl]. H atoms and Cl⁻ anions are omitted for clarity.

Similar to the crystal structure of Δ -[Ir(ppy)₂(bpy-4)][Cl], Δ -[Ir(ppy)₂(bpy-11)][Cl] molecules are connected through hydrogen bonds between chloride ion and hydrogen atoms in position 3 of **bpy-11** ligands (H_3 -Cl distances ranging from 2.596 Å to 2.729 Å). Furthermore, instead of only two adjacent Δ enantiomers involved in the hydrogen bonding pattern as for Δ -[Ir(ppy)₂(bpy-4)][Cl], three Δ -[Ir(ppy)₂(bpy-11)][Cl] molecules are assembled in this case (Figure II-39a red lines). The other chloride ions, which are not shown on Figure II-39a, are also hydrogen-bonded to H atoms of two ppy moieties (Cl-H distance of 2.92 Å). Moreover, the Cl-H hydrogen bonds guide the organization of molecules in the crystal structure leading to the packing of individual molecules. In Figure II-39b, hydrogen bonds between **bpy-11** and chloride ions are shown in circles while those between ppy and

chloride ions are depicted as triangles. For clarity, the **bpy-11** ligands are presented in red and ppy ligands are in blue in Figure II-39b. The presence of π - π interactions between adjacent **bpy-11** ligands or between ppy ligands are also observed but will not be presented and discussed here.

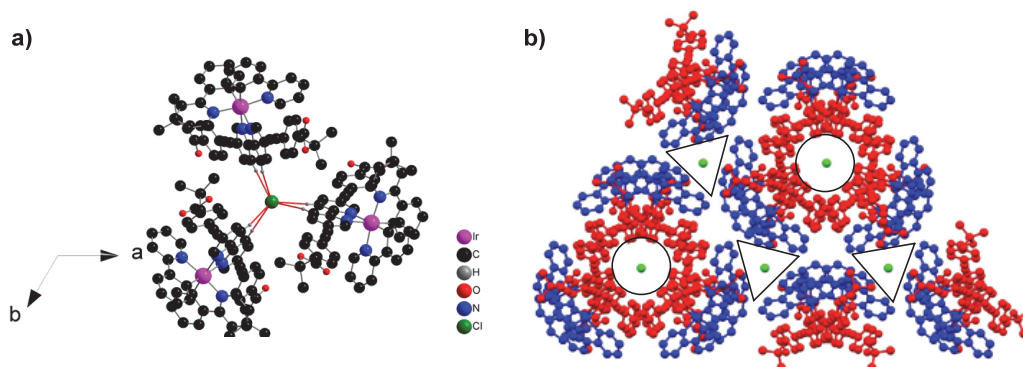


Figure II-39 : Portions of the X-ray structure of Δ -[Ir(ppy)₂(**bpy-11**)] [Cl] showing the hydrogen bonds formed between one chloride ion and three **bpy-11** units belonging to adjacent Δ -[Ir(ppy)₂(**bpy-11**)] [Cl] molecules (a) and the two types of channels formed by packing directed by hydrogen bonding (view along the c axis) (b). The **bpy-11** ligands are colored in red and ppy ligands are in blue. Hydrogen atoms not involved in H-bonding interactions are omitted for clarity.

5. Formation of a 1-D and 2-D coordination networks between racemic and enantiopure Ir(III) complex

5.1 General considerations

Having obtained and fully characterized the racemic and enantiopure Iridium complexes based on either terminal pyridyl or carboxylate coordination sites, their self-assembly with different metal salts was studied. Unfortunately, so far, the use of the metallatecton bearing terminal carboxylate groups [Ir(ppy)₂(**bpy-7**)] [Y] (Y = Cl or CF₃COO) as racemate or enantiomerically pure in self-assembly processes with different metal salts (*e.g.* Zn(NO₃)₂, Cd(NO₃)₂ *etc.*) only resulted in the formation of either precipitates or twinned crystals. Further attempts using other metal salts or by variation of the crystallization conditions still need to be carried out. However, the generation of heterometallic coordination networks with the Ir metallatectons bearing terminal pyridyl groups, [Ir(ppy)₂(**bpy-4**)] [PF₆] and [Ir(dFppy)₂(**bpy-4**)] [PF₆], was more successful and coordination polymers were obtained with Cu and Cd salts. The crystallographic study and the luminescent properties of those coordination networks is the subject of the next paragraphs.

Since the structure of *rac*-[Ir(ppy)₂(**bpy-4**)] [PF₆] and *rac*-[Ir(dFppy)₂(**bpy-4**)] [PF₆] are not centro-symmetric owing to the acentric nature of the organic tecton, they could display different

orientations within polymetallic species such as coordination networks. Here, only 1D linear chains and 2D grid-type architectures will be discussed.

For the case of 1-D linear networks, as presented in Figure II-40, the Ir(III) centers may be oriented in opposite directions (*a*) or in the same direction (*b*). This results in a non-polar arrangement in case *a* while, for case *b*, the resulting coordination network will be polar. Furthermore, for the packing arrangement of consecutive polar 1D network, if they are arranged in a head-to-tail fashion (*c*), the whole architecture is apolar, while if they are arranged in a head-to-head fashion (*d*) the resulting crystal will be polar.

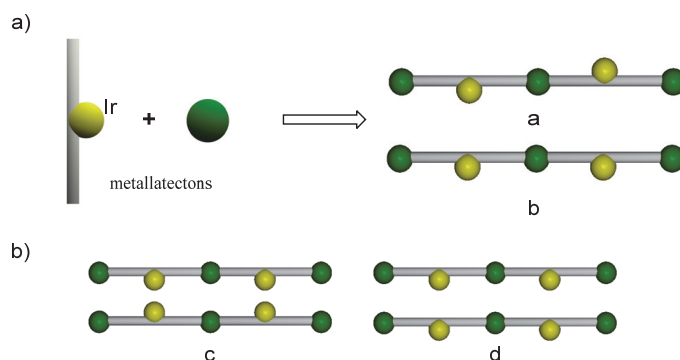


Figure II-40: Schematic representations of the arrangement of linear 1-D networks (*a* and *b*) and the packing arrangement of the latter (*c* and *d*).

In the case of the 2D grid-type network (Figure II-41), Ir(III) centres may be oriented inwardly (*i*) or outwardly (*o*). Thus for a single grid, four possibilities (i_4 , i_3o , $ioio$ and i_2o_2) may be envisaged (Figure II-41a). Furthermore, for the $ioio$ arrangement (Figure II-41b), two types of polar sheets *e* and *f* may be formed.

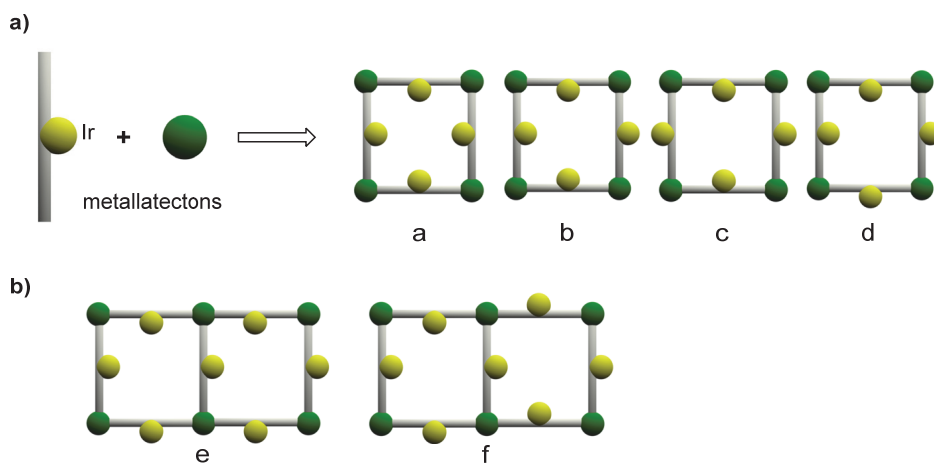


Figure II-41: Schematic representations of the possible arrangements of the Ir center within the grid (*a*) and polar sheets that may form in the case of the $ioio$ arrangement (*b*).

5.2 Heterometallic (Ir,Cu) grid-type coordination network obtained with *rac*-Ir(ppy)₂(bpy-4)PF₆ as metallatecton

The formation of extended heterometallic coordination networks was explored by combining the non-fluorinated Ir(III)-based metallatecton with different metal salts. The combination of racemic complex *rac*-[Ir(ppy)₂(bpy-4)][PF₆] in CHCl₃ with Cu(CH₃CN)₄(BF₄) in EtOH afforded red single crystals within a few days. The structural investigation by X-ray diffraction on single crystal revealed that the crystal (space group *C2/c*) is composed of the Iridium metallatecton [Ir(ppy)₂(bpy-4)]⁺, Cu²⁺ cations, BF₄⁻ and PF₆⁻ anions and solvent molecules (CHCl₃, EtOH) (Figure II-42). Owing to the severe disorder of solvent molecules not involved in direct interactions with the framework, the SQUEEZE command²⁶ was employed to process the data. It is worth noting that the copper precursor salt used for the self-assembly process was in its +I oxidation state and that oxidation of the metal occurred during the diffusion process and formation of the network taken place in the presence of air. However, no suitable single crystals were obtained when using directly Cu(BF₄)₂. The structural study revealed the formation of 2D grid-type network containing the metallatecton *rac*-[Ir(ppy)₂(bpy-4)]⁺ and Cu(BF₄)₂ complex as connecting node (Figure II-42).

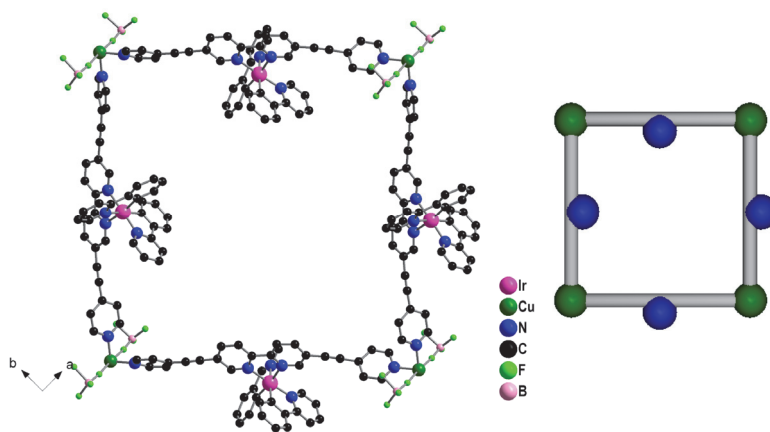


Figure II-42: Portions of the crystal structure of *rac*-[Ir(ppy)₂(bpy-4)][Cu(BF₄)₂] showing the grid type architecture resulting from the interconnection of the *Λ* enantiomer with Cu(BF₄)₂ acting as metaling node (right) and its schematic representation (left). H atoms, PF₆⁻ ions and solvent molecules are omitted for clarity.

The Iridium complex within the 2D network exhibits similar geometrical parameters (average bond lengths and angles: Ir-C_{ppy} 2.00 Å, Ir-N_{ppy} 2.04 Å, Ir-N_{bpy} 2.13 Å, N_{ppy}-Ir-N_{ppy} 174.6°, N_{ppy}-Ir-C_{ppy} 81.0°, N_{bpy}-Ir-N_{bpy} 76.5°) as those observed for the discrete metallatecton. However, while in the crystal structure of *rac*-[Ir(ppy)₂(bpy-4)][PF₆], the terminal pyridyl units connected by ethynyl

spacers to the bpy backbone were almost coplanar to the backbone, here they are tilted with respect to the **bpy-4** ligand in the grid-type network (tilt angles of -77.74° and -31.10°). The Cu(II) center adopts a slightly distorted octahedral geometry with four pyridyl groups belonging to four metallatectons occupying the square base of the octahedron (Cu-N *ca.* 2.01 Å) and two BF₄⁻ anions in axial positions (Cu-F 2.377(5) Å; F-Cu-F 176.0(2)° and N-Cu-F in the 85.7(2)°-91.7(2)° range) (Figure II-42).

Within the 2D-network, two consecutive Cu(II) metallic nodes are separated by 24.44 Å. Furthermore, unlike what has been observed before for other grid-like coordination networks,⁴¹ each grid is chiral as only one of the two enantiomers is present (Figure II-43). The consecutive homochiral sheets are packed in a staggered fashion along the *c* axis with alternation of Δ and Λ chirality leading thus to a non-chiral crystal. The inter-sheet distance of two alternated Δ and Λ homochiral sheets is 6.209 Å (distance between two mean planes defined by two consecutive grids, Figure II-43b). According to the discussion in Figure II-41, here, the *i*₂*o*₂ type arrangement is encountered for a single grid (Figure II-41a) and single sheets are of the polar *e* type (Figure II-41b). However, the homochiral and polar sheets are packed in a head-to tail fashion (Figure II-43a) leading thus to a non-polar crystal.

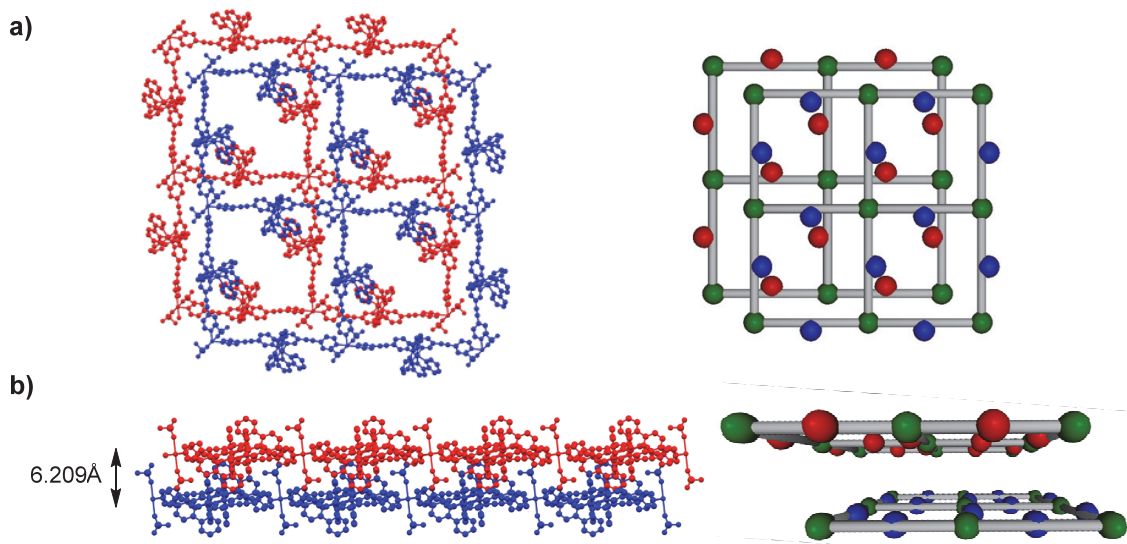


Figure II-43: Portions of the crystal structure of *rac*-[Ir(ppy)₂(**bpy-4**)]·[Cu(BF₄)₂] showing the staggered packing arrangement of two consecutive homochiral grids along the *c* axis (a) and *b* axis (b) and their schematic representations. The chiral grid containing the Λ enantiomers is depicted in red and the one with the Δ enantiomers in blue. Solvent molecules, H atoms and PF₆ anions are omitted for clarity.

The crystalline material *rac*-[Ir(ppy)₂(**bpy-4**)]·[Cu(BF₄)₂] was found to be rather air-unstable and no PXRD studies could be carried out. Degradation in less than an hour of the single crystals was

also observed using an optical microscope probably due to desolvation leading to collapse of the architecture.

Preliminary photoluminescence measurements in the solid state under ambient conditions were carried out on a standard fluorimeter. Because of the instability of the crystalline material, single crystals were embedded in a few drops of a perfluorinated-ether oil (Fomblin® Y) and deposited between two quartz coverslips adapted on the sample holder directly after their removal from the mother solution in order to prevent collapsing of the architecture. The integrity of the crystals was checked before and after the luminescence measurement by visual inspection with a microscope. Unfortunately, no emission of the coordination network could be detected with the instrument used. The luminescence quenching is probably due to the presence of the paramagnetic Cu(II) cation⁴² or to intermolecular interactions. O₂ quenching may also be expected as previously described.¹⁶ Because of the air instability of crystals, further studies in view of rationalising the emission quenching could not be carried out.

Unfortunately, the self-assembly of the enantiopure non-fluorinated metallatecton Δ - and Λ -[Ir(ppy)₂(bpy-4)][Y] (Y = Cl or PF₆) using different metal salts were also attempted but only precipitates or twinned crystals were obtained. No single crystals suitable for X-Ray diffraction have been obtained so far.

5.3 Heterometallic (Ir,Cd) 1D coordination networks obtained as racemate and enantiomerically pure with *rac*-Ir(dFppy)₂(bpy-4)PF₆ as metallatecton

The fluorinated complexes bearing terminal pyridyl moieties were used either as racemic mixture *rac*-[Ir(dFppy)₂(bpy-4)][PF₆] or as enantiopure Δ - and Λ -[Ir(dFppy)₂(bpy-4)][PF₆] complexes to generate heterometallic coordination networks upon self-assembly with different metal salts.

A-Racemic coordination network

Using as secondary metal source a metal precursor of the type MX₂ (M = metal; X = halogen) adopting an octahedral coordination geometry with the two apical positions occupied by the two X-anions, grid-type architecture could be expected.⁴³ However, another type of architecture was obtained using CdI₂ and *rac*-[Ir(dFppy)₂(bpy-4)][PF₆] as metallatecton. Thus, diffusion of an EtOH solution of CdI₂ through a EtOH/Cl₂CHCHCl₂ buffer containing two drops of trifluoroethanol and 4,4,4-trifluorobutanol into a solution of the Ir metallatecton, *rac*-[Ir(dFppy)₂(bpy-4)][PF₆], in 1,1,2,2-tetrachloroethane led to the formation of orange single crystals within few weeks. The crystal (*rac*-[Ir(dFppy)₂(bpy-4)]·[CdI₃], space group C2/c) is composed of the Iridium complex *rac*-[Ir(dFppy)₂(bpy-4)]⁺, Cd²⁺ cations, I⁻ anions and solvent molecules (EtOH, Cl₂CHCHCl₂) (Figure II-

44). It should be noted that, in the present case, all solvent molecules could be localized. Interestingly, the PF_6^- anions have been exchanged during the diffusion process with iodide ions in the resulting coordination polymer. Thus, one of the drawbacks of using a cationic metallatecton for the generation of coordination networks, *i.e.* the presence of counter ions in the crystal occupying the empty space, is circumvented. It is also worth noting that, even though the two fluorinated solvents, *i.e.* pentafluoroethanol and trifluorobutanol, were found to be indispensable for the formation of crystals, they are not present in the crystal lattice.

The Iridium center adopts a distorted octahedral geometry with bond lengths and angles ($\text{Ir}-\text{C}_{\text{ppy}}$ 2.013(7) Å; $\text{Ir}-\text{N}_{\text{ppy}}$ 2.048(6) Å; $\text{Ir}-\text{N}_{\text{bpy}}$ 2.130(4) Å; $\text{N}_{\text{ppy}}-\text{Ir}-\text{N}_{\text{ppy}}$ 175.3(3)°; $\text{N}_{\text{ppy}}-\text{Ir}-\text{C}_{\text{ppy}}$ 80.8(3)°; $\text{N}_{\text{bpy}}-\text{Ir}-\text{N}_{\text{bpy}}$ 77.1(2)°) similar to those observed for the discrete metallatecton. While the dFppy ligands are almost planar (dihedral angle $\text{N}_{\text{ppy}}-\text{C}_{\text{ppy}}-\text{C}_{\text{ppy}}-\text{C}_{\text{ppy}} = 2.051^\circ$), the bipyridyl units are not coplanar (dihedral angle $\text{N}_{\text{bpy}}-\text{C}_{\text{bpy}}-\text{C}_{\text{bpy}}-\text{N}_{\text{bpy}} = 8.159^\circ$) and the ethynyl spacers are not linear ($\text{C}\equiv\text{C}-\text{C}_{\text{bpy}}$ 171.0(8) and $\text{C}_{\text{py}}-\text{C}\equiv\text{C}$ 176.4(8)°). As a consequence, the bpy ligand is slightly curved and the tilt angle between the terminal and central pyridyl units of the bpy ligand is slightly more pronounced than for the discrete metallatecton. Within the coordination polymer, the Cd center adopts a trigonal bipyramidal geometry with the two terminal pyridyl moieties of two different metallatectons occupying the apical positions ($\text{Cd}-\text{N}$ 2.463(5) Å; $\text{N}-\text{Cd}-\text{N}$ 172.0(3)°) and three iodide atoms occupying the trigonal base ($\text{Cd}-\text{I}$ 2.7635(9) Å and 2.8114(6) Å; $\text{I}-\text{Cd}-\text{I}$ 117.33(3)° and 121.337(15)°). Thus, the $[\text{CdI}_3]^+$ complex behaves as a 2-connecting node and bridges two consecutive metallatectons of the same chirality leading thus to an infinite 1D homochiral network ((Figure II-44).

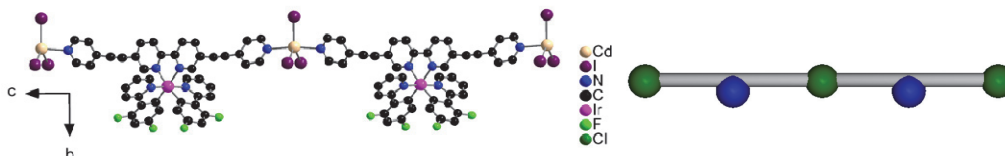


Figure II-44: Portions of the crystal structure of $\text{rac}[\text{Ir}(\text{dFppy})_2(\text{bpy}-4)] \cdot [\text{CdI}_3]$ and its schematic representation.

According to the discussion in Figure II-41, within one homochiral chain, the metallatecton are oriented in the same direction inducing formation of a polar linear chain (Figure II-41). The distance between two consecutive Cd^{2+} cations is 25.26 Å. The polar linear chains are packed in a parallel mode and slightly staggered. A rather short $\text{Cl}\cdots\text{F}$ distance of ca. 2.92 Å is observed between the chlorinated solvent molecules and the F atom in position 4 belonging to the dFppy moieties (Figures II-45a). The packing of 1D chiral networks leads to homochiral planes (Δ or Λ). Consecutive planes are of opposite chirality and packed in a parallel fashion leading thus to the formation of the crystal (Figures II-45b). The tetrachloroethane solvent molecules occupy the empty spaces within each sheet. Between consecutive sheets, a rather short distance of 3.44 Å between F atoms and the dFppy

centroids is observed. Again, the purity of microcrystalline powder was ascertained by PXRD which revealed a good match between patterns simulated from single crystal and experimental data.

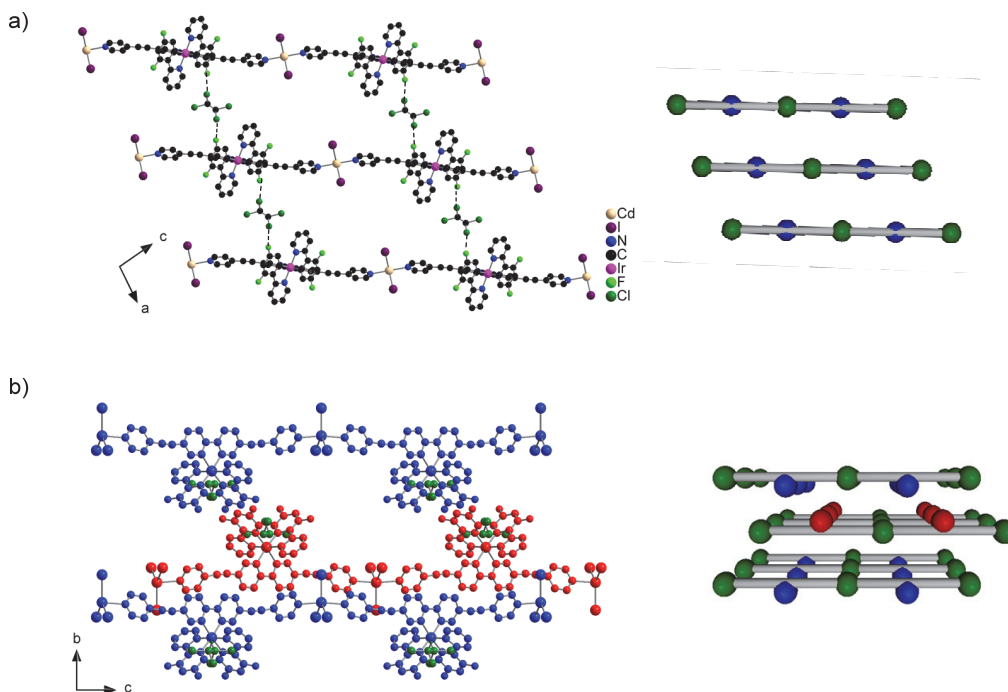


Figure II-45: Portions of the crystal structure of *rac*-[Ir(dFppy)₂(bpy-4)]·[CdI₃] showing the arrangement of homochiral parallel infinite chains containing only the Δ enantiomers and connected through Cl-F and F-F interactions (dashed lines) resulting in the formation of homochiral sheets (a); the centro-symmetric packing of consecutive homochiral planes along the *b* axis (b). The Δ enantiomers are depicted in blue while the Λ enantiomers are colored in red. The chlorinated solvent molecules are depicted in green. EtOH solvent molecules and H atoms have been omitted for clarity.

B-Enantiopure coordination network

Under the same self-assembly conditions, the enantiopure Λ -[Ir(dFppy)(bpy-4)][PF₆] metallatecton combined with CdI₂ salt afforded within two weeks orange single crystals. The structural investigation by single crystal X-ray diffraction also revealed the formation of infinite 1D-coordination network, Λ -[Ir(dFppy)₂(bpy-4)]·[CdI₃] (Figure II-46). Again, during the self-assembly process, the PF₆ counter ion of the metallatecton was exchanged with iodide anions in the final architecture. Thus, Λ -[Ir(dFppy)(bpy-4)]⁺ and Cd²⁺ cations as well as iodide anions and methanol molecules are present within the crystal lattice (chiral space group C2). It should be noted that owing to the disorder of other solvent molecules, the corresponding electron density was removed using the SQUEEZE command.²⁶ For that reason, one cannot exclude the presence of halogenated solvent molecules within the crystal. Within the enantiomerically pure 1D coordination network, the bond lengths and angles for the Λ -Ir metallatecton (average distances and angles : Ir-C_{ppy} 2.010 Å; Ir-N_{ppy}

2.065 Å; Ir-N_{bpy} 2.132 Å; N_{ppy}-Ir-N_{ppy} 176.0°; N_{ppy}-Ir-C_{ppy} 81.4°; N_{bpy}-Ir-N_{bpy} 77.1°) are similar to those observed for the achiral coordination polymer. As observed for the racemic CP, the two central pyridyl rings of the bpy ligand are not coplanar exhibiting a dihedral angle of *ca.* 8.67° while the difluorophenyl and pyridyl rings belonging to the cyclometalating unit are almost coplanar (dihedral angle in the range -2.031 to 1.221°). The ethynyl spacers are also slightly curved and the terminal pyridyl units are tilted with respect to the bidentate central bpy unit. The geometry around the Cd atom is again trigonal bipyramidal with three iodine atoms occupying the trigonal base (Cd-I 2.7734(13); 2.7824(12); 2.7879(8) and 2.8100(8) Å; I-Cd-I 119.80(2); 119.58(2); 120.41(4) and 120.85(4)°) and two nitrogen atoms belonging to the terminal pyridyl units of two different metallatecton in axial positions (Cd-N 2.485(6) and 2.465(6) Å; N-Cd-N 174.0(3) and 173.1(4)°). The bridging of two consecutive enantiopure Ir metallatectons by Cd atoms leads to the formation of infinite chiral chains with a distance of 25.32 Å between two consecutive Cd(II) metallic nodes (Figure II-46).

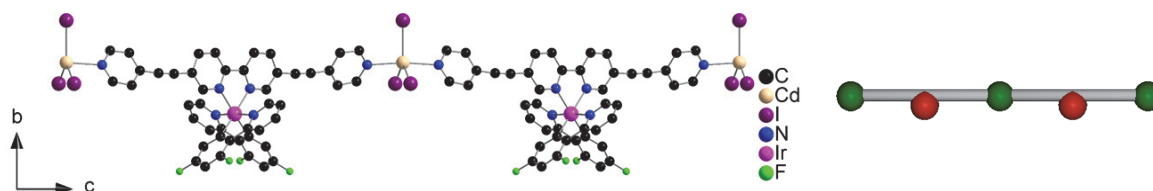


Figure II-46: Portion of the crystal structure of Λ -[Ir(dFppy)₂(bpy-4)]·[CdI₃] and its schematic representation.

Consecutive chains are parallel to each other and staggered forming layers of parallel chains. The packing within the crystal lattice is however slightly different than the one observed for the racemic coordination network *rac*-[Ir(dFppy)₂(bpy-4)]·[CdI₃]. Indeed, here two types of layers exist within the crystal, depicted either in grey or red in Figure II-47c. Each layer is polar with metallatectons oriented in the same direction, and the different layers are packed with the dFppy units pointing alternatively up or down to make the whole structure non polar. Furthermore, in the case of the grey layer, weak F-F interactions are present between two fluoride atoms in positions 2 of two dFppy units bound to two adjacent Ir complexes (F-F = 3.115 Å) (Figure II-47a). However, the red layer does not display any F-F interaction (Figure II-47b). It should be noted that, as stated above, the electron density of disordered Cl₂CHCHCl₂ solvent molecules was removed using the SQUEEZE command. Thus, Cl-F interactions between chlorinated solvent molecules and dFppy units similar to those observed in the racemic coordination polymer cannot be dismissed. Finally, the experimental PXRD pattern of microcrystalline powder matches the simulated pattern confirming the purity of the powder.

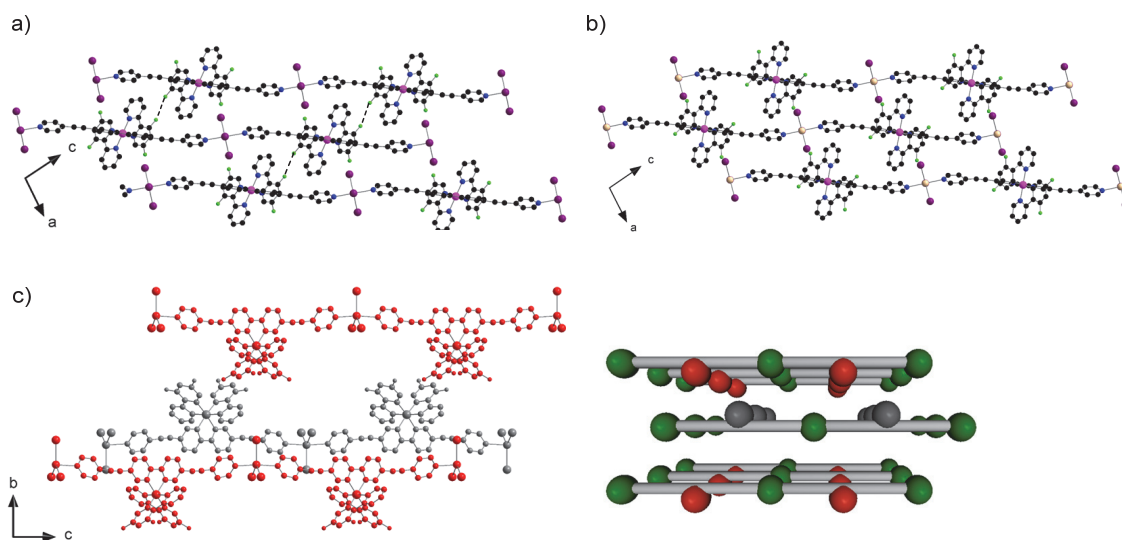


Figure II-47. Portions of the X-ray structure of Λ -[Ir(dFppy)₂(bpy-4)]·[CdI₃] showing the formation of infinite chains along the *b* axis of two types of layers (a) and (b) and the packing of consecutive homochiral chains along the *b* axis and its schematic representation (c). For the sake of clarity, the chains with dFppy units pointing up are depicted in grey and the ones with dFppy moieties pointing down are shown in red. MeOH solvent molecules and H atoms are omitted for clarity.

C-Luminescent properties

Both infinite architectures, rac -[Ir(dFppy)₂(bpy-4)]·[CdI₃] and Λ -[Ir(dFppy)₂(bpy-4)]·[CdI₃] are emissive in the solid state under ambient conditions. It should be noted that the absorption properties in the solid state of both architectures exhibit intense absorption between 300 and 650 nm similar to the discrete metallatecton. As presented in Figure II-48 and Table II-11, rac -[Ir(dFppy)₂(bpy-4)]·[CdI₃] and Λ -[Ir(dFppy)₂(bpy-4)]·[CdI₃] exhibit almost the same emission bands. This seems reasonable since the two architectures present similar structural parameters and packing modes. When compared with the discrete metallatecton, rac -[Ir(dfppy)₂(bpy-4)][PF₆], the emission bands of the two coordination polymers are slightly red-shifted by *ca.* 17 nm. This phenomena could be assigned to the slight difference in charge-transfer character arising from the Cd(II) cation. Such observation has already been reported for a (Cd,Ir) heterometallic coordination network based on the use of [Ir(ppy)₂(H₂dc bpy)][PF₆] as metallatecton (H₂dc bpy = 4, 4'-dicarboxyl-2,2'-bipyridine)^{16a} and other relevant d¹⁰ structures.⁴⁴ Indeed, assuming that the lowest excited state as a ligand centered character, the binding of Cd²⁺ cation by the pyridyl units should slightly affect the electronic properties of the bpy ligand, thus modifying the LUMO energy level of the complex.

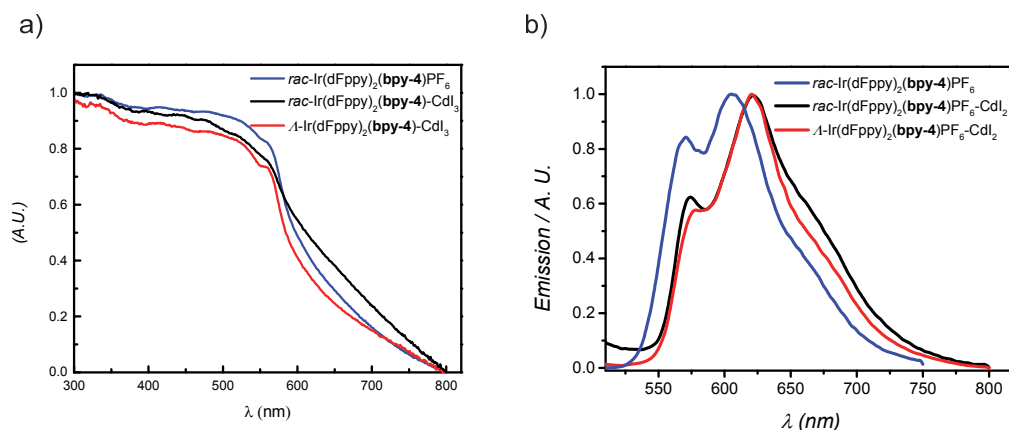


Figure II-48: Reflectance spectra (a) and emission spectra (b) of *rac*-[Ir(dFppy)₂(bpy-4)][PF₆] (blue lines), *rac*-[Ir(dFppy)₂(bpy-4)]·[CdI₃] (black lines) and Λ -[Ir(dFppy)₂(bpy-4)]·[CdI₃] (red lines).

Table II-11: Emission properties and solid state quantum yields of *rac*-[Ir(dFppy)₂(bpy-4)][PF₆], *rac*-[Ir(dFppy)₂(bpy-4)]·[CdI₃] and Λ -[Ir(dFppy)₂(bpy-4)]·[CdI₃].

| | λ_{em} (nm) ^a | Φ^a |
|--|---|----------|
| <i>rac</i> -[Ir(dFppy) ₂ (bpy-4)][PF ₆] | 570, 605 | 2 % |
| <i>rac</i> -[Ir(dFppy) ₂ (bpy-4)]·[CdI ₃] | 575, 622 | < 1 % |
| Λ -[Ir(dFppy) ₂ (bpy-4)]·[CdI ₃] | 576, 622 | < 1 % |

a: excited at 390 nm.

Quantum yields (QY) of *rac*-[Ir(dFppy)₂(bpy-4)]·[CdI₃] and Λ -[Ir(dFppy)₂(bpy-4)]·[CdI₃] which are less than 1 % were also determined. These relatively weak QY might be related to the presence of π - π interactions (different stacking arrangements compared to *rac*-[Ir(dFppy)₂(bpy-4)][PF₆]), as evidenced in the crystal structures, quenching partially the solid state emission with respect to that of *rac*-[Ir(dFppy)₂(bpy-4)][PF₆].

6. Conclusion of chapter

In this chapter, the synthesis of both racemic and enantiopure cationic Ir(III) complexes based either on pyridyl or carboxylic acid moieties as coordinating sites have been described. Several coordination networks based on these complexes have been generated and structurally investigated in the crystalline phase by X-Ray diffraction.

The luminescent properties of different complexes as well as different coordination polymers were studied. The photophysical properties of the Cd(II)-Ir(III) infinite chains are almost not affected by the coordination of Cd²⁺ ions and a luminescence arising from the Ir(III) complex is observed. However, the emission of the grid-type architecture could not be detected, the presence of Cu(II) being probably responsible for this emission quenching.⁴⁵

The use of these metallatectons to generate coordination polymers proved successful. However, this strategy presents two main drawbacks: i) the pores of the coordination polymers are not only filled with solvent molecules but also with the counter ions of the metallatecton reducing thus the available space for other guest molecules inclusion; ii) to counter balance the charge of the metallatecton within the resulting coordination networks, the counter ion, PF_6^- in our case, may be exchanged with the anions belonging to the metal salts as exemplified with the use of CdI_2 . Such ion exchange leads to the formation of neutral architectures without any counter ions in the voids but with a lower dimensionality (chains vs grid).

REFERENCES

- (1) (a) King, K. A.; Spellane, P. J.; Watts, R. J. *J. Am. Chem. Soc.* **1985**, *107*, 1431; (b) Garces, F. O.; King, K. A.; Watts, R. J. *Inorg. Chem.* **1988**, *27*, 3464; (c) Colombo, M. G.; Brunold, T. C.; Riedener, T.; Güedel, H. U.; Fortsch, M.; Büergi, H.-B. *Inorg. Chem.* **1994**, *33*, 545.
- (2) (a) Ulbricht, C.; Beyer, B.; Friebe, C.; Winter, A.; Schubert, U. S. *Adv. Mater.* **2009**, *21*, 4418; (b) Lamansky, S.; Djurovich, P.; Murphy, D.; Abdel-Razzaq, F.; Lee, H.-E.; Adachi, C.; Burrows, P. E.; Forrest, S. R.; Thompson, M. E. *J. Am. Chem. Soc.* **2001**, *123*, 4304.
- (3) Baranoff, E.; Cahill, J. F.; Flamigni, L.; Sauvage, J. P. *Chem. Soc. Rev.* **2004**, *33*, 147.
- (4) (a) Dixon, I. M.; Collin, J.-P.; Sauvage, J.-P.; Flamigni, L.; Encinas, S.; Barigelletti, F. *Chem. Soc. Rev.* **2000**, *29*, 385; (b) Basu, S.; Peng, S.-M.; Lee, G.-H.; Bhattacharya, S. *Polyhedron* **2005**, *24*, 157.
- (5) Luo, S.-X.; Wei, L.; Zhang, X.-H.; Lim, M. H.; Lin, K. X. V.; Yeo, M. H. V.; Zhang, W.-H.; Liu, Z.-P.; Young, D. J.; Hor, T. S. A. *Organometallics* **2013**, *32*, 2908.
- (6) Nonoyama, M. *J. Organomet. Chem.* **1975**, *86*, 263.
- (7) Sprouse, S.; King, K. A.; Spellane, P. J.; Watts, R. J. *J. Am. Chem. Soc.* **1984**, *106*, 6647.
- (8) (a) Lee, P. K.; Law, W. H.; Liu, H. W.; Lo, K. K. *Inorg. Chem.* **2011**, *50*, 8570; (b) Lo, K. K.-W.; Zhang, K. Y.; Li, S. P.-Y. *Pure Appl. Chem.* **2011**, *83*, 823.
- (9) Fernandez-Hernandez, J. M.; Beltran, J. I.; Lemaure, V.; Galvez-Lopez, M. D.; Chien, C. H.; Polo, F.; Orselli, E.; Frohlich, R.; Cornil, J.; De Cola, L. *Inorg. Chem.* **2013**, *52*, 1812.
- (10) (a) Auffrant, A.; Barbieri, A.; Barigelletti, F.; Lacour, J.; Mobian, P.; Collin, J. P.; Sauvage, J. P.; Ventura, B. *Inorg. Chem.* **2007**, *46*, 6911; (b) Huo, H.; Fu, C.; Harms, K.; Meggers, E. *J. Am. Chem. Soc.* **2014**, *136*, 2990.
- (11) Gong, L.; Mulcahy, S. P.; Harms, K.; Meggers, E. *J. Am. Chem. Soc.* **2009**, *131*, 9602.
- (12) Chepelin, O.; Ujma, J.; Wu, X.; Slawin, A. M.; Pitak, M. B.; Coles, S. J.; Michel, J.; Jones, A. C.; Barran, P. E.; Lusby, P. J. *J. Am. Chem. Soc.* **2012**, *134*, 19334.
- (13) Huo, H.; Shen, X.; Wang, C.; Zhang, L.; Rose, P.; Chen, L. A.; Harms, K.; Marsch, M.; Hilt, G.; Meggers, E. *Nature* **2014**, *515*, 100.
- (14) Xie, Z.; Ma, L.; deKrafft, K. E.; Jin, A.; Lin, W. *J. Am. Chem. Soc.* **2010**, *132*, 922.
- (15) (a) Barrett, S. M.; Wang, C.; Lin, W. *J. Mater. Chem.* **2012**, *22*, 10329; (b) Wang, C.; Liu, D.; Xie, Z.; Lin, W. *Inorg. Chem.* **2014**, *53*, 1331; (c) Wang, C.; Xie, Z.; deKrafft, K. E.; Lin, W. *J. Am. Chem. Soc.* **2011**, *133*, 13445.
- (16) (a) Ho, M. L.; Chen, Y. A.; Chen, T. C.; Chang, P. J.; Yu, Y. P.; Cheng, K. Y.; Shih, C. H.; Lee, G. H.; Sheu, H. S. *Dalton Trans.* **2012**, *41*, 2592; (b) Chen, Y.-T.; Lin, C.-Y.; Lee, G.-H.; Ho, M.-L. *CrystEngComm* **2015**, *17*, 2129.

- (17) (a) Li, L.; Zhang, S.; Xu, L.; Han, L.; Chen, Z.-N.; Luo, J. *Inorg. Chem.* **2013**, *52*, 12323; (b) Li, L.; Zhang, S.; Xu, L.; Wang, J.; Shi, L.-X.; Chen, Z.-N.; Hong, M.; Luo, J. *Chem. Sci.* **2014**, *5*, 3808.
- (18) Wang, C.; deKrafft, K. E.; Lin, W. *J. Am. Chem. Soc.* **2012**, *134*, 7211.
- (19) Cavazzini, M.; Quici, S.; Scalera, C.; Puntoriero, F.; La Ganga, G.; Campagna, S. *Inorg. Chem.* **2009**, *48*, 8578.
- (20) You, Y.; Park, S. Y. *J. Am. Chem. Soc.* **2005**, *127*, 12438.
- (21) Beeby, A.; Bettington, S.; Fairlamb, I. J. S.; Goeta, A. E.; Kapdi, A. R.; Niemelä, E. H.; Thompson, A. L. *New J. Chem.* **2004**, *28*, 600.
- (22) (a) Lepeltier, M.; Dumur, F.; Marrot, J.; Contal, E.; Bertin, D.; Gigmes, D.; Mayer, C. R. *Dalton Trans.* **2013**, *42*, 4479; (b) Li, L.; Wu, F.; Zhang, S.; Wang, D.; Ding, Y.; Zhu, Z. *Dalton Trans.* **2013**, *42*, 4539.
- (23) Ayme, J. F.; Beves, J. E.; Leigh, D. A.; McBurney, R. T.; Rissanen, K.; Schultz, D. *Nat Chem* **2012**, *4*, 15.
- (24) Tinker, L. L.; McDaniel, N. D.; Cline, E. D.; Bernhard, S. *Inorg. Synth.* **2010**, *35*, 168.
- (25) Gonzalo Rodriguez, J.; Martin-Villamil, R.; H. Cano, F.; Fonseca, I. *J. Chem. Soc., Perkin Trans. I* **1997**, 709.
- (26) Spek, A. L. *PLATON*; The University of Utrecht, The Netherlands, 1999.
- (27) (a) Costa, R. D.; Ortí, E.; Bolink, H. J.; Graber, S.; Schaffner, S.; Neuburger, M.; Housecroft, C. E.; Constable, E. C. *Adv. Funct. Mater.* **2009**, *19*, 3456; (b) Moriuchi, T.; Katano, C.; Hirao, T. *Chem. Lett.* **2012**, *41*, 310; (c) Leslie, W.; Batsanov, A. S.; Howard, J. A. K.; Gareth Williams, J. A. *Dalton Trans.* **2004**, 623; (d) Ladouceur, S.; Fortin, D.; Zysman-Colman, E. *Inorg. Chem.* **2010**, *49*, 5625; (e) Neve, F.; La Deda, M.; Crispini, A.; Bellusci, A.; Puntoriero, F.; Campagna, S. *Organometallics* **2004**, *23*, 5856.
- (28) Flamigni, L.; Barbieri, A.; Sabatini, C.; Ventura, B.; Barigelletti, F. *Top. Curr. Chem.* **2007**, *281*, 143.
- (29) Lowry, M. S.; Bernhard, S. *Chem. Eur. J.* **2006**, *12*, 7970.
- (30) (a) Glusac, K. D.; Jiang, S.; Schanze, K. S. *Chem. Commun.* **2002**, 2504; (b) Lafolet, F.; Welter, S.; Popović, Z.; Cola, L. D. *J. Mater. Chem.* **2005**, *15*, 2820; (c) Kim, K.-Y.; Farley, R. T.; Schanze, K. S. *The Journal of Physical Chemistry B* **2006**, *110*, 17302.
- (31) (a) Colombo, M. G.; Hauser, A.; Gudel, H. U. *Inorg. Chem.* **1993**, *32*, 3088; (b) Ohsawa, Y.; Sprouse, S.; King, K. A.; DeArmond, M. K.; Hanck, K. W.; Watts, R. J. *J. Phys. Chem.* **1987**, *91*, 1047.
- (32) Brouwer, A. M. *Pure Appl. Chem.* **2011**, *83*, 2213.
- (33) Lacour, J.; Ginglinger, C.; Grivet, C.; Bernardinelli, G. *Angew. Chem. Int. Ed. Engl.* **1997**, *36*, 608.
- (34) Lacour, J.; Vial, L.; Herse, C. *Org. Lett.* **2002**, *4*, 1351.
- (35) Meggers, E. *Chem. Eur. J.* **2010**, *16*, 752.
- (36) Schneider, G. E.; Bolink, H. J.; Constable, E. C.; Ertl, C. D.; Housecroft, C. E.; Pertegas, A.; Zampese, J. A.; Kanitz, A.; Kessler, F.; Meier, S. B. *Dalton Trans.* **2014**, *43*, 1961.
- (37) Tour, J. M.; Rawlett, A. M.; Kozaki, M.; Yao, Y.; Jagessar, R. C.; Dirk, S. M.; Price, D. W.; Reed, M. A.; Zhou, C.-W.; Chen, J.; Wang, W.; Campbell, I. *Chem. Eur. J.* **2001**, *7*, 5118.
- (38) Taylor, E. C.; Ray, P. S. *J. Org. Chem.* **1988**, *53*, 38.
- (39) Kang, S. H.; Ma, H.; Kang, M.-S.; Kim, K.-S.; Jen, A. K. Y.; Zareie, M. H.; Sarikaya, M. *Angew. Chem. Int. Ed.* **2004**, *43*, 1512.
- (40) Bunzli, A. M.; Bolink, H. J.; Constable, E. C.; Housecroft, C. E.; Junquera-Hernandez, J. M.; Neuburger, M.; Ortí, E.; Pertegas, A.; Serrano-Perez, J. J.; Tordera, D.; Zampese, J. A. *Dalton Trans.* **2014**, *43*, 738.
- (41) (a) Béziau, A.; Baudron, S. A.; Rasoloarison, D.; Hosseini, M. W. *CrystEngComm* **2014**, *16*, 4973; (b) Béziau, A.; Baudron, S. A.; Rogez, G.; Hosseini, M. W. *Inorg. Chem.* **2015**, *54*, 2032.
- (42) (a) Jayaramulu, K.; Narayanan, R. P.; George, S. J.; Maji, T. K. *Inorg. Chem.* **2012**, *51*, 10089; (b) Wu, P.; Wang, J.; He, C.; Zhang, X.; Wang, Y.; Liu, T.; Duan, C. *Adv. Funct. Mater.* **2012**, *22*, 1698.

- (43) (a) Sguerra, F.; Bulach, V.; Hosseini, M. W. *Dalton Trans.* **2012**, 41, 14683; (b) Beziau, A.; Baudron, S. A.; Fluck, A.; Hosseini, M. W. *Inorg. Chem.* **2013**, 52, 14439; (c) Larpent, P.; Jouaiti, A.; Kyritsakas, N.; Hosseini, M. W. *Dalton Trans.* **2014**, 43, 2000; (d) Ovsyannikov, A.; Ferlay, S.; Solovieva, S. E.; Antipin, I. S.; Konovalov, A. I.; Kyritsakas, N.; Hosseini, M. W. *CrystEngComm* **2014**, 16, 3765.
- (44) (a) Zheng, S.-L.; Yang, J.-H.; Yu, X.-L.; Chen, X.-M.; Wong, W.-T. *Inorg. Chem.* **2004**, 43, 830; (b) Béziau, A.; Baudron, S. A.; Guenet, A.; Hosseini, M. W. *Chem. Eur. J.* **2013**, 19, 3215.
- (45) (a) Ma, D. L.; He, H. Z.; Chan, D. S.; Wong, C. Y.; Leung, C. H. *PLoS One* **2014**, 9, e99930; (b) Lu, F.; Yamamura, M.; Nabeshima, T. *Tetrahedron Lett.* **2013**, 54, 779.

Chapter III: Synthesis of neutral Ir(III) complexes for the formation of coordination networks

As mentioned in the former chapter, cationic bis-cyclometallated Ir(III) complexes acting as metallatecton exhibit some drawbacks such as reduced available empty space since anions occupy some of the voids. Those drawbacks may be circumvented by using neutral Ir(III) metallatectons. Furthermore, neutral tris-cyclometallated Ir(III) complexes do generally exhibit more interesting luminescent properties, such as higher quantum yield and relatively longer lifetime.¹ Thus, this chapter will focus on the preparation of neutral tris-cyclometallated Ir(III) complexes and their use for the formation of luminescent heterometallic coordination networks.

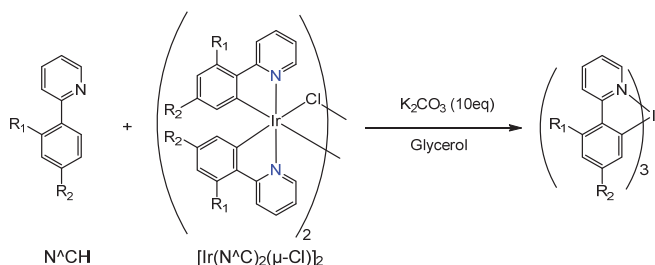
1. Introduction

This introduction part will briefly summarize the available synthetic methods to prepare neutral tris-cyclometallated Ir(III) complexes and then presents a brief overview of their luminescent properties which were already exposed in the general introduction. Finally, some literature examples of coordination networks based on neutral Ir(III) complexes will be given.

1.1 Synthesis of neutral tris-cyclometallated Ir(III) complexes

As noted in the general introduction, the synthesis of neutral tris-cyclometallated Ir(III) complexes requires harsh conditions, such as high temperature, and leads usually to the coexistence of *mer*- and *fac*- complexes. In order to overcome these difficulties, several synthetic approaches were developed in order to obtain selectively either the *mer*- or *fac*- isomers, some of which will be discussed below.

In 2003, in their pioneering work, Thompson *et al.* reported the selective synthesis of a series of facial and meridional homoleptic tris-cyclometallated Iridium(III) complexes starting in particular from the Ir dimer $[\text{Ir}(\text{N}^{\wedge}\text{C})_2(\mu\text{-Cl})_2]$ (Figure III-1).² They observed that the facial/meridional product ratios are strongly affected by temperature as well as by the nature of the cyclometallating ligands. As illustrated in Figure III-1, for ligands ppyH and tpyH (ppy = 2-phenylpyridyl; tpy = 2-(4-tolyl)pyridyl), with an excess of K_2CO_3 in glycerol, meridional products are mainly obtained at relatively low temperature (below 140 °C), while facial products are obtained at *ca* 200 °C. In contrast, using dFppyH as ligand (dFppy = 2-(2,4-difluorophenyl)pyridyl) a mixture of *mer* and *fac* products is obtained at 140 °C.



| Ligands | T < 140°C (isolated yields) | T > 200°C (isolated yields) |
|---|-----------------------------|-----------------------------|
| ppyH: R ₁ = H, R ₂ = H | <i>mer</i> (75%) | <i>fac</i> (79%) |
| tpyH: R ₁ = CH ₃ , R ₂ = H | <i>mer</i> (78%) | <i>fac</i> (81%) |
| dFppyH: R ₁ = F, R ₂ = F | <i>mer</i> / <i>fac</i> | <i>fac</i> (74%) |

Figure III-1: Thompson's method to prepare homoleptic *mer* or *fac* tris-cyclometallated Iridium(III) complexes.²

van Koten *et al.*³ expanded this study to the synthesis of heteroleptic complexes and confirmed that the *mer* isomer was photochemically converted to the *fac* isomer under irradiation (Hg lamp) (Figure III-2).

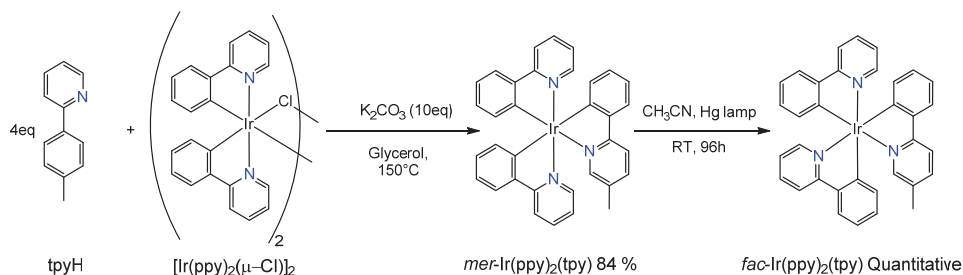


Figure III-2: Synthesis of heteroleptic *mer/fac* tris-cyclometallated Iridium (III) complexes and photochemical isomerization.³

Following the work of Güdel *et al.* who used Ag salts to obtain the complex *fac*-Ir(ppy)₃,⁴ Crutchley and co-workers expanded this method to generate heteroleptic complexes and selectively form either the *mer* or *fac* tris-cyclometallated Ir(III) complexes. Ag salts were used to scavenge the chloride ions of the Ir dimer precursors.⁵ As illustrated in Figure III-3, a lower temperature (57 °C) was required to obtain the desired *mer* isomer while a higher temperature afforded the *fac* product. Because of its relatively low required temperature, this method was then exploited by other groups using other ligands. However, temperatures up to 120 °C were sometimes necessary, and the yields were usually around 30 % to 40 %.^{for example see 6}

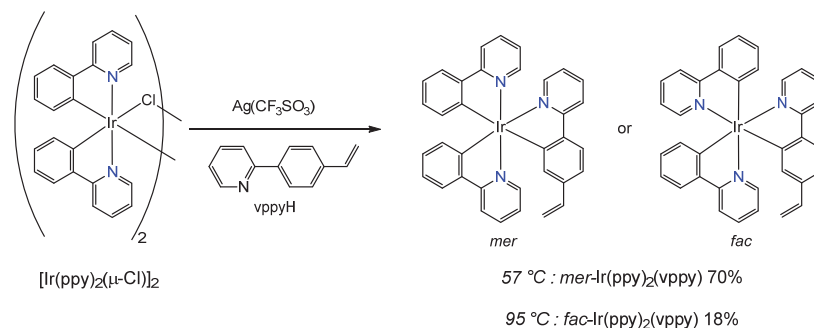


Figure III-3: Crutchley's method for the synthesis of neutral Ir(III) complexes.⁵

In 2006, Huo *et al.* obtained the *mer*-isomers with a selectivity > 99 % using a transmetalating reagent.⁷ The method is based on the use of a halide-bridged dinuclear bis-cyclometallated iridium complex $[\text{Ir}(\text{ppy})_2(\mu\text{-Br})]_2$ with $[\text{ppyZnCl}]$ as the transmetalating reagent to form tris-cyclometallated homoleptic or heteroleptic iridium complexes (Figure III-4). In these cases, meridional products were obtained with good selectivity and high yields. However, the major difficulty of this approach is the preparation of the transmetalating reagents.

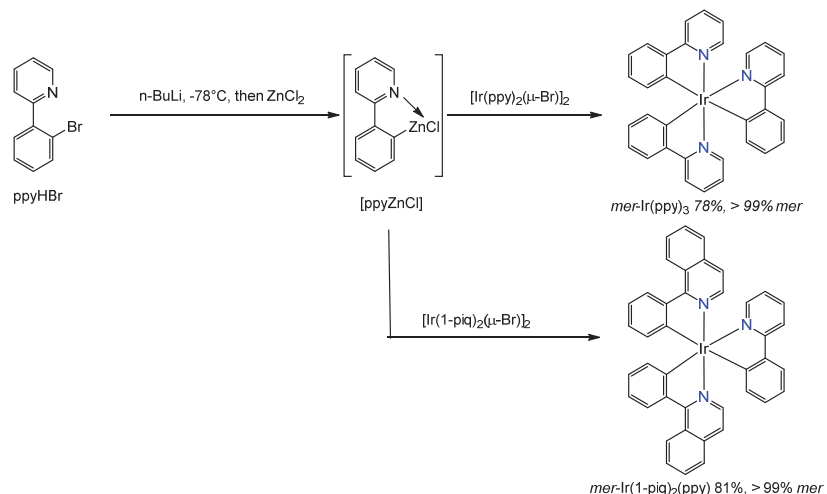


Figure III-4: Method developed by Huo *et al.* to obtain meridional products in high yields.⁷

In 2007, Mann *et al.*⁸ demonstrated that, by using “activated” Iridium (III) precursors (Figure III-5), the desired homoleptic neutral tris-cyclometallated Ir complexes could be generated. Thus, the chloro-bridged dimers $[\text{Ir}(\text{C}\wedge\text{N})_2(\mu\text{-Cl})]_2$ was either cleaved and weakly coordinating solvents such as acetonitrile would complete the coordination sphere of the Ir center to form the $[\text{Ir}(\text{C}\wedge\text{N})_2(\text{ACN})_2][\text{PF}_6]$ complex or converted to the hydroxyl-bridged dimer $[\text{Ir}(\text{C}\wedge\text{N})_2(\mu\text{-OH})]_2$ (Figure III-5a). When $[\text{Ir}(\text{C}\wedge\text{N})_2(\text{ACN})_2][\text{PF}_6]$ was employed as precursor, the facial isomer was obtained below 100 °C as the major product, while the use of $[\text{Ir}(\text{C}\wedge\text{N})_2(\mu\text{-OH})]_2$ as precursor afforded mainly the meridional isomer. Bis-cyclometallated Ir complexes bearing the acac (acetylacetonato) ligand as the third ligand are also common precursors for the synthesis of tris-

cyclometallated neutral Ir(III) complexes. Their synthesis may be achieved either by chelating the acac group in the presence of Ag salts⁹ or at high temperature¹⁰ or through a one-pot synthesis starting from $[\text{Ir}(\text{acac})(\text{coe})_2]$ ($\text{coe} = \text{cis-cyclooctene}$) obtained *in situ*.¹¹ For the latter, by varying the reaction conditions (solvents, temperature, time), the selective formation of *mer*- or *fac*- products was achieved (Figure III-5b). The efficiency of this method based on “activated” acac complexes was shown to be successful as lower reaction temperature was required. However, for the formation of heteroleptic complexes, ligand scrambling could not be efficiently avoided.

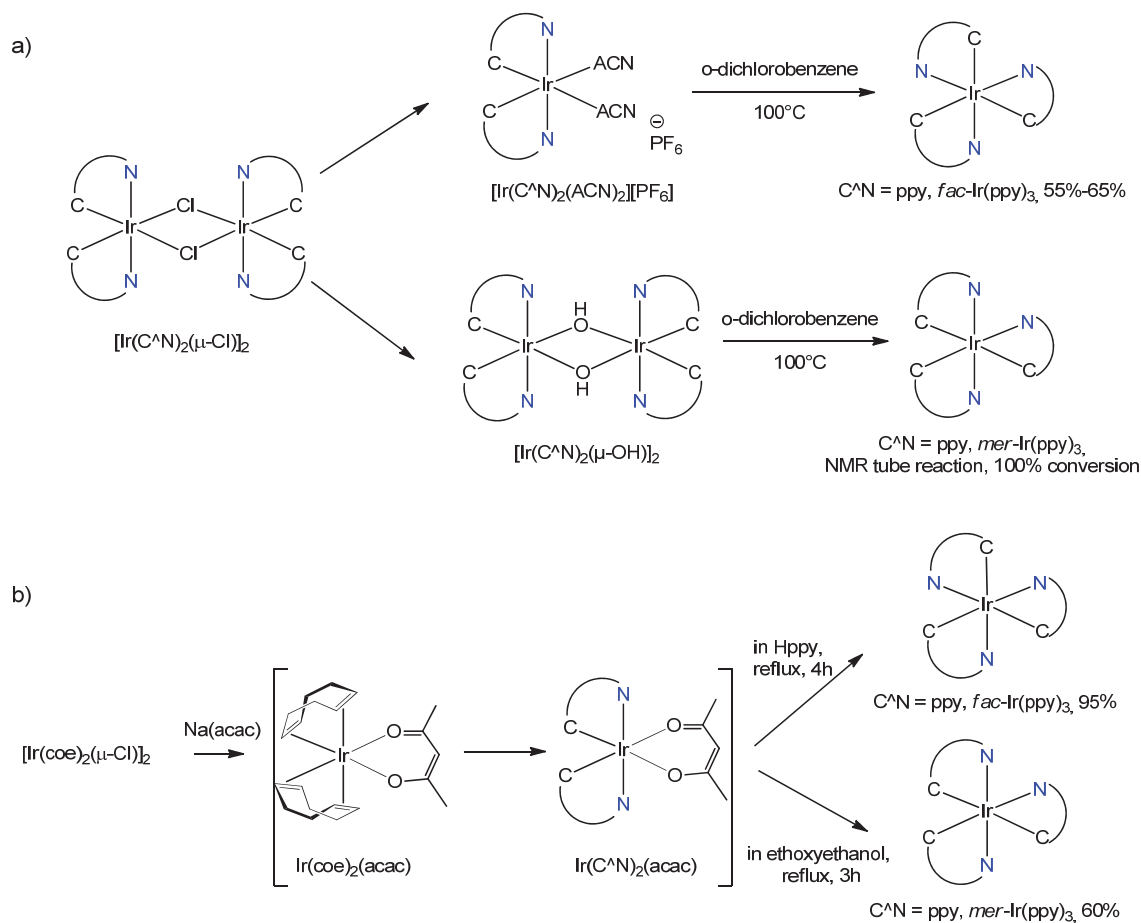


Figure III-5: Synthesis of tris-cyclometallated Iridium(III) complexes through “activated” Iridium(III) precursors.^{8,11}

All the examples presented above confirm that the selective formation of either *mer*- or *fac*-cyclometallated Ir(III) complexes can be largely affected by the ligands used. Thus, each method has pros and cons and besides choosing a proper method, optimization of the reaction conditions (*e.g.* temperature, solvent) is needed in order to obtain selectively the desired product in good yield.

It should be noted that both *fac* and *mer*-isomers exhibit two stereoisomers of the Δ and Λ type (Figure III-6). To the best of our knowledge, only one example of a homoleptic tris-cyclometallated Ir

complex bearing three achiral ppy-derivatives was reported for which the neutral Δ and Λ complexes of the *fac*-isomer could be separated by chiral supercritical fluid chromatography.¹² Another example, reported by von Zelewsky *et al.*, deals with the use of a tripodal ligand bearing three chiral ppy-derivatives based on the pinene scaffold.¹³ No other methods based on achiral bidentate cyclometallated ligands have been described so far to isolate the Δ and Λ complexes, probably because of the harsh conditions required for their synthesis.

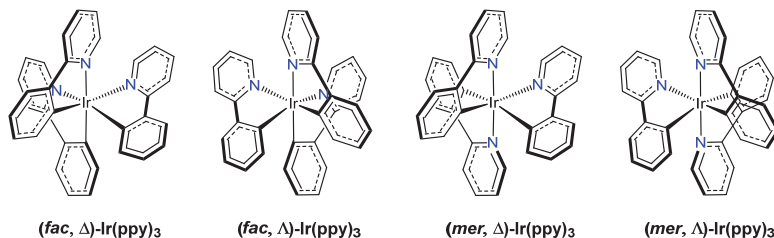


Figure II-6: Structures of the Δ and Λ type stereoisomers of *fac*-Ir(ppy)₃ and *mer*-Ir(ppy)₃.

1.2 Luminescent properties of neutral cyclometallated Ir(III) complexes

As mentioned previously, tris-cyclometallated Ir(III) complexes exhibit interesting photophysical properties that have been exploited in electroluminescent devices. Interestingly, the two isomers that exist if considering homoleptic tris-cyclometallated complexes (*e.g.* Ir(ppy)₃), namely facial (*fac*) and meridional (*mer*) isomers, display different photophysical properties. Indeed, Thompson *et al.* reported in 2003 that, compared to the facial isomer that display structured emission, the meridional products display red-shifted and broader luminescence with lower quantum yields. The phenomenon could be rationalized considering the non-radiative k_{nr} constant for the *mer* complex that is one order of magnitude larger than the one for the *fac* isomer while their radiative constants k_r are similar. One of the quenching processes that may account for such a difference is the facilitated Ir-C bond breaking in the excited states of meridional products as a consequence of strong *trans* influence of phenyl units. Broadening of the emission shows that the geometry of the excited state is distorted with respect to that of the ground state. Photolytic cleavage of Ir-C or Ir-N bonds is thus facilitated in *mer* isomers compared to the *fac* isomers, the former being thus less stable. It is usually assumed that the *mer* product, obtained at relatively low temperature, is the kinetically favored product while the *fac* isomer is thermodynamically favored requiring higher reaction temperatures. As a consequence, the facial products may be formed by photoisomerization or thermal conversion of the *mer* analogue.^{2,14} Thus, in the literature, most of the studies focus on synthesizing and exploring the photophysical properties of facial Ir(III) complexes because of their relatively photo stability and efficient photophysical properties.¹⁵

Besides 2-phenylpyridyl derivatives (ppy, dFppy), other cyclometallating ligands based for example on 2-(benzothiophen-2-yl)pyridyl (btpy), 1-phenylisoquinoliny (piq) or 1-(thiophen-2-yl)isoquinoliny (tiq) derivatives have been studied (Figure III-7). Depending on their intrinsic ligand

field strength and electronic influence towards the central Iridium atom, the photophysical properties of homoleptic tris-cyclometallated Iridium complexes may be modulated by these different ligands. Indeed, tuning the energy of the excited states, *i.e.* stabilizing or destabilizing the LUMO state, could be achieved using electron-withdrawing groups (*e.g.* F, CF₃)^{2,16} inducing a blue-shift or, on the contrary, electron-donating groups (*e.g.* OCH₃, tBu).¹⁷ Conjugation degree of the ligands also influences the emission properties. Different complexes with emission wavelengths ranging from green to red have been reported as illustrated in Figure III-7.^{2,15a,18}

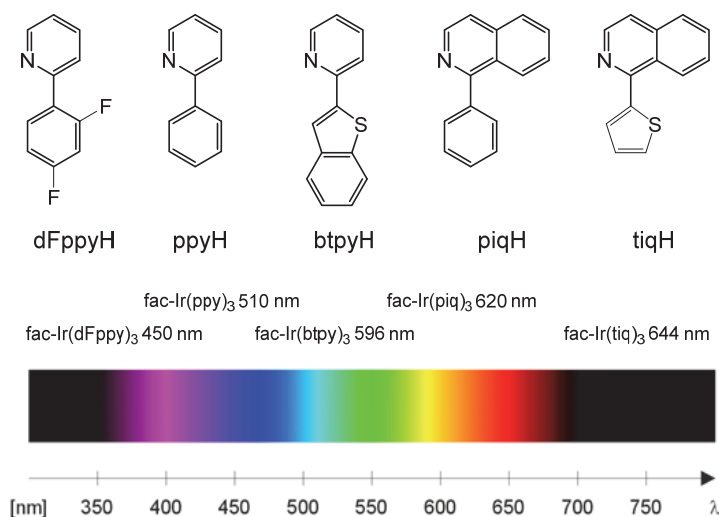


Figure III-7: examples of cyclometallating ligands and their neutral homoleptic Iridium complexes with emission wavelength ranging from green to red.^{2,15a,18}

Furthermore, Aoki and co-workers reported different amino- and pyridyl-substituted ppy derivatives to generate Iridium complexes displaying pH-dependent emission as illustrated in Figure III-8.¹⁹ The blue shift of the emission for the protonated complex $\text{fac-}[\text{Ir}(\text{atpyH}_3)_3]^{3+}$ was rationalized considering that the amino groups behaving as an electron-withdrawing group may destabilize the LUMO state. While the red-shift observed for protonated complex of $\text{fac-}[\text{Ir}(\text{pppyH}_3)_3]^{3+}$ is attributed to the larger stabilization in the excited state (LUMO, mainly localized on the protonated pyridyl rings) of the protonated complex compared to the ground state (HOMO, mainly located on the phenyl rings and the Ir d orbitals).

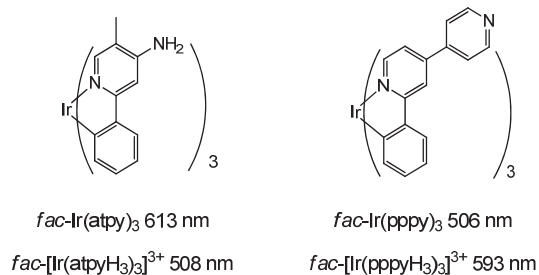


Figure III-8: Chemical structure of the two *fac*-Ir(atpy)₃ and *fac*-(pppy)₃ complexes that display pH-dependent emission and emission wavelengths for the neutral and protonated complexes.¹⁹

As for heteroleptic tris-cyclometallated Ir(III) complexes, Huo *et al.*²⁰ synthesized different heteroleptic tris-cyclometallated Ir(III) complexes bearing 2-phenylpyridyl (ppy) and 1-phenylisoquinoliny (piq) ligands. In comparison with their homoleptic analogue Ir(piq)₃, they exhibit similar photophysical properties with slightly red shifted emission wavelength (less than 7 nm) and quantum yields in solution slightly lower (with an experimental error of $\pm 10\%$). The lowest excited state for these complexes was attributed to be dominantly an ³MLCT state (Figure III-9).

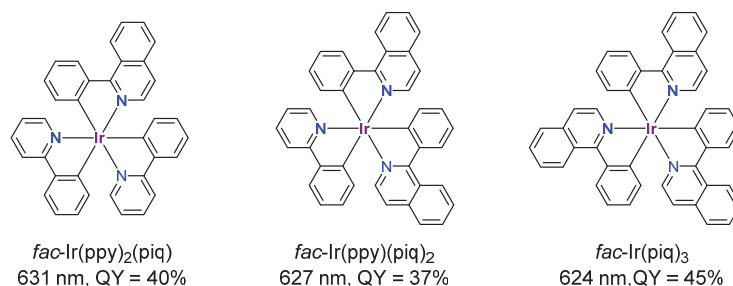


Figure III-9: Chemical structures of the two heteroleptic Ir(III) complexes *fac*-Ir(ppy)₂(piq) and *fac*-Ir(ppy)(piq)₂ and their homoleptic analogue *fac*-Ir(piq)₃.

As a summary, emission color tuning of Iridium complexes over the whole visible spectrum may be achieved through a proper choice of ligands and highly efficient photophysical performances (*e.g.* relative short lifetime and high quantum yields) are achieved making these tris-cyclometallating Ir complexes attractive for applications in diverse areas such as OLED devices, solar energy harnessing, photocatalysis, oxygen sensing or cell imaging.^{5,15a,19b,21}

1.3 Formation of coordination networks based on neutral Iridium (III) complexes

The aim of the present chapter is the synthesis of neutral Iridium complexes as metallatectons for the generation of luminescent crystalline materials in the form of heterometallic coordination polymers.

Recently, a few neutral Ir-based coordination networks have been described in the literature.²² Lin and co-workers were the first to report the use of neutral homoleptic tris-cyclometallated Iridium complexes to generate porous (Ir,Zn) heterometallic coordination polymers (Figure III-10a).^{22a} The coordination networks, obtained upon combining *fac*-Ir(4-cppy)₃ (4-cppy = 4-(2-pyridyl)benzoic acid) or *fac*-Ir(3-cppy)₃ (3-cppy = 3-(2-pyridyl)benzoic acid) with Zn(NO₃)₂, were structurally characterized by single crystal X-ray diffraction and found to be phosphorescent showing good oxygen sensing properties. They also studied the formation of (Ir,Zr) and (Ir,Zn) metal organic frameworks either by doping or using the metallatectons as linkers employing heteroleptic tris-cyclometallated Ir complex based on two ppy units and one ppy moiety substituted with carboxylic

acids.^{22b,c} The same group also reported the synthesis of a porous (Ir,Zr) heterometallic coordination polymer using an heteroleptic Ir complex ($\text{Ir}(\text{dcPhppy})\text{Cp}^*\text{Cl}$) based on an elongated ppy scaffold attached to a Cp^*Ir moiety in view of their use as water oxidation catalyst (Figure II-10b).²³ However, as stated by the authors, no single crystals suitable for X-ray diffraction were obtained owing to their small size (micro meter). The structure was thus modelled.

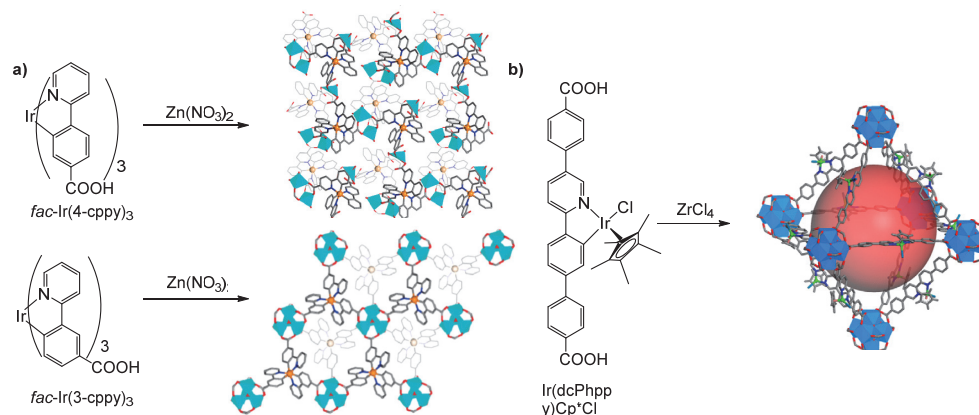


Figure III-10 : Single crystal structure of the heterometallic coordination polymers obtained upon combining fac-Ir(4-cppy)_3 (top) and fac-Ir(3-cppy)_3 (bottom) with $\text{Zn(NO}_3)_2$ (a)^{22a} and modelled structure of the heterometallic coordination polymer obtained upon combining $\text{Ir(dcPhppy)Cp}^*\text{Cl}$ with ZrCl_4 .²³

In parallel, another approach has been developed by Cohen *et al.* who used the dcppy ligand as building block for the construction of Zr and Zn-based coordination polymers that could be modified in a post-synthetic approach with $[\text{Ir}(\text{COD})(\text{OCH}_3)]$ moieties to form efficient MOF-based heterogeneous organometallic catalysts.²⁴ Depending if the framework is interpenetrated or not, the cyclometallation reaction is site-selective or not and can be controlled to introduce various amounts of Ir centers within the architecture. It is noteworthy here that the Ir center has an oxidation state of +I (Figure III-11).

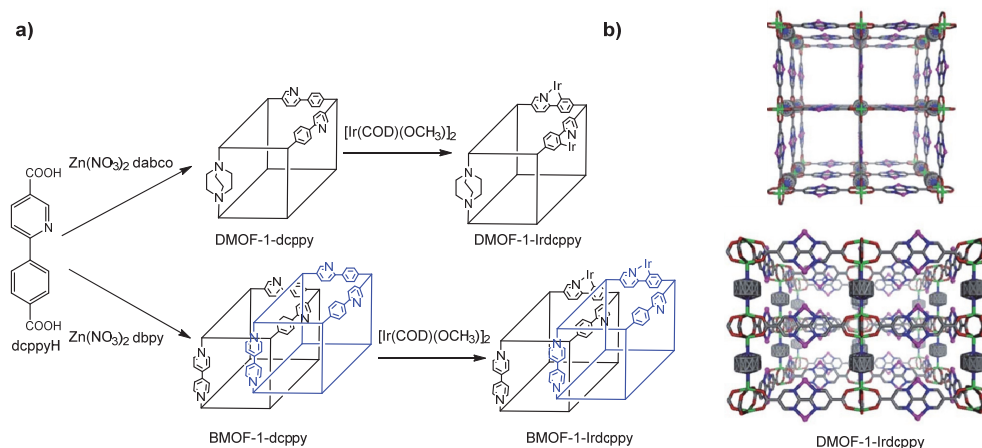


Figure III-11: Post-synthesis method to obtain Ir(I)-doped coordination networks (a) and the X-ray structure of DMOF-1-Ir₂dcppy along the *a*-(top) and *c*-axis (down) (b).

Neutral Ir(III) complexes are thus interesting building units for the generation of heterometallic luminescent coordination networks. However, the potential of tris-cyclometallated heteroleptic Iridium (III) complexes possessing either terminal carboxylic acid or pyridyl coordinating groups and acting as metallatectons has not been fully exploited for the formation of coordination networks. Indeed, most of the examples described above consist in doped coordination networks, meaning that not all the phenylpyridine derivatives acting as linker in the infinite architecture are functionalized with the Ir center.

Thus, in this chapter, the design of new neutral heteroleptic tris-cyclometallated Ir(III) complexes will be presented and the formation of coordination networks will be discussed. In order to take advantage of the knowledge gained in the previous chapter when synthesizing bis-cyclometallated cationic complexes, the design of the third ligand was based on the bipyridine ligand used in chapter II. Thus, instead of using the two bipyridine **bpy-4** and **bpy-11** substituted with either pyridyl or carboxylate groups respectively, one of the central pyridyl units was replaced by a phenyl unit to obtain the two corresponding ppy derivatives **ppy-4** and **ppy-7** (Figure III-12). A shorter substituted ppy derivative, *i.e.* **ppy-12**, was also synthesized to study the influence of the spacer on the potential voids within the final infinite architectures when compared to the one obtained with the extended **ppy-4** ligand. The synthesis and characterization of the different neutral heteroleptic Ir(III) complexes, Ir(ppy)₂(**ppy-4**), Ir(ppy)₂(**ppy-12**) and Ir(ppy)₂(**ppy-7**), functionalized either with terminal pyridyl or carboxylic acid coordinating sites will be presented. The heterometallic coordination networks obtained with those metallatectons and the difficulties encountered will then be discussed.

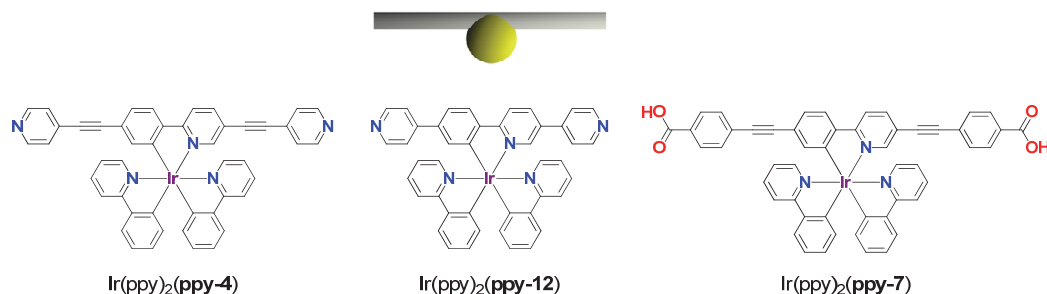


Figure III-12: Chemical structures of the three neutral tris-cyclometallated Ir(III) complexes and schematic representation of the linear metallatecton.

It should be noted that, for this whole chapter, only racemic Ir(III) complexes isolated as *fac* isomers will be discussed as the use of mild methods for the preparation of enantiopure neutral *fac*-Iridium complexes is still under investigation.

2. Synthesis and characterization of the heteroleptic neutral Ir(III) complexes based on terminal pyridyl coordinating sites

2.1 Retrosynthesis

As mentioned above, different Ir precursors may be employed to generate heteroleptic tris-cyclometallated Ir complexes. One of the common methods is based on the use of the μ -chloro bridged Ir dimer. In all cases, as depicted in Figure III-13, two synthetic pathways may be envisaged to obtain the two final Ir complexes. Following path A, the final ppy derivatives (**ppy-4** and **ppy-12**) should be first prepared and then coordinated to either the Ir dimers or, as we shall see, to other Ir precursors to form the desired complexes. Path B is based on the synthesis and coordination to the Ir center of the dibromo-substituted phenylpyridyl ligand (**ppy-1**) followed by a coupling step (e.g. Suzuki or Sonogashira coupling reactions) to connect the terminal substituted pyridyl units (4-ethynylpyridine or 4-bromophenylboronic acid) to the Ir metallatecton.

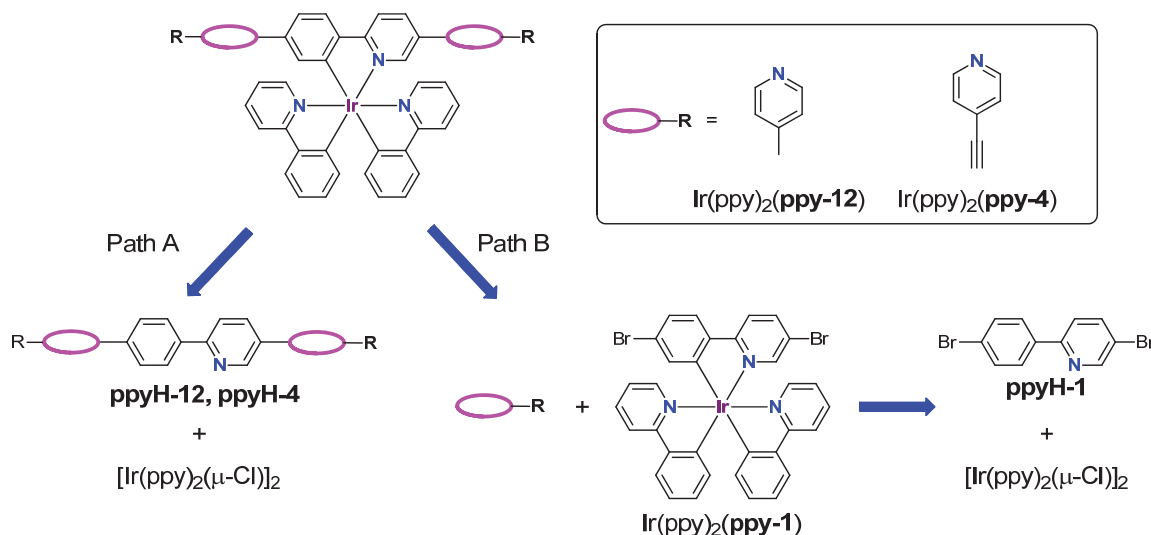
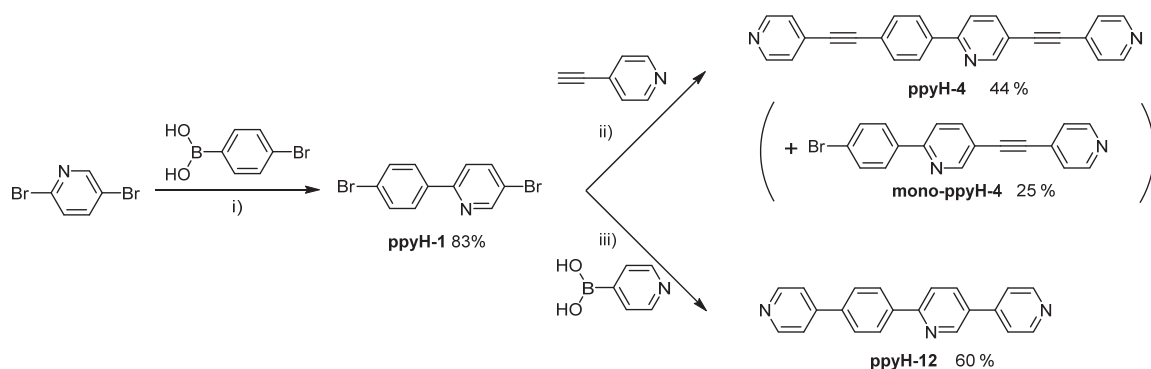


Figure III-13: Two possible retrosynthetic pathways to obtain the neutral heteroleptic Ir(III) complexes.

2.2 Synthesis of the complexes *fac*-Ir(ppy)₂(ppy-12) and *fac*-Ir(ppy)₂(ppy-4)

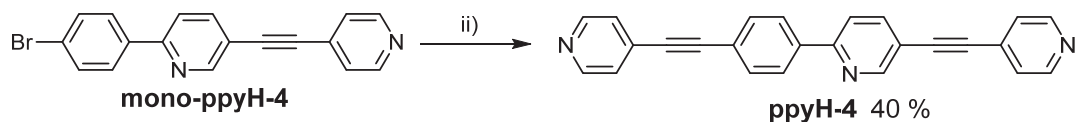
Based on different examples of synthesis of tris-cyclometallated heteroleptic complexes listed above, path A was first selected as the synthetic strategy to obtain the two complexes $\text{Ir}(\text{ppy})_2(\text{ppy-12})$ and $\text{Ir}(\text{ppy})_2(\text{ppy-4})$. In order to achieve this approach, ligands **ppyH-4** and **ppyH-12** were first prepared. The ligand synthesis, involving several Suzuki and Sonogashira coupling reactions, is detailed in Figure III-14.



=) $\text{Pd}(\text{PPh}_3)_4$, toluene/EtOH/ K_2CO_3 (1M aq) 3/2/1, 80 °C, ii) for **ppyH-4**: $\text{Pd}(\text{PPh}_3)_4$, CuI, toluene/ NEt_3 8/3, 80 °C, iii) for **ppyH-12**: $\text{Pd}(\text{PPh}_3)_4$, toluene/EtOH/ K_2CO_3 (1M aq) 3/2/1, reflux.

Figure III-14: synthesis of the two ligands **ppyH-4** and **ppyH-12**

As presented in Figure III-14, the synthesis of both organic ligands **ppyH-4** and **ppyH-12** requires the preparation of the dibromo derivative **ppyH-1**. The latter is achieved in 83 % yield *via* a Suzuki coupling reaction between 2,5-dibromopyridine and 4-bromophenylboronic acid in the presence of $\text{Pd}(\text{PPh}_3)_4$ as catalyst.²⁵ The second step is again a Pd-catalyzed coupling reaction either between ligand **ppyH-1** and 4-ethynylpyridine to form ligand **ppyH-4** (Sonogashira reaction) or between **ppyH-1** and 4-bromophenylboronic acid to afford **ppyH-12** (Suzuki reaction). Thus, in a mixture of toluene and Et_3N , in the presence of $\text{Pd}(\text{PPh}_3)_4$ and CuI, **ppyH-4** was obtained in 40 % yield starting from **ppyH-1** and 4-ethynylpyridine. The relatively low yield is due to the formation of the mono-coupling product **mono-ppyH-4** as by-product even when an excess of 4-ethynylpyridine is used. In order to further investigate the reaction, the mono-coupling product **mono-ppyH-4** was isolated and reinvested in another coupling reaction with 4-ethynylpyridine using the same reaction conditions ($\text{Pd}(\text{PPh}_3)_4$, CuI, toluene/ Et_3N) (Figure III-15). The outcome of the reaction is a 40 % yield for ligand **ppyH-4** and a substantial amount of starting material **mono-ppyH-4**. These observations might be explained by the relative low solubility of the mono-coupling product **mono-ppyH-4** in the solvent used. In order to increase the reaction yield, optimization of the reaction conditions (temperatures, solvents, bases) should be performed.



ii) 4-ethynylpyridine, $\text{Pd}(\text{PPh}_3)_4$, CuI, toluene/ NEt_3 8/3, 80 °C.

Figure III-15: synthesis of **ppyH-4** starting from **mono-ppyH-4**.

Meanwhile, ligand **ppyH-12** could be obtained in 60 % yield by reaction of **ppyH-1** and 4-bromophenylboronic acid in the presence of Pd(PPh₃)₄ and in a mixture of toluene, ethanol and an aqueous K₂CO₃ solution. Total conversion of the initial products was observed within 48 hours.

With the fully characterized ligands **ppyH-4** and **ppyH-12** in hand, the next step was the coordination of these ligands to Ir(III) precursors to form the desired tris-cyclometallated neutral Ir(III) complex. As mentioned previously, the synthesis of such heteroleptic complexes usually requires harsh reaction conditions as well as optimization. On the basis of the reported methods described in the literature, different reaction conditions as well as different Iridium precursors were tested using **ppyH-4** as the third ligand (Table III-1 and Figure III-16). The first two conditions (entries 1² and 2 in Table III-1) are based on the conventional methods starting from the μ -chloro-bridged dimer [Ir(ppy)₂(μ -Cl)]₂ as precursor in the presence of either K₂CO₃ or AgOTf. In both cases, a mixture of products that could not be purified was formed. We then turned to the use of “activated” Ir precursors such as [Ir(ppy)₂(ACN)₂][BF₄]⁸ and [Ir(ppy)₂(μ -OH)]₂⁸ (entries 3 and 5). Unfortunately, again a mixture of products that could not be purified was formed. The reaction outcome was not better using microwaves instead of classical thermal heating (entry 4, Table III-1). When using the reaction conditions described as entries 1 to 4 in Table III-1, the synthesis of Ir(ppy)₂(**ppy-12**) was also not successful affording again a mixture of complexes.

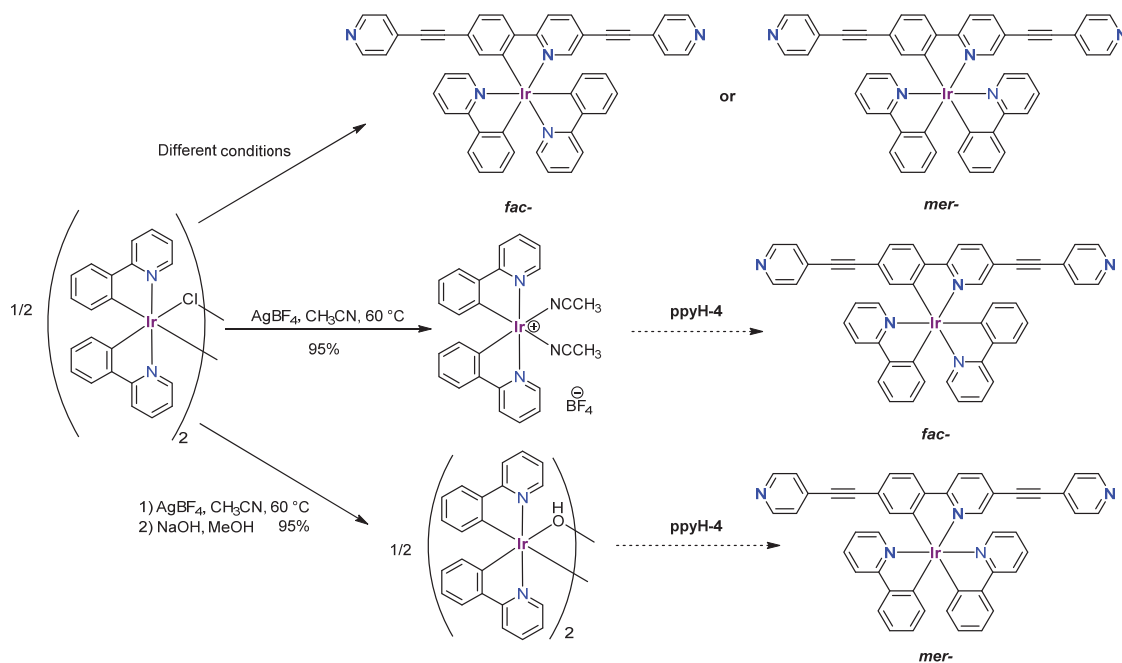
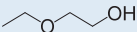
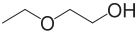
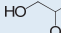
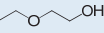
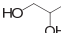
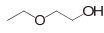
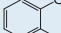
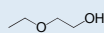


Figure III-16: Synthetic routes for the formation of Ir(ppy)₂(**ppy-4**). Reaction conditions and results are listed in Table III-1.^{2,5,8}

Table III-1: Different reaction conditions tested for the formation of $\text{Ir}(\text{ppy})_2(\text{ppy-4})$.

| Conditions | Reagents | Solvents | T (°C) | Time | Results |
|----------------------|---|---|-------------|--------------|---------------------|
| 1² | $[\text{Ir}(\text{ppy})_2(\mu\text{-Cl})]_2$, K_2CO_3 |  | 120 to 140 | 1 or 2 days | Mixture of products |
| 2⁵ | $[\text{Ir}(\text{ppy})_2(\mu\text{-Cl})]_2$, AgOTf |  | 120 | 2 days | Mixture of products |
| 3⁸ | $[\text{Ir}(\text{ppy})_2(\text{ACN})_2][\text{BF}_4]$ |  /  | 120 | 2 days | Mixture of products |
| 4 | $[\text{Ir}(\text{ppy})_2(\text{ACN})_2][\text{BF}_4]$ |  /  | 120, (120W) | Microwave 1h | Mixture of products |
| 5⁸ | $[\text{Ir}(\text{ppy})_2(\mu\text{-OH})]_2$ |  /  | 100 to 120 | 3 days | Mixture of products |

Several attempts to synthesize the final complexes $\text{Ir}(\text{ppy})_2(\text{ppy-4})$ and $\text{Ir}(\text{ppy})_2(\text{ppy-12})$ following path B (Figure III-17) were conducted in parallel. The key step for this strategy is the formation of the neutral Ir(III) precursor bearing as the third cyclometallating ligand the dibromo derivative **ppy-1**. The synthesis of **ppyH-1** was already described above. Similarly, for the formation of the dibromo-substituted complex $\text{Ir}(\text{ppy})_2(\text{ppy-1})$, different reaction conditions (solvents, temperature and reaction time) along with different precursors were tested (Figure III-17 and Table III-2).

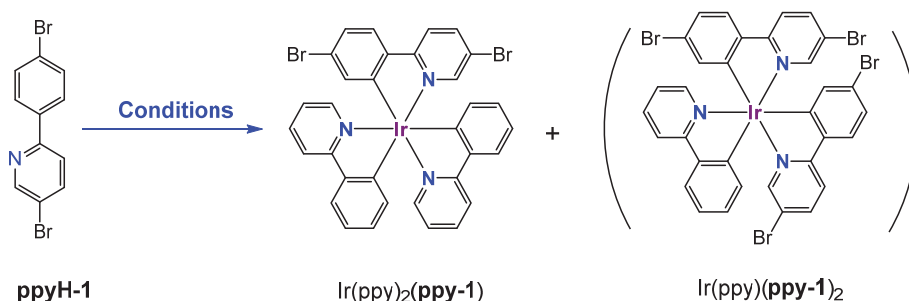
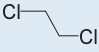
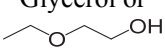
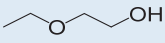
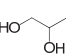
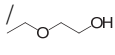
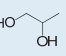
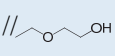


Figure III-17: Synthesis of complex $\text{fac-Ir}(\text{ppy})_2(\text{ppy-1})$ using the reaction conditions listed in Table III-2.^{2,5,8,21}

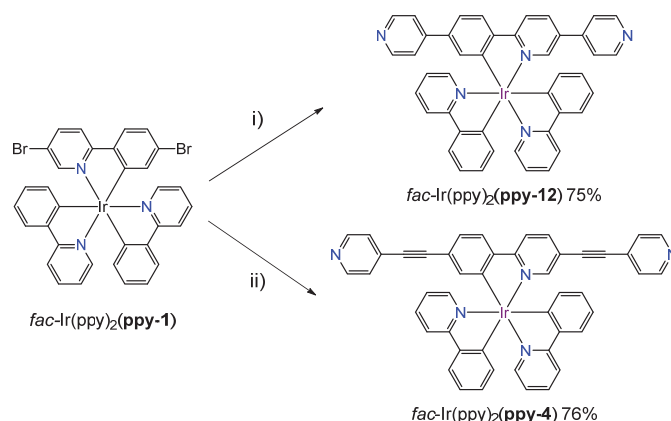
Again (entries 1 to 3 in Table III-2),²¹ the μ -chloro-bridged dimer $[\text{Ir}(\text{ppy})_2(\mu\text{-Cl})]_2$ was first employed as precursor. The use of relatively low reaction temperature (80 °C, entry 1) and the absence of conversion of the starting material confirmed that higher temperatures were required to activate this complexation reaction. Thus, the standard conditions described by Thompson *et al.*² were applied (entry 2, Table III-2). Heating the Iridium dimer in ethoxyethanol or glycerol with an excess of K_2CO_3 for one or two days resulted in the absence of starting material as evidenced by TLC. But the different products formed could not be separated by chromatography. The $^1\text{H-NMR}$ showed signals corresponding to a mixture of several products. It might originate from different isomers of $\text{Ir}(\text{ppy})_2(\text{ppy-1})$ products related to ligand scrambling. Finally (entry 3, Table III-2), when mixing the

Ir dimer $[\text{Ir}(\text{ppy})_2(\mu\text{-Cl})]_2$ with AgOTf ,⁵ *fac*- $\text{Ir}(\text{ppy})_2(\text{ppy-1})$ was obtained in *ca.* 5 % yield. The ^1H NMR spectrum of the complex and comparison with other similar facial complexes^{5,15b,26} confirm unambiguously the *fac* configuration of the complex. In parallel the “activated” Iridium complex $[\text{Ir}(\text{ppy})_2(\text{ACN})_2][\text{BF}_4]$ was also used as Ir precursor. Thus, reacting the latter with **ppyH-1** in a mixture of 1,2-propanediol and ethoxyethanol solvents at 120 °C for 30 hours (entry 4⁸ Table III-2) afforded *fac*- $\text{Ir}(\text{ppy})_2(\text{ppy-1})$ in *ca.* 40 % to 50 % yield. Small amounts of byproducts resulting from **ppy-1** ligand scrambling could be removed by recrystallization in dichloromethane and cyclohexane. The facial geometry was again confirmed by ^1H -NMR which agrees with literature values.^{15b,26-27} It is worth noting that under microwave conditions (120 W, 1 hour, entry 5 in Table III-2), the two complexes *fac*- $\text{Ir}(\text{ppy})_2(\text{ppy-1})$ and *fac*- $\text{Ir}(\text{ppy})(\text{ppy-1})_2$ were obtained in an almost 1/1 ratio. In summary, the optimized reaction conditions for the synthesis of complex *fac*- $\text{Ir}(\text{ppy})_2(\text{ppy-1})$ are those listed in Table III-2 as entry 4.

Table III-2: Different reaction conditions tested to obtain *Ir(ppy)₂(ppy-1)*

| | Reagents | Solvents | T (°C) | Time | Results |
|-----------------|--|--|----------------|-------------------------|--|
| 1 ²¹ | $[\text{Ir}(\text{ppy})_2(\mu\text{-Cl})]_2$, Et_3N , AgOTf |  | 80 | 3 days | No conversion |
| 2 ² | $[\text{Ir}(\text{ppy})_2(\mu\text{-Cl})]_2$, K_2CO_3 | Glycerol or  | 120 | 1 or 2 days | Mixture of products |
| 3 ²⁷ | $[\text{Ir}(\text{ppy})_2(\mu\text{-Cl})]_2$, AgOTf |  | 120 | 2 days | 5 % <i>fac</i> - $\text{Ir}(\text{ppy})_2(\text{ppy-1})$ |
| 4 ⁸ | $[\text{Ir}(\text{ppy})_2(\text{ACN})_2][\text{BF}_4]$ |  /  | 120 | 30 hours | 40 % to 50 % <i>fac</i> - $\text{Ir}(\text{ppy})_2(\text{ppy-1})$ |
| 5 | $[\text{Ir}(\text{ppy})_2(\text{ACN})_2][\text{BF}_4]$ |  //  | 120, (120W) | Microwave (1 hours) | <i>fac</i> - $\text{Ir}(\text{ppy})_2(\text{ppy-1})$, <i>fac</i> - $\text{Ir}(\text{ppy})(\text{ppy-1})_2$... |

Having obtained the *fac*- $\text{Ir}(\text{ppy})_2(\text{ppy-1})$ complex in reasonable yields, the conditions for the next coupling steps to prepare the final complexes *fac*- $\text{Ir}(\text{ppy})_2(\text{ppy-4})$ and *fac*- $\text{Ir}(\text{ppy})_2(\text{ppy-12})$ were investigated (Figure III-18). Thus, a Suzuki coupling reaction between *fac*- $\text{Ir}(\text{ppy})_2(\text{ppy-1})$ and 4-bromophenylboronic acid in the presence of $\text{Pd}(\text{PPh}_3)_4$ as catalyst afforded *fac*- $\text{Ir}(\text{ppy})_2(\text{ppy-12})$ in 75 % yield. Formation of complex *fac*- $\text{Ir}(\text{ppy})_2(\text{ppy-4})$ was performed *via* a Sonogashira coupling reaction between *fac*- $\text{Ir}(\text{ppy})_2(\text{ppy-1})$ and 4-ethynylpyridine in a mixture of DMF/ $i\text{Pr}_2\text{NH}$ solvents in the presence of $\text{Pd}(\text{PPh}_3)_4$ and CuI in 76 % yield. It is worth noting that no desired product could be isolated if using toluene instead of DMF as solvent. This may be rationalized considering the low solubility of the initial complex *fac*- $\text{Ir}(\text{ppy})_2(\text{ppy-1})$ in apolar solvents and, in particular, in toluene.



i) 4-bromophenylboronic acid Pd(PPh₃)₄, toluene/EtOH/K₂CO₃ (2M) 3/3/1, reflux; ii) 4-ethynylpyridine, Pd(PPh₃)₄, CuI, DMF/iPr₂NH 3/1, 80 °C

Figure III-18: Synthesis of *fac*-Ir(ppy)₂(ppy-12) and *fac*-Ir(ppy)₂(ppy-4) via coupling reactions.

It is worth noting that the chemical structure of *fac*-Ir(ppy)₂(ppy-1)₂ was ascertained performing a Suzuki coupling reaction on the crude product obtained under microwave conditions starting from [Ir(ppy)₂(ACN)₂][BF₄] (entry 5, Table III-2). The crude mixture consisted in at least two Ir complexes, *fac*-Ir(ppy)₂(ppy-1) and *fac*-Ir(ppy)₂(ppy-1)₂, as evidenced by NMR that could not be separated. Thus, reaction of the crude mixture with 4-bromophenylboronic acid in the presence of Pd(PPh₃)₄ as catalyst afforded *fac*-Ir(ppy)₂(ppy-12) and *fac*-Ir(ppy)₂(ppy-12)₂. Here, the two complexes could be purified by chromatography and were isolated in 17 % and 28 % yield respectively (based on [Ir(ppy)₂(ACN)₂][BF₄]).

In conclusion, the neutral tris-cyclometallated Ir(III) complexes, *fac*-Ir(ppy)₂(ppy-12) and *fac*-Ir(ppy)₂(ppy-4) were prepared following path B (Figure III-12) and the reaction conditions for the formation of the dibromo derivative *fac*-Ir(ppy)₂(ppy-1) was optimized. All products were characterized by standard techniques (¹H-NMR, ¹³C-NMR, HRMS, elemental analysis, IR). The luminescent properties of complexes *fac*-Ir(ppy)₂(ppy-12) and *fac*-Ir(ppy)₂(ppy-4) were also studied and complex *fac*-Ir(ppy)₂(ppy-4) has been structurally studied in the solid state by X-ray diffraction on single crystals.

2.3 Characterization of complexes *fac*-[Ir(ppy)₂(ppy-12)] and *fac*-[Ir(ppy)₂(ppy-4)]

The standard characterization information (¹H-NMR, ¹³C-NMR, HRMS) of *fac*-Ir(ppy)₂(ppy-12) and *fac*-Ir(ppy)₂(ppy-4) are listed in the experimental part. However, the crystal structure of *fac*-Ir(ppy)₂(ppy-4) and the luminescent properties of both final complexes will be highlighted and discussed in the following sections.

A-X-Ray structure of fac-Ir(ppy)₂(ppy-4)

Red single crystals of *fac*-Ir(ppy)₂(ppy-4) were obtained upon slow evaporation of a mixture of CH₂Cl₂ and MeOH solvents within one week.

The complex *fac*-Ir(ppy)₂(ppy-4) crystallizes in the monoclinic system with *P*2₁/*c* as space group with geometrical parameters similar to those described for other similar facial Iridium(III) complexes containing three phenylpyridine type ligands.^{2,4,15a,19a,28} The Ir center adopts a slightly distorted octahedral geometry (Figure III-19, Table III-3). The two ppy cyclometallating ligands are almost planar (N-C-C-C dihedral angles in the -2.63 ° to 1.03 ° range) while the ppy-4 ligand is slightly twisted (N-C-C-C dihedral angle N-C-C-C of 3.53 °). The ethynyl spacers are almost linear (C-C-C angles in the 175.59 ° - 178.59 ° range). The terminal pyridyl unit coordinated to the phenyl group through ethynyl spacer is almost coplanar to the central ppy moiety (C_{Py}-C_{Py}-C_{ppy}-C_{ppy} angle of -4.85 °) while the other terminal pyridyl unit is not (C_{Py}-C_{Py}-C_{ppy}-N_{ppy} angle of -32.88 °). It should be noted that both enantiomers, Δ and Λ , are present in the crystal as revealed by the achiral *P*2₁/*c* space group. Finally, the length of the metallatecton, *i.e.* the distance between the two terminal N atoms of ligand ppy-4, is of 20.66 Å.

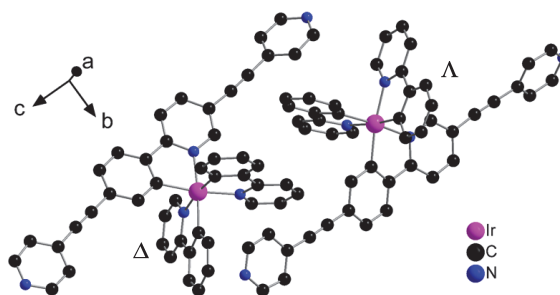


Figure III-19: Crystal structure of *fac*-Ir(ppy)₂(ppy-4). Hydrogen atoms as well as solvent molecules are omitted for clarity. For bond distances and angles, see Table III-3.

Table III-3: Selected bond distances (Å) and angles (°).

| | <i>fac</i> -Ir(ppy) ₂ (ppy-4) |
|---|--|
| Ir-C _{ppy} | 2.060 (4), 2.076 (4) |
| Ir-N _{ppy} | 2.068 (4), 2.078(4) |
| Ir-C _{ppy-4} | 2.084(4) |
| Ir-N _{ppy-4} | 2.086(4) |
| N _{ppy} -Ir-N _{ppy} | 96.75(14) |
| N _{ppy-4} -Ir-C _{ppy} | 173.97(13) |
| C _{ppy-4} -Ir-N _{ppy} | 172.17(14) |
| C _{ppy-4} -Ir-N _{ppy-4} | 78.80(14) |
| C _{ppy} -Ir-N _{ppy} | 79.38(14), 78.91(15) |

Weak π - π interactions are also observed between two adjacent ppy-4 ligands (shortest C-C distance of 3.45 Å considering the terminal pyridyl groups of one ppy-4 ligand and the central pyridyl unit of a neighbouring ppy-4 ligand belonging to two Ir complexes of opposite chirality, Figure II-20a). Additional π - π interactions between two pyridyl units of the ppy ligand belonging to two

neighbouring Ir complexes of opposite chirality (shortest C-C distance of 3.45 Å) are also present (Figure III-20b).

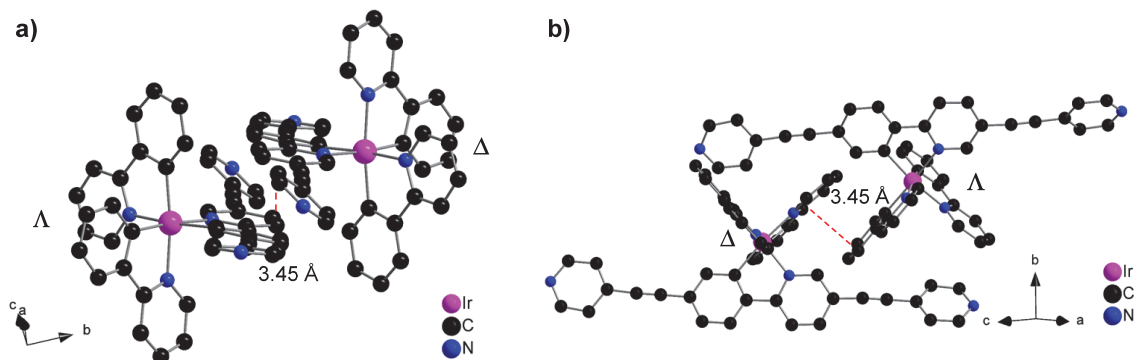


Figure III-20: Portions of the crystal structure of $\text{Ir}(\text{ppy})_2(\text{ppy-4})$ showing the π - π interactions between two **ppy-4** fragments (a) and two ppy units (b). Hydrogen atoms and solvent molecules are omitted for clarity.

B-Luminescent properties of $\text{fac-Ir}(\text{ppy})_2(\text{ppy-12})$ and $\text{fac-Ir}(\text{ppy})_2(\text{ppy-4})$

The photophysical properties (Table III-4) of complexes $\text{fac-Ir}(\text{ppy})_2(\text{ppy-12})$ and $\text{fac-Ir}(\text{ppy})_2(\text{ppy-4})$ were investigated in solution (Figure III-21) and in the solid state (Figure III-22).

The solution absorption properties of both heteroleptic complexes, $\text{fac-Ir}(\text{ppy})_2(\text{ppy-12})$ and $\text{fac-Ir}(\text{ppy})_2(\text{ppy-4})$ were investigated in THF (Figure III-21a). They show similar electronic transitions with a bathochromic shift of the absorption maxima for $\text{fac-Ir}(\text{ppy})_2(\text{ppy-4})$. According to reports on similar complexes,^{15a,b} the intense bands below 380 nm may be assigned to the ligand centered $\pi \rightarrow \pi^*$ transitions of the ppy moieties and the substituted ppy ligands (either **ppy-12** or **ppy-4**). In particular, the intense bands around 330 nm for $\text{fac-Ir}(\text{ppy})_2(\text{ppy-12})$ and 350 nm for $\text{fac-Ir}(\text{ppy})_2(\text{ppy-4})$ are not observed in the analogue homoleptic complex $\text{fac-Ir}(\text{ppy})_3$.¹⁴ Therefore, they may be attributed to the spin-allowed ligand centered (LC) or ligand centered charge transfer (¹LL'CT) transitions related to the presence of the **ppy-4** or **ppy-12** ligands.²⁰ The bathochromic shift observed ($\Delta\lambda = 18$ nm) may be related to the extended conjugation in $\text{fac-Ir}(\text{ppy})_2(\text{ppy-4})$ compared to $\text{fac-Ir}(\text{ppy})_2(\text{ppy-12})$ decreasing the HOMO-LUMO band gap.^{15a} The corresponding absorption coefficient ($\epsilon_{347} = 73.3 \times 10^3 \text{ L.mol}^{-1}.\text{cm}^{-1}$) is also higher for $\text{fac-Ir}(\text{ppy})_2(\text{ppy-4})$ than for $\text{fac-Ir}(\text{ppy})_2(\text{ppy-12})$ ($\epsilon_{329} = 57.9 \times 10^3 \text{ L.mol}^{-1}.\text{cm}^{-1}$). The relatively weaker low-energy bands extending into the visible region (up to 500 nm) could be assigned to spin allowed ¹MLCT transitions and probably ³LLCT transitions while the shoulder around 500 and 550 nm should arise from spin forbidden ³MLCT transitions. Again, these two absorption bands are red-shifted in $\text{fac-Ir}(\text{ppy})_2(\text{ppy-4})$ when compared to $\text{fac-Ir}(\text{ppy})_2(\text{ppy-12})$ ($\Delta\lambda$ around 30 nm).

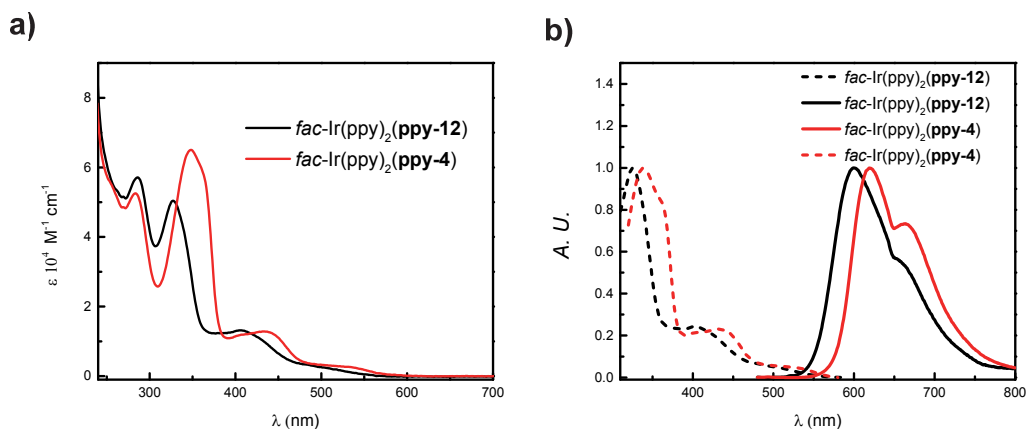


Figure III-21: Absorption (a), excitation (dotted lines, $\lambda_{em} = 660$ nm) and emission spectra (solid lines, $\lambda_{exc} = 420$ nm) of *fac-Ir(ppy)₂(ppy-12)* (black) and *fac-Ir(ppy)₂(ppy-4)* (red) at RT in degassed THF.

Table III-4: Photophysical Properties of Complexes *fac-Ir(ppy)₂(ppy-4)* and *fac-Ir(ppy)₂(ppy-12)*.

| Complexes | Absorption (aerated THF, RT) | Emission (deaerated THF, RT) ^a | | | Emission (Solid, RT) ^c | | |
|--|---|--|-------------------|---------------|--------------------------------------|----------|-------------|
| | λ (nm) ($\epsilon \cdot 10^3 \text{ M}^{-1} \cdot \text{cm}^{-1}$) | λ (nm) ^a | Φ^b | τ (ns) | λ (nm) | Φ^b | τ (ns) |
| <i>fac-Ir(ppy)₂(ppy-12)</i> | 287 (68.4), 329 (57.9), 407 (15.1), 483 (3.7). | 598, 655(sh) | 0.458 (0.030 air) | 1426 (97 air) | 626, 664, 681 | 18 % | 395 |
| <i>fac-Ir(ppy)₂(ppy-4)</i> | 284 (59.4), 347 (73.3), 432 (14.9), 515 (3.8). | 619, 664 | 0.372 (0.046 air) | 953 (129 air) | 650, 665, 680 | 2 % | 291 |

a : $\lambda_{exc} = 420$ nm; b: Relative quantum yields (Φ) measured using $[\text{Ru}(\text{bpy})_3][\text{Cl}]_2$ in degassed acetonitrile as reference ($\Phi = 0.095$);²⁹ c: $\lambda_{exc} = 430$ nm.

The photoluminescence spectra of the complexes in deaerated THF are shown in Figure III-21b. They both exhibit a relatively structured emission with one intense emission maximum (λ around 600 nm for *fac-Ir(ppy)₂(ppy-12)* and 620 nm for *fac-Ir(ppy)₂(ppy-4)*) and a less intense band around 660 nm for both complexes similar to *fac-Ir(ppy)₃*. However, due to the presence of the two differentiated cyclometallating unit, *i.e.* ppy and **ppy-4** or **ppy-12**, in these heteroleptic complexes it is difficult to conclude on the exact nature of the excited state as a combination of ³MLCT and ³LC transitions centered on either two ligands may be encountered.^{15c} Both complexes display relatively good quantum yield ($\Phi = 46$ % for *fac-Ir(ppy)₂(ppy-12)* and $\Phi = 37$ % for *fac-Ir(ppy)₂(ppy-4)*) consistent with previously reported QY for *fac-Ir(ppy)₃* ($\Phi = 40$ %)¹⁴ or other neutral homoleptic tris-cyclometallated Iridium complexes.^{15a} As expected, both complexes exhibit phosphorescence lifetimes in the microsecond domain under degassed conditions (1.4 μs for *fac-Ir(ppy)₂(ppy-12)*, 0.95 μs for *fac-Ir(ppy)₂(ppy-4)*) and are sensitive to the presence of oxygen ($\tau = 97$ ns and $\Phi = 3$ % for *fac-Ir(ppy)₂(ppy-12)*; $\tau = 129$ ns and $\Phi = 4.6$ % for *fac-Ir(ppy)₂(ppy-4)*).

Their photophysical properties in the solid state were also investigated (Figure III-22 and Table III-4). Intense absorption bands in the UV-visible region ranging from 300 to 650 nm are observed for both complexes. The emission spectra of *fac*-Ir(ppy)₂(ppy-12) and *fac*-Ir(ppy)₂(ppy-4) is again structured and the emission bands experience a bathochromic shift compared to the results obtained in solution. Furthermore, as observed in solution, the emission of *fac*-Ir(ppy)₂(ppy-12) is red-shifted ($\Delta\lambda = 24$ nm) if compared with *fac*-Ir(ppy)₂(ppy-4) which may be again attributed to the extended conjugation in *fac*-Ir(ppy)₂(ppy-4), decreasing the HOMO-LUMO band gap.^{15a} Finally, *fac*-Ir(ppy)₂(ppy-12) display a quantum yield of 18 % while *fac*-Ir(ppy)₂(ppy-4) exhibit a much smaller QY of 2 %. Different solid state interactions including π - π interactions for the two complexes may account for this discrepancy in QY.

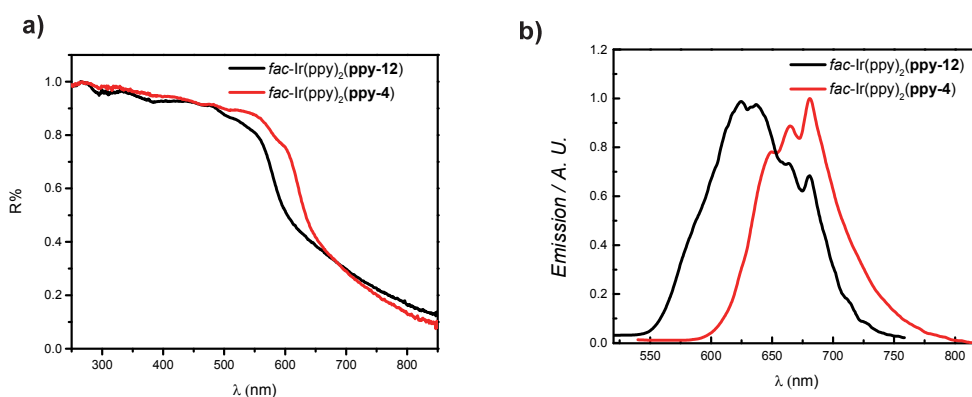
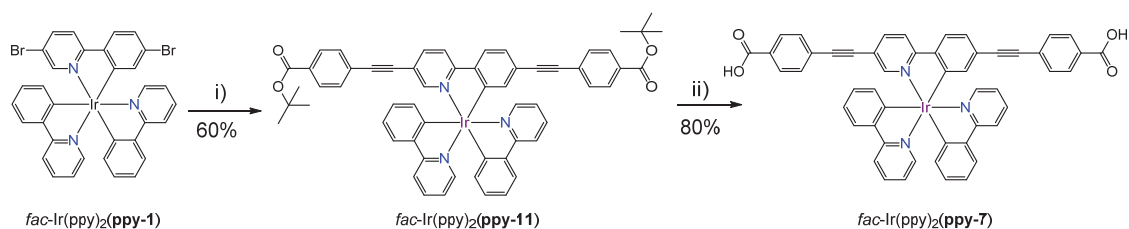


Figure III-22: Reflectance (a) and emission spectra (b) of *fac*-Ir(ppy)₂(ppy-12) (black) and *fac*-Ir(ppy)₂(ppy-4) (red) in the solid state at RT ($\lambda_{exc} = 430$ nm).

3. Synthesis and characterization of heteroleptic neutral Iridium(III) complexes based on terminal carboxylate coordinating sites

3.1 Synthesis of *fac*-Ir(ppy)₂(ppy-7)

In order to prepare the final complexes *fac*-Ir(ppy)₂(ppy-7), only the path B was employed based on the knowledge gained with the synthesis of the terminal pyridyl substituted Ir complexes (see section 2). As mentioned in chapter II, the synthesis of the dicarboxylic acid derivative requires first the synthesis of the diester *fac*-Ir(ppy)₂(ppy-11). As illustrated in Figure III-23, the latter was prepared in 60 % yield following the reaction conditions used for *fac*-Ir(ppy)₂(ppy-4). Thus, a Sonogashira coupling reaction between *fac*-Ir(ppy)₂(ppy-1) and *tert*-butyl 4-ethynylbenzoate (ligand 10, see chapter II, paragraph 5.1 for the synthetic details) in the presence of Pd(PPh₃)₄ and CuI in a mixture of DMF/*i*Pr₂NH solvents afforded the diester.



i) *tert*-butyl 4-ethynylbenzoate, $\text{Pd(PPh}_3)_4$, CuI , $\text{DMF}/i\text{Pr}_2\text{NH}$ 3/1, 80 °C; ii) 1) KOH , THF , 60 °C; 2) H_3PO_4 85 wt%, RT

Figure III-23: Synthesis of *fac*- $\text{Ir(ppy)}_2(\text{ppy-7})$.

The last step consisted in the removal of the *tert*-butyl groups. Different conditions were tried in order to obtain the desired diacid as summarized in Table III-5. The first attempt (entry 1 in Table III-5) was based on a previous report where an excess of trifluoroacetic acid in dichloromethane was used to remove the *tBu* groups.³⁰ As described in chapter II, quantitative deprotection of the ester groups to afford the cationic complex $[\text{Ir(ppy)}_2(\text{ppy-7})][\text{CF}_3\text{COO}]$ was performed using this reagent (see chapter II). However, in the present case, instead of the pure deprotected product *fac*- $\text{Ir(ppy)}_2(\text{ppy-7})$, the free ligand **ppyH-7** was also observed as a byproduct. This might be related to the strength of the acid ($\text{pK}_a = -0.25$). As the solvent (dichloromethane) may also be responsible for the decoordination of the ligand because of the possible presence of free chloride ions, it was replaced by THF in the presence of TFA (entry 2, Table III-5). Unfortunately, a certain amount of ligand **ppyH-7** was still observed. Then, phosphoric acid (85 wt %, aq) in THF³¹ ($v/v = 1/4$) was employed (entry 3 in Table III-5) but this also failed as no conversion of the starting material was observed after 15 hours of reaction time at room temperature. Finally, deprotection under basic conditions³² was attempted at different temperatures and during different reaction times followed by addition of acid to obtain the final diacid complex (entry 4 Table III-5). Thus, in the presence of aqueous KOH solution in THF at 60 °C, removal of the *tBu* groups of *fac*- $\text{Ir(ppy)}_2(\text{ppy-11})$ was complete and after addition of an aqueous H_3PO_4 solution (85 %), complex *fac*- $\text{Ir(ppy)}_2(\text{ppy-7})$ was obtained in 80 % yield.

Table III-5: Different conditions tested for the removal of the *tert*-butyl groups of *fac*- $\text{Ir(ppy)}_2(\text{ppy-11})$.³⁰⁻³²

| No. | reagents | T °C | Time | Results |
|-----|---|------|------|--|
| 1 | $\text{CF}_3\text{COOH}/\text{DCM}$ ³⁰ | RT | 1h | <i>fac</i> - $\text{Ir(ppy)}_2(\text{ppy-7})$ and ppyH-7 |
| 2 | $\text{CF}_3\text{COOH}/\text{THF}$ | RT | 15h | <i>fac</i> - $\text{Ir(ppy)}_2(\text{ppy-11})$, ppyH-7 ... |
| 3 | $\text{H}_3\text{PO}_4/\text{THF}$ ³¹ | RT | 15h | <i>fac</i> - $\text{Ir(ppy)}_2(\text{ppy-11})$ |
| 4 | KOH/THF ³² | 60°C | 48h | <i>fac</i> - $\text{Ir(ppy)}_2(\text{ppy-7})$ |

Again, the different compounds were characterized by standard techniques ($^1\text{H-NMR}$, $^{13}\text{C-NMR}$, elemental analysis or HRMS). Unfortunately, no single crystals suitable for X-Ray diffraction could be obtained. The luminescent properties of complexes *fac*- $\text{Ir(ppy)}_2(\text{ppy-11})$ and *fac*- $\text{Ir(ppy)}_2(\text{ppy-7})$ are detailed in the following paragraph.

3.2 Luminescent properties

The photophysical properties of the two complexes of *fac*-Ir(ppy)₂(**ppy-11**) and *fac*-Ir(ppy)₂(**ppy-7**) (Table III-6) were investigated both in solution (Figure III-24) and in the solid state (Figure III-25).

It is interesting to note that the two complexes exhibit almost identical absorption and emission spectra in THF solution suggesting that the tertbutyl group has little influence on the excited states of the two complexes. The UV-Visible absorption properties of both complexes, *fac*-Ir(ppy)₂(**ppy-11**) and *fac*-Ir(ppy)₂(**ppy-7**) were investigated in THF (Figure III-24a) and the electronic transitions observed are similar to those of the complex *fac*-Ir(ppy)₂(**ppy-4**) and other similar complexes.^{15a,b} Transitions between 250 and 390 nm may also be attributed to $\pi \rightarrow \pi^*$ transitions centered on the two organic ligands ppy and either **ppy-11** or **ppy-7**. In particular, the intense band around 350 nm which is not present for the analogue complex *fac*-Ir(ppy)₃ may be assigned to spin-allowed LC transitions related to the **ppy-11** or **ppy-7** ligands or to ¹LLCT transitions.¹⁴ As for complex *fac*-Ir(ppy)₂(**ppy-4**), the weaker bands at lower energy (380 to 500 nm) could be assigned to spin allowed ¹MLCT transitions and probably ³LLCT. The very weak bands between 500 to 600 nm could be assigned to the spin forbidden ³MLCT transitions. Both complexes display reasonable quantum yields under degassed conditions ($\Phi = 38\%$ for *fac*-Ir(ppy)₂(**ppy-11**) and $\Phi = 28\%$ for *fac*-Ir(ppy)₂(**ppy-7**) in the same range as other neutral tris-cyclometallated Iridium complexes reported (*e.g.* $\Phi = 40\%$ for *fac*-Ir(ppy)₃). Again, under degassed conditions, the phosphorescence lifetimes are in the microsecond range ($\tau = 1.2\ \mu\text{s}$ for both complexes) while in the presence of oxygen it drastically decreased with a more pronounced oxygen sensitivity for the ester complex ($\tau = 133\ \text{ns}$ for *fac*-Ir(ppy)₂(**ppy-11**); $\tau = 561\ \text{ns}$ for *fac*-Ir(ppy)₂(**ppy-7**)).

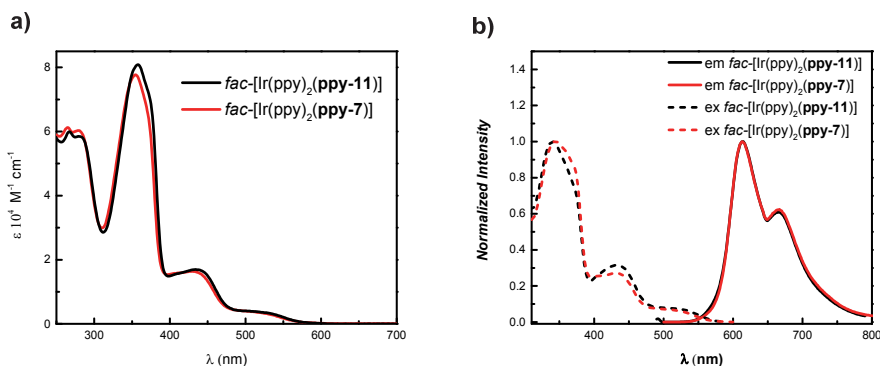


Figure III-24: Absorption (a), excitation (b, dotted lines, $\lambda_{em} = 660\ \text{nm}$) and emission (b, $\lambda_{exc} = 420\ \text{nm}$) spectra of *fac*-Ir(ppy)₂(**ppy-11**) (black) and *fac*-Ir(ppy)₂(**ppy-7**) (red) at room temperature in degassed THF.

Table III-6: Photophysical properties of *fac*-Ir(ppy)₂(ppy-11) and *fac*-Ir(ppy)₂(ppy-7).

| Complexes | Absorption (THF, r.t.) | Emission (deaerated THF, r.t.) ^a | | | Emission (Solid, r.t.) ^c |
|---|---|--|----------------------|-------------------|--|
| | λ (nm) (ε 10 ³ M ⁻¹ .cm ⁻¹) | λ (nm) ^a | Φ ^b | τ (ns) | λ (nm) |
| <i>fac</i> -Ir(ppy) ₂ (ppy-11) | 282 (70.7), 358 (97.8), 372 (sh86.8), 434 (20.5), 515 (sh4.6). | 617, 668 | 0.380 (0.052 air) | 1204 (133 air) | 667(sh), 682 |
| <i>fac</i> -Ir(ppy) ₂ (ppy-7) | 280 (66.3), 357 (85.5), 432 (18.0), 515 (4.0). | 613, 666 | 0.280 (0.033 air) | 1206 (561 air) | 638, 667, 682 |

a: λ_{exc} = 420 nm; b: Relative Quantum yields (Φ) measured using [Ru(bpy)₃][Cl]₂ in degassed acetonitrile as reference (Φ = 0.095); c: λ_{exc} = 430 nm

Their photophysical properties in the solid state were also investigated. From their reflectance spectra, intense absorption bands in the UV-visible region (650-300 nm) of both complexes could be observed. For the emission spectra, both complexes *fac*-Ir(ppy)₂(ppy-11) and *fac*-Ir(ppy)₂(ppy-7) exhibit emission bands in the almost red region (620 nm to 680 nm).

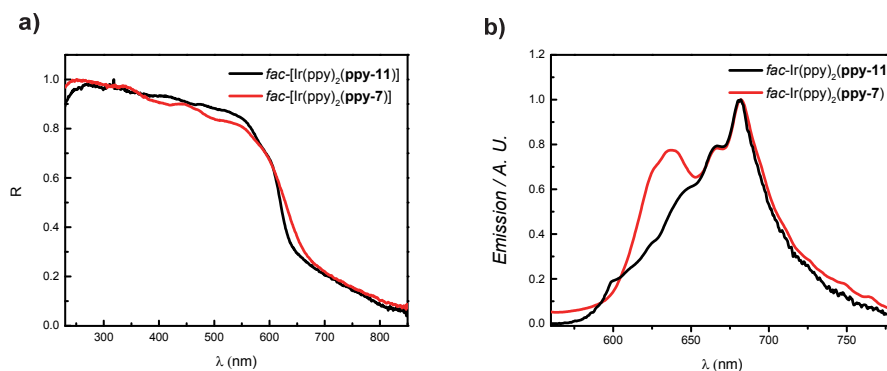


Figure III-25: Reflectance (a) and emission (b, λ_{exc} = 430 nm) spectra of *fac*-Ir(ppy)₂(ppy-11) (black) and *fac*-Ir(ppy)₂(ppy-7) (red) at room temperature in the solid state

4. Formation of coordination networks based on neutral Ir(III) complexes

Having in hand the three neutral tris-cyclometallated Ir metallatecton substituted with both terminal pyridyl and carboxylate coordinating sites, different attempts to generate heterometallic coordination networks upon self-assembly with different metal salts adopting various coordination geometries were performed. Concerning the complex *fac*-Ir(ppy)₂(ppy-7) substituted with carboxylate moieties, it was possible to grow stable single crystals using Zn(NO₃)₂ salt. Unfortunately, it was not possible to solve the structure using our diffractometer, as the crystals were poorly diffracting which prevented their structural determination.

However, generation of heterometallic coordination networks with the terminal pyridyl substituted metallatecton *fac*-Ir(ppy)₂(ppy-12) and *fac*-Ir(ppy)₂(ppy-4) was more successful and the

crystal structures of the networks obtained upon combination with CdCl_2 salts will be discussed along with their luminescent properties.

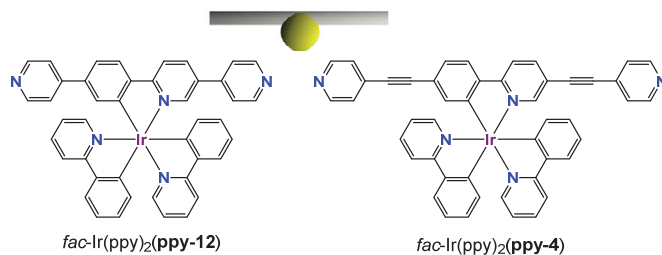


Figure III-26: Chemical structure of the neutral tris-cyclometallated Ir(III) complexes $\text{fac-Ir(ppy)}_2(\text{ppy-12})$ and $\text{fac-Ir(ppy)}_2(\text{ppy-4})$ and schematic representation of the linear metallatecton.

4.1 (Ir,Cd) Coordination networks using $\text{fac-Ir(ppy)}_2(\text{ppy-12})$ as metallatecton

The formation of extended heterometallic coordination networks was first explored by mixing complex $\text{fac-Ir(ppy)}_2(\text{ppy-12})$ with different metal salts.

Under self-assembly conditions, only the combination of the metallatecton with CdCl_2 as metallic node afforded single crystals and two different heterometallic coordination networks were obtained. As stated in chapter II, grid-type architectures³³ may be expected when using as secondary metal source a MX_2 metal salt (M = metal; X = halogen) adopting an octahedral geometry with its two apical positions occupied by the two X^- anions. This is indeed the case for the first coordination network that will be described. However, the second infinite architecture obtained present a more complicated structure as will be presented later.

Orange single crystals were obtained within three weeks by slow diffusion of an ethanol solution of CdCl_2 (2.66 eq) through a $\text{CHCl}_3/\text{EtOH}$ buffer layer into a chloroform solution containing the Ir complex $\text{fac-Ir(ppy)}_2(\text{ppy-12})$ (1 eq). However, due to the poor quality of the crystals, the final structure displays an R factor above 20 %. The results presented below are thus only for comparison with the structure that will be presented afterwards.

The structural study reveals the formation of grid-type infinite architecture $\text{fac-Ir(ppy)}_2(\text{ppy-12}) \cdot \text{Cd}$ (Figure III-27). The metallatecton $\text{fac-Ir(ppy)}_2(\text{ppy-12})$ and CdCl_2 units are present within the crystal lattice (orthorhombic, space group $Pbcn$). The solvent molecules present within the crystal were not refined. The Ir center adopts a distorted octahedral geometry with Ir-C bond lengths of ca. 2.0 Å and Ir-N bond distances of ca. 2.05 Å. The Cd center adopts also a distorted octahedral geometry with four N atoms belonging to four pyridyl units of four different metallatectons occupying the square base (Cd-N 2.36 Å and N-Cd-Cl angle in the range 86.9 ° to 92.4 °) and two chloride ions occupying the apical positions of the Cd center (Cd-Cl 2.65 Å and Cl-Cd-Cl angle 179.0 °). Within the 2D

network, two consecutive Cd atoms are separated by 20.45 Å. Each grid contains the two Ir enantiomers and the grid is thus achiral. Consecutive grids are packed in a staggered manner.

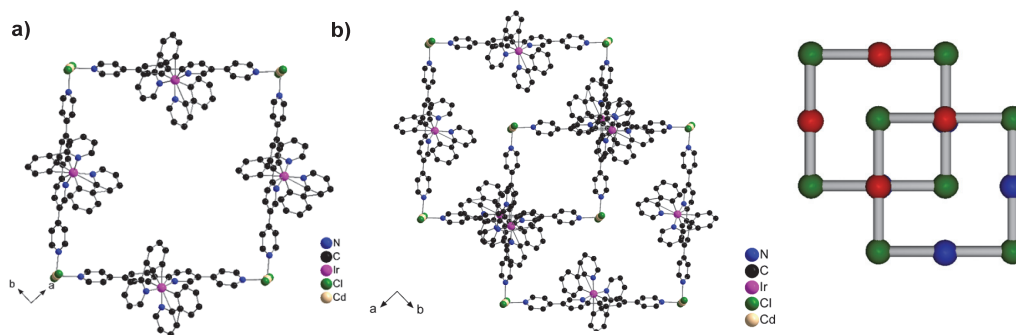


Figure III-27: Portions of the crystal structure of *fac*-Ir(ppy)₂(ppy-12)·Cd showing the grid obtained (a) and the packing of two consecutive grids along the *c* axis (b).

In order to obtain better quality crystals, other solvent systems were tested. Orange single crystals suitable for X-Ray diffraction were thus grown within one week by slow diffusion of a CdCl₂ ethanol solution (2.66 eq) through a dmsO buffer layer into a CHCl₃ solution of *fac*-Ir(ppy)₂(ppy-12). This time, even though the crystallization conditions are quite similar as before, a slightly different type of architecture was obtained as CdCl₂ salts do not behave anymore as a simple 4-connecting node but Cd atoms are arranged in a 6-membered cluster within the crystal lattice. The crystal (monoclinic, *P*2₁/*c* space group) contains the Ir metallatecton as a racemate, Cd²⁺ ions, Cl⁻ anions and water molecules. Owing to the severe disorder of other solvent molecules, the corresponding electron density was removed using the SQUEEZE command.³⁴ The Ir complex adopts a distorted octahedral geometry with geometrical parameters similar to other observed for analogous Ir complexes (Table III-7). Two crystallographically non-equivalent Ir centers are present within the lattice. The two ppy ligands are almost planar (dihedral C-C-C-N angles ranging from -3.19° to 3.11°) while the ligand ppy-12 is slightly more twisted (dihedral C-C-C-N angles of 6.95° and -4.484°). The two terminal pyridyl units are twisted relative to the central ppy moieties (dihedral angles in the -31.49° to 34.94° range). This is commonly observed for two adjacent connected pyridyl or phenyl rings for steric reasons.³⁵ Considering the Cd centers, six Cd atoms are arranged in a cluster containing three crystallographically non-equivalent Cd atoms (named Cd1, Cd2 and Cd3, Figure III-28b). Two of them (Cd2 and Cd3) are six-coordinated adopting both a distorted octahedral geometry (for distances see Table III-6). For Cd2, two pyridyl groups belonging to two perpendicular metallatectons occupy the square base and one apical position of the octahedron respectively (N-Cd-N angle of 92.39°). Four bridging chloride complete the coordination sphere of Cd2 (average N-Cd-Cl angles of 173.98° and average Cl-Cd-Cl angles of 89.1°). For Cd3 which is located in the middle of the Cd cluster, four bridging chlorides occupy the square base of the octahedron (Cl-Cd-Cl angle ranging from 85.99° to 95.77°) and a fifth bridging chloride occupies one apical position while one pyridyl unit of one

metallatecton is located on the other apical position (N-Cd-Cl angle of 173.4°). Finally, the third Cd center Cd1 adopts a distorted tetrahedral geometry (N-Cd-Cl angle ranging from 94.8° to 138.7°) with two bridging chloride ligands connecting Cd1 to either Cd3 or Cd2 (for distances see Table III-6). One monodentate chloride and one pyridyl unit of another metallatecton complete the coordination sphere. This Cd cluster can be schematically represented as a quasi-rectangular 8-connecting node with always two nodes on each edge. Selected distances and angles are presented in Table III-5. Thus, eight metallatecton *fac*-Ir(ppy)₂(ppy-12) are connected to the Cd cluster leading to a grid-type architecture with double wall edges (Figure III-28a). Furthermore, within the grid, one edge contains both Ir enantiomers, either of them oriented alternatively inwardly or outwardly leading thus to achiral grids, *i.e.* achiral 2D coordination network (Figure III-28a). Consecutive achiral 2D networks are packed in a staggered fashion along the *c* axis (Figure III-28c).

Finally, the crystals were air-stable and the purity of the microcrystalline powder was ascertained by PXRD which revealed a good match between the simulated and recorded patterns.

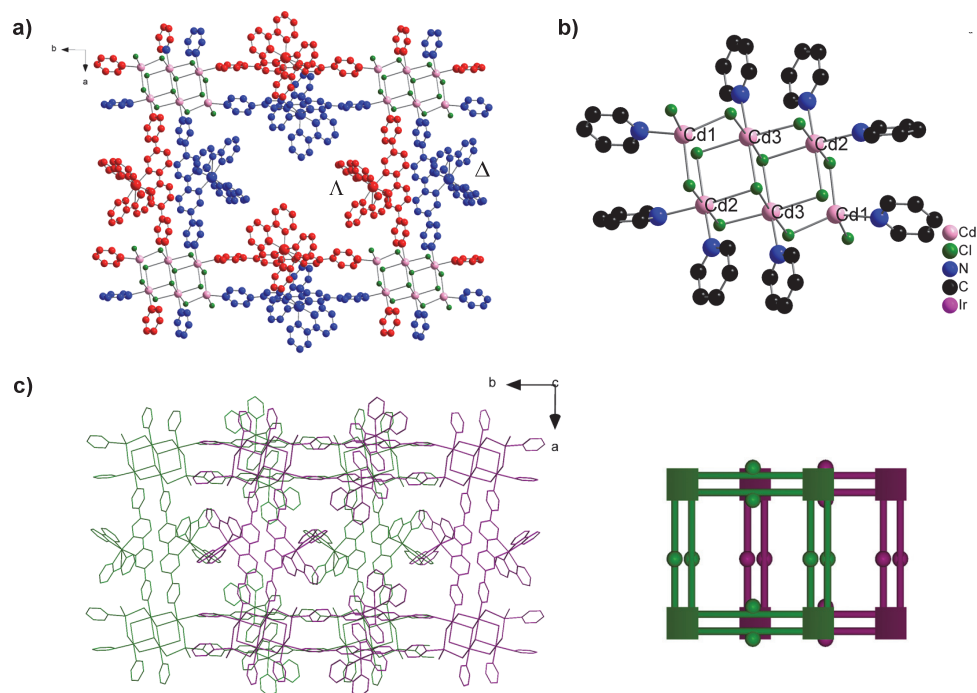


Figure III-28: Portions of the X-ray structure of *fac*-Ir(ppy)₂(ppy-12)·Cd₆ showing: the grid-type architecture with the alternated arrangement of Δ (blue) and Λ (red) complexes within the grid (a), the six-Cd membered cluster (b), the staggered packing of two consecutive grids along the *c* axis and its schematic representation (c). H atoms and solvent molecules are omitted for clarity.

Table III-7: Selected average bond distances (Å) and angles (°) for *fac*-Ir(ppy)₂(ppy-12)·Cd₆

| <i>fac</i> -Ir(ppy) ₂ (ppy-12)·Cd ₆ | | | |
|---|---------------------------------------|---|-------|
| Distances (Å) | | Angles (°) | |
| Ir-C _{ppy} | 2.03 | N _{ppy} -Ir-N _{ppy} | 96.4 |
| Ir-N _{ppy} | 2.10 | N _{ppy-4} -Ir-C _{ppy} | 170.2 |
| Ir-C _{ppy-4} | 2.05 | C _{ppy-4} -Ir-N _{ppy} | 170.7 |
| Ir-N _{ppy-4} | 2.10 | C _{ppy-4} -Ir-N _{ppy-4} | 79.2 |
| Cd-N | 2.31 (Cd1), 2.33 (Cd2), 2.33 (Cd3) | C _{ppy} -Ir-N _{ppy} | 78.1 |
| Cd1-Cl | 2.45 | | |
| Cd1-(μ-Cl) | 2.50 (Cd1), 2.64 (Cd2), 2.64(Cd3) | | |

4.2 (Ir, Cd) Coordination networks using *fac*-Ir(ppy)₂(ppy-4) as metallatecton

Combining the extended pyridyl-substituted metallatecton *fac*-Ir(ppy)₂(ppy-4) with CdCl₂ salts afforded a heterometallic coordination network that was structurally investigated by X-Ray diffraction. Single crystals suitable for X-ray structure were obtained within three weeks by slow diffusion of an EtOH solution of CdCl₂ (2.81 eq) into a benzonitrile solution containing *fac*-Ir(ppy)₂(ppy-4) (1 eq). Unlike the two examples of simple or double grid-like architectures presented above, here a monodimensional coordination network *fac*-Ir(ppy)₂(ppy-4)·CdCl₂ is obtained. The crystal (monoclinic, *P*2₁/*c*) is composed of *fac*-Ir(ppy)₂(ppy-4), Cd²⁺ cations, Cl⁻ anions and benzonitrile and water molecules (Figure III-29a). Because of the severe disorder of other solvent molecules, the structure was solved using the SQUEEZE algorithm.³⁴ The Ir center adopts a distorted octahedral geometry with geometrical parameters similar to those obtained for the discrete complex (Table III-8). It should be noted that, here, the Ir-C bonds are all equivalent and shorter than the three equivalent Ir-N bond lengths. The facial arrangement of the ligands around the Ir center is thus confirmed because of the differentiated Ir-C and Ir-N bond lengths. The three chelating ligands are almost planar (N-C-C-C angle in the -1.11 ° to 4.25 ° range). Moreover, the ethynyl junctions are almost linear (C-C-C angle ranging from 174.65 ° to 178.67 °). Both terminal pyridyl units are not coplanar to the central ppy scaffold but slightly twisted (dihedral angle of 21.00° and 10.84°). The two Cd atoms adopt a distorted octahedral geometry (Figure III-29b) with two pyridyl units of two different metallatectons occupying the apical positions of the octahedron, one water molecule and a monodentate chloride anion occupying two out of four positions of the square base of the octahedron and two bridging chloride completing the coordination sphere of the Cd atom (see Figure III-29b and Table III-8 for bond distances and angles). Thus, a 1D network is obtained consisting in two parallel chains connected through bridging chloride atoms between two adjacent Cd centers. Furthermore, the *fac*-Ir(ppy)₂(ppy-4) complex was used as a racemate and the two parallel interconnected chains consist in one homochiral chain with only the Δ enantiomers present and within the second chain only

Λ enantiomers are present (Figure III-29a, Δ complex depicted in blue, Λ complex coloured in red). The 1D coordination network is thus achiral.

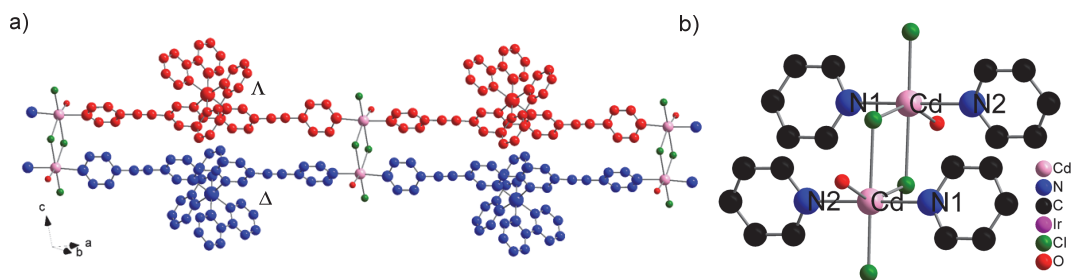


Figure III-29: Portions of the X-ray structure of *fac*-Ir(ppy)₂(ppy-4)·CdCl₂. H atoms are omitted for clarity.

Table III-8: Selected bond distances (Å) and angles (°) for *fac*-Ir(ppy)₂(ppy-4)·CdCl₂.

| <i>fac</i> -Ir(ppy) ₂ (ppy-4)·CdCl ₂ | | | |
|--|--------------------|---|----------------------|
| Distances (Å) | | Angles (°) | |
| Ir-C _{ppy} | 2.018(5), 2.024(5) | N _{ppy} -Ir-N _{ppy} | 93.19(18) |
| Ir-N _{ppy} | 2.118(4), 2.121(5) | N _{ppy-4} -Ir-C _{ppy} | 174.84(18) |
| Ir-C _{ppy-4} | 2.020(5) | C _{ppy-4} -Ir-N _{ppy} | 171.96(19) |
| Ir-N _{ppy-4} | 2.130(4) | C _{ppy-4} -Ir-N _{ppy-4} | 79.46(17) |
| | | C _{ppy} -Ir-N _{ppy} | 79.50(19), 79.45(19) |
| Cd-N | 2.347(4), 2.38(3) | N-Cd-N | 173(5) |
| Cd-O | 2.468(18) | N-Cd-O | 82(5), 91.3(4) |
| Cd-Cl | 2.389(8) | N-Cd-Cl | 89.4(2), 90(2) |
| Cd-(μ-Cl) | 2.586(8), 2.725(7) | N-Cd-(μ-Cl) | 93(4), 93.4(2) |

Two parallel double chains separated by *ca.* 7.26 Å are packed in a slightly staggered manner forming an achiral sheet (Figure III-30a). Two consecutive sheets named as sheet A and sheet B coloured in green and violet respectively, Figure III-30b) are twisted with an angle of *ca.* 47.0 ° with the 1D networks of sheet A and those of sheet B pointing in two different directions along the *c* axis. The mean distance between sheet A and sheet B is *ca.* 12.11 Å.

Finally, the crystals were air-stable and the purity of microcrystalline powder was confirmed comparing the experimental PXRD pattern with the one simulated based on single crystal data.

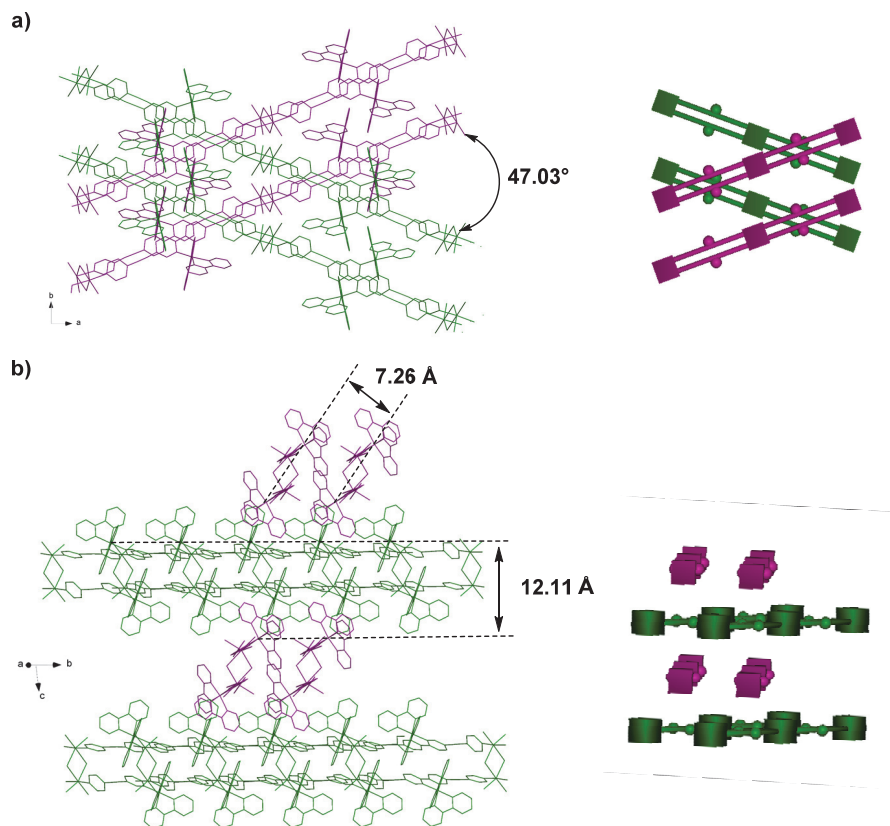


Figure III-30: Portion of X-ray structure of $\text{fac-Ir(ppy)}_2(\text{ppy-4}) \cdot \text{CdCl}_2$ showing the packing arrangement along the c axis (a) and along the axis of sheet B (b) and their schematic representations.

4.3 Luminescent properties of the two coordination networks $\text{fac-Ir(ppy)}_2(\text{ppy-12}) \cdot \text{Cd}_6$ and $\text{fac-Ir(ppy)}_2(\text{ppy-4}) \cdot \text{CdCl}_2$

The photophysical properties of the two stable coordination networks $\text{fac-Ir(ppy)}_2(\text{ppy-4}) \cdot \text{CdCl}_2$ and $\text{fac-Ir(ppy)}_2(\text{ppy-12}) \cdot \text{Cd}_6$ were investigated in the solid state (Figure III-31 and Table III-9). Both networks are emissive at room temperature. As presented in Figure III-31, they exhibit similar absorption and emission properties. Surprisingly, if compared with the related discrete complex $\text{fac-Ir(ppy)}_2(\text{ppy-4})$, no shift is observed in the emission spectra of the respective networks $\text{fac-Ir(ppy)}_2(\text{ppy-4}) \cdot \text{CdCl}_2$. Coordination of the Cd atom to the terminal pyridyl does not seem to affect strongly the excited state, unlike what was observed for the (Ir,Cd) coordination networks with cationic complexes in chapter II. This phenomena may be ascribed to a more pronounced MLCT nature of the excited state of the complex compared to the LC transition. On the contrary, a red-shift of *ca.* 24 nm was observed for $\text{fac-Ir(ppy)}_2(\text{ppy-12}) \cdot \text{Cd}_6$ compared to its discrete complex. This may be attributed to the different nature of the excited states of $\text{fac-Ir(ppy)}_2(\text{ppy-12})$ and $\text{fac-Ir(ppy)}_2(\text{ppy-4})$. This may also be related to different packing arrangement in the solid state modifying the excited

states properties of both Ir complexes. Photoluminescence quantum yields and luminescence lifetimes (Table III-9) were determined in the solid state. For the 2D coordination network $fac\text{-Ir}(\text{ppy})_2(\text{ppy-12})\cdot\text{Cd}_6$, the QY is decreased when compared to the discrete complex $fac\text{-Ir}(\text{ppy})_2(\text{ppy-12})$. While for the 1D network $fac\text{-Ir}(\text{ppy})_2(\text{ppy-4})\cdot\text{CdCl}_2$, the QY was slightly increased when compared to the discrete Ir complex $fac\text{-Ir}(\text{ppy})_2(\text{ppy-4})$. This may be related to the rigidity of the framework preventing some non-radiative deactivation pathways or to supramolecular interaction such as $\pi\text{-}\pi$ interactions.³⁶

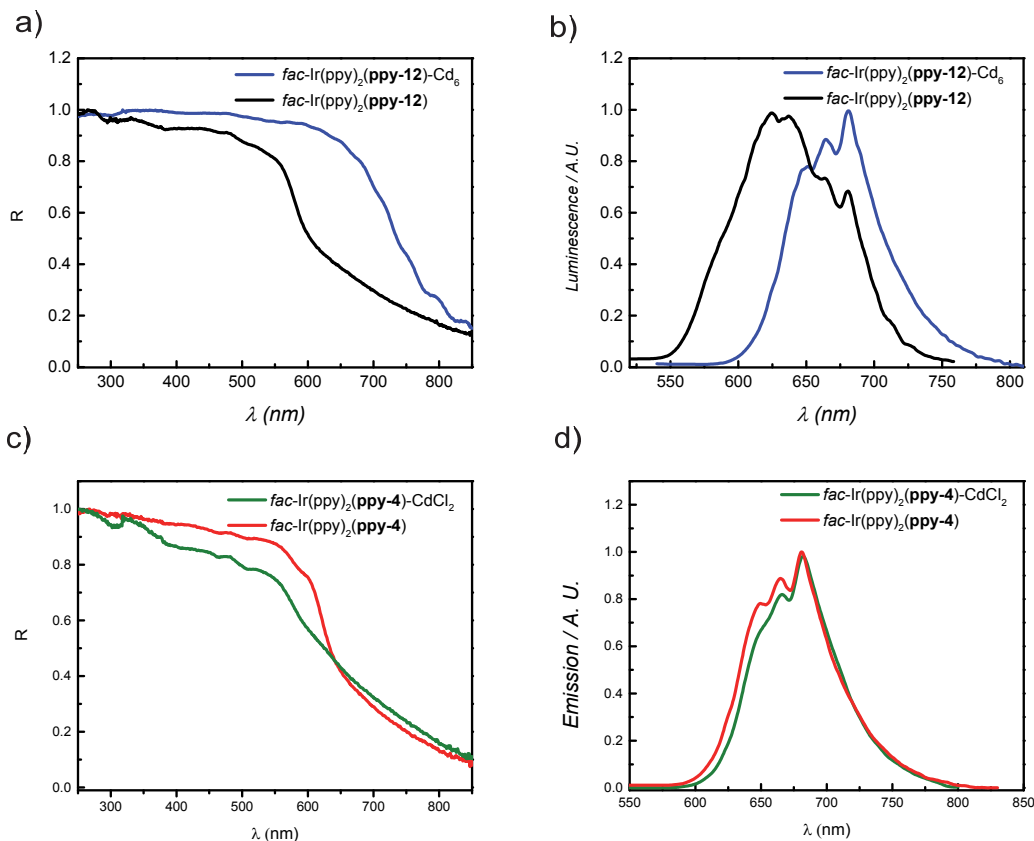


Figure III-31: Reflectance (a,c) and emission spectra (b,d) of $fac\text{-Ir}(\text{ppy})_2(\text{ppy-12})$ (black line), $fac\text{-Ir}(\text{ppy})_2(\text{ppy-4})\cdot\text{Cd}_6$ (blue line), $fac\text{-Ir}(\text{ppy})_2(\text{ppy-4})$ (red line), $fac\text{-Ir}(\text{ppy})_2(\text{ppy-4})\cdot\text{CdCl}_2$ (green line).

Table II-9: Emission properties in the solid state of $fac\text{-Ir}(\text{ppy})_2(\text{ppy-4})\cdot\text{CdCl}_2$ and $fac\text{-Ir}(\text{ppy})_2(\text{ppy-12})\cdot\text{Cd}_6$ compared to their discrete complexes.

| Complexes and networks | λ_{em} (nm) ^a | Φ^a | τ (ns) |
|---|---|----------|-------------|
| $fac\text{-}[\text{Ir}(\text{ppy})_2(\text{ppy-12})]$ | 626, 664, 681 | 18% | 395 |
| $fac\text{-}[\text{Ir}(\text{ppy})_2(\text{ppy-12})]\cdot\text{Cd}_6$ | 650, 666, 682 | 6% | 159 |
| $fac\text{-Ir}(\text{ppy})_2(\text{ppy-4})$ | 667, 683 | 2% | 291 |
| $fac\text{-Ir}(\text{ppy})_2(\text{ppy-4})\cdot\text{CdCl}_2$ | 666, 682 | 4% | 187 |

a: excited at 430 nm, RT.

5. Conclusion of chapter

In this chapter, tris-cyclometallated neutral heteroleptic Ir (III) complexes bearing either pyridyl (*fac*-Ir(ppy)₂(ppy-12) and *fac*-Ir(ppy)₂(ppy-4)) or carboxylate (*fac*-[Ir(ppy)₂(ppy-7)) groups as terminal coordinating sites have been successfully synthesized as *fac*-isomers. Structural investigation of *fac*-Ir(ppy)₂(ppy-4) was performed on single crystals using X-Ray diffraction. Furthermore, the photophysical properties of all three metallatectons were investigated both in solution and in the solid state. The three complexes are red-emitting and display QY ranging from 28 % to 46 % and lifetimes in the microsecond domain.

The linear luminescent metallatectons have been combined with different metallic salts to generate new heterometallic luminescent coordination polymers under self-assembly conditions. Two stable coordination networks have been obtained by combining either complex *fac*-Ir(ppy)₂(ppy-12) or complex *fac*-Ir(ppy)₂(ppy-4) with CdCl₂ salts. Interestingly, while both complexes are functionalized with peripheral pyridyl coordinating sites, two different networks were obtained. A 2D grid-type network was obtained using *fac*-Ir(ppy)₂(ppy-12) while the use of the other metallatecton afforded the formation of a 1D double chain network. Both networks were luminescent, depending on the network, the Ir-based luminescent properties were enhanced or slightly quenched respectively. Further studies to rationalize these observations are required.

All the neutral tris-cyclometallated Iridium complexes were prepared as racemates. In order to form heterometallic chiral coordination networks, efforts towards the resolution of the enantiomers or asymmetric synthesis are underway.

REFERENCES

- (1) Sun, J.; Wu, W.; Zhao, J. *Chem. Eur. J.* **2012**, *18*, 8100.
- (2) Tamayo, A. B.; Alleyne, B. D.; Djurovich, P. I.; Lamansky, S.; Tsyba, I.; Ho, N. N.; Bau, R.; Thompson, M. E. *J. Am. Chem. Soc.* **2003**, *125*, 7377.
- (3) McDonald, A. R.; Lutz, M.; von Chrzanowski, L. S.; van Klink, G. P. M.; Spek, A. L.; van Koten, G. *Inorg. Chem.* **2008**, *47*, 6681.
- (4) Colombo, M. G.; Brunold, T. C.; Riedener, T.; Güedel, H. U.; Fortsch, M.; Büergi, H.-B. *Inorg. Chem.* **1994**, *33*, 545.
- (5) DeRosa, M. C.; Hodgson, D. J.; Enright, G. D.; Dawson, B.; Evans, C. E. B.; Crutchley, R. J. *J. Am. Chem. Soc.* **2004**, *126*, 7619.
- (6) (a) Steunenberg, P.; Ruggi, A.; van den Berg, N. S.; Buckle, T.; Kuil, J.; van Leeuwen, F. W.; Velders, A. H. *Inorg. Chem.* **2012**, *51*, 2105; (b) Böttcher, H.-C.; Graf, M.; Krüger, H.; Wagner, C. *Inorg. Chem. Commun.* **2005**, *8*, 278; (c) Wang, X.-Y.; Kimyonok, A.; Weck, M. *Chem. Commun.* **2006**, 3933.
- (7) Huo, S.; Deaton, J. C.; Rajeswaran, M.; Lenhart, W. C. *Inorg. Chem.* **2006**, *45*, 3155.
- (8) McGee, K. A.; Mann, K. R. *Inorg. Chem.* **2007**, *46*, 7800.

- (9) Valore, A.; Colombo, A.; Dragonetti, C.; Righetto, S.; Roberto, D.; Ugo, R.; De Angelis, F.; Fantacci, S. *Chem. Commun.* **2010**, 46, 2414.
- (10) G. Park; J-H. Seo; Y. Kim; Y. S. Kim; Ha, Y. *Journal of the Korean Physical Society* **2007**, 50, 1729.
- (11) Böttcher, H.-C.; Graf, M.; Sünkel, K.; Mayer, P.; Krüger, H. *Inorg. Chim. Acta* **2011**, 365, 103.
- (12) Coughlin, F. J.; Westrol, M. S.; Oyler, K. D.; Byrne, N.; Kraml, C.; Zysman-Colman, E.; Lowry, M. S.; Bernhard, S. *Inorg. Chem.* **2008**, 47, 2039.
- (13) Schaffner-Hamann, C.; von Zelewsky, A.; Barbieri, A.; Barigelletti, F.; Muller, G.; Riehl, J. P.; Neels, A. *J. Am. Chem. Soc.* **2004**, 126, 9339.
- (14) King, K. A.; Spellane, P. J.; Watts, R. J. *J. Am. Chem. Soc.* **1985**, 107, 1431.
- (15) (a) Tsuboyama, A.; Iwawaki, H.; Furugori, M.; Mukaide, T.; Kamatani, J.; Igawa, S.; Moriyama, T.; Miura, S.; Takiguchi, T.; Okada, S.; Hoshino, M.; Ueno, K. *J. Am. Chem. Soc.* **2003**, 125, 12971; (b) Beeby, A.; Bettington, S.; Samuel, I. D. W.; Wang, Z. *J. Mater. Chem.* **2003**, 13, 80; (c) You, Y.; Nam, W. *Chem. Soc. Rev.* **2012**, 41, 7061.
- (16) (a) Coppo, P.; Plummer, E. A.; De Cola, L. *Chem. Commun.* **2004**, 1774; (b) Devery Iii, J. J.; Douglas, J. J.; Nguyen, J. D.; Cole, K. P.; Flowers Ii, R. A.; Stephenson, C. R. J. *Chem. Sci.* **2015**, 6, 537.
- (17) Okada, S.; Okinaka, K.; Iwawaki, H.; Furugori, M.; Hashimoto, M.; Mukaide, T.; Kamatani, J.; Igawa, S.; Tsuboyama, A.; Takiguchi, T.; Ueno, K. *Dalton Trans.* **2005**, 1583.
- (18) (a) Hedley, G. J.; Ruseckas, A.; Samuel, I. D. W. *J. Phys. Chem. A* **2009**, 113, 2; (b) Sajoto, T.; Djurovich, P. I.; Tamayo, A. B.; Osgaard, J.; Goddard, W. A.; Thompson, M. E. *J. Am. Chem. Soc.* **2009**, 131, 9813; (c) Chi, Y.; Chou, P. T. *Chem. Soc. Rev.* **2010**, 39, 638.
- (19) (a) Aoki, S.; Matsuo, Y.; Ogura, S.; Ohwada, H.; Hisamatsu, Y.; Moromizato, S.; Shiro, M.; Kitamura, M. *Inorg. Chem.* **2011**, 50, 806; (b) Nakagawa, A.; Hisamatsu, Y.; Moromizato, S.; Kohno, M.; Aoki, S. *Inorg. Chem.* **2014**, 53, 409.
- (20) Deaton, J. C.; Young, R. H.; Lenhard, J. R.; Rajeswaran, M.; Huo, S. *Inorg. Chem.* **2010**, 49, 9151.
- (21) Fleetham, T. B.; Wang, Z.; Li, J. *Inorg. Chem.* **2013**, 52, 7338.
- (22) (a) Xie, Z.; Ma, L.; deKrafft, K. E.; Jin, A.; Lin, W. *J. Am. Chem. Soc.* **2010**, 132, 922; (b) Barrett, S. M.; Wang, C.; Lin, W. *J. Mater. Chem.* **2012**, 22, 10329; (c) Wang, C.; Liu, D.; Xie, Z.; Lin, W. *Inorg. Chem.* **2014**, 53, 1331.
- (23) Wang, C.; Wang, J. L.; Lin, W. *J. Am. Chem. Soc.* **2012**, 134, 19895.
- (24) Dau, P. V.; Kim, M.; Cohen, S. M. *Chem. Sci.* **2013**, 4, 601.
- (25) Wang, D.; Wang, J.; Fan, H.-L.; Huang, H.-F.; Chu, Z.-Z.; Gao, X.-C.; Zou, D.-C. *Inorg. Chim. Acta* **2011**, 370, 340.
- (26) (a) Schulz, G. L.; Chen, X.; Chen, S.; Holdcroft, S. *Macromolecules* **2006**, 39, 9157; (b) Langecker, J.; Rehahn, M. *Macromol. Chem. Phys.* **2008**, 209, 258.
- (27) Maria C. DeRosa; Derek J. Hodgson; Gary D. Enright; Brian Dawson; Christopher E. B. Evans; Crutchley, R. J. *J. Am. Chem. Soc.* **2004**, 7619.
- (28) Grushin, V. V.; Herron, N.; LeCloux, D. D.; Marshall, W. J.; Petrov, V. A.; Wang, Y. *Chem. Commun.* **2001**, 1494.
- (29) Brouwer, A. M. *Pure Appl. Chem.* **2011**, 83, 2213.
- (30) Kang, S. H.; Ma, H.; Kang, M.-S.; Kim, K.-S.; Jen, A. K. Y.; Zareie, M. H.; Sarikaya, M. *Angew. Chem. Int. Ed.* **2004**, 43, 1512.
- (31) (a) Li, B.; Berliner, M.; Buzon, R.; Chiu, C. K. F.; Colgan, S. T.; Kaneko, T.; Keene, N.; Kissel, W.; Le, T.; Leeman, K. R.; Marquez, B.; Morris, R.; Newell, L.; Wunderwald, S.; Witt, M.; Weaver, J.; Zhang, Z.; Zhang, Z. *J. Org. Chem.* **2006**, 71, 9045; (b) Li, B.; Bemish, R.; Buzon, R. A.; Chiu, C. K.; Colgan, S. T.; Kissel, W.; Le, T.; Leeman, K. R.; Newell, L.; Roth, J. *Tetrahedron Lett.* **2003**, 44, 8113.
- (32) Filali, E.; Lloyd-Jones, G. C.; Sale, D. A. *Synlett* **2009**, 2009, 205.
- (33) (a) Sguerra, F.; Bulach, V.; Hosseini, M. W. *Dalton Trans.* **2012**, 41, 14683; (b) Beziau, A.; Baudron, S. A.; Fluck, A.; Hosseini, M. W. *Inorg. Chem.* **2013**, 52, 14439; (c) Larpent, P.; Jouaiti, A.; Kyritsakas, N.; Hosseini, M. W. *Dalton Trans.* **2014**, 43, 2000; (d) Ovsyannikov,

- A.; Ferlay, S.; Solovieva, S. E.; Antipin, I. S.; Konovalov, A. I.; Kyritsakas, N.; Hosseini, M. W. *CrystEngComm* **2014**, *16*, 3765.
- (34) Spek, A. L. *PLATON*; The University of Utrecht, The Netherlands, 1999.
- (35) Merz, T. A.; Waddell, P. G.; Cole, J. M. *J. Phys. Chem. C* **2013**, *117*, 8429.
- (36) Li, L.; Zhang, S.; Xu, L.; Han, L.; Chen, Z.-N.; Luo, J. *Inorg. Chem.* **2013**, *52*, 12323.

Chapter IV: Conclusions and Perspectives

This PhD project focused on the synthesis of octahedral tris-chelate Iridium(III) complexes that are stereogenic at the metal center only. Applying the concepts of molecular tectonics, combinations of such chiral metallatectons with metallic ions or clusters, acting as metallic nodes, lead to the formation of homochiral heterometallic coordination networks. Besides their intrinsic chirality, Iridium(III) complexes are also known as triplet emitters. Thus, the formation of homochiral and luminescent heterometallic coordination polymers was explored under self-assembly conditions.

To achieve those goals, two types of Ir metallatectons (Figure IV-1) were synthesised. Cationic bis-cyclometallated Iridium complexes bearing two anionic phenylpyridyl type ligands and a third neutral substituted bipyridyl moiety were first investigated. The chiral complexes were isolated either as a racemate or as enantiopure species (chapter II). The second type of metallatecton was a neutral heteroleptic tris-cyclometallated Ir(III) complexes for which two phenylpyridyl and one substituted phenylpyridyl ligands are coordinated to the Ir center. For the latter, only the *fac* isomers were isolated as racemates since the resolution of the two enantiomers (*fac*, Δ) and (*fac*, Λ) could not be achieved (chapter III).

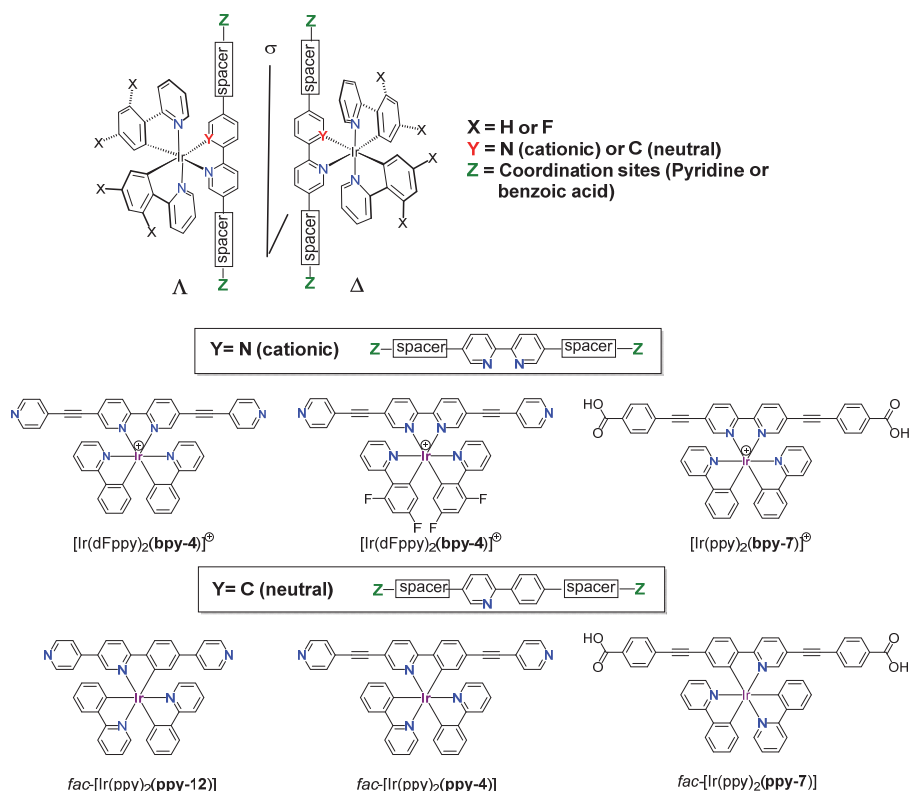


Figure IV-1: The two types of Iridium complexes (cationic or neutral) investigated during this PhD work and their chemical structures.

In order to generate coordination networks, for both types of complexes, the third ligand is equipped with two peripheral coordinating sites, either 4-pyridyl units or 4-benzoate moieties. Except for one metallatecton, *fac*-Ir(ppy)₂(ppy-12), ethynyl spacers between the central and peripheral coordinating sites were used to ensure extended conjugation of the ligand. It should be noted that all three chelating ligands coordinated to the Ir center are achiral. With the aim of generating under self-assembly conditions hybrid periodic architectures in the crystalline phase, all five Ir complexes, behaving as metallatectons, were combined to interact with different metal salts (Figure IV-2).

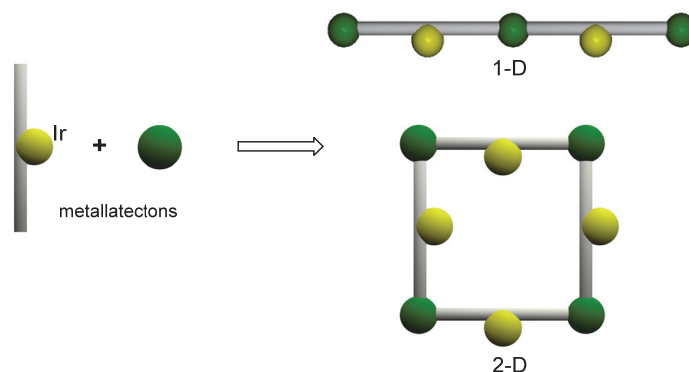


Figure IV-2: Schematic representation of the formation of 1D linear and 2D grid-type coordination networks with the designed Ir metallatectons

In chapter II, the synthesis of the three cationic Iridium complexes represented in Figure IV-1 is described. Two of them bear 2-phenylpyridine units and for the third one, 2-phenylpyridyl units are substituted with two fluorine atoms. The third ligand is a 2,2'-bipyridyl substituted in positions 5 and 5' either by 4-ethynylpyridyl or 4-ethynylbenzoic acid. The three Ir complexes were obtained as racemates or enantiomerically pure using a chiral Ir precursor. Photophysical properties of the three metallatectons were studied and exhibited no unexpected features. For the preparation of coordination networks, different metal salts such as Cd²⁺, Co²⁺ or Cu²⁺ have been combined with the metallatectons. Single crystals suitable for X-ray diffraction were only obtained with the linear metallatecton bearing peripheral pyridyl moieties. Using Cu^{II} salt a 2D grid-type infinite architecture was obtained whereas with Cd^{II} salt a 1D network was generated. The 2D network presented two main features: i) the presence of PF₆⁻ anions within the cavities of the network reducing thus the empty space within the framework; ii) the resulting network was not luminescent, probably because of the presence of Cu^{II} cations. The 1D network could be obtained as a racemate when starting from the racemic metallatecton or enantiopure when using the Λ enantiomer. In both cases, the PF₆⁻ anions were not present within the infinite architecture but exchanged within iodide anions. Furthermore, both 1D networks were found to be red-emitter in the solid state.

In chapter III, the optimised synthesis of three neutral heteroleptic tris-cyclometalated Ir(III) complexes is presented. Thus, two Ir complexes substituted with peripheral 4-pyridyl coordinating units, *fac*-Ir(ppy)₂(**ppy-12**) and *fac*-Ir(ppy)₂(**ppy-4**), and one Ir complex substituted with peripheral 4-benzoate coordinating sites, *fac*-Ir(ppy)₂(**ppy-7**) have been obtained as *fac* isomers and as a racemate (Figure IV-1). They all display good luminescent properties. Different single crystals suitable for X-Ray diffraction have been obtained for the three complexes. Unfortunately, when the 4-benzoate substituted Ir complex was used as metallatecton, the crystals were not diffracting enough. However, combination of the two complexes substituted with peripheral 4-pyridyl units with CdCl₂ salts afforded single crystals and the infinite architecture obtained could be investigated by X-Ray diffraction. Thus, depending on the metallatecton used, either 2D grid-type or 1D linear coordination networks could be obtained. In all cases, the networks were luminescent.

In conclusion, our strategy based on the use of cationic chiral-at-metal Ir metallatectons bearing only achiral ligands proved successful for the generation of homochiral heterometallic coordination networks. By a proper choice of the metallic node, the luminescence of the final architecture could be maintained which may be of interest for chemical sensing. However, even if the metallic node quenches the Ir-centered luminescence, as observed for the (Cu,Ir) 2D grid-type network, one may use such system to sense guest molecules interacting with the Cu ion and thus possibly restoring the luminescence. Such phenomena could not be investigated because of the poor stability of the 2D architecture. In order to generate stable porous infinite architectures, the formation of coordination networks with other metal salts and under other crystallization conditions is still under investigation.

The use of neutral tris-cyclometalated Iridium complexes, isolated as *fac*-isomers, as metallatectons was also successful. Thus, heterometallic 1D and 2D coordination networks exhibiting red emitting properties were obtained and investigated by X-Ray diffraction. However, so far the two enantiomers of the *fac*-isomers were not resolved and efforts towards this goal are still undergoing. Having achieved this goal, it will be possible to generate heterometallic homochiral coordination polymers with neutral chiral-at-metal Ir metallatectons displaying luminescence properties. Such materials may be of interest for chemical sensing.

Chapter V: Experimental Part

1. General

Synthesis:

All air sensitive and anhydrous reactions were carried out under argon. Light sensitive reactions were protected from light by covering with an aluminum foil. The glassware was dried in an oven at 100 °C and cooled under argon flow. Commercially available chemicals were used without further purification.

Anhydrous di-isopropylamine, toluene, chloroform, dichloromethane and methanol were used as supplied by commercial sources without further purification. THF was dried and distilled over sodium respectively. Triethylamine was dried and distilled over KOH. Methanol was distilled and dried over magnesium methoxide under argon.

Thin layer chromatography analyses were performed on silica gel Merck 60 F₂₅₄ sheets or aluminium oxide F254 sheets. A UV lamp (254 nm or 365 nm) lamp was used for detection.

Microwave reactions were conducted using the Discover BenchMate microwave apparatus (CEM Corporation) and the corresponding vials. Reactions were performed in glass vials (capacity 10 mL) sealed with a septum, and the liquid was mixed by magnetic stirring.

NMR (Nuclear magnetic resonance):

Nuclear magnetic resonance spectra were recorded on Bruker Avance AV 300 (300 MHz), AV 400 (400 MHz) or AV500 (500 MHz) spectrometers at 20 °C.

Chemicals shifts (δ , ppm) were determined relative to the residual undeuterated solvent as internal reference (CDCl₃: 7.26 ppm for ¹H, 77.2 ppm for ¹³C; CD₃OD: 3.34 ppm for ¹H, 49.9 ppm for ¹³C; CD₃CN: 1.94 ppm for ¹H, 118.3 ppm and 1.3 ppm for ¹³C; DMSO-D₆: 2.50 ppm for ¹H and 39.52 ppm for ¹³C). Spin multiplicities are given with the following abbreviations: s (singlet), brs (broad singlet), d (doublet), dd (doublet of doublet), t (triplet), q (quadruplet), m (multiple). Coupling constants (J) are given in Hz.

¹H-NMR spectra were assigned by standard methods combined when necessary with 2D COSY and ROESY ¹H-¹H correlated experiments. ¹³C-NMR spectra were assigned by standard methods combined when necessary with DEPT-135 experiment and 2D HMQC and HMBC ¹H-¹³C correlation experiments.

MS (Mass spectrometry):

Mass spectrometry was performed at the Service de Spectrométrie de Masse, Université de Strasbourg. Low (LRMS) and high-resolution mass spectra (HRMS) (positive and negative mode ESI: Electro Spray Ionization) were recorded on Thermoquest AQA Navigator® with time of flight detector.

Elemental analyses:

Elemental analyses were performed on a Thermo Scientific Flash 2000 by the “Service d’Analyses”, Université de Strasbourg.

X-Ray diffraction:

X-ray single crystal structure determination was carried out on a Bruker SMART CCD Diffractometer with Mo-K α radiation. The structures were solved using SHELX-97 and refined by full matrix least squares on F² using SHELX-97 with anisotropic thermal parameters for all non-hydrogen atoms. The hydrogen atoms were introduced at calculated positions and not refined (riding model).

Powder X-ray diffraction (PXRD) data were recorded on a Bruker D8 AV diffractometer using Cu-K α radiation ($\lambda = 1.5406 \text{ \AA}$) operating at 40 kV and 40 mA with a scanning rate between 3.8 and 70° by a scan step size of 2°/min. For comparison, simulated patterns were calculated using the data obtained for single crystals by the Mercury software.

Photophysical measurements:

UV/Vis spectra in solution and in the solid state were recorded on Uvikon XL spectrophotometer or a Perkin-Elmer Lambda 650S spectrophotometer (spectra in the solid state recorded in the reflection mode, using a 150 mm integrating sphere and spectralon® as light spectral reference for the reflection corrections). Wavelengths (λ) are given in nm and molar absorption coefficients (ϵ) are given in L.mol⁻¹.cm⁻¹. Steady-state emission spectra in solution were recorded on a HORIBA Jobin-Yvon IBH FL-322 Fluorolog 3 spectrometer equipped with a 450 W xenon arc lamp, double grating excitation and emission monochromators (2.1 nm mm⁻¹ dispersion; 1200 grooves mm⁻¹) and a Hamamatsu R928 photomultiplier tube. Steady-state emission spectra in the solid state were recorded on a Perkin Elmer LS55 spectrometer equipped with a Hamamatsu R928 photomultiplier tube. Emission and excitation spectra were corrected for source intensity (lamp and grating) and emission spectral response (detector and grating) by standard correction curves.

Photoluminescence quantum yields in the solid state were performed by using an absolute photo-luminescence quantum yield spectrometer Quantaaurus C11347-11(Hamamatsu, Japan) exciting the samples from 300 nm to 500 nm. In solution, quantum yields in the visible range were measured using the method of Crosby and Demas using Ru(bipy)₃Cl₂ in degassed acetonitrile as the standard ($\Phi = 0.095$).¹

All solvents were spectrometric grade. Measurements in solution were performed on optically dilute solutions ($A_{\lambda_{exc}} < 0.10$). Deaerated samples were prepared by the freeze-pump-thaw technique.

Time-resolved measurements were performed using the PicoHarp 300 equipped with time correlated single photon counting (TCSPC) system on the Fluoro Time 300 (PicoQuant), where a laser source 375 nm (LDH-P-C-375) was applied to excite the samples. The laser was mounted directly on the sample chamber at 90° and collected by a PMA-C 192M single-photon-counting detector. Signals were collected using EasyTau software, and data analysis was performed using FluoFit software (PicoQuant). while data analysis was performed using the commercially available software FluoFit (PicoQuant GmbH, Germany).

CD (Circular Dichroism)

Circular dichroism was performed on a JASCO J-810 spectropolarimeter. Data were collected over a wavelength range of 200-600 nm, at a scan speed of 100 nm/min, bandwidth of 1 nm and data pitch of 0.1 nm. Samples were measured at RT (23°C) and at given concentrations using a 10 mm path length cuvette (Starna Ltd.).

Optical rotation ([α]_D)

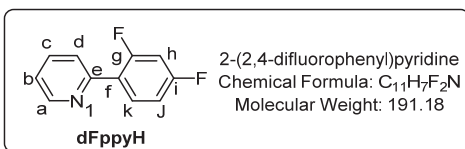
Polarimetric measurements were performed on a Perkin Elmer (model 341) instrument at a wavelength of 589 nm (Na). The [α]_D²⁰ values are measured at 20 °C and given in 10⁻¹ deg.cm².g⁻¹ and concentrations are given in g/100mL.

Crystallization methods:

All solvents used for crystallization were commercial analytical solvents used without purification. Under self-assembly conditions, crystallization were performed for combinations of the metallatecton with metal salts by liquid-liquid slow diffusion in a crystallization tube (height = 12 cm diameter = 0.4 cm). At room temperature, a solution containing the desired metal salts was allowed to diffuse (over few days or weeks) into a solution containing the metallatecton through a 1/1 buffer layer composed of the two solvents.

For crystallization of metallatectons by vapor diffusion, a solution of the compound in a small vial (height = 6.5 cm, diameter = 2 cm) was placed into a closed jar (100 mL) containing volatile solvent (*ca.* 40 mL) at RT.

2. Synthesis and characterization of compounds



Ligand dFppyH:²

2, 4-difluorophenylboronic acid (1.00 g, 6.3 mmol) and Pd(PPh₃)₄ (0.30 g, 0.25 mmol) were dissolved in dry THF (13 mL) to form a light yellow solution. The solution was degassed several times before adding 2-bromopyridine (0.50 mL, 5.3 mmol). Then a degassed solution of K₂CO₃ (2 M in distilled water, 7.5 mL) was added. The mixture was refluxed for 33 hr before distilled water (20 mL) was added. The resulting solution was washed with CH₂Cl₂ (20 mL × 3) and the combined yellow organic layers were dried over Mg₂SO₄ and filtered. The solvent was evaporated and the crude product was purified by column chromatography (SiO₂, CH₂Cl₂/cyclohexane 25 % to 50 %), 2,4-difluorophenylpyridine (0.70 g, 70 %) was obtained as a light yellow oil.

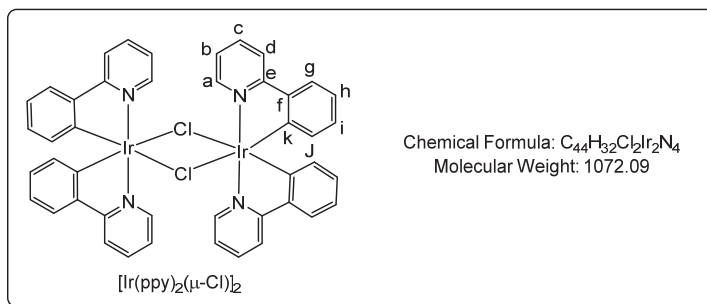
¹H NMR (CDCl₃, 300 MHz) δ (ppm): 8.72 (td, 1H, ³J = 4.8 Hz, ⁴J = 1.5 Hz, H_a), 8.03 (td, 1H, ⁴J_{H-F} = 8.8 Hz, ⁴J_{H-H} = 6.8 Hz, H_k), 7.78-7.71 (m, 2H, H_d, H_b), 7.24-7.30 (m, 1H, H_c), 7.03 (ddd, 1H, ³J_{H-F} = 8.5 Hz, ³J_{H-H} = 8.7 Hz, ⁴J_{H-H} = 2.4 Hz, H_j), 6.93 (ddd, 1H, ³J_{H-F} = 11.4 Hz, ³J_{H-F} = 8.7 Hz, ⁴J_{H-H} = 2.4 Hz, H_h).

¹⁹F NMR (CDCl₃, 282 MHz) δ (ppm): -109.34 (d, 1F, ⁴J_{F-F} = 9.0 Hz), -112.94 (d, 1F, ⁴J_{F-F} = 9.0 Hz).

¹³C NMR (CDCl₃, 75 MHz) δ (ppm): 163.1 (dd, ¹J_{C-F} = 240.8 Hz, ³J_{C-F} = 11.9 Hz, C_g), 160.5 (dd, ¹J_{CF} = 240.8 Hz, ³J_{C-F} = 11.9 Hz, C_i), 152.5 (C_e), 149.7 (C_a), 136.4 (C_c), 132.1 (dd, ³J_{C-F} = 9.7 Hz, ³J_{C-F} = 4.4 Hz, C_k), 124.1 (d, ⁴J_{C-F} = 9.7 Hz, C_d), 123.7 (d, ²J_{C-F} = 9.7 Hz, C_f), 122.3 (C_b), 111.7 (dd, ²J_{C-F} = 21.1 Hz, ⁴J_{C-F} = 2.8 Hz, C_j), 104.3 (dd, ²J_{C-F} = 17.4 Hz, ²J_{C-F} = 17.4 Hz, C_h).

IR: ν cm⁻¹ 1619, 1599, 1588, 1504 (aromatic C=C), 1466 (aromatic C=N), 1441, 1418, 1283, 1263, 1139, 1105 (CF), 1060, 966, 909, 850, 778, 734.

Elem. Anal. Calcd for C₁₁H₇F₂N·0.1H₂O: C, 68.46; H, 3.76; N, 7.26. **Found:** C, 68.16; H, 3.79; N, 7.00.



Compound [Ir(ppy)₂(μ-Cl)]₂:³

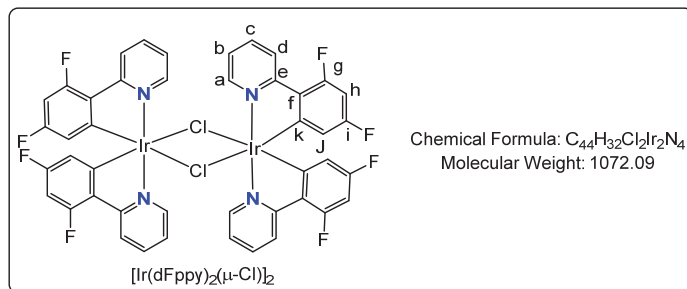
IrCl₃·xH₂O (0.42 g, 1.41 mmol) and 2-phenylpyridine (0.46 mL, 3.22 mmol) were dissolved into a 2-EtOEtOH/H₂O mixture (20 mL/7 mL) and the resulting solution was heated at 130 °C for 20 hr. After cooling, the yellow precipitate was filtered and washed with an acetone/ethanol mixture (10 mL/10 mL). The resulting powder was dissolved in dichloromethane (ca. 30 mL) and the suspension was filtered. The yellow solution was concentrated to give a fine yellow microcrystalline powder (0.652 g, 86 %).

¹H NMR (CDCl₃, 300 MHz) δ (ppm): 9.24 (dd, 4H, ³J = 5.7 Hz, ⁴J = 1.0 Hz, H_a), 7.86 (d, 4H, ³J = 7.8 Hz, H_d), 7.73 (td, 4H, ³J = 7.5 Hz, ⁴J = 1.5 Hz, H_c), 7.48 (dd, 4H, ³J = 7.8 Hz, ⁴J = 1.2 Hz, H_g),

6.73-6.78 (m, 8H, H_b, H_i), 6.56 (ddd, 4H, ³J = 8.0 Hz, ³J = 8.0 Hz, ⁴J = 1.4 Hz, H_h), 5.93 (dd, 4H, ³J = 7.7 Hz, ⁴J = 1.0 Hz, H_j).

¹³C NMR (CDCl₃, 75 MHz) δ (ppm): 168.6 (C_e), 151.7 (C_a), 145.4 (C_f), 143.7 (C_k), 136.1 (C_j), 130.6 (C_c), 124.1 (C_b), 123.7 (C_d), 122.1 (C_i), 121.3 (C_g), 118.3 (C_h).

IR: ν cm⁻¹ 1605, 1582, 1477 (C=N), 1416, 1268, 1225, 1160, 1062, 1030, 793, 753, 735, 727.



Complex [Ir(dFppy)₂(μ-Cl)]₂.⁴

IrCl₃·xH₂O (0.20 g, 0.67 mmol) and 2,4-difluorophenylpyridine (0.38 g, 1.98 mmol) were dissolved in a 2-EtOH/H₂O mixture (4 mL/2 mL) and heated at 130 °C for 20 hr. After cooling, the yellow precipitate was filtered and washed with water (5 mL) and an acetone/ethanol mixture (6 mL/6 mL). The resulting powder was recrystallized in a mixture of cyclohexane/dichloromethane (10 mL/30 mL) to give a fine yellow microcrystalline powder (0.29 g, 68 %).

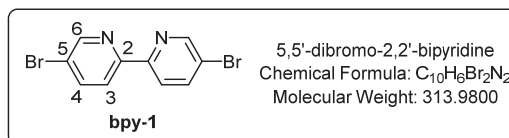
¹H NMR (CDCl₃, 300 MHz) δ (ppm): 9.12 (dd, 4H, J_d = 5.7 Hz, J_d = 1.0 Hz, H_a), 8.31 (d, 4H, J_d = 8.3 Hz, H_d), 7.83 (td, 4H, J_i = 7.8 Hz, J_d = 1.3 Hz, H_b), 6.83 (ddd, 4H, ³J_{H-H} = 7.2 Hz, ³J_{H-H} = 7.2 Hz, ⁴J_{H-H} = 1.2 Hz, H_c), 6.33 (ddd, 4H, ³J_{H-F} = 12.6 Hz, ³J_{H-F} = 9.2 Hz, ⁴J_{H-H} = 2.4 Hz, H_h), 5.28 (dd, 4H, ³J_{H-F} = 9.3 Hz, ⁴J_{H-H} = 2.4 Hz, H_j).

¹⁹F NMR (CDCl₃, 282 MHz) δ (ppm): -107.72 (d, 1F, ⁴J_{F-F} = 10.2 Hz), -110.32 (d, 1F, ⁴J_{F-F} = 10.2 Hz).

¹³C NMR (CDCl₃, 125 MHz) δ (ppm): 165.3 (d, ²J_{C-F} = 6.7 Hz, C_f), 162.4 (dd, ¹J_{C-F} = 253.5 Hz, ³J_{C-F} = 12.9 Hz, C_g), 160.4 (dd, ¹J_{C-F} = 253.5 Hz, ³J_{C-F} = 12.9 Hz, C_j), 151.3 (C_b), 147.6 (d, ³J_{C-F} = 7.1 Hz, C_e), 137.6 (C_a), 127.8 (C_k), 122.7 (d, ⁴J_{C-F} = 19.9 Hz, C_d), 122.6 (C_c), 112.7 (d, ²J_{C-F} = 18.2 Hz, C_j), 98.2 (t, ²J_{C-F} = 26.5 Hz, C_h).

IR: ν cm⁻¹ 1602, 1572, 1558, 1478 (C=N), 1428, 1400, 1292, 1268, 1250, 1231, 1165, 1116, 1102 (C-F), 1043, 989, 848, 832, 819, 811, 792, 786, 762, 756.

Elem. Anal. Calcd for C₄₄H₃₂Cl₂Ir₂N₄·H₂O: C, 42.83; H, 2.12; N, 4.54. Found: C, 42.65; H, 2.20; N, 4.23.



Compound bpy-1.⁵

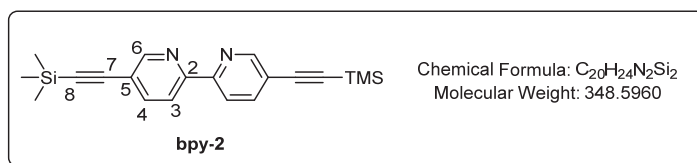
5-Bromo-2-iodopyridine (0.80 g, 2.82 mmol) was dissolved in anhydrous toluene (15 mL). After degassing the solution by argon several times, Pd(PPh₃)₄ (0.02 g, 0.02 mmol) and *n*-Bu₆Sn₂ (0.75 mL, 1.48 mmol) were added. The mixture was refluxed for 3 days. The reaction mixture was cooled to room temperature and diethyl ether (about 80 mL) was added. The white-brown precipitate that formed was filtered and washed consecutively with distilled water 3 mL×3 and diethyl ether 5 mL×3. The precipitate was dissolved in CHCl₃ 20 mL and the solution was washed with brine 20 mL, dried (MgSO₄), filtered and concentrated under reduced pressure to afford bpy-1 as a colorless solid (0.31 g, 69 %).

¹H NMR (CDCl₃, 500 MHz) δ (ppm): 8.70 (d, 2H, J_d = 2.4 Hz, **H**₆), 8.29 (d, 2H, J_d = 8.6 Hz, **H**₃), 7.93 (dd, 2H, J_d = 2.4 Hz, J_d = 8.6 Hz, **H**₄).

¹³C NMR (CDCl₃, 125MHz) δ (ppm): 153.8 (**C**^{IV}_{ar}, **C**₅), 150.4 (**C**_{ar}, **C**₆), 139.7 (**C**_{ar}, **C**₃), 122.3 (**C**_{ar}, **C**₄), 121.5 (**C**^{IV}_{ar}, **C**₂).

IR: ν cm⁻¹ 1544, 1455 (C=N), 1357, 1261, 1233, 1124, 1087, 1007, 827, 801, 726, 702, 638 (C-Br).

Elem. Anal. Calcd for C₁₀H₆Br₂N₂: C, 38.25; H, 1.93; N, 8.92. **Found:** C, 38.16; H, 2.12; N, 8.57.



Compound **bpy-2**:⁵

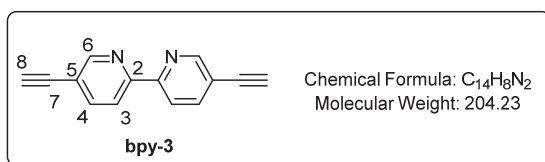
Trimethylsilylacetylene (0.25 mL, 1.84 mmol) was added to a degassed solution of 5,5'-dibromo-2,2'-bipyridine (0.20 g, 0.64 mmol) in a mixture of toluene (14 mL) and distilled NEt₃ (4 mL). The resulting mixture was degassed several times with argon. Then Pd(PPh₃)₄ (0.02 g, 0.017 mmol) and CuI (0.01 g, 0.52 mmol) were added. The mixture was stirred at 60 °C overnight. The solution was filtered through a celite pad then concentrated under reduced pressure. The residue was dissolved in CH₂Cl₂ (30 mL), washed with an aqueous saturated NH₄Cl solution (30 mL) and brine (30 mL), dried over MgSO₄ and evaporated to dryness. The solid thus obtained was then purified by chromatography (silica gel, CH₂Cl₂/Cyclohexane 50% to 100%) to afford the desired product as a white solid (0.19 g, 83%).

¹H NMR (CDCl₃, 300 MHz) δ (ppm): 8.71 (d, 2H, J_d = 1.8 Hz, **H**₆), 8.35 (d, 2H, J_d = 8.5 Hz, **H**₃), 7.85 (dd, 2H, J_d = 1.9 Hz, J_d = 8.2 Hz, **H**₄), 0.27 (s, 18H, Si(CH₃)₃).

¹³C NMR (CDCl₃, 100MHz) δ (ppm): 154.2 (**C**^{IV}_{ar}, **C**₂), 152.1 (**C**_{ar}, **C**₆), 139.8 (**C**_{ar}, **C**₄), 120.5 (**C**_{ar}, **C**₃), 120.4 (**C**^{IV}_{ar}, **C**₅), 101.8 (**C**₇), 99.5 (**C**₈), -0.1 (Si(CH₃)₃).

IR: ν cm⁻¹ 2161, 1457, 1363, 1249, 1220, 1024, 866, 834, 760, 738, 661, 646.

Elem. Anal. Calcd for C₂₀H₂₄N₂Si₂: C, 68.91; H, 6.94; N, 8.04. **Found:** C, 67.95; H, 6.96; N, 7.93.



Compound **bpy-3**:⁵

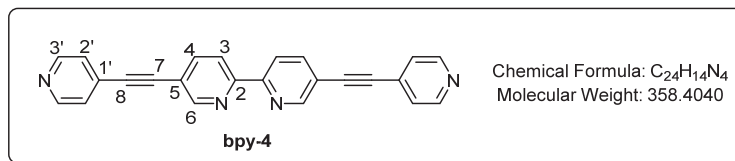
5,5'-bis((trimethylsilyl)ethynyl)-2,2'-bipyridine (0.26 g, 0.75 mmol) was dissolved in a methanol: THF (1:1, 12 mL) mixture and powdered K₂CO₃ (0.10 g, 0.72 mmol) was added. The mixture was stirred overnight at room temperature and the solvent was evaporated to dryness. CH₂Cl₂ (15 mL) was added and the mixture was washed with a saturated NH₄Cl solution (15 mL) and brine (15 mL). The organic layer was dried over MgSO₄ and concentrated to dryness. Purification by chromatography (Al₂O₃, CH₂Cl₂/cyclohexane 0% to 70%) afforded the pure product as a beige solid (0.13 g, 87 %).

¹H NMR (CDCl₃, 300 MHz) δ (ppm): 8.76 (s, 2H, **H**₆), 8.39 (d, 2H, J_d = 8.2 Hz, **H**₃), 7.90 (dd, 2H, J_d = 1.4 Hz, J_d = 8.2 Hz, **H**₄), 3.30 (s, 2H, **H**₈).

¹³C NMR (CDCl₃, 125MHz) δ (ppm): 154.6 (**C**^{IV}_{ar}, **C**₅), 152.3 (**C**_{ar}, **C**₆), 140.1 (**C**_{ar}, **C**₃), 120.6 (**C**_{ar}, **C**₄), 119.5 (**C**^{IV}_{ar}, **C**₂), 81.7 (**C**_{7/8}), 80.6 (**C**_{8/7}).

IR: ν cm⁻¹ 3263, 1585, 1531, 1464, 1365, 1234, 1025, 838, 737, 706, 679, 631, 514.

Elem. Anal. Calcd for C₁₄H₈N₂·0.1H₂O: C, 81.61; H, 4.01; N, 13.60. **Found:** C, 81.45; H, 3.94; N 13.75.



Compound bpy-4:

To a solution of 5,5'-diethynyl-2,2'-bipyridine (0.09 g, 0.44 mmol) in anhydrous toluene (18 mL), 5-iodopyridine (0.19 g, 0.88 mmol) and Pd(PPh₃)₄ (0.04 g, 0.03 mmol) were added. After degassing the yellow solution several times with argon, diisopropylamine (6 mL) was added. The mixture was heated at 60 °C for two days. The dark red mixture was filtered on a celite pad and the filtrate was evaporated. The crude product was purified by column chromatography (Al₂O₃, CH₂Cl₂/MeOH 0 % to 1 %). The powder obtained after evaporation of solvents was dissolved in a 1M aqueous HCl solution (5 mL) and H₂O (20 mL). The aqueous layer was washed with CH₂Cl₂ (2x30 mL). A 1M aqueous NaOH solution (10 mL) was then added that resulted in precipitation of a white powder. The resulting suspension was extracted with CH₂Cl₂ (2x30 mL) and the organic layers were collected and evaporated to dryness to afford the product as a beige solid (0.087 g, 72%).

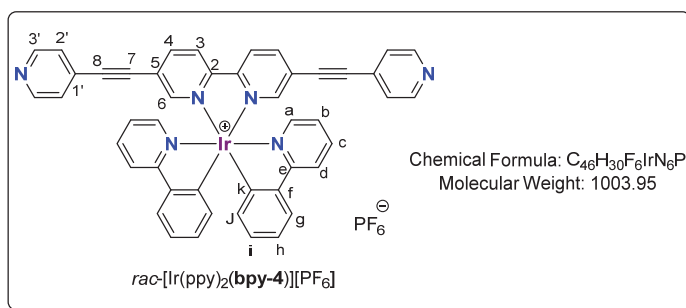
¹H NMR (CDCl₃, 500 MHz) δ (ppm): 8.84 (d, 2H, ⁴J = 1.7 Hz, H₆), 8.65 (dd, 4H, ³J = 4.4 Hz, ⁵J = 1.5 Hz, H_{3'}), 8.48 (d, 2H, ³J = 8.3 Hz, H₃), 7.98 (dd, 2H, ³J = 8.2 Hz, ⁴J = 2.1 Hz, H₄), 7.43 (dd, 4H, ³J = 4.5 Hz, ⁵J = 1.5 Hz, H_{2'}).

¹³C NMR (CDCl₃, 125 MHz) δ (ppm): 154.6 (C₅), 151.9 (C₆), 149.8 (C_{3'}), 139.7 (C₄), 130.7 (C_{1'}), 125.5 (C_{2'}), 120.8 (C₃), 119.5 (C₂), 90.9 (C_{7/8}), 90.7 (C_{7/8}).

IR: ν cm⁻¹ 1584, 1529, 1492, 1411, 1364, 1219, 1022, 839, 819, 735, 718, 649, 549, 520, 466.

Elem. Anal. Calcd for C₂₄H₁₄N₄·0.25H₂O: C, 79.43; H, 4.03; N, 15.44. **Found:** C, 79.35; H, 4.02; N, 15.39.

UV-Visible (CH₂Cl₂): λ (nm) (ϵ) (10³ L.mol⁻¹.cm⁻¹) 279 (15.6), 340 (64.6).



Compound *rac*-[Ir(ppy)₂(bpy-4)][PF₆]:

To a solution of [Ir(ppy)₂(μ -Cl)]₂ (0.05 g, 0.046 mmol) in a mixture of MeOH/CH₂Cl₂/CH₃CN (6 mL/6 mL/2 mL) was added 5,5'-diethynylpyridine-2,2'-bipyridine (0.035 g, 0.097 mmol). The yellow solution was heated at 60 °C overnight. After cooling, water (30 mL) was added and the aqueous layer was washed with Et₂O (30 mL x3). The aqueous layer was heated at 70 °C and an aqueous KPF₆ solution (100 mg in 5 mL H₂O) was added. An orange precipitate formed immediately and the suspension was placed in an ice bath for 2 hours. The suspension was filtered, washed with H₂O (5 mL) and Et₂O (5 mL). The product was obtained as a red powder (0.078 g, 85 %) by recrystallization from acetonitrile (1.5 mL) and diethylether (30 mL). Single crystals suitable for X-ray diffraction were obtained by vapor diffusion of Et₂O (15 mL) into an acetonitrile solution containing the Ir complex (5 mg in 1 mL).

¹H NMR (CD₃CN, 400 MHz) δ (ppm): 8.62 (br s, 4H, H_{3'}), 8.56 (d, 2H, ³J = 8.6 Hz, H₃), 8.27 (dd, 2H, ³J = 8.6 Hz, ⁴J = 2.0 Hz, H₄), 8.06-8.09 (m, 4H, H_d, H₆), 7.87 (ddd, 2H, ³J = 7.8 Hz, ³J = 7.8 Hz, ⁴J = 1.4 Hz, H_c), 7.81 (d, 2H, ³J = 7.7 Hz, H_g), 7.70 (d, 2H, ³J = 5.8 Hz, H_a), 7.36 (d, 4H, ³J = 5.7 Hz, H_{2'}), 7.04-7.09 (m, 4H, H_b, H_h), 6.94 (ddd, 2H, ³J = 7.5 Hz, ³J = 7.5 Hz, ⁴J = 1.0 Hz, H_i), 6.27 (d, 2H, ⁴J = 7.6 Hz, H_j).

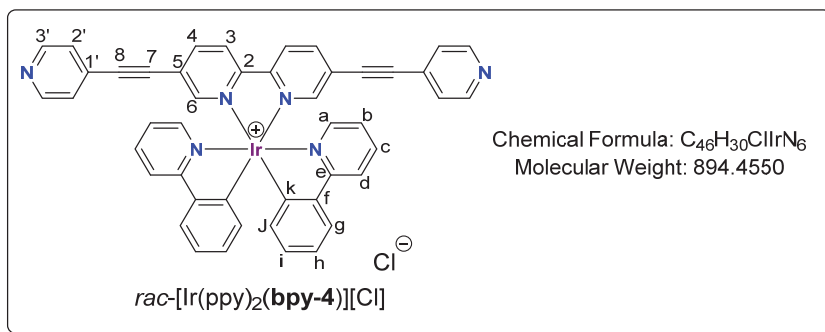
¹³C NMR (CD₃CN, 100 MHz) δ (ppm): 168.1 (C_e), 155.6 (C₂), 153.5 (C₆), 151.1 (C_{3'}), 150.6 (C_a), 150.0 (C_f), 145.0 (C_k), 142.7 (C₄), 139.7 (C_c), 132.4 (C_j), 131.5 (C_i), 129.9 (C₅), 126.3 (C_{2'}), 126.0 (C_{3/g}), 125.9 (C_{3/g}), 124.8 (C_{1'}), 124.6 (C_{b/h}), 123.9 (C_{b/h}), 121.0 (C_d), 94.3 (C₈), 88.4 (C₇).

MS (ESI⁺): calcd for [M-PF₆]⁺ C₄₆H₃₀IrN₆ 859.22, found 859.22.

UV-Visible (CH₃CN): λ (nm), ε (10³ L.mol⁻¹.cm⁻¹) 256 (43.8), 303 (37.4), 359 (45.9).

UV-Visible (THF): λ (nm), ε (10³ L.mol⁻¹.cm⁻¹) 303 (40.4), 359 (48.8).

Elem. Anal. Calcd for C₄₆H₃₀F₆IrN₆P: C, 55.03; H, 3.01; N, 8.37. Found: C, 54.71; H, 3.27; N, 8.81.



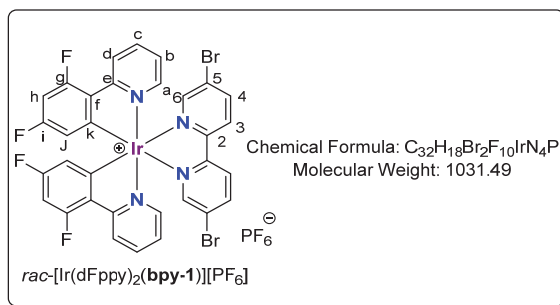
Compound *rac*-[Ir(ppy)₂(bpy-4)][Cl]:

To a solution of *rac*-[Ir(ppy)₂(μ-Cl)]₂ (0.05 g, 0.047 mmol) in a mixture of MeOH/CH₂Cl₂/CH₃CN (5 mL/5 mL/1.5 mL) was added 5,5'-diethynylpyridine-2,2'-bipyridine (0.036 g, 0.100 mmol). The yellow solution was heated at 60 °C overnight. The solvent was evaporated to dryness. Then the mixture was dissolved into 3 mL acetonitrile, filtered and concentrated. *rac*-[Ir(ppy)₂(bpy-4)][Cl] (0.065 g, 78 %) was obtained by recrystallization from acetonitrile (2 mL) and Et₂O (20 mL).

¹H NMR (CD₃CN, 400 MHz) δ (ppm): 8.64 (2H, d, ³J = 8.6, H₃), 8.56 (4H, d, ³J = 5.7, H_{3'}), 8.28 (2H, dd, ³J = 8.6, ⁴J = 1.9, H₄), 8.09 (2H, d, ³J = 8.6, H_d), 8.05 (2H, d, ³J = 1.9, H₆), 7.88 (2H, ddd, ³J = 7.8, ³J = 7.8, ⁴J = 1.4, H_c), 7.83 (2H, d, ³J = 7.7, H_g), 7.70 (2H, d, ³J = 5.8, H_a), 7.37 (4H, d, ³J = 5.7, H_{2'}), 7.04-7.09 (4H, m, H_b, H_h), 6.95 (2H, ddd, ³J = 7.5, ³J = 7.5, ⁴J = 1.0, H_i), 6.27 (2H, d, ⁴J = 7.6, H_j).

¹³C NMR (CD₃CN, 100 MHz) δ (ppm): 168.1 (C_e), 155.6 (C₂), 153.5 (C₆), 151.1 (C_{3'}), 150.6 (C_a), 150.0 (C_f), 145.0 (C_k), 142.7 (C₄), 139.7 (C_c), 132.4 (C_j), 131.5 (C_i), 129.9 (C₅), 126.2 (C_{2'}), 126.1 (C_{3/g}), 125.9 (C_{3/g}), 124.8 (C_{1'}), 124.6 (C_{b/h}), 123.9 (C_{b/h}), 121.0 (C_d), 94.3 (C₈), 88.4 (C₇).

UV-Visible (CH₃CN): λ (nm), ε (10³ L.mol⁻¹.cm⁻¹) 256 (43.3), 301 (37.9), 359 (45.4).



Compound *rac*-[Ir(dFppy)₂(bpy-1)][PF₆]:⁶

To a solution of *rac*-[Ir(dFppy)₂(μ-Cl)]₂ (0.22 g, 0.18 mmol) in a mixture of MeOH/CH₂Cl₂ (5 mL/5 mL), was added 5,5'-dibromo-2,2'-bipyridine **2** (0.12 g, 0.37 mmol). The yellow solution was heated at 60 °C overnight. After cooling, water (30 mL) was added and the aqueous layer was washed with ether (30 mL x2). After heating the aqueous layer at 70 °C, an aqueous KPF₆ solution (100 mg in 5 mL H₂O) was added. A yellow precipitate formed immediately and the suspension was placed in an ice bath for 2 hours. The suspension was filtered, washed with H₂O (5 mL) and ether (5 mL). The pure product *rac*-[Ir(dFppy)₂(bpy-1)][PF₆] was obtained as a yellow powder (0.23 g, 60 %) by recrystallization from acetonitrile (2 mL) and diethylether (20 mL).

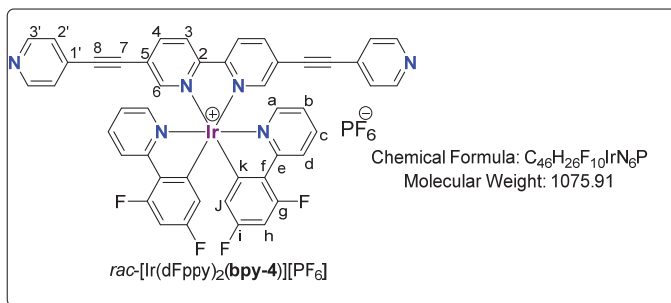
¹H NMR (CD₃CN, 300 MHz) δ (ppm): 8.43 (d, 2H, ³J_{H-H} = 8.6 Hz, H₃), 8.34-8.31 (m, 4H, H₄, H_{a/d}), 7.96-7.91 (m, 4H, H₆ and H_{b/c}), 7.67 (d, 2H, ³J_{H-H} = 5.7 Hz, H_{a/d}), 7.11 (ddd, 2H, ³J_{H-H} = 7.5 Hz, ³J = 5.8 Hz, ⁴J_{H-H} = 1.3 Hz, H_{b/c}), 6.71 (ddd, 2H, ³J_{H-F} = 12.4 Hz, ³J_{H-F} = 9.0 Hz, ⁴J_{H-H} = 2.5 Hz, H_h), 5.68 (dd, 2H, ³J_{H-F} = 8.8 Hz, ⁴J_{H-H} = 2.3 Hz, H_j).

¹⁹F NMR (CD₃CN, 282 MHz) δ (ppm): -73.9 (d, 6F, ¹J_{P-F} = 706.2 Hz, PF₆), -108.8 (d, 2F, ⁴J_{F-F} = 10.7 Hz), -110.7 (d, 2F, ⁴J_{F-F} = 10.7 Hz).

¹³C NMR (CD₃CN, 125 MHz) δ (ppm): 164.3 (dd, ¹J_{C-F} = 256.6 Hz, ²J_{C-F} = 13.3 Hz, C_{g/i}), 164.3 (d, ¹J_{C-F} = 7.0 Hz, C_{e/f}), 162.1 (dd, ¹J_{C-F} = 260.3 Hz, ²J_{C-F} = 12.7 Hz, C_{g/i}), 154.6 (C₅), 153.4 (d, ¹J_{C-F} = 6.7 Hz, C_{e/f}), 152.7 (C₆), 151.0 (C_{a/d}), 143.6 (C₄), 140.6 (C_{b/c}), 129.0 (C_k), 127.0 (C₃), 126.0 (C₂), 124.9 (C_{a/b/c/d}), 124.8 (C_{a/b/c/d}), 114.8 (dd, ³J_{C-F} = 18.1 Hz, ⁴J_{C-F} = 2.3 Hz, C_j), 100.1 (t, ³J_{C-F} = 26.8 Hz, C_h).

UV-Visible (CH₃CN): λ (nm), ε (10³ L.mol⁻¹.cm⁻¹) 244 (44.4), 266 (45.4), 314 (28.1), 328 (24.0), 364 (6.5).

HRMS (ESI⁺): calcd for [M-PF₆]⁺ C₃₂H₁₈Br₂F₄IrN₄ 884.9419, found 884.9308.



Compound *rac*-[Ir(dFppy)₂(bpy-4)][PF₆]:

To a solution of *rac*-[Ir(dFppy)₂(bpy-1)][PF₆] (0.108 g, 0.096 mmol) in a mixture of toluene/iPr₂NH/CH₃CN (20 mL/8 mL/1.5 mL) was added 4-ethynylpyridine (0.025 g, 0.24 mmol). After degassing the resulting yellow solution with argon, Pd(PPh₃)₄ (10 mg, 0.0086 mmol) and CuI (5 mg, 0.026 mmol) were added. The solution was heated at 70 °C overnight. Then the yellow mixture was filtered over a celite pad, washed with CH₂Cl₂ (5 mL x3) and concentrated to dryness. The yellow powder was purified by chromatography (Al₂O₃, MeOH/CH₂Cl₂ 0% to 2%) and recrystallized from

acetonitrile (2 mL) and diethylether (20 mL) to afford the product *rac*-[Ir(dFppy)₂(bpy-4)][PF₆] as an orange solid (0.055 g, 46%). Single crystals were obtained by vapor diffusion of Et₂O (15 mL) into an acetonitrile solution containing the desired product (5 mg in 1 mL).

¹H NMR (CD₃CN, 400 MHz) δ (ppm): 8.62 (dd, 4H, ³J_{H-H} = 4.4 Hz, ⁴J_{H-H} = 1.5 Hz, H_{3'}), 8.59 (d, 2H, ³J = 8.4 Hz, H₃), 8.36-8.30 (m, 4H, H₄, H_{a/d}), 8.11 (d, 2H, ⁴J = 1.7 Hz, H₆), 7.93 (ddd, 2H, ³J_{H-H} = 8.6 Hz, ³J_{H-H} = 7.3 Hz, ⁴J_{H-H} = 1.3 Hz, H_{b/c}), 7.71 (dd, 2H, ³J_{H-H} = 5.8 Hz, ⁴J_{H-H} = 0.9 Hz, H_{a/d}), 7.41 (dd, 4H, ³J_{H-H} = 4.4 Hz, ⁴J_{H-H} = 1.6 Hz, H_{2'}), 7.12 (ddd, 2H, ³J_{H-H} = 7.5 Hz, ³J_{H-H} = 5.9 Hz, ⁴J_{H-H} = 1.3 Hz, H_{b/c}), 6.71 (ddd, 2H, ³J_{H-F} = 12.6 Hz, ³J_{H-F} = 9.5 Hz, ⁴J_{H-H} = 2.4 Hz, H_b), 5.71 (dd, 2H, ³J_{H-F} = 8.7 Hz, ⁴J_{H-H} = 2.3 Hz, H_j).

¹⁹F NMR (CD₃CN, 282 MHz) δ (ppm): -72.91 (d, 6F, ¹J_{F-F} = 706.2 Hz, PF₆), -107.78 (d, 2F, ⁴J_{F-F} = 10.8 Hz), -109.75 (d, 2F, ⁴J_{F-F} = 10.28 Hz).

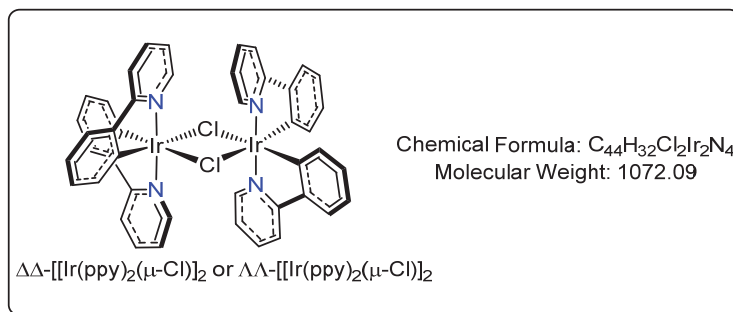
¹³C NMR (CD₃CN, 125 MHz) δ (ppm): 164.4 (dd, ¹J_{C-F} = 255.4 Hz, ³J_{C-F} = 12.5 Hz, C_i), 164.4 (d, ¹J_{C-F} = 6.9 Hz, C_{e/f}), 162.2 (dd, ¹J_{C-F} = 259.9 Hz, ³J_{C-F} = 12.7 Hz, C_g), 155.3 (C₅), 153.9 (C₆), 153.7 (d, ¹J_{C-F} = 6.0 Hz, C₂, C_{e/f}), 151.1 (C_{3'}), 150.9 (C_{a/d}), 143.2 (C₄), 140.6 (C_{b/c}), 130.0 (C_{1'}), 128.9 (C_k), 126.3 (C_{2'}), 126.2 (C₃), 125.1 (C₂), 124.9 (C_{a/b/c/d}), 124.8 (C_{a/b/c/d}), 114.7 (d, ³J_{C-F} = 17.8 Hz, C_j), 100.1 (d, ³J_{C-F} = 27.2 Hz, C_h), 94.6 (C₈), 88.3 (C₇).

UV-Visible (CH₃CN): λ (nm), ε (10³ L.mol⁻¹.cm⁻¹) 243 (49.8), 303 (37.5), 356 (42.4).

UV-Visible (THF): λ (nm), ε (10³ L.mol⁻¹.cm⁻¹) 362 (45.2).

HRMS (ESI⁺): calcd for [M-PF₆]⁺ C₄₆H₂₆F₄Ir₁N₆ 931.1782, found 931.1702.

Elem. Anal. Calcd for C₄₆H₂₆F₁₀IrN₆P·1.5H₂O: C, 50.09; H, 2.65; N, 7.62. Found: C, 50.10; H, 2.70; N, 7.47.



Compounds ΔΔ-[Ir(ppy)₂(μ-Cl)]₂ and ΛΛ-[Ir(ppy)₂(μ-Cl)]₂:⁷

The enantiopure iridium dimers ΔΔ-[Ir(ppy)₂(μ-Cl)]₂ and ΛΛ-[Ir(ppy)₂(μ-Cl)]₂ were obtained according to the procedure described by Lusby *et al.*⁷ with slight modifications. The crude products obtained after reaction of the racemic dimer with L- or D-serine respectively were purified by column chromatography (SiO₂) using a mixture of CH₂Cl₂/CH₃OH/NEt₃ as eluent with a gradient elution of 99:0:1 to 97:3:1 (instead of CH₂Cl₂/CH₃OH/NEt₃ 96:3:1 only). ΔΔ-[Ir(ppy)₂(μ-Cl)]₂ and ΛΛ-[Ir(ppy)₂(μ-Cl)]₂ were obtained as yellow solids (32 mg and 36 mg respectively) in 43 % and 48 % yields respectively (starting from 150 mg of *rac*-[Ir(ppy)₂(μ-Cl)]₂).

ΔΔ-[Ir(ppy)₂(μ-Cl)]₂ :

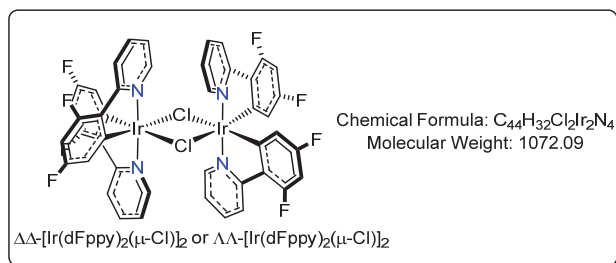
¹H and ¹³C NMR spectra were identical to *rac*-[Ir(ppy)₂(μ-Cl)]₂.

[α]_D²⁰ (c 0.052 g/100 mL in CH₂Cl₂): +433°.

ΛΛ-[Ir(ppy)₂(μ-Cl)]₂ :

¹H and ¹³C NMR spectra were identical to *rac*-[Ir(ppy)₂(μ-Cl)]₂.

[α]_D²⁰ (c 0.054 g/100 mL in CH₂Cl₂): -468°



Compounds $\Delta\Delta$ -[Ir(dFppy) $_2$ (μ -Cl)] $_2$ and $\Lambda\Lambda$ -[Ir(dFppy) $_2$ (μ -Cl)] $_2$:

The enantiopure iridium dimers $\Delta\Delta$ -[Ir(dFppy) $_2$ (μ -Cl)] $_2$ and $\Lambda\Lambda$ -[Ir(dFppy) $_2$ (μ -Cl)] $_2$ were obtained by adapting the procedure described by Lusby *et al.*⁷ for their non-fluorinated analogue with slight modifications. The crude products obtained after reaction of the racemic dimer with L- or D-serine respectively were purified by column chromatography (SiO $_2$) using a mixture of CH $_2$ Cl $_2$ /CH $_3$ OH/NEt $_3$ as eluent with a gradient elution of 99:0:1 to 97:3:1 (instead of CH $_2$ Cl $_2$ /CH $_3$ OH/NEt $_3$ 96:3:1 only). Starting from *rac*-[Ir(dFppy) $_2$ (μ -Cl)] $_2$ (150 mg, 0.123 mmol) and L- or D-serine respectively (26 mg, 0.246 mmol), the enantiopure dimers $\Delta\Delta$ -[Ir(dFppy) $_2$ (μ -Cl)] $_2$ and $\Lambda\Lambda$ -[Ir(dFppy) $_2$ (μ -Cl)] $_2$ were obtained as yellow solids (30 mg and 28 mg) in 40 % and 37 % yields respectively.

$\Delta\Delta$ -[Ir(dFppy) $_2$ (μ -Cl)] $_2$:

1H NMR, ^{13}C NMR and ^{19}F NMR spectra were identical to *rac*-[Ir(dFppy) $_2$ (μ -Cl)] $_2$.

$[\alpha]_D^{20}$ (0.063 g/100 mL, CH $_2$ Cl $_2$): +205°.

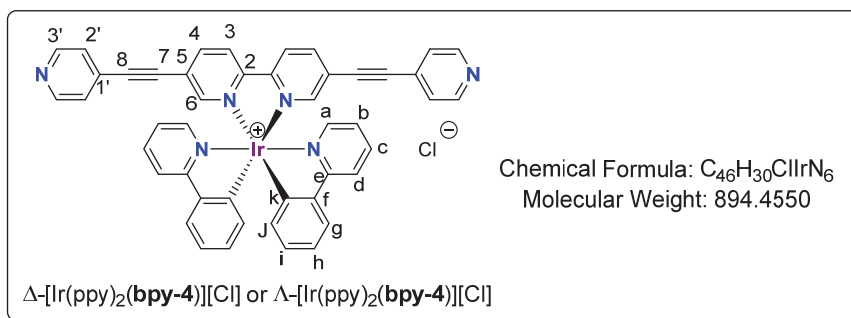
UV-Visible (CH $_2$ Cl $_2$): λ (nm), ϵ (10 3 L.mol $^{-1}$.cm $^{-1}$) 254 (73.2), 297 (29.9), 338 (12.7), 382 (6.7).

$\Lambda\Lambda$ -[Ir(dFppy) $_2$ (μ -Cl)] $_2$:

1H NMR, ^{13}C NMR and ^{19}F NMR spectra were identical to *rac*-[Ir(dFppy) $_2$ (μ -Cl)] $_2$.

$[\alpha]_D^{20}$ (0.060 g/100 mL, CH $_2$ Cl $_2$): -183°.

UV-Visible (CH $_2$ Cl $_2$): λ (nm), ϵ (10 3 L.mol $^{-1}$.cm $^{-1}$) 254 (70.9), 297 (28.7), 338 (12.5), 382 (6.5).



Compounds Δ - and Λ -[Ir(ppy) $_2$ (bpy-4)][Cl]:

The same procedure as the one followed for the racemic compound *rac*-[Ir(ppy) $_2$ (bpy-4)][Cl] was used for the synthesis of Δ - and Λ -[Ir(ppy) $_2$ (bpy-4)][Cl] complexes starting from the enantiopure Iridium dimers ($\Delta\Delta$ and $\Lambda\Lambda$ -[Ir(ppy) $_2$ (μ -Cl)] $_2$ respectively; 0.02g, 0.018 mmol). The enantiopure products Δ -[Ir(ppy) $_2$ (bpy-4)][Cl] (0.024 g, 74 %) and Λ -[Ir(ppy) $_2$ (bpy-4)][Cl] (0.025 g, 76 %) were obtained by recrystallization in acetonitrile (2 mL) and Et $_2$ O (20 mL). Single crystals suitable for X-ray diffraction were obtained by slow diffusion of toluene into a toluene/CH $_3$ CN 1/1 solution of the desired complex.

Δ -[Ir(ppy) $_2$ (bpy-4)][Cl]:

^1H NMR and ^{13}C NMR were identical to *rac*-[Ir(ppy)₂(bpy-4)][Cl].

$[\alpha]_{\text{D}}^{20}$ (c 0.047 g/100 mL in CH₃CN): -317°

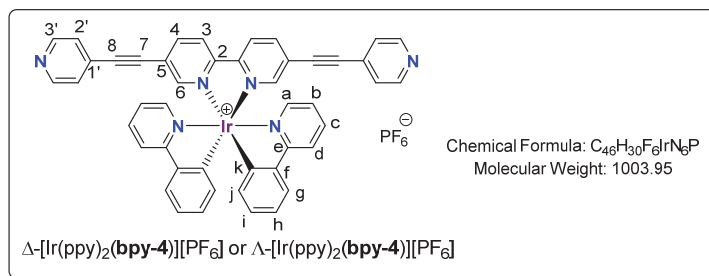
UV-Visible (CH₃CN): λ (nm), ϵ (10³ L.mol⁻¹.cm⁻¹) 256 (42.8), 301 (39.6), 359 (47.8).

Δ -[Ir(ppy)₂(1)][Cl]:

^1H NMR and ^{13}C NMR were identical to *rac*-[Ir(ppy)₂(bpy-4)][Cl].

$[\alpha]_{\text{D}}^{20}$ (c 0.048 g/100 mL in CH₃CN): +323°.

UV-Visible (CH₃CN): λ (nm), ϵ (10³ L.mol⁻¹.cm⁻¹) 256 (42.2), 301 (39.4), 359 (48.6).



Compounds Δ - and Λ -[Ir(ppy)₂(bpy-4)][PF₆] :

Syntheses of Δ - and Λ -[Ir(ppy)₂(bpy-4)][PF₆] complexes follow the same procedure as for the parent racemic complex *rac*-[Ir(ppy)₂(bpy-4)][PF₆] starting from the enantiopure Iridium dimers ($\Delta\Delta$ and $\Lambda\Lambda$ -[Ir(ppy)₂(μ -Cl)]₂ respectively). Red solids (60 mg for Δ -[Ir(ppy)₂(bpy-4)][PF₆] and 62 mg for Λ -[Ir(ppy)₂(bpy-4)][PF₆]) were obtained by recrystallization from acetonitrile (3 mL) and Et₂O (20 mL) in 80 % and 83 % yield respectively.

Δ -[Ir(ppy)₂(bpy-4)][PF₆]:

^1H NMR and ^{13}C NMR were identical to *rac*-[Ir(ppy)₂(bpy-4)][PF₆].

$[\alpha]_{\text{D}}^{20}$ (c 0.068 g/100 mL in CH₃CN): -299°.

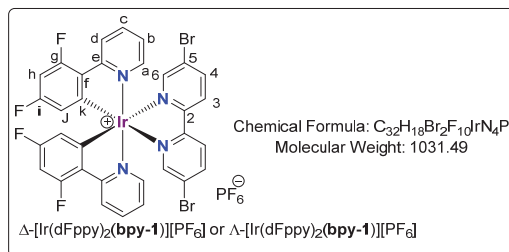
UV-Visible (CH₃CN) λ (nm), ϵ (10³ L.mol⁻¹.cm⁻¹) 256 (45.4), 301 (40.3), 359 (47.7).

Λ -[Ir(ppy)₂(bpy-4)][PF₆]:

^1H NMR and ^{13}C NMR were identical to *rac*-[Ir(ppy)₂(bpy-4)][PF₆].

$[\alpha]_{\text{D}}^{20}$ (c 0.064 g/100 mL in CH₃CN): +238°.

UV-Visible (CH₃CN) λ (nm), ϵ (10³ L.mol⁻¹.cm⁻¹) 256 (44.5), 301 (40.5), 359 (47.1).



Compounds Δ - and Λ -[Ir(dFppy)₂(bpy-1)][PF₆] :

Syntheses of Δ - and Λ -[Ir(dFppy)₂(bpy-1)][PF₆] complexes follow the same procedure as for the parent racemic complex starting from the enantiopure Iridium dimers ($\Delta\Delta$ and $\Lambda\Lambda$ -[Ir(dFppy)₂(μ -Cl)]₂ respectively). Yellow solids (31 mg for Δ -[Ir(dFppy)₂(bpy-1)][PF₆] and 28 mg for Λ -[Ir(dFppy)₂(bpy-1)][PF₆]) were obtained by recrystallization from acetonitrile (3 mL) and Et₂O (20 mL) in 60 % and 55 % yield respectively.

Δ -[Ir(dFppy)₂(bpy-1)][PF₆]:

Single crystals of Δ -[Ir(dFppy)₂(bpy-1)][PF₆] suitable for X-ray diffraction were obtained by slow diffusion of Et₂O into a CH₃CN solution of the desired complex.

¹H NMR, ¹⁹F NMR and ¹³C NMR were identical to *rac*-[Ir(dFppy)₂(bpy-1)][PF₆].

[α]_D²⁰ (0.047 g/100 mL, CH₃CN) -314°

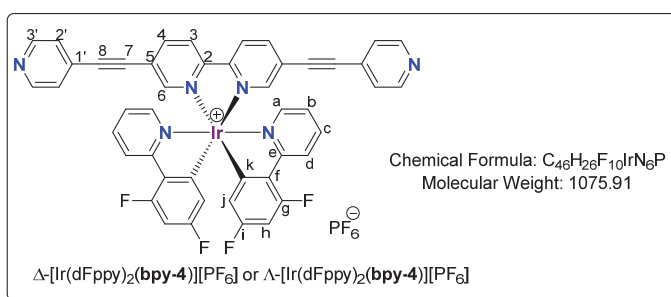
UV-Visible (CH₃CN): λ (nm), ϵ (10³ L.mol⁻¹.cm⁻¹) 244 (47.6), 266 (47.5), 314 (30.4), 328 (26.4), 364 (7.0)

Λ -[Ir(dFppy)₂(bpy-1)][PF₆]:

¹H NMR, ¹⁹F NMR and ¹³C NMR were identical to *rac*-[Ir(dFppy)₂(bpy-1)][PF₆].

[α]_D²⁰ (0.049 g/100 mL, CH₃CN) +311°

UV-Visible (CH₃CN): λ (nm), ϵ (10³ L.mol⁻¹.cm⁻¹) 244 (46.3), 266 (47.7), 314 (29.3), 328 (25.1), 364 (7.4)



Compounds Δ - and Λ -[Ir(dFppy)₂(bpy-4)][PF₆]:

The enantiopure Δ - and Λ -[Ir(dFppy)₂(bpy-4)][PF₆] complexes were obtained through a Sonogashira coupling reaction following the procedure described above for the racemic compound *rac*-[Ir(dFppy)₂(bpy-4)][PF₆] starting with Δ - and Λ -[Ir(dFppy)₂(bpy-1)][PF₆] (42 mg, 0.041 mmol and 45 mg, 0.041 mmol respectively) to afford yellow powders after recrystallization from acetonitrile/Et₂O in 46 % and 45 % yield respectively.

Δ -[Ir(dFppy)₂(bpy-4)][PF₆]:

¹H, ¹³C and ¹⁹F NMR spectra were identical to *rac*-[Ir(dFppy)₂(bpy-4)][PF₆].

[α]_D²⁰ (0.068 g/100 mL, CH₃CN): -209°.

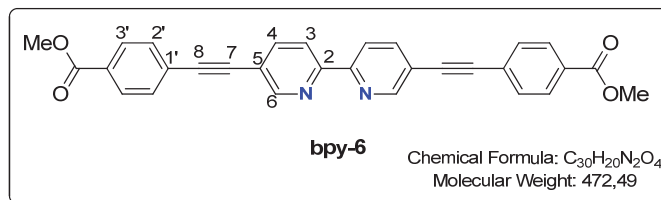
UV-Visible (CH₃CN): λ (nm), ϵ (10³ L.mol⁻¹.cm⁻¹) 243 (49.8), 303 (40.0), 356 (48.2).

Λ -[Ir(dFppy)₂(bpy-4)][PF₆]:

¹H, ¹³C and ¹⁹F NMR spectra were identical to *rac*-[Ir(dFppy)₂(bpy-4)][PF₆].

[α]_D²⁰ (20°C, 0.069 g/100 mL, CH₃CN): +213°.

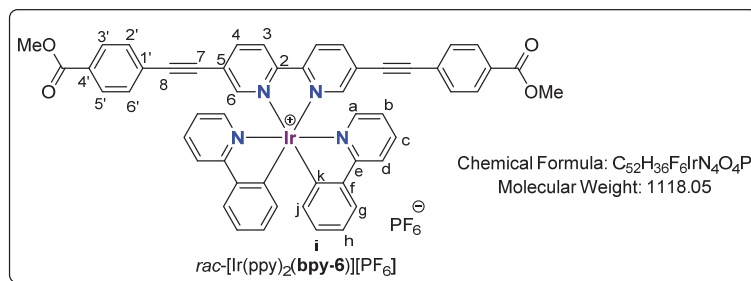
UV-Visible (CH₃CN): λ (nm), ϵ (10³ L.mol⁻¹.cm⁻¹) 243 (47.6), 303 (39.8), 356 (47.5).



Compound **bpy-6**:

To a solution of 5,5'-diethynyl-2,2'-bipyridine **bpy-3** (0.05 g, 0.24 mmol) in anhydrous toluene (8 mL), methyl 5-iodobenzoate (0.13 g, 0.52 mmol) and Pd(PPh₃)₄ (0.02 g, 0.015 mmol) were added. After degassing the yellow solution several times, diisopropylamine (3 mL) was added. The mixture was heated at 80 °C for two days. The dark red mixture was then filtered through a celite pad and the filtrate was evaporated. The crude product was purified by column chromatography (Al₂O₃, CH₂Cl₂/cyclohexane 0/100 to 60/40) to afford the product as a beige solid (0.025 g, 22 %).

¹H NMR (CDCl₃, 300 MHz) δ (ppm): 8.83 (d, 2H, J_d = 1.9 Hz, **H**₆), 8.47 (d, 2H, J_d = 8.2 Hz, **H**₃), 8.06 (d, 4H, J_d = 8.2 Hz, **H**₂), 7.97 (dd, 2H, J_d = 8.2 Hz, J_d = 1.9 Hz, **H**₄), 7.64 (dd, 4H, J_d = 8.2 Hz, **H**₃), 3.94 (s, 6H, 2Me).



Compound *rac*-[Ir(ppy)₂(**bpy-6**)]PF₆:

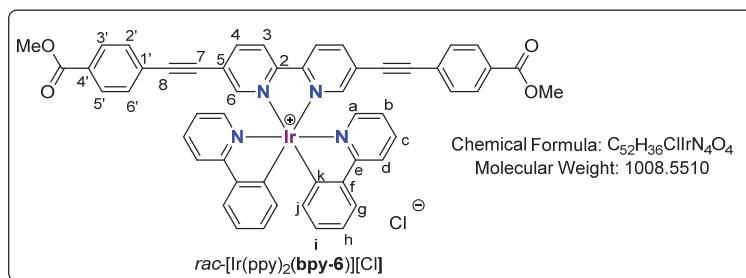
Path A: To a solution of *rac*-[Ir(ppy)₂Cl]₂ (0.01 g, 0.01 mmol) in a mixture of CH₂Cl₂/MeOH/CH₃CN (2 mL/2 mL/1 mL) was added ligand **bpy-6** (0.01 g, 0.021 mmol). The solution was degassed with argon several times and then heated at 60 °C overnight. After removal of solvents, acetonitrile (1 mL) and water (20 mL) were added. The mixture was washed with diethyl ether (20 mL x 2). The aqueous layer was then heated at 70 °C and a solution of KPF₆ (25 mg in 3 mL H₂O) was added dropwise to precipitate the red product. The pure red solid was recrystallized by slow vapour diffusion of diethyl ether into an acetonitrile solution containing the complex (15 mg, 67 %).

Path B: To a solution of *rac*-[Ir(ppy)₂(**bpy-1**)]PF₆ (0.150 g, 0.16 mmol) in a mixture of toluene/iPr₂NH/ACN (6 mL/6 mL/1 mL) was added methyl 4-ethynylbenzoate **5** (0.060 g, 0.38 mmol). The yellow solution was degassed with argon several times. Then, Pd(PPh₃)₄ (0.02g, 0.017 mmol) and CuI (0.01 mg, 0.052 mmol) were added. The resulting solution was heated at 60 °C overnight. The yellow mixture was then filtered over a celite pad that was washed with CH₂Cl₂ (5 mL x 3). The filtrate was evaporated and purified by chromatography (Al₂O₃, MeOH/CH₂Cl₂ 0 % to 2 %) to afford the product as a red solid (0.14 g, 83 %).

¹H NMR (CD₃CN, 400 MHz) δ (ppm): 8.54 (d, 2H, ³J = 8.4 Hz, **H**₃), 8.26 (dd, 2H, ³J = 8.4 Hz, ⁴J = 1.8 Hz, **H**₄), 8.08 (d, 2H, ³J = 8.1 Hz, **H**_d), 8.4 (d, 2H, ⁴J = 1.8 Hz, **H**₆), 8.01 (d, 4H, ³J = 8.4 Hz, **H**₃), 7.88 (ddd, 2H, ³J = 8.4 Hz, ³J = 8.4 Hz, ⁴J = 1.4 Hz, **H**_c), 7.83 (d, 2H, ³J = 7.8 Hz, **H**_g), 7.70 (d, 2H, ³J = 5.4 Hz, **H**_a), 7.58 (d, 4H, ³J = 8.4 Hz, **H**₂), 7.09-7.05 (m, 4H, **H**_b, **H**_h), 6.95 (ddd, 2H, ³J = 8.4 Hz, ³J = 8.4 Hz, ⁴J = 1.4 Hz, **H**_i), 6.27 (d, 2H, ³J = 7.0 Hz, **H**₁), 3.88 (s, 6H, 2OCH₃).

¹³C NMR (CD₃CN, 125 MHz) δ (ppm): 167.7 (C_e), 166.5 (COO), 154.9 (C₂), 153.0 (C₆), 150.2 (C_f), 149.7 (C_a), 144.6 (C_k), 142.0 (C₄), 139.3 (C_c), 132.4 (C₁), 132.0 (C₂, C₆), 131.7 (C_i), 131.1 (C_j), 130.1 (C₃, C₅), 126.1 (C_{3/g}), 125.6 (C₄), 125.5 (C_{g/3}), 124.8 (C₅), 124.2 (C_{b/h}), 123.4 (C_{h/b}), 120.6 (C_d), 96.0 (C₈), 86.9 (C₇), 52.6 (2OCH₃).

HRMS (ESI⁺): calcd for [M-PF₆]⁺ C₄₆H₂₆F₄IrN₆ 973.2364, found 973.2376.

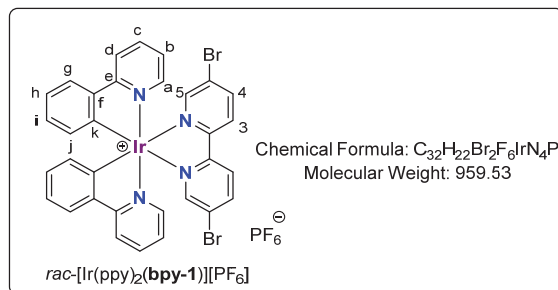


Compound *rac*-[Ir(ppy)₂(bpy-6)][Cl]:

To a solution of [Ir(ppy)₂(bpy-1)][Cl] (0.150 g, 0.16 mmol) in a mixture of toluene/*i*Pr₂NH/ACN (6 mL/6 mL/1 mL) was added methyl 4-ethynylbenzoate (0.060 g, 0.38 mmol). The yellow solution was degassed with argon several times. Pd(PPh₃)₄ (0.02g, 0.017 mmol) and CuI (0.01 mg, 0.052 mmol) were then added. The solution was heated at 60 °C overnight. The resulting yellow mixture was filtered over a celite pad that was washed with CH₂Cl₂ (5 mL x 3). The filtrate was concentrated to dryness and purified by chromatography (Al₂O₃, MeOH/CH₂Cl₂ 0 % to 2 %) to afford the product as a red solid (0.11 g, 63 %).

¹H NMR (CD₃CN, 400 MHz) δ (ppm): 8.54 (d, 2H, ³J = 8.4 Hz, H₃), 8.26 (dd, 2H, ³J = 8.4 Hz, ⁴J = 1.8 Hz, H₄), 8.08 (d, 2H, ³J = 8.1 Hz, H_d), 8.4 (d, 2H, ⁴J = 1.8 Hz, H₆), 8.01 (d, 4H, ³J = 8.4 Hz, H_{3'}), 7.88 (ddd, 2H, ³J = 8.4 Hz, ³J = 8.4 Hz, ⁴J = 1.4 Hz, H_c), 7.83 (d, 2H, ³J = 7.8 Hz, H_g), 7.70 (d, 2H, ³J = 5.4 Hz, H_a), 7.58 (d, 4H, ³J = 8.4 Hz, H_{2'}), 7.09-7.05 (m, 4H, H_b, H_h), 6.95 (ddd, 2H, ³J = 8.4 Hz, ³J = 8.4 Hz, ⁴J = 1.4 Hz, H_i), 6.27 (d, 2H, ³J = 7.0 Hz, H_j), 3.88 (s, 6H, 2OCH₃).

¹³C NMR (CD₃CN, 125 MHz) δ (ppm): 167.7 (C_e), 166.5 (COO), 154.9 (C₂), 153.0 (C₆), 150.2 (C_f), 149.7 (C_a), 144.6 (C_k), 142.0 (C₄), 139.3 (C_c), 132.4 (C_{1'}), 132.0 (C_{2'}, C_{6'}), 131.7 (C_i), 131.1 (C_j), 130.1 (C_{3'}, C_{5'}), 126.1 (C_{3/g}), 125.6 (C_{4'}), 125.5 (C_{g/3}), 124.8 (C₅), 124.2 (C_{b/h}), 123.4 (C_{h/b}), 120.6 (C_d), 96.0 (C₈), 86.9 (C₇), 52.6 (2OCH₃).



Compound *rac*-[Ir(ppy)₂(bpy-1)][PF₆]:⁸

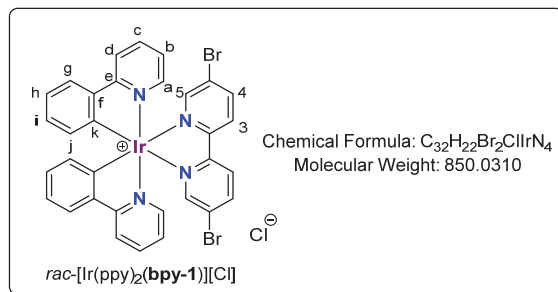
rac-[Ir(ppy)₂(μ-Cl)]₂ (0.05 g, 0.047 mmol) was dissolved into a 1/1 MeOH/DCM mixture (3 mL /3 mL). Then, 5,5'-dibromo-2,2'-bipyridine **bpy-1** (0.034 g, 0.10 mmol) was added. The yellow solution was heated at 60 °C overnight. Distilled water (50 mL) was then added and the resulting solution was washed with diethyl ether (30 mL x2). The aqueous layer was heated to 70 °C and a solution of KPF₆ (100 mg in 5 mL distilled water) was added. A yellow precipitate formed immediately. The aqueous solution was cooled using an ice bath for 2 hours, then filtered and washed with water (2 mL x3) and ether (2 mL x3). The product was obtained as an orange powder (0.075 g, 83%) by recrystallization in acetonitrile and diethyl ether.

¹H NMR (CD₃CN, 300 MHz) δ (ppm): 8.18 (d, 2H, J_d = 8.6 Hz, H₃), 8.07 (dd, 2H, J_d = 8.6 Hz, J_d = 1.6 Hz, H₄), 7.85 (d, 2H, J_d = 8.1 Hz, H_d), 7.70 (d, 2H, J_d = 2.0 Hz, H₆), 7.65 (ddd, 2H, J_d = 8.0 Hz, J_d = 8.0 Hz, J_d = 1.3 Hz, H_c), 7.60 (dd, 2H, J_d = 8.0 Hz, J_d = 1.0 Hz, H_g), 7.44 (d, 2H, J_d = 6.5 Hz, H_a), 6.81-6.88 (m, 4H, H_b, H_h), 6.71 (ddd, 2H, J_d = 7.5 Hz, J_d = 7.5 Hz, J_d = 1.3 Hz, H_i), 6.02 (dd, 2H, J_d = 7.5 Hz, J_d = 0.8 Hz, H_j).

¹³C NMR (CD₃CN, 125MHz) δ (ppm): 168.3 (C^{IV}_{ar}, C_e), 155.3 (C^{IV}_{ar}, C₂), 152.8 (C_{ar}, C₆), 151.0 (C_{ar}, C_a), 150.1 (C_{ar}, C_f), 145.4 (C^{IV}_{ar}, C_k), 143.3 (C_{ar}, C₄), 140.1 (C_{ar}, C_c), 132.8 (C_{ar}, C_j), 131.8 (C_{ar}, C_i), 127.3 (C_{ar}, C₅), 126.3 (C_{ar}, C_{3/g}), 126.1 (C^{IV}_{ar}, C_{g/3}), 125.0 (C_{ar}, C_{b/h}), 124.3 (C_{ar}, C_{h/b}), 121.4 (C_{ar}, C_d).

MS (ESI⁺): calcd for M⁺ (M = C₃₂H₂₂Br₂IrN₄) 812.98, found 812.98

UV-Visible (CH₂Cl₂): λ (nm), ε (10³ L.mol⁻¹.cm⁻¹) 268 (48.4), 288 (38.9), 331 (24.0), 380 (7.0), 401 (5.8).

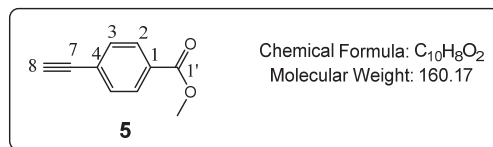


Compound *rac*-[Ir(ppy)₂(bpy-1)][Cl]:

rac-[Ir(ppy)₂(μ-Cl)]₂ (0.15 g, 0.14 mmol) was dissolved in a mixture of methanol/DCM (12 mL/12 mL), then 5,5'-dibromo-2,2'-dipyridine (0.90 g, 0.29 mmol) was added. The yellow solution was heated at 60 °C overnight. After cooling to RT, the solution was evaporated to dryness and acetonitrile (1.5 mL) was added. The mixture was filtered and washed with acetonitrile (1 mL x 2). The complex was obtained as an orange powder (0.22 g, 94%) after slow diffusion of diethyl ether into the filtrate.

¹H NMR (CD₃CN, 300 MHz) δ (ppm): 8.19 (d, 2H, J_d = 8.6 Hz, H₃), 8.07 (dd, 2H, J_d = 8.6 Hz, J_d = 1.6 Hz, H₄), 7.85 (d, 2H, J_d = 8.1 Hz, H₄), 7.70 (d, 2H, J_d = 2.0 Hz, H₆), 7.65 (ddd, 2H, J_d = 8.0 Hz, J_d = 8.0 Hz, J_d = 1.3 Hz, H_c), 7.60 (dd, 2H, J_d = 8.0 Hz, J_d = 1.0 Hz, H_g), 7.44 (d, 2H, J_d = 6.5 Hz, H_a), 6.81-6.88 (m, 4H, H_b, H_h), 6.71 (ddd, 2H, J_d = 7.5 Hz, J_d = 7.5 Hz, J_d = 1.3 Hz, H_i), 6.02 (dd, 2H, J_d = 7.5 Hz, J_d = 0.8 Hz, H_j).

¹³C NMR (CD₃CN, 125MHz) δ (ppm): 168.3 (C^{IV}_{ar}, C_e), 155.3 (C^{IV}_{ar}, C₂), 152.8 (C_{ar}, C₆), 151.0 (C_{ar}, C_a), 150.1 (C_{ar}, C_f), 145.4 (C^{IV}_{ar}, C_k), 143.3 (C_{ar}, C₄), 140.1 (C_{ar}, C_c), 132.8 (C_{ar}, C_j), 131.8 (C_{ar}, C_i), 127.3 (C_{ar}, C₅), 126.3 (C_{ar}, C_{3/g}), 126.1 (C^{IV}_{ar}, C_{g/3}), 125.0 (C_{ar}, C_{b/h}), 124.3 (C_{ar}, C_{h/b}), 121.4 (C_{ar}, C_d).



Compound **5**.⁹

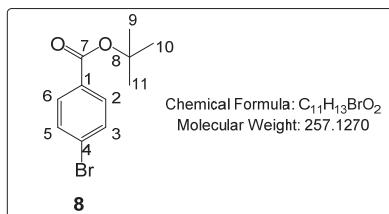
Methyl 4-iodobenzoate (0.5 g, 1.90 mmol) was dissolved into a mixture of THF/iPr₂NH 2/1 ((24 mL/12 mL). The resulting mixture was degassed with argon several times before ethynyltrimethylsilane (0.35 mL, 2.47 mmol), Pd(PPh₃)₄ (10 mg, 0.0086 mmol) and CuI (5 mg, 0.026 mmol) were added. The mixture was heated at 60 °C overnight. After removal of the solvents, the crude mixture was purified by chromatography (silica gel, Cylohexane/CH₂Cl₂ 40 %). The TMS protected product obtained was then dissolved in anhydrous methanol (20 mL) and K₂CO₃ (500 mg) was added. The mixture was stirred at room temperature for 3 h. Distilled water (60 mL) was added and the resulting solution was washed with dichloromethane (60 mL x 2). The combined organic layers were dried over MgSO₄, filtered over a silica gel pad using dichloromethane as eluent to afford the pure product as white solid (0.26 g, 85 %).

^1H NMR (CDCl_3 , 500 MHz) δ (ppm): 7.99 (dd, 2H, $^3J = 6.7$ Hz, $^4J = 1.7$ Hz, H_2), 7.55 (dd, 2H, $^3J = 6.7$ Hz, $^4J = 1.7$ Hz, H_3), 3.92 (s, 3H, CH_3), 3.23 (s, 1H, H_8).

^{13}C NMR (CDCl_3 , 125 MHz) δ (ppm): 166.5 ($\text{C}_{1'}$), 132.1 (C_2), 130.2 (C_1), 129.5 (C_4), 126.8 (C_3), 82.8 ($\text{C}_{7/8}$), 80.1 ($\text{C}_{8/7}$), 52.3 (CH_3).

IR: ν cm^{-1} 2221, 1579, 1539, 1469, 1489, 1407, 1216, 1106, 827, 815, 760, 709, 547, 520, 466.

Elem. Anal. Calcd for $\text{C}_{10}\text{H}_8\text{O}_2$: C, 74.99; H, 5.03; Found: C, 74.80; H, 5.02.



Compound **8** (*tert*-butyl 4-bromobenzoate):¹⁰

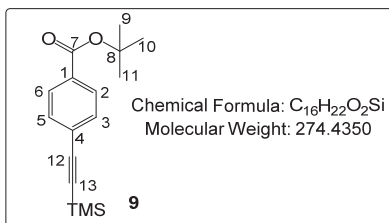
To a solution of 4-bromobenzoyl chloride (2.0 g, 9.1 mmol) in anhydrous CH_2Cl_2 (10 mL), was added dropwise a solution of *tert*-butanol (1.4 g, 18.9 mmol) and pyridine (1.5 mL, 19.0 mmol) in anhydrous CH_2Cl_2 (18 mL). The mixture was stirred at room temperature under argon for 2 days. Then CH_2Cl_2 (30 mL) was added and the resulting solution was washed with distilled water (50 mL x 2). The organic layer was dried over MgSO_4 , filtered and concentrated. Purification by chromatography (silica gel, Cyclohexane/ CH_2Cl_2 100/0 to 70/30) afforded compound **8** as a colorless oil (2.1 g, 90 %).

^1H NMR (CDCl_3 , 500 MHz) δ (ppm): 7.84 (d, 2H, $^3J = 8.5$ Hz, H_3, H_5), 7.54 (d, 2H, $^3J = 8.5$ Hz, H_2, H_6), 1.59 (s, 9H, tBu).

^{13}C NMR (CDCl_3 , 125 MHz) δ (ppm): 165.1 (C_7), 131.6 (C_2, C_6), 131.1 (C_3, C_5), 131.0 (C_4), 127.6 (C_1), 81.6 (C_8), 28.3 ($\text{C}_{11}, \text{C}_9, \text{C}_{10}$).

IR: ν cm^{-1} 2974 (Ar-H), 1711 ($\text{C}=\text{O}$ ester), 1588, 1479, 1395 (tBu), 1367 (tBu), 1291, 1255, 1161, 1114, 1102, 1069, 1011, 846 (*p*-Ar), 756, 682, 510 (C-Br).

Elem. Anal. Calcd for $\text{C}_{11}\text{H}_{13}\text{BrO}_2 + \text{H}_2\text{O}$: C, 46.50; H, 5.68 Found: C, 46.70; H, 5.42.



Compound **9**:¹⁰

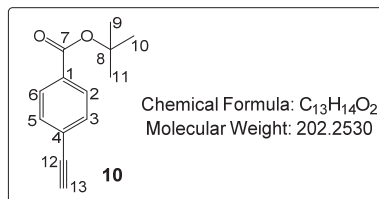
tert-butyl 4-bromobenzoate (1.8 g, 6.0 mmol) and ethynyltrimethylsilane (1.0 g, 10.0 mmol) were dissolved in anhydrous triethylamine (15 mL) and toluene (15 mL). The resulting solution was degassed with argon several times. $\text{Pd}(\text{PPh}_3)_4$ (10 mg, 0.0086 mmol) and CuI (10 mg, 0.051 mmol) were then added. The reaction mixture was heated at 100 $^\circ\text{C}$ overnight. After cooling to room temperature, the reaction mixture was diluted in CH_2Cl_2 (100 mL) and washed with distilled water (100 mL x3). The combined organic layers were dried over MgSO_4 , filtered, concentrated. Purification by chromatography (silica gel, cyclohexane/ CH_2Cl_2 100/0 to 70/30) afforded the compound as a light yellow oil (1.8 g, 93 %).

^1H NMR (CDCl_3 , 500 MHz) δ (ppm): 7.91 (d, 2H, $^3J = 8.4$ Hz, H_2, H_6), 7.48 (d, 2H, $^3J = 8.4$ Hz, H_3, H_5), 1.59 (s, 9H, tBu), 0.26 (s, 9H, TMS).

¹³C NMR (CDCl₃, 125 MHz) δ (ppm): 165.3 (C₇), 131.8 (C₅, C₃), 131.7 (C₄), 129.3 (C₆, C₂), 127.3 (C₁), 104.4 (C₁₂), 97.3 (C₁₃), 81.4 (C₈), 28.3 (C₉, C₁₀, C₁₁), 0.01 (Si (CH₃)₃).

IR: ν cm⁻¹ 2974 (Ar-H), 2162 (C≡C), 1713 (C=O ester), 1604, 1367 (tBu), 1306, 1292, 1281, 1249 (Si-CH₃), 1162, 1117, 1106, 1094, 1018, 839 (*p* Ar), 769, 694, 665, 540, 534. 453 Vibrations ?

Elem. Anal. Calcd for C₁₆H₂₂O₂Si: C, 70.03; H, 8.08 Found: C, 69.92; H, 7.95.



Compound **10** (*tert*-butyl 4-ethynylbenzoate):¹⁰

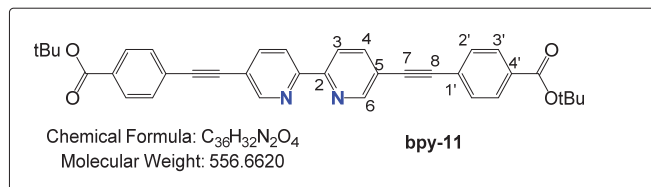
A solution of compound **9** (1.3 g, 4.74 mmol) in anhydrous CH₃OH (25 mL) containing 0.1 g of K₂CO₃ was stirred at room temperature under argon for 1 hour until no more starting material could be detected by TLC. The solution was then diluted with CH₂Cl₂ (100 mL), washed with water (100 mL x3) and dried over anhydrous Mg₂SO₄. After filtration and removal of the solvent, the residue was purified by chromatography (silica gel, cyclohexane/ CH₂Cl₂ 100/0 to 70/30) to give **10** as a white solid (0.9 g, 95 %).

¹H NMR (CDCl₃, 500 MHz) δ (ppm): 7.93 (d, 2H, ³J = 8.4 Hz, H₂, H₆), 7.52 (d, 2H, ³J = 8.4 Hz, H₃, H₅), 3.21 (s, H₁₃), 1.59 (s, 9H, tBu).

¹³C NMR (CDCl₃, 125 MHz) δ (ppm): 165.2 (C₇), 132.2 (C₄), 132.0 (C₅, C₃), 129.4 (C₆, C₂), 126.3 (C₁), 83.1 (C₁₂), 81.5 (C₈), 79.8 (C₁₃), 28.3 (C₉, C₁₀, C₁₁).

IR: ν cm⁻¹ 3254 (C≡C-H), 2982 (Ar-H), 1704 (C=O ester), 1606, 1367 (tBu), 1308, 1296, 1281, 1257, 1158, 1118, 1017, 850, 769 (*p* Ar), 698, 683, 529.

Elem. Anal. Calcd for C₁₃H₁₄O₂: C, 77.20; H, 6.98; Found: C, 76.80; H, 6.93.



Compound **bpy-11**:

5,5'-dibromo-2,2'-bipyridine **bpy-1** (0.4 g, 1.27 mmol) and **10** (0.54 g, 2.67 mmol) were dissolved in a DMF/Toluene/*i*Pr₂NH mixture (20 mL/15 mL/15 mL). After degassing the solution with argon, Pd(PPh₃)₄ (50 mg, 0.043 mmol) and CuI (20 mg, 0.1 mmol) were added. The mixture was heated at 80 °C overnight. After removal of the solvent, the crude product was purified by chromatography (Al₂O₃, cyclohexane/dichloromethane 100/0 to 60/40). The light brown solid obtained (0.48 g) was recrystallized in dichloromethane/cyclohexane (4 mL / 20 mL) to afford the pure product as a white solid (0.41 g, 67 %).

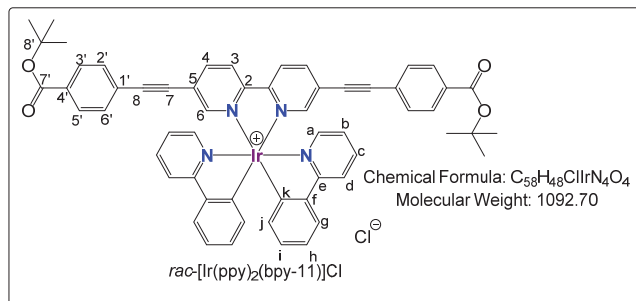
¹H NMR (CDCl₃, 500 MHz) δ (ppm): 8.83 (d, 2H, J_d = 1.9 Hz, H₆), 8.45 (d, 2H, J_d = 8.2 Hz, H₃), 7.99 (d, 4H, J_d = 8.2 Hz, H_{3'}), 7.95 (dd, 2H, J_d = 8.2 Hz, J_d = 1.9 Hz, H₄), 7.60 (dd, 4H, J_d = 8.2 Hz, H_{2'}), 1.61 (s, 18H, tBu).

¹³C NMR (CDCl₃, 125 MHz) δ (ppm): 165.2 (COO), 154.5 (C₂), 151.9 (C₆), 139.7 (C₄), 132.1 (C_{1'}), 131.6 (C_{2'}), 129.6 (C_{3'}), 126.7 (C_{4'}), 120.9 (C₃), 120.3 (C₅), 93.3 (C_{8/7}), 88.9 (C_{7/8}), 81.6 (tBu), 28.3 (tBu).

Elem. Anal. Calcd for C₃₂H₂₃N₂O₃+0.75H₂O: C, 77.32; H, 4.97; N, 5.64 Found: C, 77.18; H, 5.02; N, 5.59.

IR: ν cm⁻¹ 2965 (Ar-H), 1706 (C=O ester), 1607, 1584, 1457, 1366 (tBu), 1309, 1294, 1282, 1256, 1168, 1146, 1116, 1019, 854, 840, 768 (p Ar), 736, 694.

UV-Visible (CH₂Cl₂): λ (nm), ϵ (10³ L.mol⁻¹.cm⁻¹) 352 (74.3).



Compound *rac*-[Ir(ppy)₂(bpy-11)][Cl]:

Path A: To a solution of *rac*-[Ir(ppy)₂(μ-Cl)]₂ (0.20 g, 0.187 mmol) in a mixture of CH₂Cl₂/MeOH/CH₃CN (15 mL/15 mL/5 mL) was added ligand **5** (0.21 g, 0.434 mmol, 2.3eq). After degassing the solution with argon several times, it was heated at 60 °C overnight. After removal of the solvents, acetonitrile (5 mL) was added and the mixture was filtered. The pure product was obtained as red solid (0.38 g, 93 %) after recrystallization by slow vapour diffusion of diethyl ether into an acetonitrile solution containing the complex.

Path B: To a solution of *rac*-[Ir(ppy)₂(bpy-1)][Cl] (0.050 g, 0.059 mmol) in a mixture of toluene/iPr₂NH/ACN (6 mL/6 mL/1 mL) was added ligand **5** (0.025 g, 0.012 mmol). After degassing the yellow solution with argon several times, Pd(PPh₃)₄ (0.01g, 0.0086 mmol) and CuI (5 mg, 0.026 mmol) were added. The solution was then heated at 80 °C overnight. The resulting yellow mixture was filtered over a celite pad that was washed with CH₂Cl₂ (5 mL x3). The filtrate was evaporated and after purification by chromatography (Al₂O₃, CH₂Cl₂/MeOH 0 % to 2 %) the product was obtained as a red solid (0.040 g, 68 %).

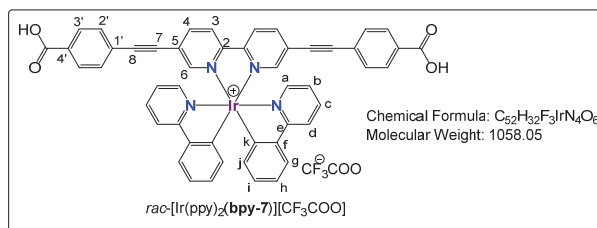
¹H NMR (CDCl₃, 300 MHz) δ (ppm): 9.57 (d, 2H, ³J = 8.5 Hz, H₃), 8.33 (dd, 2H, ³J = 8.5 Hz, ⁴J = 1.9 Hz, H₄), 7.98-7.95 (m, 8H, H_{3'}, H_{5'}, H₆, H_d), 7.81 (ddd, 2H, ⁴J = 7.4 Hz, H_c), 7.72 (d, 2H, ³J = 7.0 Hz, H_g), 7.56 (d, 2H, ³J = 7.4 Hz, H_a), 7.49 (d, 4H, ³J = 8.5 Hz, H_{2'}, H_{6'}), 7.10-7.05 (m, 4H, H_b, H_h), 6.95 (ddd, 2H, ³J = 7.4 Hz, H_i), 6.29 (d, 2H, ³J = 7.4 Hz, H_j), 1.59 (s, 18H, tBu).

¹³C NMR (CDCl₃, 125 MHz) δ (ppm): 167.9 (C_e), 164.9 (COO), 154.2 (C₂), 152.0 (C₆), 149.4 (C_f), 148.7 (C_a), 143.4 (C_k), 142.5 (C₄), 138.4 (C_c), 132.9 (C_{1'}), 131.9 (C_{2'}, C_{6'}), 131.8 (C_i), 131.2 (C_j), 129.6 (C_{3'}, C_{5'}), 127.5 (C_{3/g}), 125.3 (C_{4'}), 125.2 (C_{g/3}), 124.6 (C₅), 123.6 (C_{h/b}), 123.1 (C_{b/h}), 120.0 (C_d), 96.9 (C₈), 86.5 (C_{7/8}), 81.8 (C_{8/7}), 28.3 (tBu).

MS (ESI⁺): calcd for [M-Cl]⁺ C₅₇H₄₆IrN₃O₄⁺ 1057.32, found 1057.33.

UV-Visible (CH₂Cl₂): λ (nm), ϵ (10³ L.mol⁻¹.cm⁻¹) 255 (64.0), 295 (41.2), 320 (34.0), 380 (60.6).

UV-Visible (THF): λ (nm), ϵ (10³ L.mol⁻¹.cm⁻¹) 260 (59.3), 297 (43.3), 373 (62.0).



Compound *rac*-[Ir(ppy)₂(bpy-7)][CF₃COO]:

To a solution of *rac*-[Ir(ppy)₂(bpy-11)][Cl] (0.10 g, 0.092 mmol) in distilled CH₂Cl₂ (8 mL) was added trifluoroacetic acid (2 mL). The resulting mixture was stirred at RT for 1 hour and then concentrated to dryness to afford the pure product as a red solid (0.096 g, quantitative).

¹H NMR (DMSO-D₆, 500 MHz) δ (ppm): 9.01 (d, 2H, ³J = 8.5 Hz, H₃), 8.52 (dd, 2H, ³J = 8.5 Hz, ⁴J = 1.8 Hz, H₄), 8.29 (d, 2H, ³J = 8.5 Hz, H_d), 7.99-7.94 (m, 8H, H_{3'}, H_{5'}, H_c, H_g), 7.88 (d, 2H, ⁴J = 1.9 Hz, H₆), 7.83 (d, 2H, ³J = 7.5 Hz, H_a), 7.62 (d, 4H, ³J = 8.5 Hz, H_{2'}, H_{6'}), 7.18 (ddd, 2H, ³J = 7.5 Hz, H_b), 7.06 (ddd, ³J = 7.5 Hz, 4H, H_h), 6.95 (ddd, 2H, ³J = 7.4 Hz, H_i), 6.20 (d, 2H, ³J = 7.4 Hz, H_j).

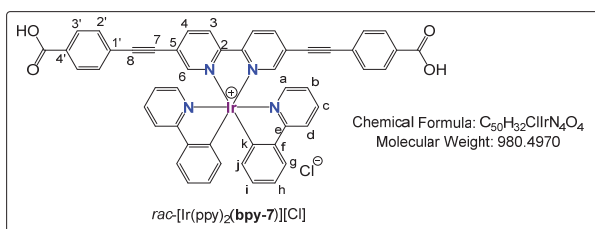
¹³C NMR (DMSO-D₆, 125 MHz) δ (ppm): 206.8 (CF₃COO), 166.5 (C_e/COO), 166.4 (COO/C_e), 158.3 (CF₃), 154.2 (C₂), 151.4 (C₆), 149.7 (C_a), 149.3 (C_f), 143.8 (C_k), 142.0 (C₄), 139.0 (C_c), 132.0 (C_{2'}, C_{6'}), 131.7 (C_{1'}), 131.1 (C_i), 130.4 (C_j), 129.7 (C_{3'}, C_{5'}), 125.6 (C_{3/g}), 125.2 (C_{g/3}), 124.7 (C_{4'}), 124.2 (C_b), 123.4 (C₅), 122.6 (C_h), 120.2 (C_d), 95.5 (C₈), 86.7 (C₇).

¹⁹F NMR (DMSO-D₆, 282 MHz) δ (ppm): -75.7 (CF₃COO).

HRMS (ESI⁺): calcd for [M-CF₃COO]⁺ C₅₀H₃₂IrN₄O₄⁺ 945.2051, found 945.2108

UV-Visible (DMSO): λ (nm), ε (10³ L.mol⁻¹.cm⁻¹) 269 (106.2), 372 (56.5).

UV-Visible (THF): λ (nm), ε (10³ L.mol⁻¹.cm⁻¹) 258 (58.2), 304 (40.9), 371 (59.0).



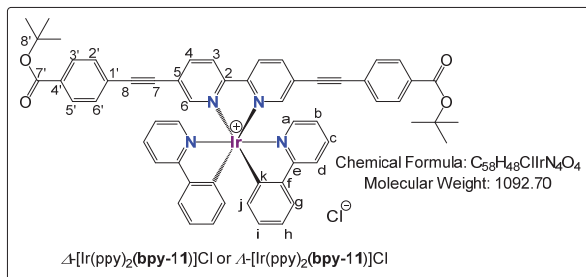
Compound *rac*-[Ir(ppy)₂(bpy-7)][Cl]:

To a solution of *rac*-[Ir(ppy)₂(bpy-11)][Cl] (0.20 g, 0.183 mmol) in 1,4-dioxane (40 mL) was added dropwise a solution of HCl (15 mL, 37 % aq) in 1,4-dioxane (15 mL) under argon. The resulting mixture was stirred at RT for 6 h until no more red precipitate was present. The reaction mixture was then concentrated to 20 mL and water (50 mL) was added. After filtration, the red precipitate was washed with distilled water (5 mL x3) and 1,4-dioxane (5 mL x3) and then dried under vacuum to afford the pure product as a red solid (0.15 g, 83 %).

¹H NMR (DMSO-D₆, 500 MHz) δ (ppm): 9.02 (d, 2H, ³J = 8.5 Hz, H₃), 8.51 (dd, 2H, ³J = 8.5 Hz, ⁴J = 1.8 Hz, H₄), 8.29 (d, 2H, ³J = 8.5 Hz, H_d), 7.99-7.94 (m, 8H, H_{3'}, H_{5'}, H_c, H_g), 7.88 (d, 2H, ⁴J = 1.9 Hz, H₆), 7.83 (d, 2H, ³J = 7.5 Hz, H_a), 7.62 (d, 4H, ³J = 8.5 Hz, H_{2'}, H_{6'}), 7.18 (ddd, 2H, ³J = 7.5 Hz, H_b), 7.06 (ddd, ³J = 7.5 Hz, 4H, H_h), 6.95 (ddd, 2H, ³J = 7.4 Hz, H_i), 6.20 (d, 2H, ³J = 7.4 Hz, H_j).

¹³C NMR (DMSO-D₆, 125 MHz) δ (ppm): 166.5 (C_e/COO), 166.4 (COO/C_e), 154.2 (C₂), 151.3 (C₆), 149.7 (C_a), 149.3 (C_f), 143.8 (C_k), 142.0 (C₄), 139.0 (C_c), 131.9 (C_{2'}, C_{6'}), 131.7 (C_{1'}), 131.1 (C_i), 130.4 (C_j), 129.7 (C_{3'}, C_{5'}), 125.6 (C_{3/g}), 125.2 (C_{g/3}), 124.7 (C_{4'}), 124.2 (C_b), 123.4 (C₅), 122.6 (C_h), 120.2 (C_d), 95.5 (C₈), 86.7 (C₇).

UV-Visible (THF): λ (nm), ε (10³ L.mol⁻¹.cm⁻¹) 258 (52.1), 305 (37.4), 371(50.9).



Δ -[Ir(ppy)₂(bpy-11)][Cl]:

Enantiopure Δ - and Λ -[Ir(ppy)₂(bpy-11)][Cl] complexes were obtained following the same procedure (path B) described above for the racemic compound *rac*-[Ir(ppy)₂(bpy-11)][Cl] starting with the enantiopure Iridium dimers ($\Delta\Delta$ and $\Lambda\Lambda$ -[Ir(ppy)₂(μ -Cl)]₂ respectively) (50 mg, 0.047 mmol and 40 mg, 0.037 mmol respectively) to afford red powders after recrystallization in acetonitrile/Et₂O (1 mL/20 mL) in 80 % and 75 % yield respectively.

Δ -[Ir(ppy)₂(bpy-11)][Cl]:

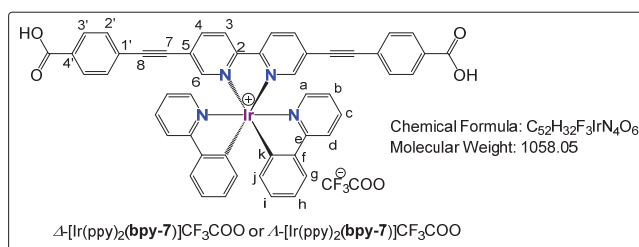
¹H NMR and ¹³C NMR were identical to *rac*-[Ir(ppy)₂(bpy-11)][Cl].

[α]_D²⁰ (0.064 g/100 mL, CH₃CN) -277°

Λ -[Ir(ppy)₂(bpy-11)][Cl]:

¹H NMR and ¹³C NMR were identical to *rac*-[Ir(ppy)₂(bpy-11)][Cl].

[α]_D²⁰ (0.066 g/100 mL, CH₃CN) -280°



Enantiopure Δ - and Λ -[Ir(ppy)₂(bpy-7)][CF₃COO] complexes were obtained following the same procedure (path B) described above for the racemic compound *rac*-[Ir(ppy)₂(bpy-7)][CF₃COO] starting with the enantiopure Iridium complexes (Δ and Λ -[Ir(ppy)₂(bpy-11)][Cl] respectively) (20 mg, 0.018 mmol for both experiments) to afford red powders quantitatively.

Δ -[Ir(ppy)₂(bpy-7)][CF₃COO]:

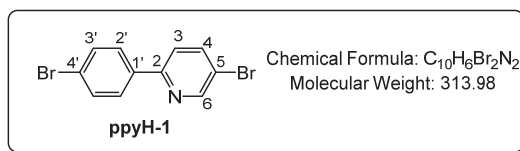
¹H NMR and ¹³C NMR ¹⁹F NMR were identical to *rac*-[Ir(ppy)₂(bpy-7)][CF₃COO].

[α]_D²⁰ (0.068 g/100 mL, DMSO) -254°

Λ -[Ir(ppy)₂(bpy-7)][CF₃COO]:

¹H NMR and ¹³C NMR ¹⁹F NMR were identical to *rac*-[Ir(ppy)₂(bpy-7)][CF₃COO].

[α]_D²⁰ (0.068 g/100 mL, DMSO) +257°



Compound ppyH-1:¹¹

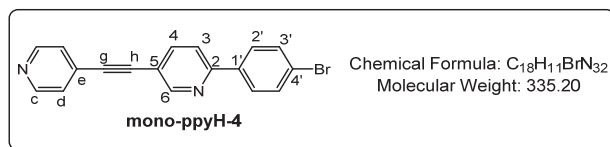
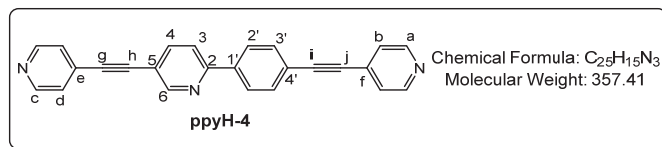
Under argon, in a three-necked round bottom flask containing 2,5- dibromopyridine (1.00 g, 4.22 mmol) and 4-bromophenylboronic acid (0.77 g, 3.84 mmol), were added toluene (45 mL), ethanol (15 mL), Pd(PPh₃)₄ (0.10 g, 0.086 mmol) and an aqueous saturated K₂CO₃ solution (15 mL). After refluxing for 2 days, the two organic and aqueous layers were separated and the organic layer was evaporated to dryness. Chromatography of the resulting residue (silica gel, cyclohexane/dichloromethane 100/0 to 50/50) afforded a white solid that was recrystallized in ethanol (20 mL) to afford colorless crystals as pure product (1.20 g, 80 %).

¹H NMR (CDCl₃, 500 MHz) δ (ppm): 8.7 (d, 1H, ⁴J = 2.3 Hz, H₆), 7.85 (dd, 1H, ³J = 8.5 Hz, ⁴J = 2.3Hz, H₄), 7.82 (d, ³J = 8.5 Hz, 2H, H₂), 7.59-7.57 (m, 3H, H₃, H₃).

^{13}C NMR (CDCl_3 , 125 MHz) δ (ppm): 154.7 (C_2), 150.9 (C_6), 139.5 (C_4), 137.1 ($\text{C}_{1'}$), 132.1 ($\text{C}_{3'}$), 128.3 ($\text{C}_{2'}$), 123.9 ($\text{C}_{4'}$), 121.4 (C_3), 119.7 (C_5).

IR: ν cm^{-1} 2918 (Ar-H), 1586 ($\text{C}=\text{N}$), 1575, 1462, 1452, 1398, 1361, 1095, 1072, 1001, 812, 745, 686, 638, 541($\text{C}-\text{Br}$), 462.

Elem. Anal. Calcd for $\text{C}_{10}\text{H}_6\text{Br}_2\text{N}_2$: C, 42.21; H, 2.25; N, 4.48 Found: C, 42.31; H, 2.12; N, 4.35.



Compounds ppyH-4 and mono-ppyH-4:

To a degassed solution of ppyH-1 (0.30 g, 0.958 mmol) in anhydrous toluene (24 mL) under argon, was added $\text{Pd}(\text{PPh}_3)_4$ (0.030 g, 0.026 mmol) and CuI (0.010 g, 0.052 mmol). Then 4-ethynylpyridine (0.22 g, 2.133 mmol) and diisopropylamine (9 mL) were added. After heating at 80 $^\circ\text{C}$ for 2 days, the reaction mixture was extracted and the organic layer was evaporated to dryness. The crude product was purified by chromatography (Al_2O_3 , $\text{CH}_3\text{OH}/\text{CH}_2\text{Cl}_2$ 0 % to 0.5 %). The first fraction obtained as a white solid was mono-ppyH-4 (0.08 g, 25 %) while the second fraction also obtained as a white solid was pure ligand ppyH-4 (0.15 g, 44 %).

For compound mono-ppyH-4:

^1H NMR (CDCl_3 , 400 MHz) δ (ppm): 8.83 (d, 1H, $^4J = 1.9$ Hz, H_6), 8.64 (dd, 2H, $^3J = 8.4$ Hz, $^4J = 1.9$ Hz, H_c), 7.93-7.88 (m, 3H, $\text{H}_{2'}$, H_4), 7.73 (d, 1H, $^3J = 8.4$ Hz, H_3), 7.61 (d, 1H, $^3J = 8.1$ Hz, H_3), 7.41 (d, 1H, $^3J = 8.1$ Hz, H_d).

^{13}C NMR (CDCl_3 , 125 MHz) δ (ppm): 155.8 (C_2), 152.4 (C_6), 149.9 (C_c), 139.6 (C_4), 137.2 ($\text{C}_{1'}$), 132.1 ($\text{C}_{3'}$), 130.7 (C_e), 128.5 ($\text{C}_{2'}$), 125.5 (C_d), 124.2 ($\text{C}_{4'}$), 119.5 (C_3), 117.9 (C_5), 90.6, 90.4 (C_g , C_h).

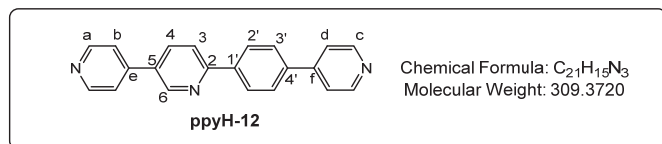
For compound ppyH-4 :

^1H NMR (CDCl_3 , 500 MHz) δ (ppm): 8.85 (d, 1H, $^4J = 1.9$ Hz, H_6), 8.65-8.62 (m, 4H, H_a , H_c), 8.06 (d, 2H, $^3J = 8.4$ Hz, $\text{H}_{2'}$), 7.90 (dd, 1H, $^3J = 8.1$ Hz, $^4J = 2.0$ Hz, H_4), 7.78 (d, 1H, $^3J = 8.1$ Hz, H_3), 7.67 (d, 2H, $^3J = 8.4$ Hz, $\text{H}_{3'}$), 8.42-8.39 (m, 4H, H_d , H_b).

^{13}C NMR (CDCl_3 , 125 MHz) δ (ppm): 155.7 (C_2), 152.5 (C_6), 149.9, 149.8 (C_a , C_c), 139.6 (C_4), 138.9 ($\text{C}_{1'}$), 132.6 ($\text{C}_{3'}$), 131.3, 130.7 (C_e , C_f), 127.0 ($\text{C}_{2'}$), 125.6, 125.5 (C_b , C_d), 123.3 ($\text{C}_{4'}$), 119.9 (C_3), 118.0 (C_5), 93.7 (C_i), 90.6, 90.5, 88.3 (C_g , C_h , C_j).

IR: ν cm^{-1} 2221, 1579, 1539, 1469, 1489, 1407, 1216, 1106, 827, 815, 760, 709, 547, 520, 466.

Elem. Anal. Calcd for $\text{C}_{25}\text{H}_{15}\text{N}_3 \cdot 0.25\text{H}_2\text{O}$: C, 82.97; H, 4.32; N, 11.61. Found: C, 83.18; H, 4.16; N, 11.60.

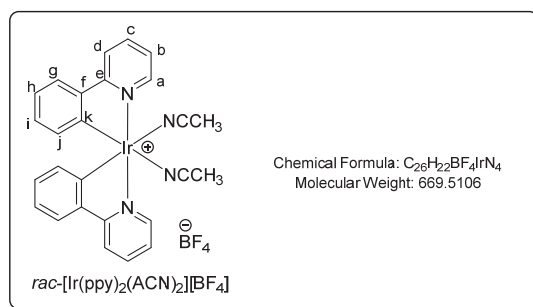


Compound ppyH-12:

To a solution of ligand **ppyH-1** (0.40 g, 1.27 mmol) and 4-pyridylboronic acid (0.35 g, 2.80 mmol) in toluene (21 mL) and ethanol (7 mL) under argon, was added Pd(PPh₃)₄ (0.10 g, 0.0086 mmol) and an aqueous saturated K₂CO₃ solution (7 mL). After refluxing for 2 days, the layers were separated and the organic layer was evaporated to dryness. Chromatography of the resulting residue (silica gel, CH₃OH/CH₂Cl₂ 0 % to 0.5 %) afforded a beige solid that was recrystallized using dichloromethane (5 mL) and cyclohexane (20 mL) to obtain a white solid as pure **ppyH-12** (0.39 g, 60 %).

¹H NMR (DMSO-D₆, 500 MHz) δ (ppm): 9.17 (d, 1H, ⁴J = 1.6 Hz, H₆), 8.71 (dd, 2H, ³J = 8.5 Hz, ⁴J = 1.6 Hz, H_{a/c}), 8.68 (dd, 2H, ³J = 8.5 Hz, ⁴J = 1.6 Hz, H_{c/a}), 8.39-8.33 (m, 3H, H_{2'}, H₄), 8.23 (d, 1H, ³J = 8.5 Hz, H₃), 7.99 (d, 1H, ³J = 8.5 Hz, H_{3'}), 7.88 (dd, 2H, ³J = 8.5 Hz, ⁴J = 1.6 Hz, H_{b/d}), 7.81 (dd, 4H, 2H, ³J = 8.4 Hz, ⁴J = 1.6 Hz, H_{d/b}).

¹³C NMR (DMSO-D₆, 125 MHz) δ (ppm): 156.1 (C₂), 150.9, 150.8 (C_a, C_c), 148.4 (C₆), 146.7 (C_{e/f}), 144.3 (C_{f/c}), 139.1 (C_{1'/4'}), 138.4 (C_{4'/1'}), 136.1 (C₄), 132.1 (C₅), 127.9, 127.8 (C_{2'}, C_{3'}), 121.7 (C_b, C_d), 121.1 (C₃)



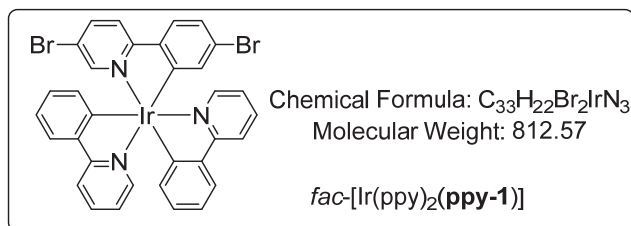
Compound *rac*-[Ir(ppy)₂(ACN)₂][BF₄]:¹²

To a degassed yellow solution of *rac*-[Ir(ppy)₂(μ-Cl)]₂ (0.50 g, 0.46 mmol) in acetonitrile (100 mL) was added a solution of AgBF₄ (0.20 g, 1.03 mmol) in acetonitrile (30 mL). The resulting mixture was protected from light and heated at 60 °C for 2 hours. After cooling at RT, the suspension was filtered over a celite pad. The resulting powder was washed several times with acetonitrile (*ca.* 10 mL) until the filtrate was colourless. The filtrate was then concentrated to dryness. The pure product was obtained quantitatively by precipitation with acetonitrile (3 mL) and ether (50 mL).

¹H NMR (CD₂Cl₂, 500 MHz) δ (ppm): 9.02 (d, 2H, J_t = 6.0 Hz, J_d = 1.0 Hz, H_a), 8.04-8.02 (m, 4H, H_c, H_d), 7.70 (dd, 4H, J_t = 7.6 Hz, J_d = 1.2 Hz, H_g), 7.48 (dt, 2H, J_t = 5.7 Hz, J_d = 3.6 Hz, H_b), 6.97 (ddd, 2H, J_t = 7.6 Hz, J_t = 7.6 Hz, J_d = 1.2 Hz, H_i), 6.84 (ddd, 4H, J_d = 7.6 Hz, J_d = 7.6 Hz, J_d = 1.2 Hz, H_h), 6.08 (d, 2H, J_t = 6.0 Hz, J_d = 1.0 Hz, H_j), 2.34 (s, 6H, 2CH₃CN).

¹³C NMR (CD₃Cl₂, 125 MHz) δ (ppm): 166.1 (C^{IV}_{ar}, C_e), 151.1 (C_{ar}, C_a), 144.7 (C^{IV}_{ar}, C_f), 141.5 (C^{IV}_{ar}, C_k), 138.9 (C_{ar}, C_j), 130.3 (C_{ar}, C_c), 128.5 (C_{ar}, C_b), 124.9 (C_{ar}, C_d), 124.1 (C_{ar}, C_i), 123.5 (C_{ar}, C_g), 120.0 (C_{ar}, C_h), 119.3 (CN), 3.6 (CH₃).

Elem. Anal. Calcd for C₂₆H₂₃BF₄N₄·0.5H₂O: C, 46.96; H, 3.56; N, 8.25 Found: C, 47.18; H, 3.54; N, 8.29.



Compound *fac*-Ir(ppy)₂(ppy-1):

[Ir(ppy)₂(ACN)₂][BF₄] (0.50 g, 0.75 mmol) and **ppyH-1** (0.40 g, 1.27 mmol) were suspended in ethoxyethanol (12 mL) and propane-1,2-diol (12 mL). Under argon, the mixture was protected from light and stirred at 120 °C for 36 hours. After cooling, ethyl acetate (100 mL) was added and the organic layer was washed with brine (100 mL) and water (100 mL). The organic layer was then dried over MgSO₄, filtered and evaporated. The crude product was purified by chromatography (Al₂O₃, cyclohexane/DCM 0 % to 50 %). The yellow solid obtained was recrystallized from dichloromethane (5 mL) and cyclohexane (40 mL) to afford the pure product as yellow solid (0.34 g, 45 %).

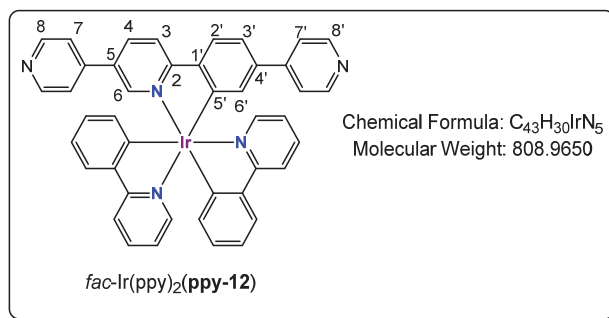
¹H NMR (CDCl₃, 400 MHz) δ (ppm): 7.92-7.88 (m, 2H), 7.72-7.62 (m, 6H), 7.52 (d, 1H, J_d = 1.3 Hz), 7.48-7.44 (m, 3H), 7.05 (dd, 1H, J_d = 8.4 Hz, J_d = 1.2 Hz), 6.93-6.82 (m, 8H), 6.76 (dd, 1H, J_d = 7.5 Hz, J_d = 1.0 Hz, H_d).

¹H NMR (DMSO-D₆, 500 MHz) δ (ppm): 8.19-8.15 (m, 3H), 8.06 (dd, 1H, J_d = 8.5 Hz, J_d = 1.8 Hz), 7.86-7.82 (m, 2H), 7.79 (d, 1H, J_d = 7.6 Hz), 7.76 (d, 1H, J_d = 8.5 Hz), 7.60 (d, 1H, J_d = 5.3 Hz), 7.47 (d, 1H, J_d = 5.3 Hz), 7.40 (d, 1H, J_d = 1.8 Hz), 7.19-7.16 (m, 2H), 6.70 (dd, 1H, J_d = 8.5 Hz, J_d = 1.8 Hz), 6.87-6.83 (m, 2H), 6.77-6.71 (m, 2H), 6.69 (d, 1H, J_d = 1.8 Hz), 6.59-6.57 (m, 2H).

¹³C NMR (DMSO-D₆, 125 MHz) δ (ppm): 165.4 (C^{IV}_{ar}), 165.1 (C^{IV}_{ar}), 164.7 (C^{IV}_{ar}), 163.7 (C^{IV}_{ar}), 159.2 (C^{IV}_{ar}), 158.3 (C^{IV}_{ar}), 147.5 (C_{ar}), 147.0 (C_{ar}), 146.9 (C_{ar}), 143.8 (C^{IV}_{ar}), 143.7 (C^{IV}_{ar}), 142.3 (C^{IV}_{ar}), 139.8 (C_{ar}), 137.8 (C_{ar}), 137.5 (2C, C_{ar}), 136.1 (2C, C_{ar}), 129.6 (C_{ar}), 129.4 (C_{ar}), 126.8 (C_{ar}), 124.6 (C^{IV}_{ar}), 124.5 (C_{ar}, 2C), 123.3 (C_{ar}), 123.1 (C_{ar}), 122.6 (C_{ar}), 121.0 (C_{ar}), 120.3 (C_{ar}, 2C), 119.4 (2C, C_{ar}), 117.6 (C, C^{IV}_{ar}).

UV-Visible (CH₂Cl₂): λ (nm), ε (10³ L.mol⁻¹.cm⁻¹) 244 (47.8), 283 (48.6), 378 (12.9).

HRMS (ESI⁺): calcd for [M+Na]⁺ C₃₃H₂₂Br₂IrN₃Na⁺ 835.9675, found 835.9618.



Compound *fac*-Ir(ppy)₂(ppy-12):

To a degassed suspension of *fac*-Ir(ppy)₂(ppy-1) (0.18 g, 0.22 mmol) in a mixture of toluene/EtOH/aq K₂CO₃ (2M) (20 mL/8 mL/8 mL) was added Pd(PPh₃)₄ (20 mg, 0.017 mmol). The reaction mixture was refluxed overnight. After cooling to RT, the mixture was concentrated to about 5 mL, and dichloromethane (30 mL) was added. The organic layer was washed with distilled water (30 mL x3). The combined organic layers were dried over MgSO₄, filtered and concentrated to dryness. The crude product was purified by chromatography (Al₂O₃, dichloromethane/cyclohexane 50/50 to 100/0). The solid was then recrystallized from dichloromethane (2 mL) and cyclohexane (20 mL) to afford an orange solid (0.135 g, 75 %).

¹H NMR (CDCl₃, 500 MHz) δ (ppm): 8.58 (dd, 2H, ³J = 4.5 Hz, ⁴J = 1.5 Hz, H₈), 8.50 (dd, 2H, ³J = 4.4 Hz, ⁴J = 1.5 Hz, H₈), 7.98 (d, 1H, ³J = 8.4 Hz, H₂), 7.94 (d, 1H, ³J = 8.4 Hz), 7.91 (d, 1H, ³J = 8.4 Hz), 7.82 (dd, 1H, ⁴J = 8.4 Hz, ⁴J = 2.2 Hz, H₃), 7.79 (d, 1H, ⁴J = 2.2 Hz, H₅), 7.77 (d, 1H, ³J = 8.4 Hz, H₂), 7.70-7.58 (m, 6H), 7.29 (dd, 2H, ³J = 4.5 Hz, ⁴J = 1.5 Hz, H₇), 7.24 (dd, 1H, ³J = 8.4 Hz, ⁴J = 1.5 Hz, H₃), 7.21 (d, 1H, ⁴J = 1.5 Hz, H₅), 7.12 (dd, 2H, ³J = 8.4 Hz, ⁴J = 1.4 Hz, H₇), 6.97-6.85 (m, 8H, ³J = 7.0 Hz).

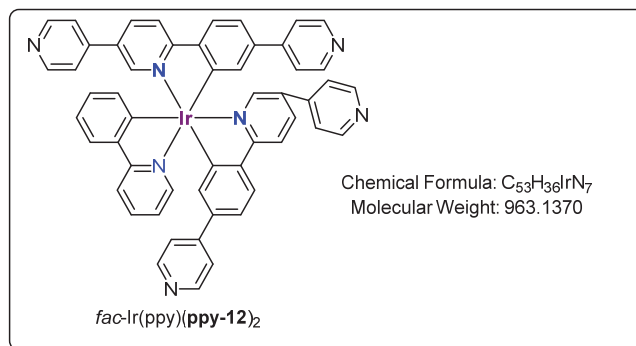
¹³C NMR (CDCl₃, 125 MHz) δ (ppm): 166.8 (2C, C^{IV}_{ar}), 166.6 (C^{IV}_{ar}), 163.2 (C^{IV}_{ar}), 160.5 (C^{IV}_{ar}), 159.8 (C^{IV}_{ar}), 150.6 (2C, C_{ar}), 149.9 (2C, C_{ar}), 148.8 (C^{IV}_{ar}), 147.2 (C_{ar}), 147.0 (C_{ar}), 145.1 (C_{ar}), 144.2 (C^{IV}_{ar}), 143.6 (C^{IV}_{ar}), 143.5 (C^{IV}_{ar}), 138.6 (C^{IV}_{ar}), 137.3 (C_{ar}), 137.1 (C_{ar}), 136.4 (C_{ar}), 136.3 (C_{ar}), 135.2 (C_{ar}), 134.3 (C_{ar}), 131.9 (C^{IV}_{ar}), 130.2 (C_{ar}), 130.1 (C_{ar}), 125.0 (C_{ar}).

124.1(C_{ar}), 124.0 (C_{ar}), 122.2 (C_{ar}), 122.1 (C_{ar}), 121.6 (2C, C_{ar}), 120.5 (2C, C_{ar}), 120.4 (C_{ar}), 120.2 (C_{ar}), 119.2 (C_{ar}), 119.0 (2C, C_{ar}), 118.9 (C_{ar}).

HRMS (ESI⁺): calcd for [M+H]⁺ C₄₃H₃₁IrN₅⁺ 810.2206, found 810.2206.

UV-Visible (CH₂Cl₂): λ (nm), ε (10³ L.mol⁻¹.cm⁻¹) 286 (57.1), 327 (50.4), 483 (3.3).

UV-Visible (THF): λ (nm), ε (10³ L.mol⁻¹.cm⁻¹) 287 (68.4), 329 (57.9), 407 (15.1), 483 (3.7).



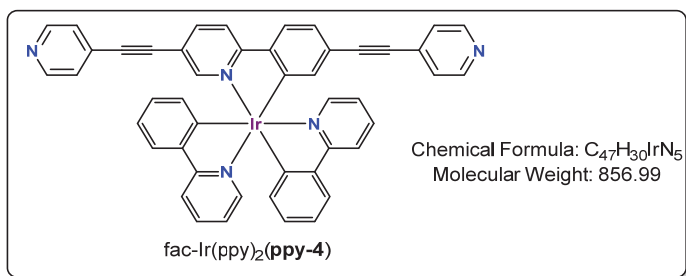
Compound *fac*-Ir(ppy)(ppy-12)₂:

In a microwave vial, [Ir(ppy)₂(ACN)₂][BF₄] (0.10 g, 0.15 mmol) and **ppyH-12** (0.08 g, 0.26 mmol) were suspended in ethoxyethanol (1.5 mL) and propane-1,2-diol (1.5 mL). After bubbling argon into the solution for 10 min, the vial was sealed and heated to 120 °C (120 W, 1 h). Ethyl acetate (20 mL) was added and the resulting mixture was washed with brine (20 mL) and water (20 mL). The organic layer was then dried over MgSO₄, filtered and concentrated to dryness. The crude product was purified by chromatography (Al₂O₃, Cyclohexane/CH₂Cl₂ 100/0 to 50/50) to afford a yellow powder (0.10 g) consisting in a mixture of different isomers including (*fac*-Ir(ppy)₂(ppy-12) and *fac*-Ir(ppy)(ppy-12)₂. The crude mixture was then suspended in a toluene/EtOH/aq K₂CO₃(2M) mixture of solvents (10 mL/4 mL/4 mL). After degassing with argon, Pd(PPh₃)₄ (15 mg, 0.013 mmol) was added. The reaction mixture was refluxed overnight. After cooling to RT, the mixture was concentrated to about 5 mL and dichloromethane (20 mL) was added. The organic layer was washed with distilled water (20 mL x3), dried over MgSO₄, filtered and concentrated to dryness. The crude product was purified by chromatography (Al₂O₃). The first orange eluting fraction obtained was *fac*-Ir(ppy)₂(ppy-12) (0.02 g, 17%) with a gradient eluent of cyclohexane/dichloromethane (50/50 to 0/100) while the second orange-to-red eluting fraction was obtained with 1% methanol in dichloromethane as eluent, the second fraction, *fac*-Ir(ppy)(ppy-12)₂ was recrystallized with dichloromethane (3 mL) and cyclohexane (15 mL) to afford the pure *fac*-Ir(ppy)(ppy-12)₂ as orange solid (0.04 g, 28%).

¹H NMR (CDCl₃, 500 MHz) δ (ppm): 8.60 (d, 2H, ³J = 4.5 Hz), 8.57 (d, 2H, ³J = 4.4 Hz), 8.52 (d, 2H, ³J = 8.4 Hz), 8.46 (d, 2H, ³J = 8.4 Hz), 8.06-8.10 (m, 2H), 7.99 (d, 1H, ⁴J = 8.4 Hz), 7.96 (dd, 1H, ⁴J = 2.2 Hz), 7.92 (dd, 1H, ³J = 8.4 Hz), 7.85-7.86 (m, 2H), 7.81-7.84 (m, 2H, ³J = 4.5 Hz, ⁴J = 1.5 Hz), 7.70-7.75 (m, 2H), 7.24-7.31 (m, 4H), 7.21 (d, 1H, ³J = 2.0 Hz), 7.13-7.15 (m, 4H, ³J = 7.0 Hz), 6.96-7.01 (m, 2H), 6.90-6.95 (m, 2H).

¹³C NMR (CDCl₃, 125 MHz) δ (ppm): 166.8 (C^{IV}_{ar}), 166.6 (C^{IV}_{ar}), 166.6 (C^{IV}_{ar}), 162.3 (C^{IV}_{ar}), 161.8 (C^{IV}_{ar}), 159.0 (C^{IV}_{ar}), 150.7 (2C, C_{ar}), 150.7 (2C, C_{ar}), 149.9 (2C, C_{ar}), 149.9 (2C, C_{ar}), 148.8 (C^{IV}_{ar}), 148.7 (C^{IV}_{ar}), 147.2 (C_{ar}), 145.2 (C_{ar}), 145.1 (C_{ar}), 144.1 (C^{IV}_{ar}), 144.1 (C^{IV}_{ar}), 143.8 (C^{IV}_{ar}), 143.6 (C^{IV}_{ar}), 143.5 (C^{IV}_{ar}), 140.0 (2C, C^{IV}_{ar}), 137.2 (C_{ar}), 136.7 (C_{ar}), 135.3 (C_{ar}), 135.2 (C_{ar}), 134.8 (C_{ar}), 134.7 (C_{ar}), 132.3 (2C, C^{IV}_{ar}), 130.5 (C_{ar}), 125.2 (C_{ar}), 125.2 (C_{ar}), 124.4 (C_{ar}), 122.4 (C_{ar}), 121.6 (2C, C_{ar}), 121.5 (2C, C_{ar}), 120.8 (C_{ar}), 120.6 (2C, C_{ar}), 120.5 (2C, C_{ar}), 119.5 (2C, C_{ar}), 119.4 (C_{ar}), 119.4 (C_{ar}), 119.3 (C_{ar}).

HRMS (ESI⁺): calcd for [M+H]⁺ C₅₃H₃₆IrN₇⁺ 964.2740, found 964.2747.



Compound **fac-Ir(ppy)₂(ppy-4)**:

fac-Ir(ppy)₂(ppy-1) (0.45 g, 0.055 mmol) and 4-ethynylpyridine (0.15 g, 0.145 mmol) were dissolved into a DMF/*i*Pr₂NH mixture (50 mL/18 mL). To the argon degassed solution, were added Pd(PPh₃)₄ (60 mg, 0.052 mmol) and CuI (50 mg, 0.26 mmol). The resulting mixture was heated at 80 °C overnight. After removal of the solvents, the crude product was purified by chromatography (Al₂O₃, cyclohexane/dichloromethane 100/0 to 0/100). Recrystallization from dichloromethane (5 mL) and cyclohexane (30 mL) afforded the pure product as a red solid (0.36 g, 76%).

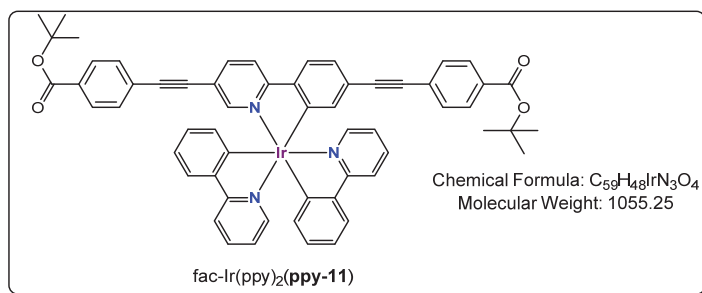
¹H NMR (CDCl₃, 300 MHz) δ (ppm): 8.56 (dd, 2H, ³J = 4.5 Hz, ⁴J = 1.5 Hz), 8.50 (dd, 2H, ³J = 4.4 Hz, ⁴J = 1.5 Hz), 7.92-7.87 (m, 3H), 7.72-7.58 (m, 7H), 7.54-7.51 (m, 2H), 7.28-7.25 (m, 4H), 7.11-7.06 (m, 2H), 6.95-6.76 (m, 8H).

¹³C NMR (CDCl₃, 125 MHz) δ (ppm): 166.7 (C^{IV}_{ar}), 166.6 (C^{IV}_{ar}), 166.1 (C^{IV}_{ar}), 162.7 (C^{IV}_{ar}), 160.0 (C^{IV}_{ar}), 159.3 (C^{IV}_{ar}), 150.2 (C_{ar}), 150.0 (2C, C_{ar}), 149.7 (2C, C_{ar}), 147.2 (C_{ar}), 147.1 (C_{ar}), 144.3 (C^{IV}_{ar}), 143.8 (C^{IV}_{ar}), 143.5 (C^{IV}_{ar}), 140.3 (C_{ar}), 139.1 (C_{ar}), 137.4 (C_{ar}), 136.9 (C_{ar}), 136.5 (2C, C_{ar}), 132.1 (C^{IV}_{ar}), 130.5 (C^{IV}_{ar}), 130.4 (C_{ar}), 130.2 (C_{ar}), 125.7 (2C, C_{ar}), 125.5 (2C, C_{ar}), 124.6 (C_{ar}), 124.3 (2C, C_{ar}), 124.2 (C_{ar}), 123.5 (C^{IV}_{ar}), 122.4 (C_{ar}), 122.1 (C_{ar}), 120.4 (2C, C_{ar}), 119.2 (2C, C_{ar}), 118.9 (C_{ar}), 117.6 (C^{IV}_{ar}), 96.1 (C≡C), 90.5 (C≡C), 90.1 (C≡C), 87.5 (C≡C).

HRMS (ESI⁺): calcd for [M]⁺ C₄₇H₃₀IrN₅⁺ 857.2128, found 857.2125.

UV-Visible (CH₂Cl₂): λ (nm), ε (10³ L.mol⁻¹.cm⁻¹) 283 (52.5), 348 (65.0), 433 (12.8), 521 (2.9).

UV-Visible (THF): λ (nm), ε (10³ L.mol⁻¹.cm⁻¹) 284 (59.4), 347(73.3), 432(14.9), 515 (3.8).



Compound **fac-Ir(ppy)₂(ppy-11)**:

To an argon degassed solution of *fac*-Ir(ppy)₂(ppy-1) (0.10 g, 0.120 mmol) and *tert*-butyl 4-ethynylbenzoate **10** (0.06 g, 0.296 mmol) in a DMF/*i*Pr₂NH mixture (30 mL/10 mL), were added Pd(PPh₃)₄ (20 mg, 0.017 mmol) and CuI (15 mg, 0.079 mmol) were added. The resulting mixture was heated at 80 °C overnight. After removal of the solvents, the crude product was purified by chromatography (Al₂O₃, cyclohexane/dichloromethane 100/0 to 0/100). Recrystallization from dichloromethane (2 mL) and cyclohexane (15 mL) afforded the pure product as a red solid (0.06 g, 60 %).

¹H NMR (CDCl₃, 500 MHz) δ (ppm): 7.93 (m, 7H), 7.71 (dd, 1H, J_d = 8.4 Hz, J_d = 1.4 Hz), 7.69-7.60 (m, 6H), 7.55-7.52 (m, 2H), 7.45 (d, 1H, J_d = 4.9 Hz), 7.44 (d, 1H, J_d = 4.9 Hz), 7.12 (dd,

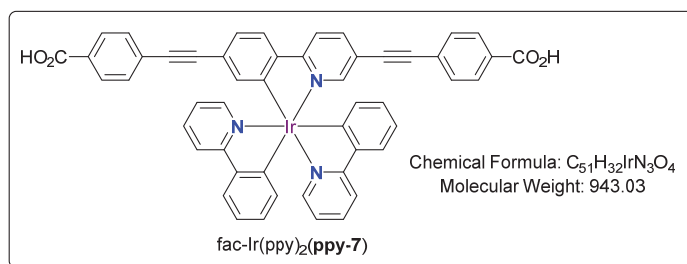
^1H NMR (CDCl_3 , 125 MHz) δ (ppm): 7.07 (d, 1H, $J_d = 1.4$ Hz), 6.95-6.84 (m, 7H), 6.80 (d, 1H, $J_d = 6.8$ Hz), 1.59 (s, 9H, tBu), 1.58 (s, 9H, tBu).

^{13}C NMR (CDCl_3 , 125 MHz) δ (ppm): 166.7 ($\text{C}^{\text{IV}}_{\text{ar}}$), 166.6 ($\text{C}^{\text{IV}}_{\text{ar}}$), 165.7 ($\text{C}^{\text{IV}}_{\text{ar}}$), 165.5 ($\text{C}^{\text{IV}}_{\text{ar}}$), 165.1 ($\text{C}^{\text{IV}}_{\text{ar}}$), 162.3 ($\text{C}^{\text{IV}}_{\text{ar}}$), 160.2 ($\text{C}^{\text{IV}}_{\text{ar}}$), 159.6 ($\text{C}^{\text{IV}}_{\text{ar}}$), 150.0 (C_{ar}), 147.3 (C_{ar}), 147.2 (C_{ar}), 144.0 ($\text{C}^{\text{IV}}_{\text{ar}}$), 143.8 ($\text{C}^{\text{IV}}_{\text{ar}}$), 143.5 ($\text{C}^{\text{IV}}_{\text{ar}}$), 140.1 (C_{ar}), 138.9 (C_{ar}), 137.5 (C_{ar}), 136.9 (C_{ar}), 136.4 (C_{ar}), 136.3 (C_{ar}), 132.1 ($\text{C}^{\text{IV}}_{\text{ar}}$), 131.5 (2C, C_{ar}), 131.4 (2C, C_{ar}), 131.0 ($\text{C}^{\text{IV}}_{\text{ar}}$), 130.3 (C_{ar}), 130.1 (C_{ar}), 129.5 (2C, C_{ar}), 129.3 (2C, C_{ar}), 128.1 ($\text{C}^{\text{IV}}_{\text{ar}}$), 126.5 ($\text{C}^{\text{IV}}_{\text{ar}}$), 124.4 (C_{ar}), 124.3 (C_{ar}), 124.2 (C_{ar}), 124.1 (C_{ar}), 124.0 ($\text{C}^{\text{IV}}_{\text{ar}}$), 122.3 (C_{ar}), 122.1 (C_{ar}), 120.4 (C_{ar}), 120.3 (C_{ar}), 119.2 (2C, C_{ar}), 118.8 (C_{ar}), 118.2 ($\text{C}^{\text{IV}}_{\text{ar}}$), 94.2 ($\text{C}\equiv\text{C}$), 92.7 ($\text{C}\equiv\text{C}$), 89.6 ($\text{C}\equiv\text{C}$), 88.3 ($\text{C}\equiv\text{C}$), 81.7 (tBu), 81.3 (tBu), 28.3 (2tBu).

HRMS (ESI^+): calcd for $[\text{M}]^+ \text{C}_{59}\text{H}_{48}\text{IrN}_3\text{O}_4^+$ 1055.3273, found 1055.3269.

UV-Visible (CH_2Cl_2): λ (nm), ϵ ($10^3 \text{ L}\cdot\text{mol}^{-1}\cdot\text{cm}^{-1}$) 280 (83.7), 357 (99.6), 373 (86.4), 432 (22.7), 515 (4.9).

UV-Visible (THF): λ (nm), ϵ ($10^3 \text{ L}\cdot\text{mol}^{-1}\cdot\text{cm}^{-1}$) 282 (70.7), 358 (97.8), 372 (sh86.8), 434 (20.5), 515 (sh4.6).



Compound *fac*-Ir(ppy) $_2$ (ppy-7):

To an argon degassed solution of *fac*-Ir(ppy) $_2$ (ppy-11) (0.10 g, 0.012 mmol) in THF (15 mL), grinded solid KOH (400 mg) was added. The reaction suspension was heated at 60 °C for 2 days until no starting material could be detected by TLC. After removal of the solvent, water (100 mL) was added and acidified with an aqueous 85wt % H_3PO_4 solution (*ca.* 2 mL) until pH = 2 was reached. The red precipitate was filtered and washed with distilled water (2 mL \times 3) and THF (1 mL \times 3). To recover the powder, it was dissolved in a minimum amount of DMF (*ca.* 3 mL) and concentrated to dryness to afford the pure product as a red solid (0.08 g, 89 %).

^1H NMR ($\text{DMSO}-d_6$, 500 MHz) δ (ppm): 8.30 (d, 1H), 8.19 (d, 1H), 8.02 (d, 1H), 7.95-7.80 (m, 10H), 7.63-7.52 (m, 7H), 7.19-7.16 (m, 2H), 7.07 (d, 1H), 6.95-6.80 (m, 3H), 6.76-6.73 (m, 2H), 6.64-6.60 (m, 2H).

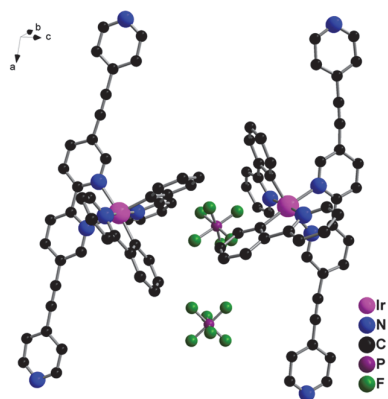
^{13}C NMR ($\text{DMSO}-d_6$, 125 MHz) δ (ppm): 167.2 ($\text{C}^{\text{IV}}_{\text{ar}}$), 167.1 ($\text{C}^{\text{IV}}_{\text{ar}}$), 165.8 ($\text{C}^{\text{IV}}_{\text{ar}}$), 165.6 ($\text{C}^{\text{IV}}_{\text{ar}}$), 165.3 ($\text{C}^{\text{IV}}_{\text{ar}}$), 162.8 ($\text{C}^{\text{IV}}_{\text{ar}}$), 160.0 ($\text{C}^{\text{IV}}_{\text{ar}}$), 159.4 ($\text{C}^{\text{IV}}_{\text{ar}}$), 149.4 (C_{ar}), 148.0 (C_{ar}), 147.4 (C_{ar}), 145.0 ($\text{C}^{\text{IV}}_{\text{ar}}$), 144.3 ($\text{C}^{\text{IV}}_{\text{ar}}$), 144.2 ($\text{C}^{\text{IV}}_{\text{ar}}$), 140.2 (C_{ar}), 139.1 (C_{ar}), 137.8 (C_{ar}), 137.8 (C_{ar}), 136.7 (C_{ar}), 136.5 (C_{ar}), 132.1 (2C, C_{ar}), 131.9 (2C, C_{ar}), 131.6 ($\text{C}^{\text{IV}}_{\text{ar}}$), 130.8 ($\text{C}^{\text{IV}}_{\text{ar}}$), 130.1 (2C, C_{ar}), 130.0 (2C, C_{ar}), 129.9 (C_{ar}), 129.8 (C_{ar}), 127.2 ($\text{C}^{\text{IV}}_{\text{ar}}$), 126.0 ($\text{C}^{\text{IV}}_{\text{ar}}$), 125.7 (C_{ar}), 125.2 ($\text{C}^{\text{IV}}_{\text{ar}}$), 124.9 (C_{ar}), 124.9 (C_{ar}), 124.1 (C_{ar}), 123.6 (2C, C_{ar}), 123.0 ($\text{C}^{\text{IV}}_{\text{ar}}$), 120.7 (C_{ar}), 120.6 (C_{ar}), 120.2 (C_{ar}), 119.9 (C_{ar}), 119.8 (C_{ar}), 118.1 ($\text{C}^{\text{IV}}_{\text{ar}}$), 94.2 ($\text{C}\equiv\text{C}$), 93.0 ($\text{C}\equiv\text{C}$), 89.7 ($\text{C}\equiv\text{C}$), 88.4 ($\text{C}\equiv\text{C}$).

UV-Visible (DMSO): λ (nm), ϵ ($10^3 \text{ L}\cdot\text{mol}^{-1}\cdot\text{cm}^{-1}$) 280 (66.3), 357 (85.5), 432 (18.0), 515 (sh4.0).

UV-Visible (THF): λ (nm), ϵ ($10^3 \text{ L}\cdot\text{mol}^{-1}\cdot\text{cm}^{-1}$) 280 (60.3), 355 (77.7), 427 (16.4), 515 (sh3.6).

HRMS (ESI^+): calcd for $[\text{M}]^+ \text{C}_{51}\text{H}_{32}\text{IrN}_3\text{O}_4^+$ 943.2026, found 943.2017.

3. Crystallization, crystallographic data, NMR data



Single crystal X-Ray diffraction data

rac-[Ir(ppy)₂(bpy-4)][PF₆]

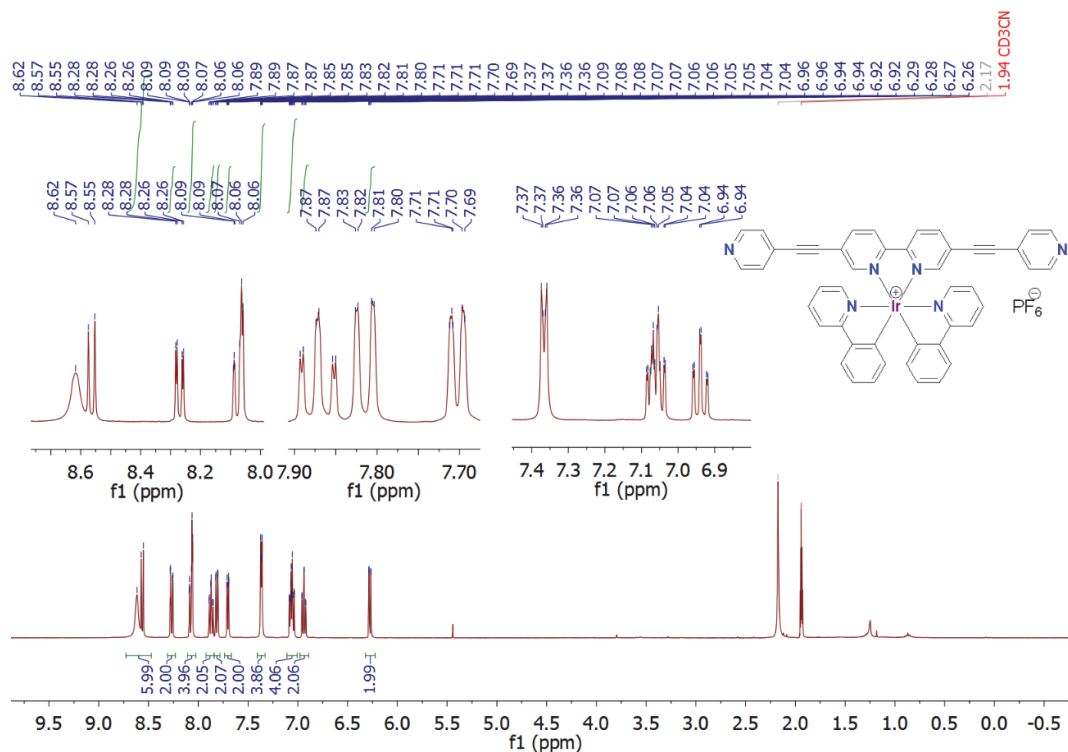
Crystallization Method: Diethyl ether vapor (*ca.* 30 mL) was slowly diffused into an acetonitrile solution of *rac*-[Ir(ppy)₂(bpy-4)][PF₆] (*ca.* 50 mg in 3 mL ACN). Red single crystals were obtained in a few days.

Crystallographic data (Lab code: s2726):

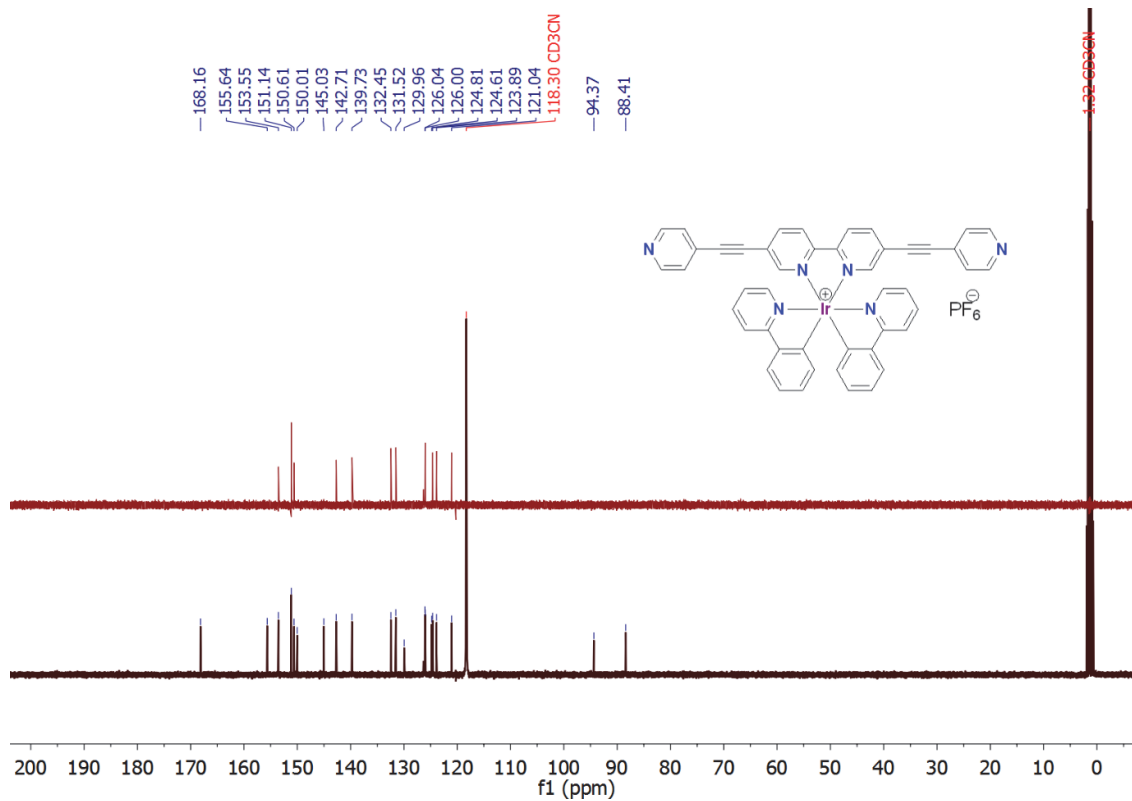
| | | |
|-----------------------------------|--|--------------------|
| Formula weight | C ₄₆ H ₃₂ F ₆ IrN ₆ OP | |
| Temperature | 1021.95 | |
| Wavelength | 173(2) K | |
| Crystal size | 0.71073 Å | |
| Crystal system | Triclinic | |
| Space group | P-1 | |
| Unit cell dimensions | a = 13.9900(3) Å | α = 104.5710(10)°. |
| | b = 15.4250(3) Å | β = 106.4530(10)°. |
| | c = 23.9686(7) Å | γ = 93.4910(10)°. |
| Volume | 4752.1(2) Å ³ | |
| Z | 4 | |
| Density (calculated) | 1.428 Mg/m ³ | |
| Absorption coefficient | 2.906 mm ⁻¹ | |
| F(000) | 2016 | |
| Crystal size | 0.06 x 0.05 x 0.04 mm ³ | |
| Theta range for data collection | 1.86 to 30.10°. | |
| Index ranges | -19 ≤ h ≤ 18, -21 ≤ k ≤ 20, 0 ≤ l ≤ 33 | |
| Reflections collected | 24960 | |
| Independent reflections | 24960 [R(int) = 0.0210] | |
| Completeness to theta = 29.10° | 98.3 % | |
| Absorption correction | Semi-empirical from equivalents | |
| Max. and min. transmission | 0.8926 and 0.8450 | |
| Refinement method | Full-matrix least-squares on F ² | |
| Data / restraints / parameters | 24960 / 27 / 1160 | |
| Goodness-of-fit on F ² | 1.004 | |
| Final R indices [I > 2σ(I)] | R1 = 0.0421, wR2 = 0.0964 | |
| Final R indices (all data) | R1 = 0.0722, wR2 = 0.1038 | |
| Largest diff. peak and hole | 1.085 and -0.848 e.Å ⁻³ | |

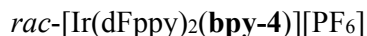
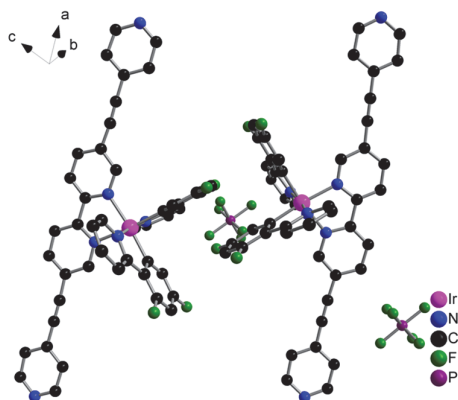
NMR data for *rac*-[Ir(ppy)₂(bpy-4)][PF₆]

¹H NMR



¹³C NMR + DEPT 145°





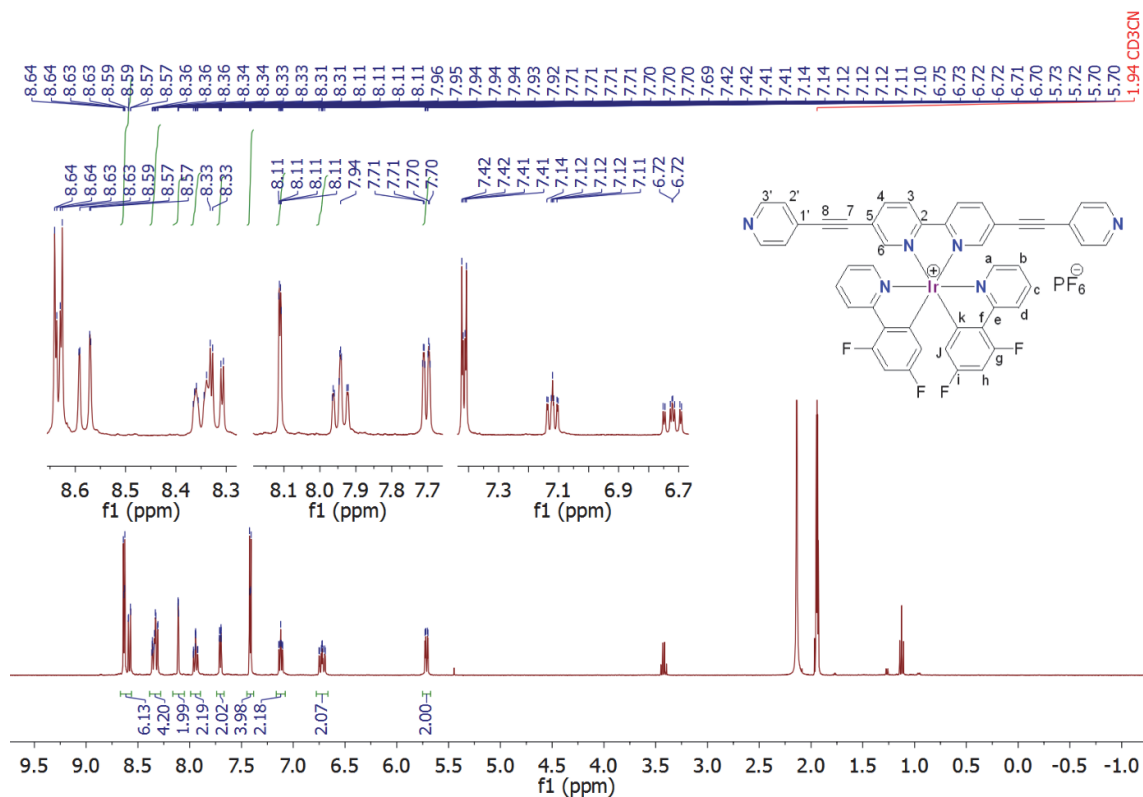
Crystallization Method: Vapors of diethyl ether (*ca.* 30 mL) were slowly diffused into an acetonitrile solution of *rac*-[Ir(dFppy)₂(bpy-4)][PF₆] (*ca.* 30 mg in 2 mL ACN). Orange single crystals were obtained in a few days.

Crystallographic data (Lab code: e2971):

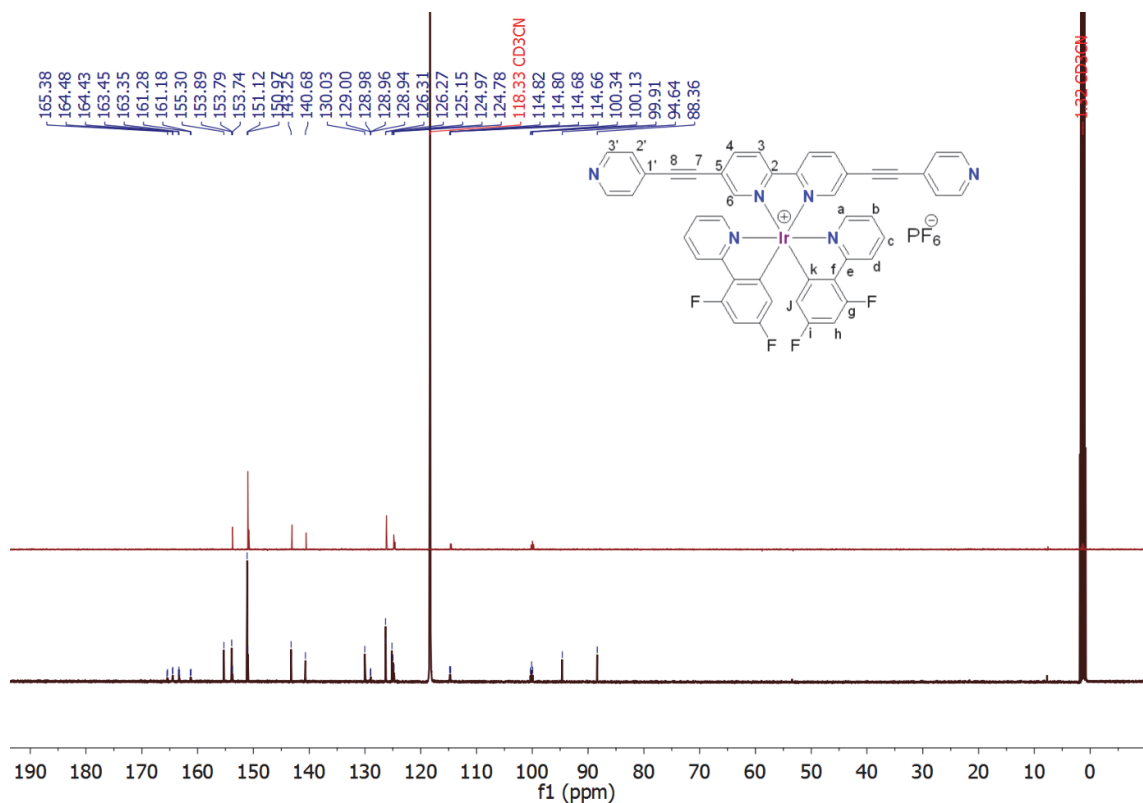
| | | |
|---|---|------------------|
| Empirical formula | C ₁₈₄ H ₁₁₀ F ₄₀ Ir ₄ N ₂₄ O ₃ P ₄ | |
| Formula weight | 4357.64 | |
| Temperature | 173(2) K | |
| Wavelength | 0.71073 Å | |
| Crystal system | Triclinic | |
| Space group | P-1 | |
| Unit cell dimensions | a = 13.7634(3) Å | α = 71.3150(10)° |
| | b = 15.9262(5) Å | β = 82.8320(10)° |
| | c = 23.4390(6) Å | γ = 83.3790(10)° |
| Volume | 4813.4(2) Å ³ | |
| Z | 1 | |
| Density (calculated) | 1.503 Mg/m ³ | |
| Absorption coefficient | 2.885 mm ⁻¹ | |
| F(000) | 2134 | |
| Crystal size | 0.06 x 0.06 x 0.04 mm ³ | |
| Theta range for data collection | 1.94 to 28.90° | |
| Index ranges | -15 ≤ h ≤ 18, -21 ≤ k ≤ 22, 0 ≤ l ≤ 33 | |
| Reflections collected | 24677 | |
| Independent reflections | 24677 [R(int) = 0.0456] | |
| Completeness to theta = 28.90° | 97.3 % | |
| Absorption correction | Semi-empirical from equivalents | |
| Max. and min. transmission | 0.8933 and 0.8460 | |
| Refinement method | Full-matrix least-squares on F ² | |
| Data / restraints / parameters | 24677 / 0 / 1171 | |
| Goodness-of-fit on F² | 1.093 | |
| Final R indices [I > 2σ(I)] | R ₁ = 0.0401, wR ₂ = 0.1118 | |
| R indices (all data) | R ₁ = 0.0651, wR ₂ = 0.1204 | |
| Largest diff. peak and hole | 1.438 and -1.131 e.Å ⁻³ | |

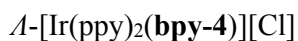
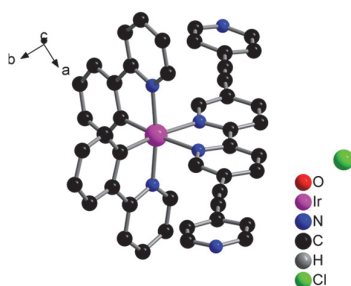
NMR data for *rac*-[Ir(ppy)₂(bpy-4)][PF₆]

¹H NMR



¹³C NMR + DEPT 145°

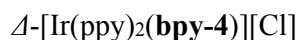
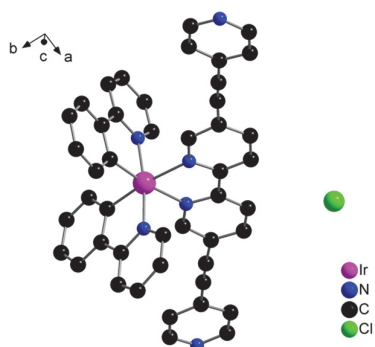




Crystallization Method: Slow vapor diffusion of toluene (*ca.* 5 mL) into a 1/1 acetonitrile/toluene solution containing *A*-[Ir(dFppy)₂(bpy-4)][Cl] (*ca.* 8 mg in *ca.* 2 mL). Red single crystals were obtained in two weeks.

Crystallographic data (Lab code: e3109):

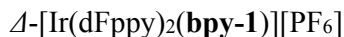
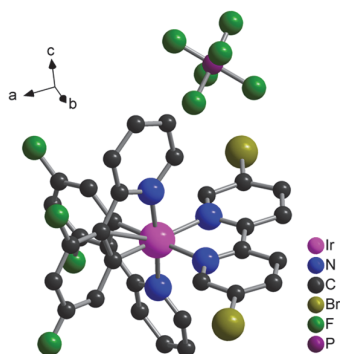
| | | |
|---|--|---------------------------|
| Chemical formula | C ₆₀ H ₄₈ ClIrN ₆ O | |
| Formula weight | 1096.69 | |
| Temperature | 173(2) K | |
| Wavelength | 0.71073 Å | |
| Crystal size | 0.050 x 0.060 x 0.060 mm | |
| Crystal system | orthorhombic | |
| Space group | P 21 21 2 | |
| Unit cell dimensions | a = 32.7712(7) Å | α = 90° |
| | b = 12.3271(4) Å | β = 90° |
| | c = 13.9638(4) Å | γ = 90° |
| Volume | 5641.0(3) Å ³ | |
| Z | 4 | |
| Density (calculated) | 1.291 g/cm ³ | |
| Absorption coefficient | 2.457 mm ⁻¹ | |
| F(000) | 2208 | |
| Theta range for data collection | 1.92 to 30.06° | |
| Index ranges | 29 ≤ h ≤ 17, 19 ≤ k ≤ -29, -17 ≤ l ≤ -19 | |
| Reflections collected | 15562 | |
| Max. and min. transmission | 0.8870 and 0.8670 | |
| Structure solution technique | direct methods | |
| Structure solution program | SHELXS-97 (Sheldrick, 2013) | |
| Refinement method | Full-matrix least-squares on F ² | |
| Refinement program | SHELXL-2013 (Sheldrick, 2013) | |
| Function minimized | Σ w(F _o ² - F _c ²) ² | |
| Data / restraints / parameters | 15257 / 0 / 617 | |
| Goodness-of-fit on F² | 0.923 | |
| Δ/σ_{max} | 0.016 | |
| Final R indices | 13322 data; I > 2σ(I) | R1 = 0.0337, wR2 = 0.0659 |
| | all data | R1 = 0.0427, wR2 = 0.0685 |
| Weighting scheme | w = 1/[σ ² (F _o ²)] where P = (F _o ² + 2F _c ²)/3 | |
| Absolute structure parameter | 0.0(0) | |
| Largest diff. peak and hole | 0.870 and -0.972 eÅ ⁻³ | |
| R.M.S. deviation from mean | 0.081 eÅ ⁻³ | |



Crystallization Method: Slow vapor diffusion of toluene (*ca.* 5 mL) into a 1/1 acetonitrile/toluene solution containing $\Delta\text{-}[\text{Ir}(\text{dFppy})_2(\text{bpy-4})][\text{Cl}]$ (*ca.* 8 mg in *ca.* 2 mL). Red single crystals were obtained in two weeks.

Crystallographic data (Lab code: s3042 squeeze):

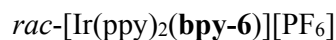
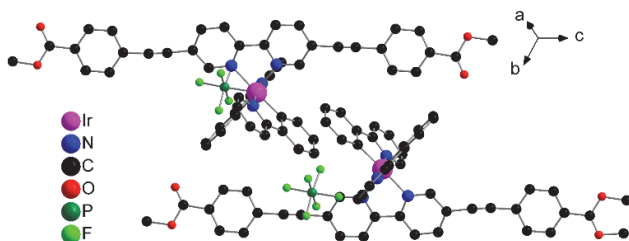
| | | |
|--|---|---------------------------|
| Chemical formula | $\text{C}_{60}\text{H}_{48}\text{ClIrN}_6\text{O}$ | |
| Formula weight | 1096.69 | |
| Temperature | 173(2) K | |
| Wavelength | 0.71073 Å | |
| Crystal size | 0.060 x 0.060 x 0.070 mm | |
| Crystal system | orthorhombic | |
| Space group | P 21 21 2 | |
| Unit cell dimensions | $a = 32.5454(6)$ Å | $\alpha = 90^\circ$ |
| | $b = 12.2814(2)$ Å | $\beta = 90^\circ$ |
| | $c = 13.9420(2)$ Å | $\gamma = 90^\circ$ |
| Volume | $5572.66(16)$ Å ³ | |
| Z | 4 | |
| Density (calculated) | 1.307 g/cm ³ | |
| Absorption coefficient | 2.487 mm ⁻¹ | |
| F(000) | 2208 | |
| Theta range for data collection | 1.59 to 30.15° | |
| Reflections collected | 15818 | |
| Independent reflections | 15815 [R(int) = 0.0345] | |
| Max. and min. transmission | 0.8651 and 0.8452 | |
| Structure solution technique | direct methods | |
| Structure solution program | SHELXS-97 (Sheldrick, 2008) | |
| Refinement method | Full-matrix least-squares on F ² | |
| Refinement program | SHELXL-97 (Sheldrick, 2008) | |
| Function minimized | $\Sigma w(\text{F}_\text{o}^2 - \text{F}_\text{c}^2)^2$ | |
| Data / restraints / parameters | 15815 / 0 / 617 | |
| Goodness-of-fit on F² | 1.098 | |
| Δ/σ_max | 0.005 | |
| Final R indices | 14466 data; I > 2σ(I) | R1 = 0.0322, wR2 = 0.0566 |
| | all data | R1 = 0.0383, wR2 = 0.0569 |
| Weighting scheme | $w = 1/[\sigma^2(\text{F}_\text{o}^2)]$ where $P = (\text{F}_\text{o}^2 + 2\text{F}_\text{c}^2)/3$ | |
| Absolute structure parameter | 0.0(0) | |
| Largest diff. peak and hole | 1.262 and -1.326 eÅ ⁻³ | |
| R.M.S. deviation from mean | 0.091 eÅ ⁻³ | |



Crystallization Method: Vapors of diethyl ether (*ca.* 30 mL) were slowly diffused into an acetonitrile solution of $\Delta\text{-}[\text{Ir}(\text{dFppy})_2(\text{bpy-1})][\text{PF}_6]$ (*ca.* 20 mg in 2 mL ACN). Orange single crystals were obtained in a few days.

Crystallographic data (Lab code: s3224 squeeze):

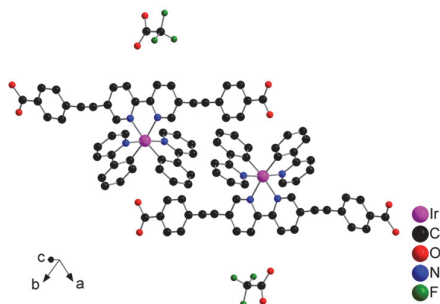
| | | |
|--|---|---------------------------|
| Chemical formula | $\text{C}_{164}\text{H}_{100}\text{Br}_{10}\text{F}_{50}\text{Ir}_5\text{N}_{20}\text{OP}_5$ | |
| Formula weight | 5231.58 | |
| Temperature | 173(2) K | |
| Wavelength | 0.71073 Å | |
| Crystal size | 0.040 x 0.040 x 0.050 mm | |
| Crystal system | orthorhombic | |
| Space group | C 2 2 21 | |
| Unit cell dimensions | $a = 21.6255(5)$ Å | $\alpha = 90^\circ$ |
| | $b = 25.9383(6)$ Å | $\beta = 90^\circ$ |
| | $c = 39.2268(8)$ Å | $\gamma = 90^\circ$ |
| Volume | 22003.4(8) Å ³ | |
| Z | 4 | |
| Density (calculated) | 1.579 g/cm ³ | |
| Absorption coefficient | 4.954 mm ⁻¹ | |
| F(000) | 9968 | |
| Theta range for data collection | 1.88 to 29.98° | |
| Index ranges | -30 ≤ h ≤ 28, -36 ≤ k ≤ 23, -42 ≤ l ≤ 45 | |
| Reflections collected | 73194 | |
| Independent reflections | 27030 [R(int) = 0.0946] | |
| Max. and min. transmission | 0.8260 and 0.7900 | |
| Structure solution technique | direct methods | |
| Structure solution program | SHELXS-97 (Sheldrick, 2008) | |
| Refinement method | Full-matrix least-squares on F ² | |
| Refinement program | SHELXL-97 (Sheldrick, 2008) | |
| Function minimized | $\sum w(\text{F}_\text{o}^2 - \text{F}_\text{c}^2)^2$ | |
| Data / restraints / parameters | 27030 / 2 / 1139 | |
| Goodness-of-fit on F² | 1.056 | |
| Δ/σ_max | 0.001 | |
| Final R indices | 15912 data; I > 2σ(I) | R1 = 0.0540, wR2 = 0.1039 |
| | all data | R1 = 0.1139, wR2 = 0.1163 |
| Weighting scheme | $w = \frac{1}{[\sigma^2(\text{F}_\text{o}^2) + (0.0459\text{P})^2]}$ where $\text{P} = (\text{F}_\text{o}^2 + 2\text{F}_\text{c}^2)/3$ | |
| Absolute structure parameter | 0.0(0) | |
| Largest diff. peak and hole | 1.703 and -1.959 eÅ ⁻³ | |
| R.M.S. deviation from mean | 0.150 eÅ ⁻³ | |



Crystallization Method: Vapors of diethyl ether (*ca.* 30 mL) were slowly diffused into an acetonitrile solution of *Δ*-[Ir(ppy)₂(bpy-1)][PF₆] (*ca.* 20 mg in 2 mL ACN). Orange single crystals were obtained in a few days.

Crystallographic data (Lab code: s3256):

| | | |
|---|---|---------------------------|
| Chemical formula | C ₁₁₆ H ₁₀₂ F ₁₂ Ir ₂ N ₈ O ₁₁ P ₂ '2(C ₅₂ H ₃₆ IrN ₄ O ₄ , 2(F ₆ P), 3(C ₄ H ₁₀ O)' | |
| Formula weight | 2458.39 | |
| Temperature | 173(2) K | |
| Wavelength | 0.71073 Å | |
| Crystal size | 0.050 x 0.050 x 0.060 mm | |
| Crystal system | triclinic | |
| Space group | P -1 | |
| Unit cell dimensions | a = 12.1607(6) Å | α = 111.0540(9)° |
| | b = 14.4048(7) Å | β = 93.2930(10)° |
| | c = 17.0571(7) Å | γ = 97.0730(10)° |
| Volume | 2750.5(2) Å ³ | |
| Z | 1 | |
| Density (calculated) | 1.484 g/cm ³ | |
| Absorption coefficient | 2.529 mm ⁻¹ | |
| F(000) | 1234 | |
| Theta range for data collection | 2.02 to 31.31° | |
| Index ranges | -17 ≤ h ≤ 17, -21 ≤ k ≤ 21, -15 ≤ l ≤ 21 | |
| Reflections collected | 76358 | |
| Independent reflections | 16006 [R(int) = 0.0336] | |
| Max. and min. transmission | 0.8920 and 0.8610 | |
| Structure solution technique | direct methods | |
| Structure solution program | SHELXS-97 (Sheldrick, 2014) | |
| Refinement method | Full-matrix least-squares on F ² | |
| Refinement program | SHELXL-97 (Sheldrick, 2014) | |
| Function minimized | Σ w(F _o ² - F _c ²) ² | |
| Data / restraints / parameters | 16006 / 10 / 720 | |
| Goodness-of-fit on F² | 1.086 | |
| Δ/σ_{max} | 0.012 | |
| Final R indices | 14528 data; I > 2σ(I) | R1 = 0.0302, wR2 = 0.0847 |
| | all data | R1 = 0.0354, wR2 = 0.0876 |
| Weighting scheme | w = 1/[σ ² (F _o ²) + (0.0507P) ² + 2.8529P] where P = (F _o ² + 2F _c ²)/3 | |
| Largest diff. peak and hole | 2.288 and -0.863 eÅ ⁻³ | |
| R.M.S. deviation from mean | 0.117 eÅ ⁻³ | |



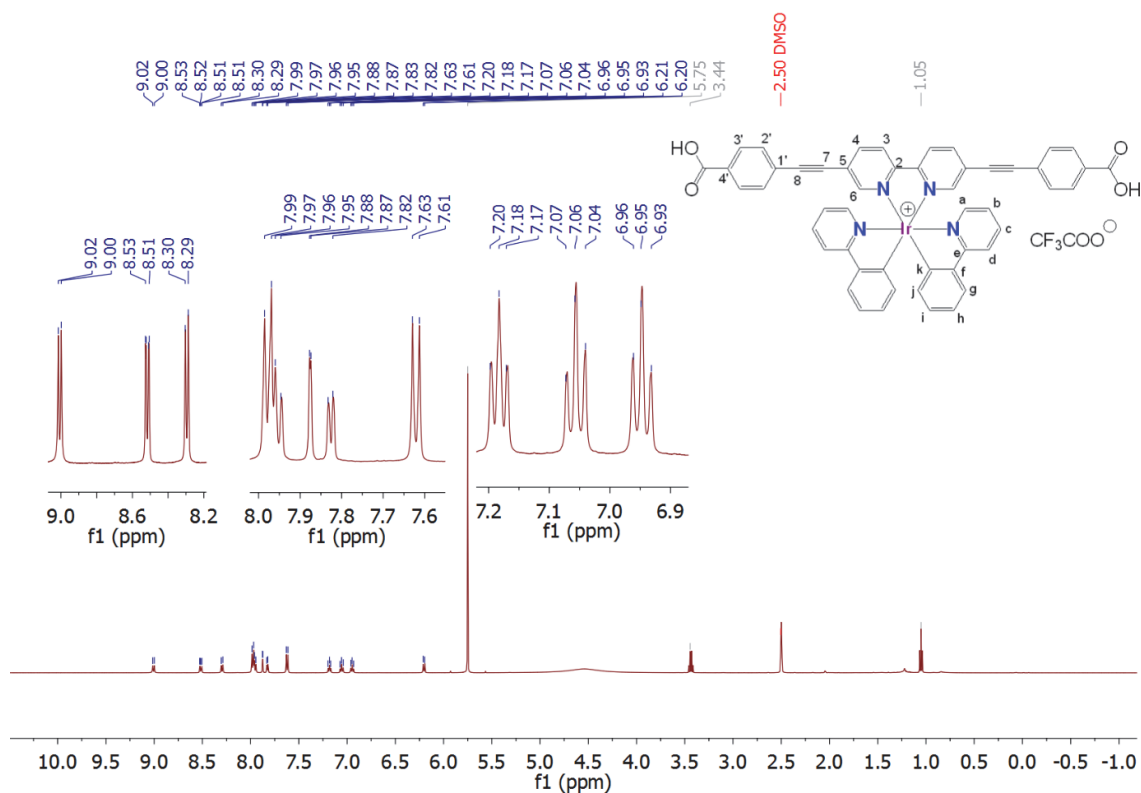
Crystallization Method: Vapor diffusion of diethyl ether (*ca.* 30 mL) into a DMF solution containing *rac*-[Ir(ppy)₂(bpy-7)][CF₃COO] (*ca.* 20 mg in 2 mL DMF) afforded red single crystals within a week.

Crystallographic data (Lab code: s3443):

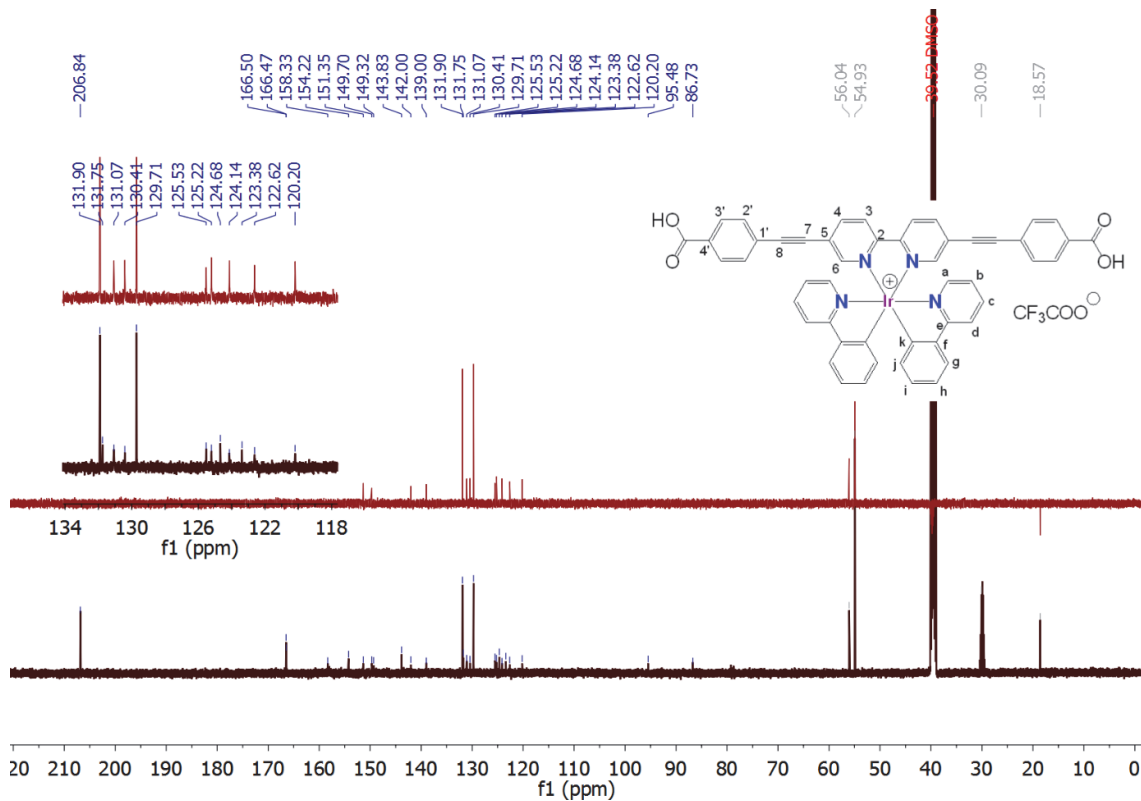
| | | |
|---|---|---------------------------|
| Chemical formula | C ₅₈ H ₄₈ F ₃ IrN ₆ O ₉ | |
| Formula weight | 1222.22 g/mol | |
| Temperature | 173(2) K | |
| Wavelength | 0.71073 Å | |
| Crystal size | 0.040 x 0.050 x 0.050 mm | |
| Crystal system | triclinic | |
| Space group | P -1 | |
| Unit cell dimensions | a = 12.9811(6) Å | α = 78.160(2)° |
| | b = 14.1622(6) Å | β = 82.392(2)° |
| | c = 17.1945(6) Å | γ = 71.130(2)° |
| Volume | 2920.1(2) Å ³ | |
| Z | 2 | |
| Density (calculated) | 1.390 g/cm ³ | |
| Absorption coefficient | 2.353 mm ⁻¹ | |
| F(000) | 1228 | |
| Theta range for data collection | 1.21 to 27.70° | |
| Index ranges | -16 ≤ h ≤ 16, -18 ≤ k ≤ 18, -22 ≤ l ≤ 19 | |
| Reflections collected | 25141 | |
| Independent reflections | 12530 [R(int) = 0.0491] | |
| Max. and min. transmission | 0.9130 and 0.8910 | |
| Structure solution technique | direct methods | |
| Structure solution program | SHELXS-97 (Sheldrick, 2008) | |
| Refinement method | Full-matrix least-squares on F ² | |
| Refinement program | SHELXL-97 (Sheldrick, 2008) | |
| Function minimized | Σ w(F _o ² - F _c ²) ² | |
| Data / restraints / parameters | 12530 / 65 / 715 | |
| Goodness-of-fit on F² | 1.037 | |
| Δ/σ_{max} | 0.004 | |
| Final R indices | 8380 data; I > 2σ(I) | R1 = 0.0885, wR2 = 0.2413 |
| | all data | R1 = 0.1288, wR2 = 0.2780 |
| Weighting scheme | w = 1/[σ ² (F _o ²) + (0.1800P) ² + 7.3114P] where P = (F _o ² + 2F _c ²)/3 | |
| Largest diff. peak and hole | 1.156 and -2.533 eÅ ⁻³ | |
| R.M.S. deviation from mean | 0.241 eÅ ⁻³ | |

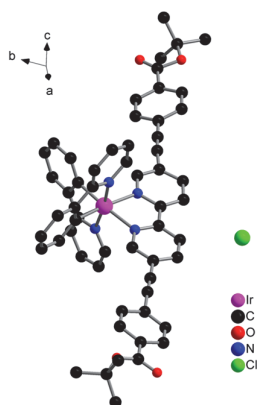
NMR data for *rac*-[Ir(ppy)₂(bpy-4)][PF₆]

¹H NMR



¹³C NMR + DEPT 145°



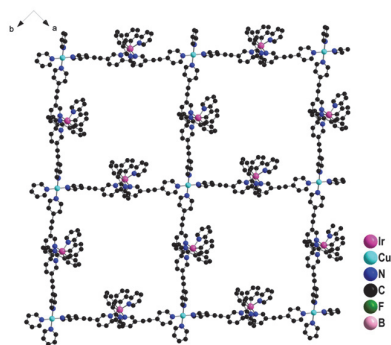


Δ -[Ir(ppy)₂(bpy-11)][Cl]

Crystallization Method: Slow vapor diffusion of toluene (*ca.* 5 mL) into a 1/1 acetonitrile/toluene solution containing Δ -[Ir(ppy)₂(bpy-11)][Cl] (*ca.* 8 mg in *ca.* 2 mL). Red single crystals were obtained in two weeks.

Crystallographic data (Lab code: s3580):

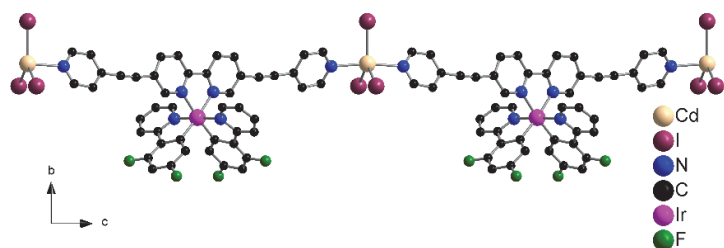
| | | |
|--|---|---------------------------|
| Chemical formula | C ₅₈ H ₄₈ ClIrN ₄ O ₄ | |
| Formula weight | 1092.65 g/mol | |
| Temperature | 293(2) K | |
| Wavelength | 0.71073 Å | |
| Crystal size | 0.050 x 0.050 x 0.060 mm | |
| Crystal system | trigonal | |
| Space group | P 3 2 1 | |
| Unit cell dimensions | a = 20.8216(12) Å | $\alpha = 90^\circ$ |
| | b = 20.8216(12) Å | $\beta = 90^\circ$ |
| | c = 27.2953(18) Å | $\gamma = 120^\circ$ |
| Volume | 10248.2(14) Å ³ | |
| Z | 6 | |
| Density (calculated) | 1.062 g/cm ³ | |
| Absorption coefficient | 2.031 mm ⁻¹ | |
| F(000) | 3300 | |
| Theta range for data collection | 1.49 to 30.15° | |
| Index ranges | -21 ≤ h ≤ 29, -29 ≤ k ≤ 21, -38 ≤ l ≤ 38 | |
| Reflections collected | 127626 | |
| Independent reflections | 20155 [R(int) = 0.0710] | |
| Max. and min. transmission | 0.9200 and 0.8810 | |
| Structure solution technique | direct methods | |
| Structure solution program | SHELXS-97 (Sheldrick, 2008) | |
| Refinement method | Full-matrix least-squares on F ² | |
| Refinement program | SHELXL-2014/6 (Sheldrick, 2014) | |
| Function minimized | $\Sigma w(F_o^2 - F_c^2)^2$ | |
| Data / restraints / parameters | 20155 / 34 / 501 | |
| Goodness-of-fit on F² | 1.058 | |
| Δ/σ_{\max} | 0.022 | |
| Final R indices | 13444 data; I > 2σ(I) | R1 = 0.0783, wR2 = 0.2123 |
| | all data | R1 = 0.1270, wR2 = 0.2597 |
| Weighting scheme | w = $\frac{1}{[\sigma^2(F_o^2) + (0.1542P)^2 + 19.1405P]}$ where P = (F _o ² + 2F _c ²)/3 | |
| Absolute structure parameter | -0.0(0) | |
| Largest diff. peak and hole | 3.882 and -4.177 eÅ ⁻³ | |
| R.M.S. deviation from mean | 0.217 eÅ ⁻³ | |



Crystallization Method: In a crystallization tube (height = 12 cm, diameter = 0.4 cm), slow diffusion of an ethanol solution (*ca.* 0.7 mL, 4 mg) of [Cu(ACN)₄][BF₄] into a chloroform solution of *rac*-[Ir(ppy)₂(bpy-4)][PF₆] (*ca.* 3 mg in 0.6 mL CHCl₃) with a buffer layer of CHCl₃/EtOH 1/1 (*ca.* 0.1 mL). Red single crystals were obtained in a few days.

Crystallographic data (Lab code: e2907 squeeze):

| | | |
|---|---|---------------------------|
| Chemical formula | C ₉₇ H ₆₈ B ₂ Cl ₁₂ CuF ₂₀ Ir ₂ N ₁₂ OP ₂ | |
| Formula weight | 2754.53 | |
| Temperature | 173(2) K | |
| Wavelength | 0.71073 Å | |
| Crystal size | 0.050 x 0.060 x 0.060 mm | |
| Crystal system | monoclinic | |
| Space group | C 1 2/c 1 | |
| Unit cell dimensions | a = 33.6718(17) Å | α = 90° |
| | b = 33.6481(16) Å | β = 110.2790(10)° |
| | c = 13.8979(6) Å | γ = 90° |
| Volume | 14770.2(12) Å ³ | |
| Z | 4 | |
| Density (calculated) | 1.239 g/cm ³ | |
| Absorption coefficient | 2.242 mm ⁻¹ | |
| F(000) | 5396 | |
| Theta range for data collection | 1.98 to 29.80° | |
| Reflections collected | 20368 | |
| Independent reflections | 20368 [R(int) = 0.0456] | |
| Max. and min. transmission | 0.8961 and 0.8772 | |
| Structure solution technique | direct methods | |
| Structure solution program | SHELXS-97 (Sheldrick, 2008) | |
| Refinement method | Full-matrix least-squares on F ² | |
| Refinement program | SHELXL-97 (Sheldrick, 2008) | |
| Function minimized | Σ w(F _o ² - F _c ²) ² | |
| Data / restraints / parameters | 20368 / 12 / 690 | |
| Goodness-of-fit on F² | 1.043 | |
| Δ/σ_{max} | 0.005 | |
| Final R indices | 10500 data; I > 2σ(I) | R1 = 0.0737, wR2 = 0.1925 |
| | all data | R1 = 0.1251, wR2 = 0.2082 |
| Weighting scheme | w = 1/[σ ² (F _o ²) + (0.1026P) ²] where P = (F _o ² + 2F _c ²)/3 | |
| Largest diff. peak and hole | 3.634 and -1.904 eÅ ⁻³ | |
| R.M.S. deviation from mean | 0.147 eÅ ⁻³ | |



rac-[Ir(dFppy)₂(bpy-4)]·[CdI₃]

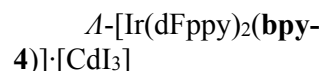
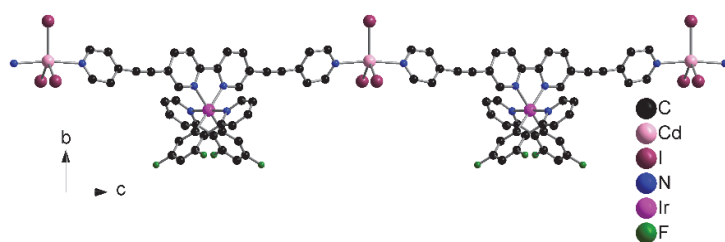
Crystallization Method:

In a crystallization tube (height = 12 cm, diameter = 0.4 cm), slow diffusion of an ethanol solution (*ca.* 0.7 mL, 2 mg) of

CdI₂ into a tetrachloroethane solution of *rac*-[Ir(dFppy)₂(bpy-4)][PF₆] (*ca.* 3 mg in 0.6 mL Cl₂CHCHCl₂) with a 1/1 buffer layer of Cl₂CHCHCl₂/EtOH containing two drops of 1,1,1-trifluoroethanol and 4,4,4-trifluorobutanol (*ca.* 0.1 mL). Orange single crystals were obtained in two weeks.

Crystallographic data (Lab code: s3209):

| | | |
|-----------------------------------|--|---------------------------|
| Chemical formula | C ₉₈ H ₆₅ Cd ₂ Cl ₂ F ₈ I ₆ Ir ₂ N ₁₂ O ₂ | |
| Formula weight | 3036.12 | |
| Temperature | 173(2) K | |
| Wavelength | 0.71073 Å | |
| Crystal size | 0.040 x 0.050 x 0.060 mm | |
| Crystal system | monoclinic | |
| Space group | C 1 2/c 1 | |
| Unit cell dimensions | a = 15.0314(3) Å | α = 90° |
| | b = 33.2661(7) Å | β = 97.8500(11)° |
| | c = 11.2295(3) Å | γ = 90° |
| Volume | 5562.5(2) Å ³ | |
| Z | 2 | |
| Density (calculated) | 1.813 g/cm ³ | |
| Absorption coefficient | 4.537 mm ⁻¹ | |
| F(000) | 2854 | |
| Theta range for data collection | 2.20 to 30.09° | |
| Index ranges | -20 ≤ h ≤ 18, -46 ≤ k ≤ 45, -15 ≤ l ≤ 15 | |
| Reflections collected | 26425 | |
| Independent reflections | 8024 [R(int) = 0.0305] | |
| Max. and min. transmission | 0.8390 and 0.7720 | |
| Structure solution technique | direct methods | |
| Structure solution program | SHELXS-97 (Sheldrick, 2013) | |
| Refinement method | Full-matrix least-squares on F ² | |
| Refinement program | SHELXL-97 (Sheldrick, 2013) | |
| Function minimized | Σ w(F _o ² - F _c ²) ² | |
| Data / restraints / parameters | 8024 / 5 / 318 | |
| Goodness-of-fit on F ² | 1.078 | |
| Δ/σ _{max} | 0.001 | |
| Final R indices | 6248 data; I > 2σ(I) | R1 = 0.0483, wR2 = 0.1434 |
| | all data | R1 = 0.0664, wR2 = 0.1545 |
| Weighting scheme | w = 1/[σ ² (F _o ²) + (0.0903P) ² + 18.3937P] where P = (F _o ² + 2F _c ²)/3 | |
| Largest diff. peak and hole | 2.403 and -0.883 eÅ ⁻³ | |
| R.M.S. deviation from mean | 0.200 eÅ ⁻³ | |



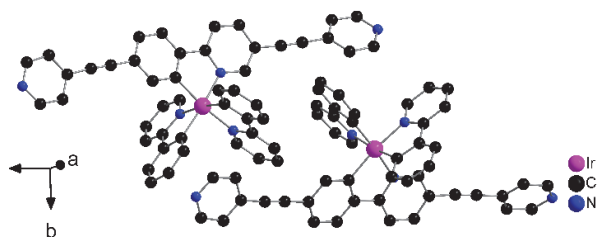
Crystallization

Method: In a crystallization tube (height = 12 cm, diameter = 0.4 cm), slow diffusion of an ethanol solution (ca. 0.7 mL, 2

mg) of CdI₂ into a tetrachloroethane solution of Δ -[Ir(dFppy)₂(bpy-4)][PF₆] (ca. 3 mg in 0.6 mL Cl₂CHCHCl₂) with a 1/1 buffer layer of Cl₂CHCHCl₂/EtOH containing two drops of 1,1,1-trifluoroethanol and 4,4,4-trifluorobutanol (ca. 0.1 mL). Orange single crystals were obtained in two weeks.

Crystallographic data (Lab code: s3257 squeeze):

| | | |
|--|---|-----------------------------|
| Chemical formula | C ₄₇ H ₃₀ CdF ₄ I ₃ IrN ₆ O | |
| Formula weight | 1456.07 | |
| Temperature | 173(2) K | |
| Wavelength | 0.71073 Å | |
| Crystal size | 0.040 x 0.040 x 0.050 mm | |
| Crystal system | monoclinic | |
| Space group | C 1 2 1 | |
| Unit cell dimensions | a = 14.8505(4) Å | $\alpha = 90^\circ$ |
| | b = 33.5574(11) Å | $\beta = 97.7720(10)^\circ$ |
| | c = 11.3102(3) Å | $\gamma = 90^\circ$ |
| Volume | 5584.6(3) Å ³ | |
| Z | 4 | |
| Density (calculated) | 1.732 g/cm ³ | |
| Absorption coefficient | 4.468 mm ⁻¹ | |
| F(000) | 2728 | |
| Theta range for data collection | 1.82 to 31.83° | |
| Index ranges | -21 ≤ h ≤ 17, -49 ≤ k ≤ 49, -15 ≤ l ≤ 16 | |
| Reflections collected | 188612 | |
| Independent reflections | 17002 [R(int) = 0.0314] | |
| Max. and min. transmission | 0.8420 and 0.8070 | |
| Structure solution technique | direct methods | |
| Structure solution program | SHELXS-97 (Sheldrick, 2008) | |
| Refinement method | Full-matrix least-squares on F ² | |
| Refinement program | SHELXL-97 (Sheldrick, 2008) | |
| Function minimized | $\Sigma w(F_o^2 - F_c^2)^2$ | |
| Data / restraints / parameters | 17002 / 15 / 582 | |
| Goodness-of-fit on F² | 1.057 | |
| Δ/σ_{\max} | 0.056 | |
| Final R indices | 13920 data; I > 2σ(I) | R1 = 0.0327, wR2 = 0.0942 |
| | all data | R1 = 0.0448, wR2 = 0.0987 |
| Weighting scheme | w = 1/[σ ² (F _o ²) + (0.0614P) ² + 0.7428P] where P = (F _o ² + 2F _c ²)/3 | |
| Absolute structure parameter | 0.0(0) | |
| Largest diff. peak and hole | 2.242 and -0.842 eÅ ⁻³ | |
| R.M.S. deviation from mean | 0.140 eÅ ⁻³ | |



fac-Ir(ppy)₂(bpy-4)

Crystallization Method: Vapor diffusion of methanol (*ca.* 30 mL in a big vial) into a mixture of MeOH/CH₂Cl₂/CHCl₃ (1.5 mL/1.5 mL/1 mL) solvents containing *fac*-Ir(ppy)₂(bpy-4) (*ca.* 20 mg) afforded red single crystals

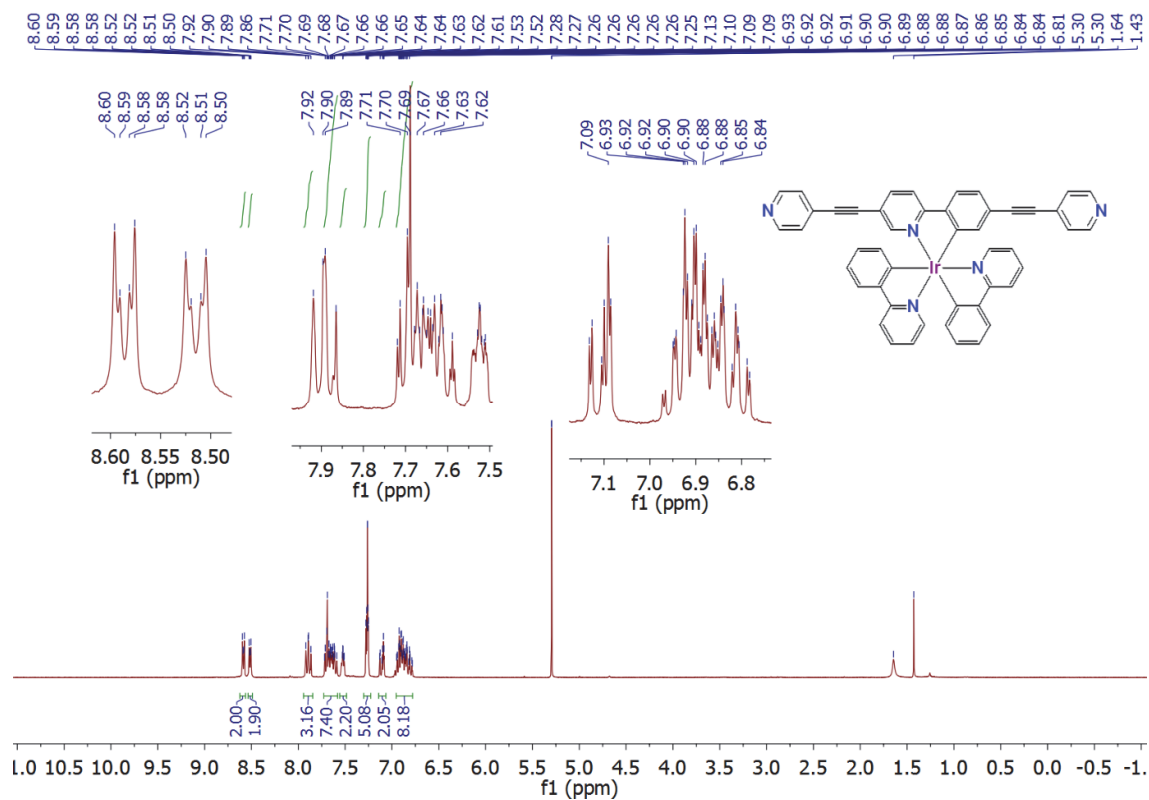
in a few days.

Crystallographic data (Lab code: s3609):

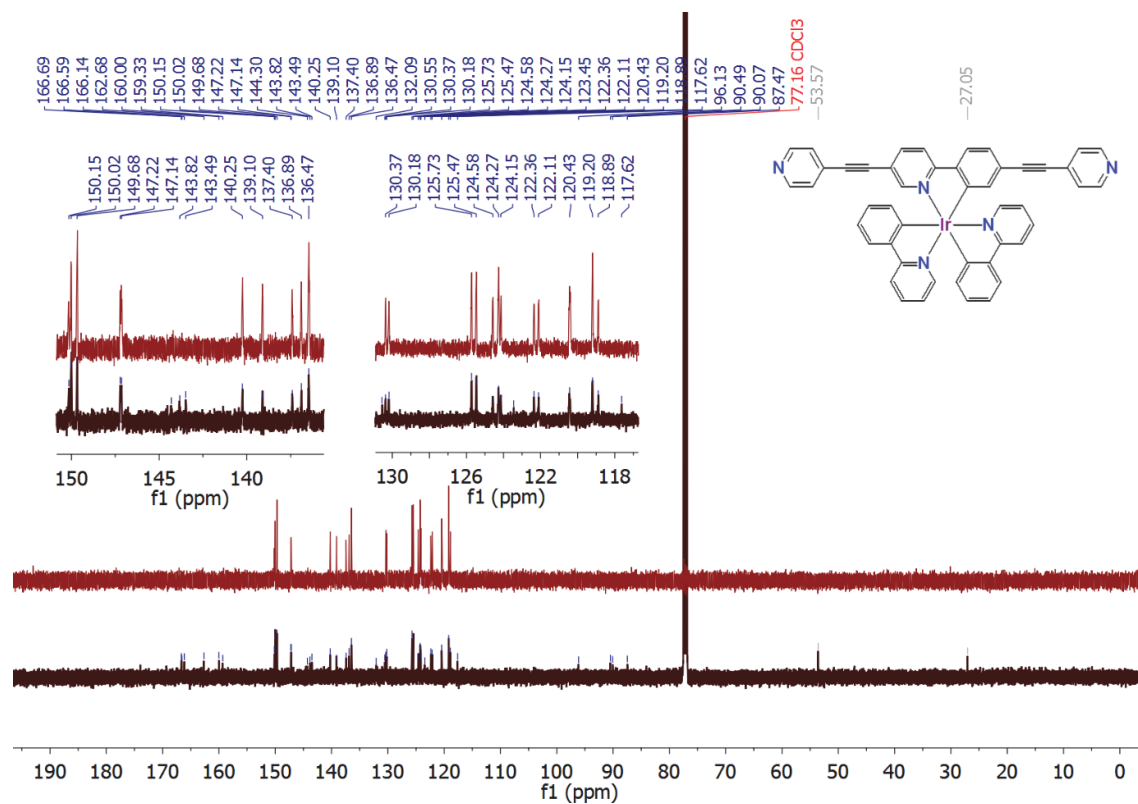
| | | |
|---|---|---------------------------|
| Chemical formula | C ₄₈ H ₃₂ Cl ₂ IrN ₅ | |
| Formula weight | 941.88 g/mol | |
| Temperature | 173(2) K | |
| Wavelength | 0.71073 Å | |
| Crystal size | 0.060 x 0.060 x 0.070 mm | |
| Crystal system | monoclinic | |
| Space group | P 1 21/c 1 | |
| Unit cell dimensions | a = 11.5371(5) Å | α = 90° |
| | b = 18.9198(10) Å | β = 102.705(2)° |
| | c = 17.7528(10) Å | γ = 90° |
| Volume | 3780.2(3) Å ³ | |
| Z | 4 | |
| Density (calculated) | 1.655 g/cm ³ | |
| Absorption coefficient | 3.717 mm ⁻¹ | |
| F(000) | 1864 | |
| Theta range for data collection | 1.59 to 30.06° | |
| Index ranges | -15 ≤ h ≤ 8, -26 ≤ k ≤ 19, -24 ≤ l ≤ 24 | |
| Reflections collected | 19759 | |
| Independent reflections | 10808 [R(int) = 0.0350] | |
| Max. and min. transmission | 0.8150 and 0.7750 | |
| Structure solution technique | direct methods | |
| Structure solution program | SHELXS-97 (Sheldrick, 2008) | |
| Refinement method | Full-matrix least-squares on F ² | |
| Refinement program | SHELXL-2014/6 (Sheldrick, 2014) | |
| Function minimized | Σ w(F _o ² - F _c ²) ² | |
| Data / restraints / parameters | 10808 / 0 / 505 | |
| Goodness-of-fit on F² | 1.006 | |
| Δ/σ_{max} | 0.001 | |
| Final R indices | 7900 data; I > 2σ(I) | R1 = 0.0373, wR2 = 0.0773 |
| | all data | R1 = 0.0644, wR2 = 0.0861 |
| Weighting scheme | w = 1/[σ ² (F _o ²) + (0.0385P) ² + 0.5057P] where P = (F _o ² + 2F _c ²)/3 | |
| Largest diff. peak and hole | 1.435 and -1.180 eÅ ⁻³ | |
| R.M.S. deviation from mean | 0.139 eÅ ⁻³ | |

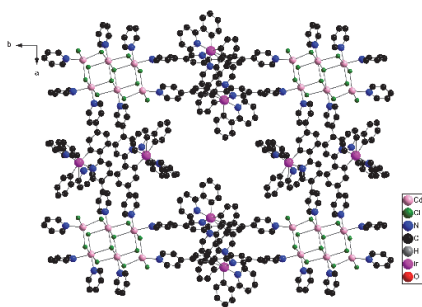
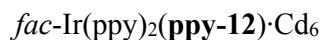
NMR data for *rac*-[Ir(ppy)₂(bpy-4)][PF₆]

¹H NMR



¹³C NMR + DEPT 145°

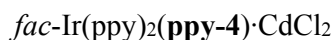
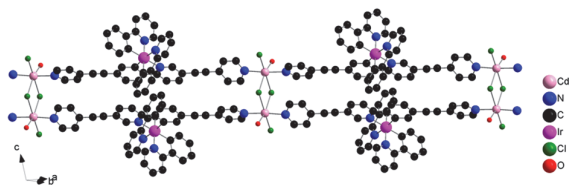




Crystallization Method: In a crystallization tube (height = 12 cm, diameter = 0.4 cm), slow diffusion of an ethanol solution of CdCl₂·2.5H₂O (*ca.* 0.7 mL, 1.5 mg, 6.57·10⁻³ mmol) into a chloroform solution of *fac*-Ir(ppy)₂(ppy-12) (*ca.* 2 mg in 0.6 mL, 2.47·10⁻³ mmol) with a DMSO buffer layer (*ca.* 0.1 mL) afforded orange single crystals in three weeks.

Crystallographic data (Lab code: s3487):

| | | |
|---|--|---------------------------|
| Chemical formula | C ₁₇₂ H ₁₂₂ Cd ₆ Cl ₁₂ Ir ₄ N ₂₀ O | |
| Formula weight | 4353.49 g/mol | |
| Temperature | 173(2) K | |
| Wavelength | 0.71073 Å | |
| Crystal size | 0.040 x 0.040 x 0.050 mm | |
| Crystal system | monoclinic | |
| Space group | P 1 21/c 1 | |
| Unit cell dimensions | a = 23.1344(7) Å | α = 90° |
| | b = 25.8883(10) Å | β = 117.109(2)° |
| | c = 23.1246(7) Å | γ = 90° |
| Volume | 12328.1(7) Å ³ | |
| Z | 2 | |
| Density (calculated) | 1.173 g/cm ³ | |
| Absorption coefficient | 2.824 mm ⁻¹ | |
| F(000) | 4204 | |
| Theta range for data collection | 1.26 to 28.13° | |
| Reflections collected | 29629 | |
| Max. and min. transmission | 0.9000 and 0.8700 | |
| Structure solution technique | direct methods | |
| Structure solution program | SHELXS-97 (Sheldrick, 2008) | |
| Refinement method | Full-matrix least-squares on F ² | |
| Refinement program | SHELXL-2014/6 (Sheldrick, 2014) | |
| Function minimized | Σ w(F _o ² - F _c ²) ² | |
| Data / restraints / parameters | 29629 / 0 / 656 | |
| Goodness-of-fit on F² | 1.076 | |
| Δ/σ_{max} | 0.001 | |
| Final R indices | 8805 data; I > 2σ(I) | R1 = 0.1119, wR2 = 0.2451 |
| | all data | R1 = 0.2302, wR2 = 0.2822 |
| Weighting scheme | w = 1/[σ ² (F _o ²) + (0.0930P) ²] where P = (F _o ² + 2F _c ²)/3 | |
| Largest diff. peak and hole | 2.381 and -2.271 eÅ ⁻³ | |
| R.M.S. deviation from mean | 0.235 eÅ ⁻³ | |



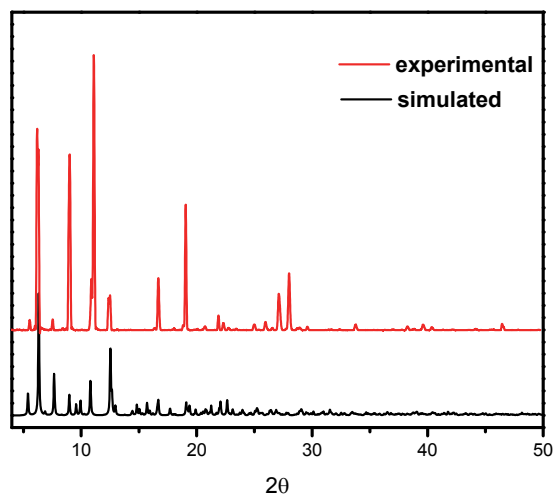
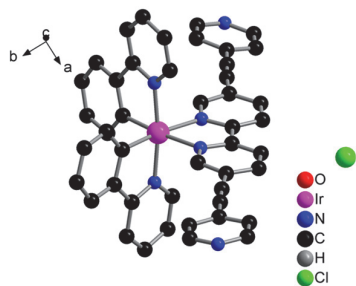
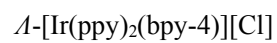
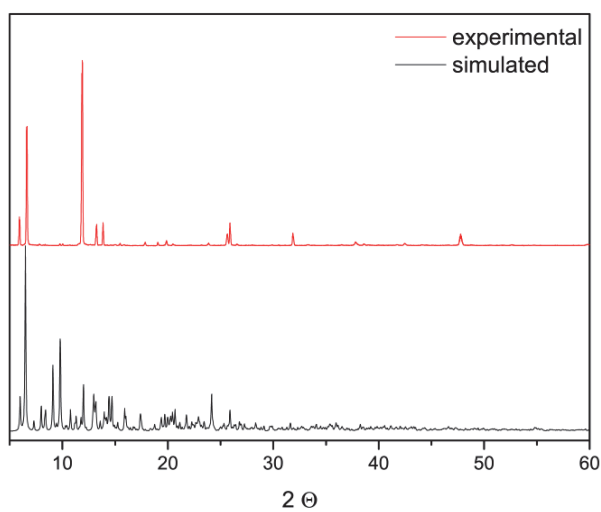
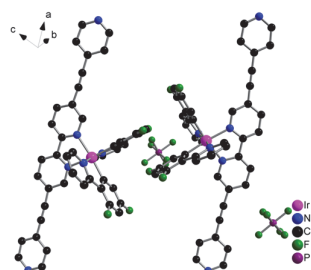
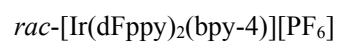
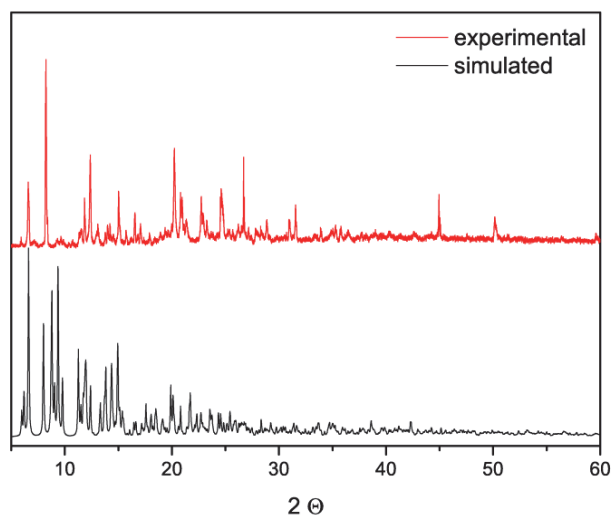
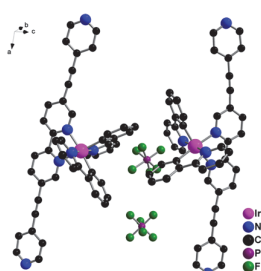
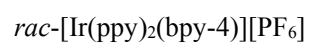
Crystallization Method: In a crystallization tube (height = 12 cm, diameter = 0.4 cm), slow diffusion of an ethanol solution of CdCl₂·2.5H₂O (*ca.* 0.7 mL, 1.5 mg, 6.57·10⁻³ mmol) into a

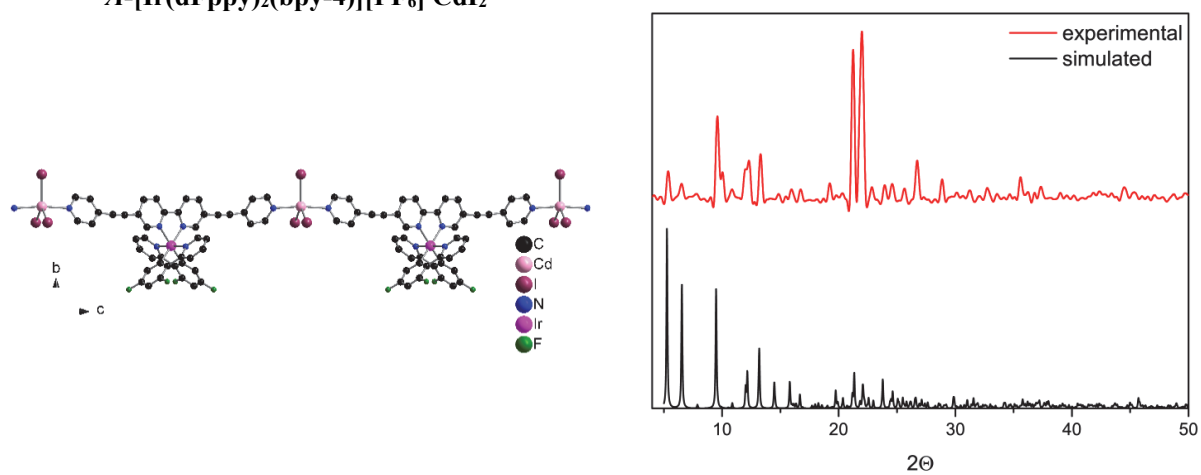
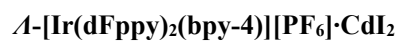
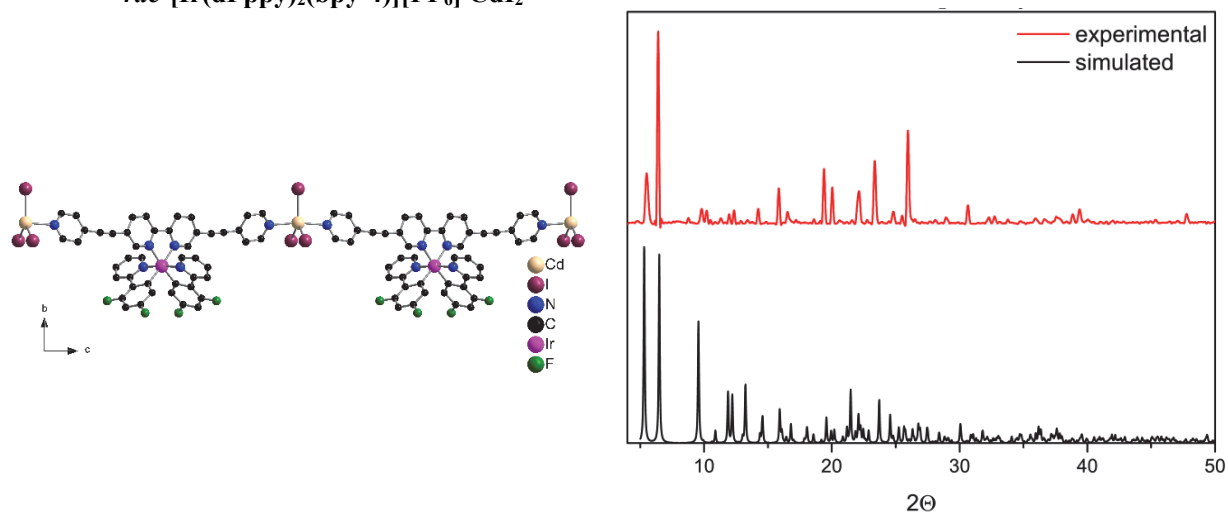
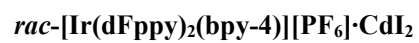
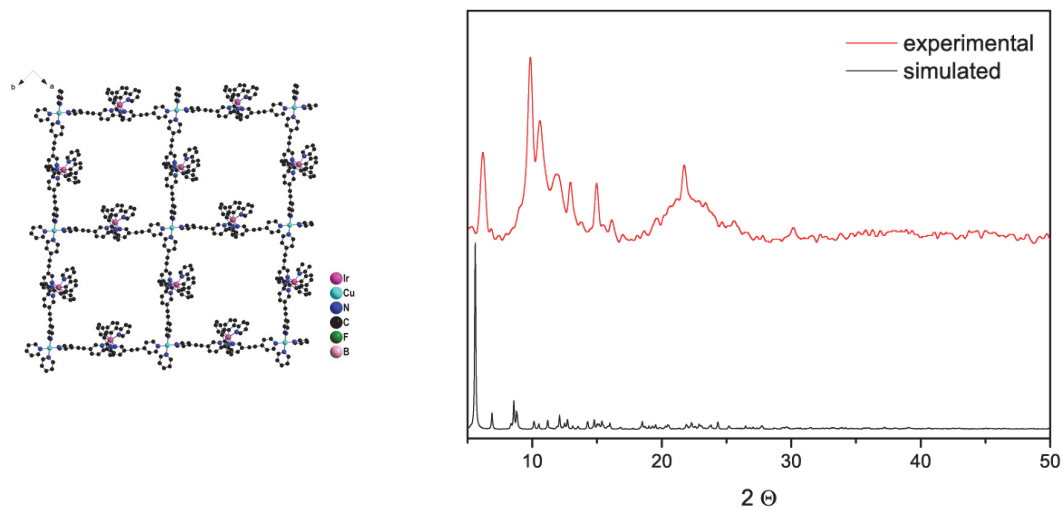
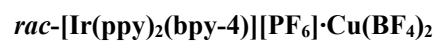
benzonitrile solution of *fac*-Ir(ppy)₂(ppy-4) (*ca.* 2 mg in 0.6 mL, 2.33·10⁻³ mmol) with a buffer layer of 1/1 benzonitrile/EtOH mixture (*ca.* 0.1 mL) afforded red single crystals within three weeks.

Crystallographic data (Lab code: s3587):

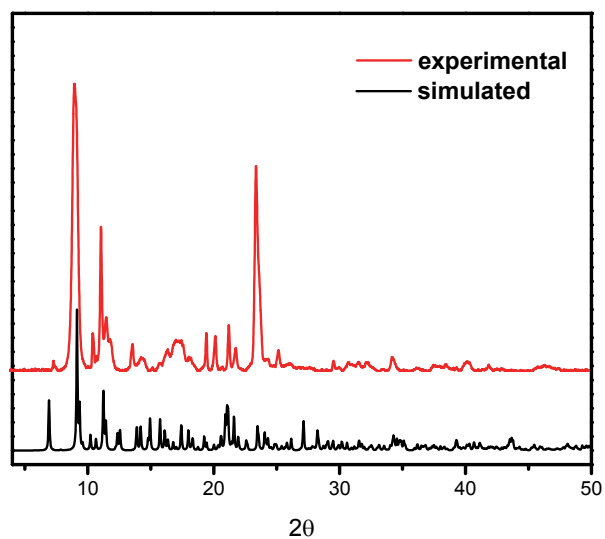
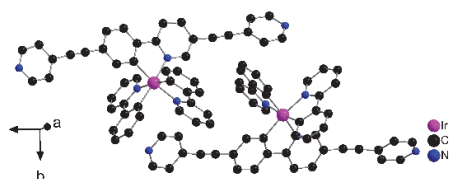
| | | |
|---|--|---------------------------|
| Chemical formula | C ₅₄ H ₃₇ CdCl ₂ IrN ₆ O | |
| Formula weight | 1161.39 g/mol | |
| Temperature | 173(2) K | |
| Wavelength | 0.71073 Å | |
| Crystal size | 0.040 x 0.050 x 0.050 mm | |
| Crystal system | monoclinic | |
| Space group | P 1 21/c 1 | |
| Unit cell dimensions | a = 23.4459(8) Å | α = 90° |
| | b = 9.5514(4) Å | β = 106.9370(10)° |
| | c = 25.3263(10) Å | γ = 90° |
| Volume | 5425.6(4) Å ³ | |
| Z | 4 | |
| Density (calculated) | 1.422 g/cm ³ | |
| Absorption coefficient | 2.981 mm ⁻¹ | |
| F(000) | 2280 | |
| Theta range for data collection | 1.66 to 30.01° | |
| Index ranges | -32 ≤ h ≤ 24, -13 ≤ k ≤ 12, -35 ≤ l ≤ 35 | |
| Reflections collected | 15773 | |
| Independent reflections | 15773 [R(int) = 0.0375] | |
| Max. and min. transmission | 0.9010 and 0.8610 | |
| Structure solution technique | direct methods | |
| Structure solution program | SHELXS-97 (Sheldrick, 2008) | |
| Refinement method | Full-matrix least-squares on F ² | |
| Refinement program | SHELXL-2014/6 (Sheldrick, 2014) | |
| Function minimized | Σ w(F _o ² - F _c ²) ² | |
| Data / restraints / parameters | 15773 / 8 / 526 | |
| Goodness-of-fit on F² | 1.078 | |
| Δ/σ_{max} | 0.006 | |
| Final R indices | 13135 data; I > 2σ(I) | R1 = 0.0584, wR2 = 0.1619 |
| | all data | R1 = 0.0690, wR2 = 0.1673 |
| Weighting scheme | w = 1/[σ ² (F _o ²) + (0.0910P) ² + 22.5809P] where P = (F _o ² + 2F _c ²)/3 | |
| Largest diff. peak and hole | 4.948 and -3.865 eÅ ⁻³ | |
| R.M.S. deviation from mean | 0.177 eÅ ⁻³ | |

4. Powder X-ray diffraction data

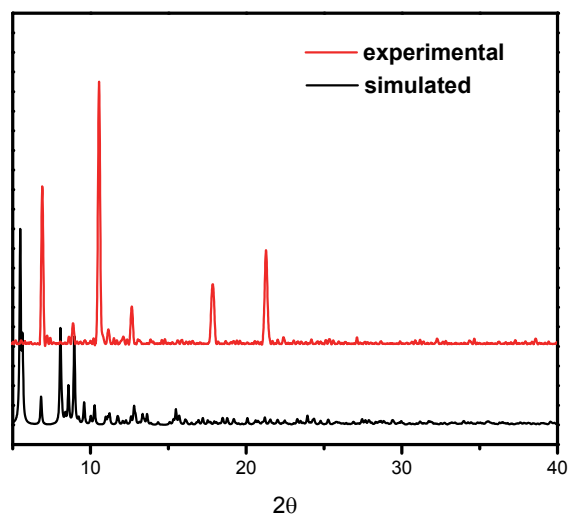
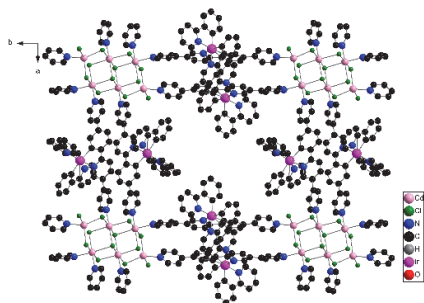




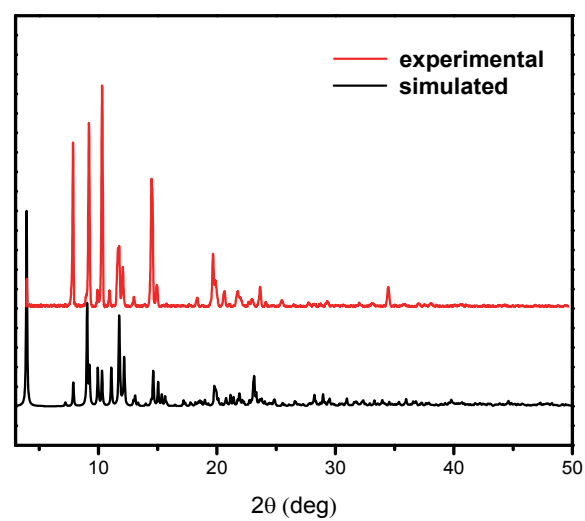
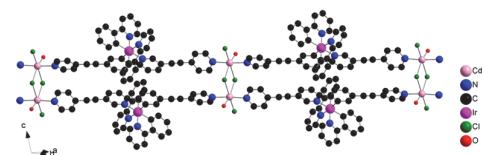
fac-Ir(ppy)₂(ppy-4)



fac-Ir(ppy)₂(ppy-12)·Cd₆



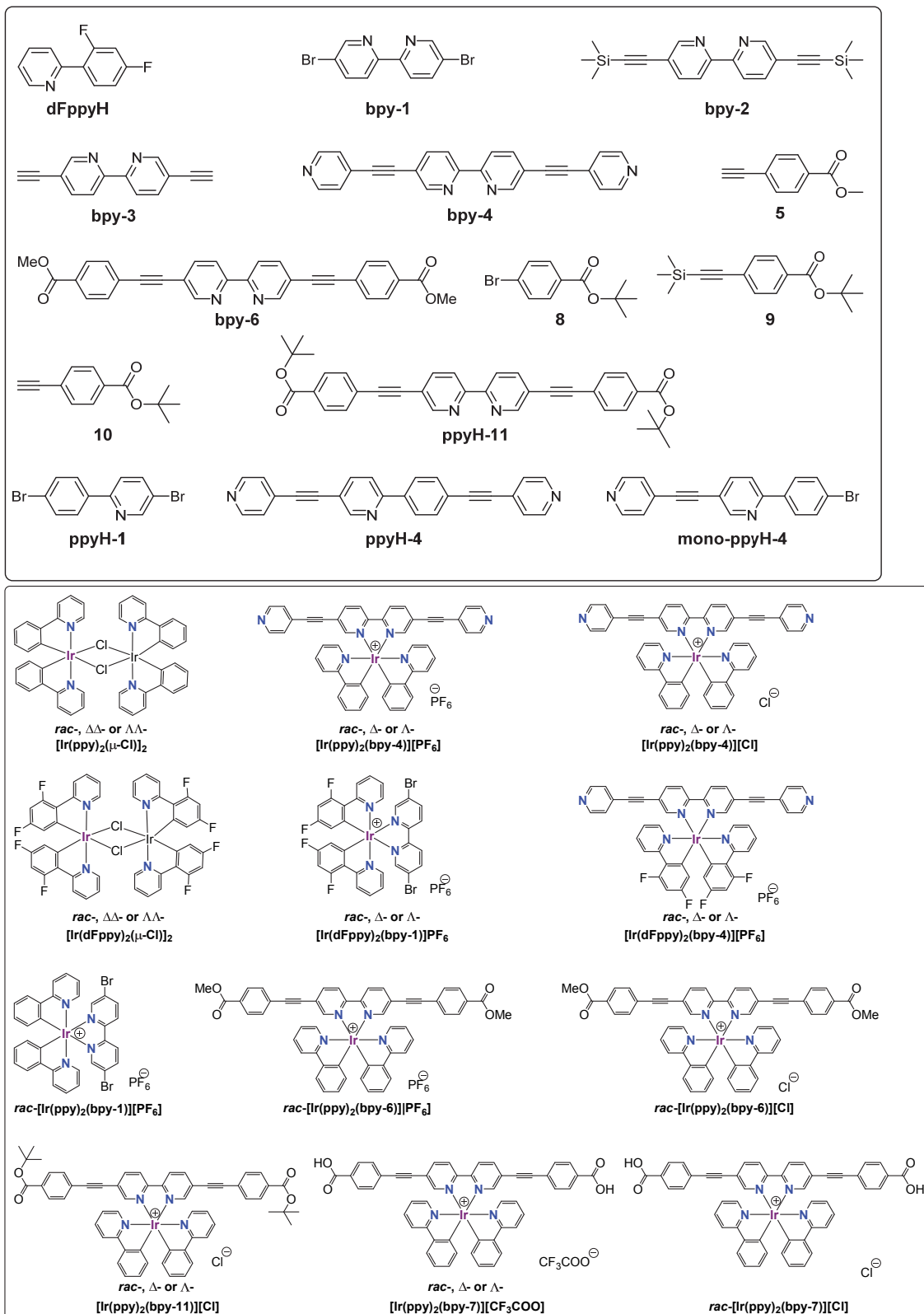
fac-Ir(ppy)₂(ppy-4)·CdCl₂

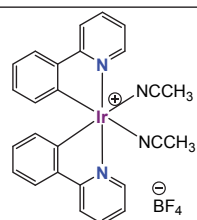


REFERENCES

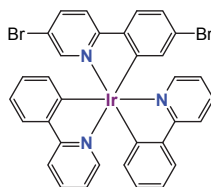
- (1) Brouwer, A. M. *Pure Appl. Chem.* **2011**, 83, 2213.
- (2) Beeby, A.; Bettington, S.; Fairlamb, I. J. S.; Goeta, A. E.; Kapdi, A. R.; Niemelä, E. H.; Thompson, A. L. *New J. Chem.* **2004**, 28, 600.
- (3) Sprouse, S.; King, K. A.; Spellane, P. J.; Watts, R. J. *J. Am. Chem. Soc.* **1984**, 106, 6647.
- (4) You, Y.; Park, S. Y. *J. Am. Chem. Soc.* **2005**, 127, 12438.
- (5) Ayme, J. F.; Beves, J. E.; Leigh, D. A.; McBurney, R. T.; Rissanen, K.; Schultz, D. *Nat Chem* **2012**, 4, 15.
- (6) Cavazzini, M.; Quici, S.; Scalera, C.; Puntoriero, F.; La Ganga, G.; Campagna, S. *Inorg. Chem.* **2009**, 48, 8578.
- (7) Chepelin, O.; Ujma, J.; Wu, X.; Slawin, A. M.; Pitak, M. B.; Coles, S. J.; Michel, J.; Jones, A. C.; Barran, P. E.; Lusby, P. J. *J. Am. Chem. Soc.* **2012**, 134, 19334.
- (8) Tinker, L. L.; McDaniel, N. D.; Cline, E. D.; Bernhard, S. *Inorg. Synth.* **2010**, 35, 168.
- (9) Tour, J. M.; Rawlett, A. M.; Kozaki, M.; Yao, Y.; Jagessar, R. C.; Dirk, S. M.; Price, D. W.; Reed, M. A.; Zhou, C.-W.; Chen, J.; Wang, W.; Campbell, I. *Chem. Eur. J.* **2001**, 7, 5118.
- (10) Taylor, E. C.; Wong, G. S. K. *J. Org. Chem.* **1989**, 54, 3618.
- (11) Wang, D.; Wang, J.; Fan, H.-L.; Huang, H.-F.; Chu, Z.-Z.; Gao, X.-C.; Zou, D.-C. *Inorg. Chim. Acta* **2011**, 370, 340.
- (12) McGee, K. A.; Mann, K. R. *Inorg. Chem.* **2007**, 46, 7800.

List of Products

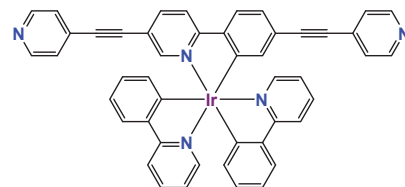




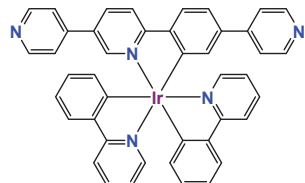
***rac*-[Ir(ppy)₂(ACN)₂][BF₄]**



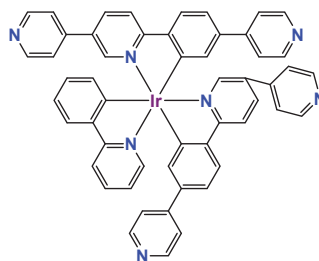
***fac*-Ir(ppy)₂(ppy-1)**



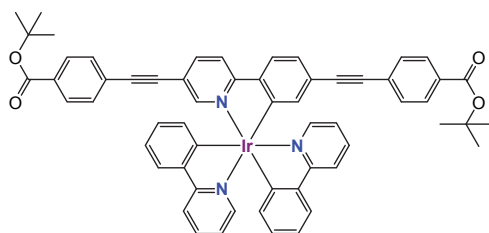
***fac*-Ir(ppy)₂(ppy-4)**



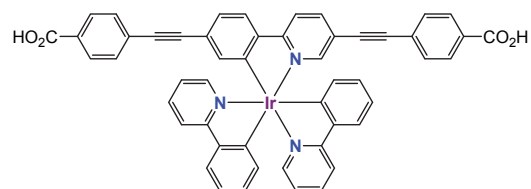
***fac*-Ir(ppy)₂(ppy-12)**



***fac*-Ir(ppy)(ppy-12)₂**



***fac*-Ir(ppy)₂(ppy-11)**



***fac*-Ir(ppy)₂(ppy-7)**

Publications

1). Chaojie Xu, Aurélie Guenet, Nathalie Kyritsakas, Jean-Marc Planeix, and Mir Wais Hosseini, “Molecular tectonics: heterometallic (Ir,Cu) grid-type coordination networks based on cyclometallated Ir(III) chiral metallatectons”, *Chem. Commun.* **2015**, DOI: 10.1039/C5CC06427A

2). Chaojie Xu, Aurélie Guenet, Nathalie Kyritsakas, Jean-Marc Planeix, and Mir Wais Hosseini, “Molecular Tectonics: design of enantiopure luminescent heterometallic Cd(II)-Ir(III) coordination network” *Inorg. Chem.*, **2015**, DOI: 10.1021/acs.inorgchem.5b01910.

Oral communication

1). Chaojie Xu, Aurélie Guenet, Nathalie Kyritsakas, Jean-Marc Planeix and Mir Wais Hosseini, “Chiral Luminescent Iridium Complexes based Coordination Networks”, Joint group meeting with Pr. Makoto Fujita’s group, 12th September, **2014**, Strasbourg, France.

2). Chaojie Xu, Aurélie Guenet, Nathalie Kyritsakas, Jean-Marc Planeix and Mir Wais Hosseini, “Chiral Luminescent Iridium Complexes based Coordination Networks”, Journée des Doctorants en Chimie, 7th November, **2014**, Strasbourg, France.

3). Chaojie Xu, Aurélie Guenet, Nathalie Kyritsakas, Jean-Marc Planeix and Mir Wais Hosseini, “Synthesis of Iridium Complexes for the formation of Coordination Networks”, 6 oral presentation in the frame of the Interreg IV project “CHIRANET”.

Poster presentation

1). Chaojie Xu, Aurélie Guenet, Nathalie Kyritsakas, Jean-Marc Planeix and Mir Wais Hosseini, “Synthesis of Chiral Iridium Complexes for the formation of Coordination Networks”, Strasbourg summer school “Challenges in Supramolecular Chemistry”, 8th-12th September, **2014**, Strasbourg, France.

2). Chaojie Xu, Aurélie Guenet, Nathalie Kyritsakas, Jean-Marc Planeix and Mir Wais Hosseini, “Enantiopure Luminescent Heterometallic Coordination Polymers” GECOM-CONCOORD, 26th-29th May, **2015**, Lyon, France. (**Best Poster Prize**).

3). Chaojie Xu, Aurélie Guenet, Nathalie Kyritsakas, Jean-Marc Planeix and Mir Wais Hosseini, “Luminescent Heterometallic Coordination Polymers” ISMSC, 28th June – 2nd July, **2015**, Strasbourg, France.

Tectonique Moléculaire :
Réseaux de coordination hétérométalliques basés sur des complexes d'Iridium(III) chiraux et luminescents

Résumé

Les réseaux de coordination sont des architectures cristallines hybrides organiques-inorganiques pouvant présenter des propriétés découlant de leurs compositions et de leurs architectures. L'objectif de ce travail fut la synthèse de réseaux de coordination hétérométalliques à base de complexes d'Iridium (III) chiraux et luminescents.

Dans un premier temps, la synthèse de nouveaux complexes d'Iridium cationiques bis-cyclométallés sous forme racémique et énantiopure a été réalisée avec succès. L'étude de leurs propriétés photophysiques a montré une émission dans le rouge par excitation dans le visible. La formation de réseaux de coordination à partir de ces metallatectons cationiques a ensuite été étudiée. Un réseau de coordination homochiral monodimensionnel luminescent a notamment été obtenu *via* l'auto-assemblage d'un complexe énantiopure avec un sel de cadmium(II).

D'autre part, la synthèse de complexes d'Iridium neutres tris-cyclométallés possédant un troisième ligand dérivé de l'unité 2-phénylpyridine comportant des sites de coordination périphériques a été optimisée et les propriétés photophysiques de ces complexes discrets ont été étudiées. L'utilisation de ces complexes comme metallatectons neutres a conduit à la formation de différents réseaux de coordination luminescents.

Mots clés : Réseau de coordination, complexes d'Iridium (III), Chiralité, metallatectons, luminescence, tectonique moléculaire.

Abstract :

Coordination networks or Metal Organic Frameworks (MOFs) are hybrid organic-inorganic crystalline architectures that, depending on their composition and organization, may display tailored properties. The aim of this PhD work was to synthesize heterometallic coordination networks based on chiral luminescent Iridium(III) complexes.

On the one hand, the synthesis of cationic bis-cyclometallated Ir(III) complexes, both as racemate and as enantiopure species, was achieved. These complexes display red emission upon excitation in the visible domain. Formation of coordination networks using the prepared cationic metallatectons was studied. Notably, a luminescent enantiopure 1D coordination network was obtained upon self-assembly of one of the enantiopure cationic metallatectons with Cd(II) salts.

On the other hand, synthesis of racemic neutral tris-cyclometallated Ir(III) complexes was also optimized and their photophysical properties studied. Different coordination networks have been also generated and studied.

Keywords: Coordination networks, Iridium (III) complexes, Chirality, metallatectons, luminescence, molecular tectonics.